High throughput proteomic analysis of *Mycobacterium tuberculosis* associated Immune Reconstitution Inflammatory Syndrome (TB-IRIS)

Liam Bell

Thesis presented for the degree of Doctor of Philosophy
In the Department of Clinical and Laboratory Sciences
University of Cape Town
December 2012

Abstract

Currently more than 70 % of people with active tuberculosis (TB) in South Africa are dually infected with HIV. The incidence of new TB cases in South Africa is approximately 1 % of the adult population per year and the incidence of new HIV cases is over 15 % of the adult population; in some townships this figure is 33 %. The past decade has seen the emergence of the immune reconstitution inflammatory syndrome (IRIS) in HIV patients who have a concurrent infection and who have recently initiated their highly active anti-retroviral therapy (HAART), the most common co-infection associated with IRIS being TB. IRIS is characterised by an excessive inflammatory immune reaction to the co-infecting pathogen, normally within the first three months of initiation of HAART. The incidence of TB associated IRIS (TB-IRIS) varies between 7 - 43 % of TB positive and HIV positive patients. Currently there is no pre-symptomatic diagnostic test available for clinicians and TB-IRIS patients are therefore only diagnosed after presenting clinical symptoms. In 2009, a double blinded, randomised, placebo controlled drug trial was performed to assess the effectiveness of prednisone in the treatment of TB-IRIS cases. The outcome determined that prednisone treatment reduced the need for hospitalization and therapeutic procedures and hastened improvements in symptoms, performance, and quality of life. However, the underlying molecular mechanism of action of this treatment still remains largely unknown.

Immune responses to *Mycobacterium tuberculosis* antigens are known to differ *in vivo* between TB-IRIS and control patients who are dually infected with HIV and TB and who are on HAART and anti-TB therapies but who do not develop IRIS symptoms ('TBART' patients). This thesis therefore describes proteomic research aimed at determining the molecular origin of these differences using an *in vitro* model of TB-IRIS, based on use of cultured peripheral blood mononuclear cells (PBMCs) isolated from TB-IRIS and TBART patients, the goals being to 1) identify a potential diagnostic protein biomarker for the TB-IRIS condition, 2) provide an improved understanding of the molecular origin of TB-IRIS, and 3) aid development of more targeted suppression of TB-IRIS.

Results from this study have determined a fundamental difference in the proteomic profiles of TB-IRIS and TBART patient derived PBMCs in response to re-stimulation using heat killed H37Rv as well as to treatment using dexamethasone. These results form the bases of a new hypothesis that TB-IRIS derived PBMCs mount an uncoordinated immune response which appears to become a co-ordinated innate response in the presence of dexamethasone, whereas TBART derived PBMCs display the capacity to produce a co-ordinated adaptive immune response that is better equipped to clear antigen and contain infection to sites of disease.

Declaration

1. I know that plagiarism is wrong. Plagiarism is to use another's work and pretend that it is one's own.

2. I have used the …..... convention for citation and referencing. Each contribution to, and quotation in, this thesis from the work(s) of other people has been attributed, and has been cited and referenced.

3. This thesis is my own work

4. I have not allowed, and will not allow, anyone to copy my work with the intention of passing it off as his or her own work.

5. I acknowledge that copying some else's assignment or essay, or part of it, is wrong and declare that this is my own work.

Signature _____

Acknowledgements

This thesis has taken many years of sacrifice from many people who are involved in my life. I would firstly like to thank my mother, Colleen, without whose support emotionally and financially I would never have made it to the start of my thesis, never mind the end. You have been the single greatest blessing in my life mom and I hope this thesis makes you proud. Equally I would like to thank my supervisor, Prof. Jonathan Blackburn who has given me the opportunity to explore this fantastic field of Science and whose guidance during troubled times can not be overstated enough. There are many others who have helped along the way with encouraging words in times of need (and there were many), too numerous to name here but you know who you are. I would also like to thank those who helped me by providing tools that I have used for my thesis. In this regard I would like to thank my fellow lab members, chief amongst them are Shaun Garnett and Katie Viljoen, who respectively; single handedly put together our proteomic data processing pipeline, and who conquered the scripting language R to make sense of the processed data. I have been fortunate enough to complete my Ph.D in a lab filled with fantastic people and to all of you I have had the pleasure of working with along the way I want to say thank you for making my journey memorable. I would also like to thank Dr Salome Smit at the Central Analytical Facility based at the University of Stellenbosch who helped me to generate my proteomics data, although overworked you always have a smile. Lastly I would like to thank the Big Guy upstairs, this journey has been illuminating for myself about myself and I thank you for being there when I needed it.

I would also like to thank the University of Cape Town and the National Research Foundation for providing me with financial support during my studies.

Contents

List of Figures

List of Tables

Nomenclature

1DE	One-dimensional electrophoresis
2D	Two-dimensional
2DE	Two-dimensional electrophoresis
3TC	Lamivudine
ABC	50 mM Ammonium bicarbonate
ACN	Acetonitrile
AFB+	Acid-fast bacilli
AIDS	Acquired immunodeficiency syndrome
APCs	Antigen presenting cells
APEX	Absolute protein index
ARP	Actin-related protein
ART	Anti-retroviral treatment
AZT	Zidovudine
BCG	Bacillus Calmette–Guérin
BSL	Bio-safety level
CCB	Colloidal coomasie blue

Cdc42	Cell division cycle 42 protein
cDNA	Complimentary DNA
CFL	Cofilin
CFP-10	Culture filtrate protein-10
CFU	Colony forming unit
CHAPS	3-[(3-cholamidopropyl)dimethylammonio]-1-propanesulfonate
CID	Collision induced dissociation
CNS	Central Nervous System
CPGR	Centre for Proteomic and Genomic Research
CSF	Crude sub-cellular fractionation
CV	Column volume
DEAE	Diethylaminoethyl
DHB	2,5-dihydroxybenzoic acid
DIGE	Differential gel electrophoresis
DMSO	Dimethyl sulfoxide
dNTPs	Deoxynucleoside triphosphates
DOC	Deoxcycholate
DOTS	Directly observed treatment, short course
DST	Drug susceptibility test
DTH	Delayed type hypersensitivity

DTT	Di-thiothreitol
ECM	Extra-cellular matrix
eIF2	Eukaryotic initiation factor-2
ELISA	Enzyme-Linked Immunosorbent Assay
ELISpot	Enzyme-Linked Immunospot Assay
emPAI	Exponentially modified protein abundance index
ESAT-6	Early secreted antigenic target 6 KDa protein
ETD	Electron transfer dissociation
FA	Formic acid
FASP	Filter aided sample preparation
FcγR	Fc-gamma receptor
FCS	Fetal calf serum
FDR	False discovery rate
H37Rv	Mycobacterium tuberculosis strain type
HAART	Highly active anti-retroviral therapy
HILIC	Hydrophilic interaction liquid chromatography
IAA	50 mM Iodoacetamide in 8M Urea and 0.1 M Tris-Cl pH 8.5
iBAQ	Intensity based absolute quantitation
ICAT	Isotope-coded affinity tag
ICF	Informed consent form

IFN	Interferon gamma
IGRA	Interferon gamma release assay
IIDMM	Institute for Infectious Diseases and Molecular Medicine
IMAC	Immobilized metal affinity chromatography
INH	Isoniazid
IPA	Ingenuity Pathway Analysis
IPI	International Protein Index
IPT	Isoniazid preventive therapy
IRD	Immune Restoration Disease
IRIS	Immune reconstitution inflammatory syndrome
IRS	Immune Reconstitution Syndrome
IT	Ion trap
ITAM	Immunoreceptor tyrosine activation motifs
iTRAQ	Isobaric tags for relative and absolute quantitationb
LC	Liquid chromatography
LIMK	LIM-kinase
LOPIT	Localisation of organelle proteins by isotope tagging
LTBI	Latent TB infection
M.tb	Mycobacterium tuberculosis
m/z	Mass-to-charge ratio

MDR	Multi-drug resistant
MHC	Major histocompatibility complex
MLCP	Myosin light chain phosphatase
MM	Minus dexamethasone / Minus re-stimulation with H37Rv
MMTS	S-methylmethanethiosulphonate
MOAC	Metal oxide affinity chromatography
MOI	Multiplicity of infection
MP	Minus dexamethasone / Plus re-stimulation with H37Rv
MRM	Multiple reaction monitoring
MS	Mass spectrometry
MudPIT	Multi-dimensional protein identification technology
MWCO	Molecular weight cut-off filter, measured in Daltons
MYL	Myosin light chain
NAAT	Nucleic acid amplification testing
NK	Natural killer
NSAF	Normlised spectral abundance factor
OGP	n-octyl 3-D-glucopyranoside
OI	Opportunistic infection
PAGE	Polyacrylamide Gel Electrophoresis
PBMCs	Peripheral blood mononuclear cells

PBS	Phosphate buffered saline
PD	Phospho-depleted
PDE	Phospho-depleted and -enriched
PDGF	Platelet-derived growth factor
PE	Phospho-enriched
PFF	Peptide fragment fingerprinting
PI	Protease inhibitor
pI	Iso-electric point
PMF	Peptide mass fingerprinting
PP	Plus dexamethasone / Plus re-stimulation with H37Rv
PPD	Purified protein derivative
ppm	Parts per million
PSMs	Peptide-spectrum matches
PTM	Post translational modification
PTPs	Proteotypic peptides
Q	Quadrupole
qPCR	Quantitative real-time PCR
R-10	RPMI-1640 and 10 percent Fetal calf serum
Rif	Rifampicin
ROCK	Rho kinase

RP	Reverse phase
RT-PCR	Real-time PCR
S/N	Signal to noise ratio
SAB	Laemmli gel sample application buffer
SAX	Strong anion exchange
SCX	Strong cation exchange
SDS	Sodium dodecyl sulfate
SILAC	Stable isotope labelling by amino acids in cell culture
SRM	Selected reaction monitoring
SYK	Spleen tyrosine kinase
TB	Tuberculosis
TB-IRIS	TB associated immune reconstitution inflammatory syndrome
TBART	Patients receiving TB and ART treatment who do not develop IRIS
TCEP	Tris(2-carboxyethyl)phosphine
TDR-TB	Totally drug resistant TB
TEAB	Tri-ethyl ammonium bicarbonate
TFA	Tri-fluoro-acetic acid
Th1	Type 1 helper T cell
Th17	Type 17 helper T cell
Th2	Type 2 helper T cell

TiO2	Titanium dioxide
TNF-alpha	Tumour necrosis factor alpha
ToF	Time-of-flight
TPP	Trans-Proteomic Pipeline
TR	Retention time
TST	Tuberculin skin test
UA	8M Urea in 0.1 M Tris-Cl pH 8.5
UnitProtKB	UniProt Knowledge Base
WAX	Weak anion exchange
WHO	World Health Organisation
XDR	Extensively drug resistant
ZN	Ziehl-Neelson

1 Immunology Literature Review

1.1 Tuberculosis

Mycobacterium tuberculosis (*M.tb*) is the primary infectious agent responsible for tuberculosis (TB), a common infectious disease - especially in resource poor countries. Other mycobacteria, such as *M. bovis*, *M. africanum* and *M. microti*, can cause non-granulomatous TB, however they do not normally infect healthy or immunocompetent human adults. The most common site of disease for TB is the lungs (pulmonary TB). However, *M.tb* can also be found in tissues and organs outside of the lungs, referred to as extra-pulmonary TB, such as the central nervous system (CNS), lymph nodes, gastro-intestinal tract, bones, skin and even the heart (pericardial TB). It is estimated that as many as a third of the world's population are latently infected with *M.tb* [1].

1.1.1 The bacterium

M.tb is an Actinomycete, first discovered by Robert Koch in 1882, although archaeological evidence of human infection with *M.tb* dates back thousands of years [2]. *M.tb* is a small rod-like aerobic bacterium that has a very slow metabolism, dividing approximately every 15 - 20 hours. It has a waxy cell wall, due to the high lipid content, and is fairly impermeable to most dyes unless they are attached to phenol. Consequently, *M.tb* is classified neither as a gram negative or gram positive bacterium, but is rather identified as being acid fast since, once stained, it resists decolourisation with acidified solvents.

The nature of the unique architecture of the mycobacterial cell wall envelope and how it anchors to the plasma membrane results in a very well protected environment for the bacteria that makes it difficult for small molecules, such as drugs, to permeate and also provides a source for a large number of antigenic compounds. The mycobacterial plasma membrane is surrounded by three covalently linked structural layers that can loosely be described as a peptidoglycan/arabino-galactan layer, linked to a mycolic acid layer, which (as a result of the covalent linkages between

the mycolic acids) provides a hydrophobic layer of extremely low fluidity. The outermost section of the mycolic acid layer contains various free lipids, such as phenolic glycolipids, phthiocerol dimycocerosates, and phosphatidylinositol mannosides, that are intercalated with the mycolic acids, the majority of which are specific for mycobacteria. The mycolic acid layer is in turn linked to the outer polysaccharide layer, which is generally called the capsule, contains molecules such as glucan and arabinomannan. A basic diagram of these layers and their relation to the mycobacterial plasma membrane can be seen in Figure 1.1.

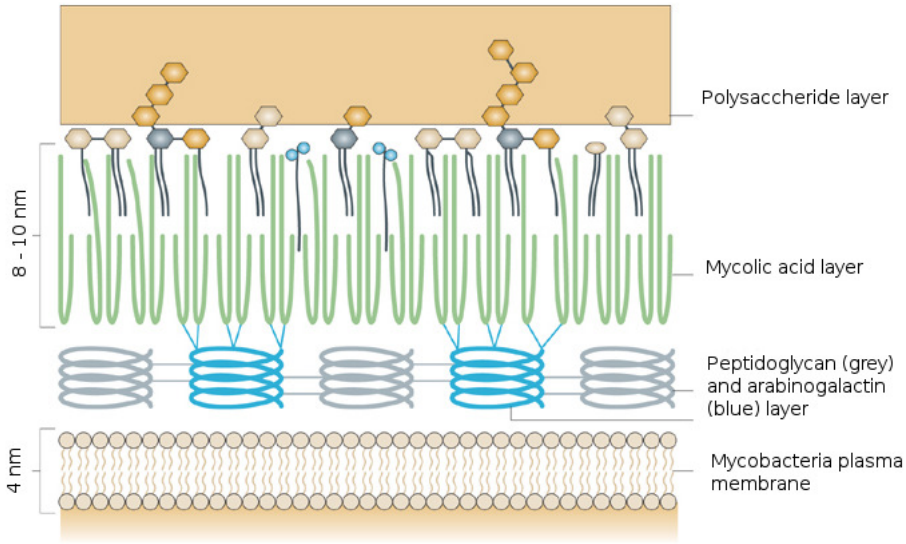

Figure 1.1: Schematic representation of the cell envelope of *Mycobacterium tuberculosis* The diagram represents a basic cross section of a typical mycobacterial cell envelope, containing three different linked structures, namely: the peptidoglycan/arabinogalactan layer (grey and blue); the mycolic acids layer (green) which is also referred to as the mycomembrane; and the outer polysaccharide layer. Figured sourced from Abdallah *et al* 2007 [3].

1.1.2 Distribution and burden of disease

The global distribution of TB is skewed mainly towards resource limited countries with over 80 % of TB infections occurring in 22 countries across Africa and Asia - as shown in Figure 1.2.

The five countries with the largest number of incident cases of TB in 2010 were India (2.0 million–2.5 million), China (0.9 million–1.2 million), South Africa (0.40 million–0.59 million), Indonesia (0.37 million–0.54 million) and Pakistan (0.33 million–0.48 million). India alone accounted for an estimated one quarter (26%) of all TB cases worldwide, and China and India combined accounted for 38% [4].

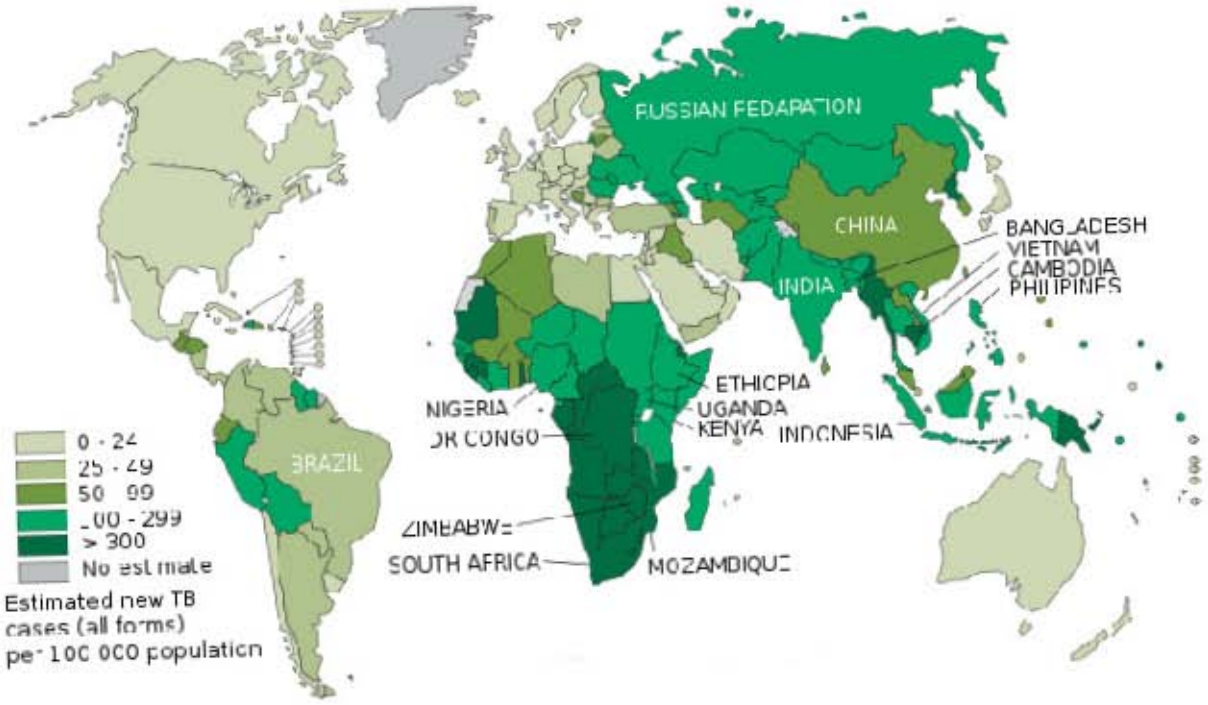

Figure 1.2: Estimated global incidence rates of TB in 2010
The global distribution of new cases of TB in 2010. Source = *Global Tuberculosis Control: WHO report 2011* [4].

In South Africa, the incidence rate for TB has more than tripled from 301 to 981 new cases per 100 000 population between 1990 and 2010. Currently the incidence of new TB infection is approximately 1 % of the population of which more than half are co-infected with HIV [4]. In specific informal settlements in South Africa, e.g. Kayelitsha, Cape Town, the incidence of active TB is currently 1.6 %, with 70 % of new active TB patients being HIV positive.

This co-incidence of HIV and TB disease causes major complications in disease management for a number of reasons, such as adverse drugs reactions, incompatible dosing regimes and the development of life threatening secondary syndromes. The net result being that in co-infected individuals, TB and HIV can no longer realistically be viewed as separate diseases. The high level of HIV/TB co-infection has led the South African National AIDS Council to call for integration of care for these two diseases in their National Strategic Plan [5, 6].

The *M.tb* genome has been shown to exhibit a large amount of variation and currently thousands of strains have been identified using various genetic methods, these strains also exhibit considerable differences in clinical phenotype. The distribution of these strains has been shown to be phylogeographical in nature and each lineage appears to have links to specific sympatric human populations [7**?**].

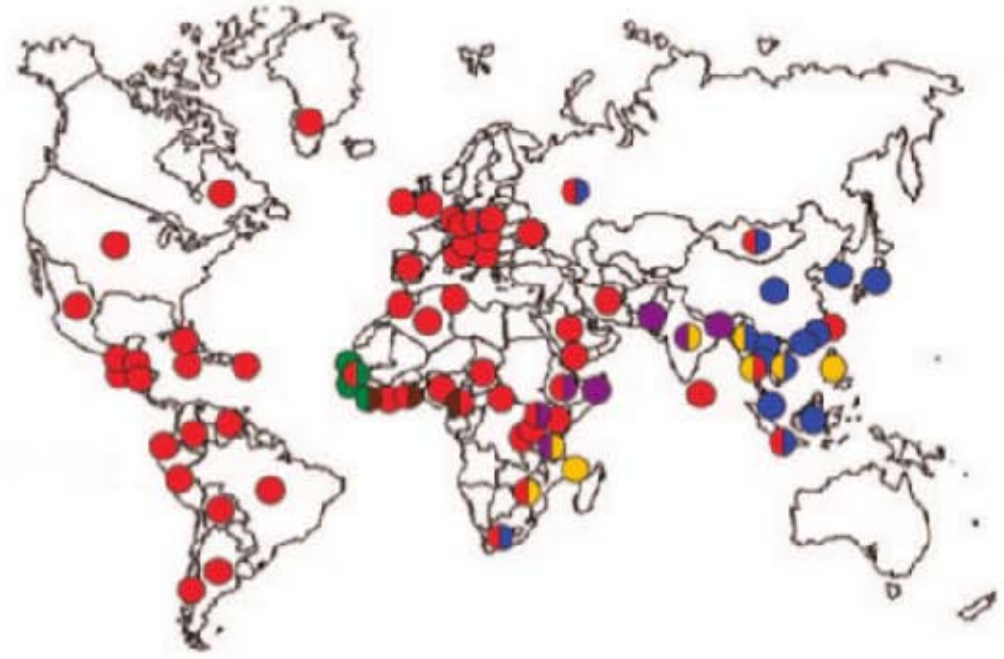

Geographic region (no. of countries)	Total strains	Indo-Oceanic lineage	East-Asian lineage	East-African-Indian lineage	Euro-American lineage	West-African lineage 1	West-African lineage 2
Americas (18)	207	6	7		194		
Europe (14)	35	1	4		30		
North Africa/ Middle East (6)	10				10		
West Africa (8)	28				12	9	7
Central Africa (5)	15			1	14		
South Africa (1)	5		2		3		
East Africa (6)	20	3		8	9		
Indian Subcontinent (4)	17	3	1	10	3		
Southeast Asia (9)	272	159	73	1	29		
East Asia (7)	262	17	190		55		
Pacific Islands (2)	4				4		
Total (80)	875	199	277	20	368	9	7

Figure 1.3: Global geographic distribution of *M.tb* phylogenetic lineages

The six main lineages of *M.tb* are geographically distributed, each dot corresponds to 1 of 80 countries represented in the global strain collection. The colours of the dots relate to the six main lineages as represented in the table provided below the figure and indicate the dominant lineage(s) in respective countries. Figured sourced from Gagneux *et al*. 2006 [8].

1.1.3 Aetiology and pathogenesis

It is important to distinguish active TB disease (primary and reactivation) from a latent TB infection (LTBI) when discussing aetiology and pathogenesis. Primary disease is the result of active disease on first exposure to the TB bacillus, whereas reactivation disease occurs when a LTBI infection becomes an active infection. Re-infection occurs in people who have been able to eliminate *M.tb* entirely but are then subsequently exposed and infected at a later stage.

A latent TB infection is thought to occur when inhaled TB bacilli are engulfed by the host macrophages but then prevent the fusion of the host macrophage with lysozyme vesicles (highly acidic and contains proteases). Fusion of these two entities would normally results in a highly destructive phagolysosome that is capable of eliminating intracellular pathogens effectively - however this prevented during an LTBI infection. The mechanism of prevention of fusion amongst these vesicles is poorly understood, and it is thought that the host response maintains the infected macrophages in a contained, hypoxic environment within a granuloma. In some cases the host response are capable of eradicating bacilli effectively, however in LTBI or active disease this is not the case. The *M.tb* bacilli revert to a low metabolic or dormant state until such time as the host response in maintaining the granulomatous is disturbed and presents the *M.tb* bacilli with a chance to regroup and develop into an active TB infection. This is not the only way that active disease may be acquired however, as it is possible for active TB to develop from a infection with TB bacilli.

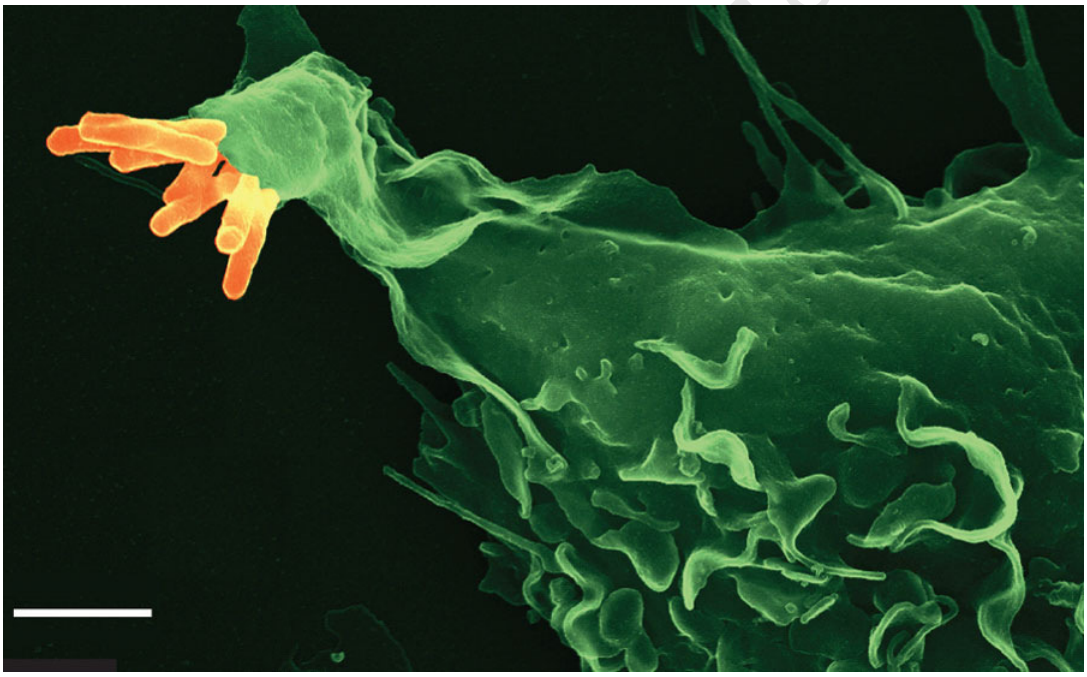

Figure 1.4: Macrophage phagocytosing *M.tb* bacilli
This scanning electron micrograph shows the phagocytosis of *Mycobacterium tuberculosis* bacilli (orange) by the host macrophage (green) in the lungs. (Scale: White bar = 2 μm.) Sourced from Kaufmann, Stefan H E, *Deadly combination*, Nature 453, May (2008) [9].

In a typical TB infection, droplet nuclei containing the infectious *M.tb* antigens are inhaled into the lungs from the air where they come to rest in the pulmonary alveoli. The infectious bacilli stimulate alveolar macrophage toll-like receptors, resulting in cytokine and chemokine release and the subsequent recruitment of circulating monocyte and local dendritic cells. Monocytes

become macrophages and engulf bacilli and remain in the lung (Figure 1.4 illustrates a macrophage phagocytosing *M.tb* bacilli). Dendritic cells that are also present at the site of infection, engulf the bacilli and migrate to local draining lymph nodes to activate lymphocytes. The infected dendritic cells are capable of presenting *M.tb* antigens from the replicating bacilli to circulating CD4 lymphocytes using MHC class II proteins on their cell surface, triggering a cell-mediated adaptive immune response [10]. An initial clonal expansion of the lymphocytes occurs before migrating to the site of infection. Here the infected phagocytic antigen presenting cells (APCs) skew the balance of IL-12:IL-4 and results in a Type 1 helper T cell (Th1) response as opposed to a Type 2 helper T cell (Th2) response. The Th1 response is characterised by the clonal expansion of CD8+ T-cells and natural killer (NK) cells and an increase in the production of interferon-gamma (IFN-γ) - an end product of the Th1 response - at the site of infection. The increased production of IFN-γ activates macrophages to improve their microbicidal activity and drives the release of chemokines, other pro-inflammatory cytokines and tumour necrosis factor alpha (TNFα). There is a delay of approximately two weeks after initial exposure before the cell mediated immune response kicks in as the lymphocytes have to be activated in the lymph nodes. IL-12 has also been shown to be a growth factor for preactivated T- and NK cells, thus enhancing the cytotoxic activity of CD8+ T-cells and NK cells, and is important for optimal differentiation of CD8+ T-cells. Patients who have a strong Th2 response (anti-inflammatory) to *M.tb* infections have been shown to have a decreased cell mediated immune response and subsequently have been more susceptible to TB infection. The balance between the Th1/Th2 response mechanism can be seen in Figure 1.5.

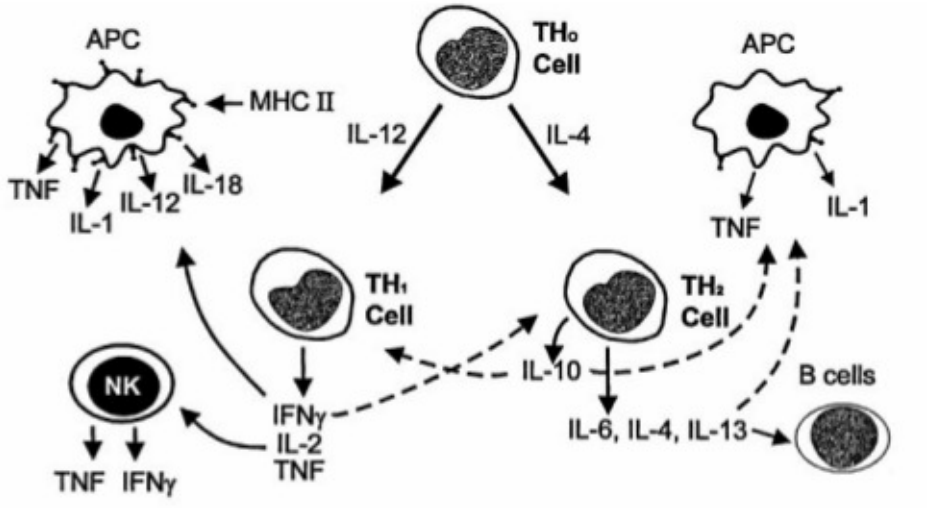

Figure 1.5: The drivers behind a Th1 and Th2 response

The mechanisms behind the balance of the Th1 and Th2 response. Solid lines indicate stimulatory pathways and dotted lines indicate inhibitory pathways. APC = Antigen presenting cell, Th0 = uncommitted CD4+ T helper cell precursor. Figure adapted from [11].

The Th1 response results in the recruitment of a number of different cells that form a granuloma to contain the infected APCs [12]. The infected macrophages are surrounded by foamy macrophages and multinucleate Langerhans giant cells [13]. These in turn are surrounded by CD4 and CD8 lymphocytes as well as B cells. The final layer of an established granuloma is characterised by collagen producing fibroblasts. If the granuloma fails to contain the *M.tb* infected macrophages, it breaks open and releases bacteria that then infect surrounding macrophages, leading to cavities forming at other locations in the lung and eventually to a disseminated infection [10]. Damage to lung tissue also results in a persistent cough, providing the mechanism for transmission of *M.tb* bacilli through aerosols, thus beginning the cycle again. For individuals with a latent TB infection, it is thought that lipid vacuoles in macrophages latently infected with TB bacilli actually provide nutrition for the latent bacilli, as they have switched their metabolism from carbohydrates (their preferred energy-source) to lipids. Interestingly, there is some evidence to suggest that accumulation of tri-acyl gycerol lipids in bacilli in sputum correlates with a more dormant-like phenotype which may conceivably differ between clinical strains of *M.tb* and may also link to observed differences in virulence [14].

1.1.4 Diagnosis and testing

It is important to distinguish between LTBI and active infections when discussing diagnosis and treatment of TB, with latent infection being defined as "the presence of any tuberculous lesion which fails to produce symptoms of its presence" [15]. The chance of disease progression from asymptomatic latent TB, to active TB is approximately five to 10% per lifetime and the chance of acquiring a TB infection from a person who has an active infection is also approximately 10 % per lifetime [16].

The *M.tb* genome was first sequenced in 1998 [17, 18] but despite this, there have been few advancements in how active or latent TB is diagnosed in patients. Diagnosis of TB still relies heavily on techniques that were developed over 100 years ago, the most widely spread method being the tuberculin skin test (TST) [4]. The TST is often used in conjunction with other more modern methods, such as chest radiography, sputum smear microscopy or culture from infected fluids; these techniques are currently the predominant methods used in resource limited settings for the diagnosis of TB.

Typically the first test done on adult patients suspected of having TB (based on clinical symptoms and history of exposure) is sputum smear microscopy, with or without a chest x-ray. The trouble with chest x-rays is that because TB can resemble various other pulmonary pathologies, it is difficult to differentiate TB from these pathologies, and also from previous

lung damage which may leave residual signs on x-ray (this requires the presence of a baseline x-ray in order to compare the new x-ray to, and this is often not available). Children and HIV+ patients often have a low sputum bacillary load, meaning that they have more false negative sputum smear microscopy results. The gold standard for diagnosis is a positive culture result (the material to be cultured is determined by the clinical site of disease, e.g. sputum for pulmonary TB, ascitic fluid for GIT TB, blood for disseminated TB, etc), although this takes time.

The main underlying issue with the TST and certain other assays is that they are incapable of distinguishing latent infection from active disease as their outcome is determined due to the patient having acquired an immune response to a previous infection that is detectable when re-challenged with an antigen, thus the outcome is not directly linked to the presence of viable bacilli. The TST test is also usually reactive in people from high-prevalence areas (because almost everyone has been exposed to TB in these areas, and therefore their immune systems are primed by TB antigens), and also in people who have received the Bacillus Calmette–Guérin (BCG) vaccine. Whilst the last decade has seen the development of newer diagnostic techniques based primarily on PCR technology, the major obstacles for many of the TB diagnostic tests currently in use world wide remain the relationship between the sensitivity and the accuracy of detection of *M.tb* as well as the cost of the test: some tests are sensitive but can give a high number of false positives whilst others are not as sensitive and can be prone to false negatives depending on the stage and duration of infection, see Table 1.1.

Test		Exposed	Infected	Diseased	Days to result
X-ray		-	±	+ / ++	1
TST		-	+	++	3
ZN smear microscopy		-	-	++	1
Culture methods	Solid media	-	+	++	42 - 56
	Liquid media (MGIT)	-	+	++	3 - 14
Serological tests		-	+	+	2
Urine LAM		-	± (HIV+)	+	1
ELISpot		±	++	++	1 - 2
Quantiferon		-	++	+++	1 - 2
NAAT/PCR (XPERT)		±	± (HIV+)	+++	2

Table 1.1: Array of some TB diagnostic tests currently in use

The table illustrates the potential role of different tests in diagnosis of tuberculosis at different stages of disease. TST = tuberculin skin test; LAM = lipoarabinomanan; PCR = polymerase chain reaction; -, not helpful; +, helpful; ++, very helpful; +++, very reliable; ±, may or may not be helpful in diagnosis [19].

Test		Sensitivity (%)	Specificity (%)	Additional information
Active TB infections				
Automated liquid culture				Quicker to result than solid culture
ZN smear microscopy				Quick, inexpensive and relatively easy to implement
Urinary LAM ELISA [20]		80.3	99	Higher sensitivity in HIV co-infected patients
XPERT [21]		80 - 99	98.4	Capable of determining Rif resistance
Latent TB infections				
TST				Sensitive to prior BCG vaccination
IGRAs	QuantiFERON Gold			Not sensitive to prior BCG vaccination
	ELISpot.TB	90	23 - 81	Not sensitive to prior BCG vaccination

Table 1.2: Comparison of sensitivities and specificities of commonly used TB diagnostic tests

1.1.4.1 Tuberculin skin test

The TST, is the diagnostic test still used in many countries today. Tuberculin, or purified protein derivative (PPD), used for this test is a composition of over 200 antigens crudely purified from *M.tb*, *M. bovis*, the BCG vaccine strain and many other common mycobacteria [22]. A small amount of the PPD is injected into the epidermal layer of the skin, this results in an inflammatory response, mediated by the recruitment of antigen specific lymphocytes that is generally exaggerated in patients that have previously been been exposed to any of those antigens [23]. The difference in the inflammatory response between naive and infected patients is crudely determined by the size of the indentured ring that forms at the site of the infection. A positive test result would be a ring of inflammation that has a diameter greater than 10 mm in width. However, the TST does not distinguish well between active or latent TB infections (since both have prior exposure to TB antigens) [24], especially where patients are infected with HIV [25, 26]. Furthermore false positives occur because the purified protein derivative contains many antigens that are present in BCG and non-pathogenic mycobacteria, and false negatives occur in immunocompromised patients, early in primary tuberculosis, and in disseminated tuberculosis.

1.1.4.2 Sputum smear staining

The high lipid content in the waxy *M.tb* cell envelope makes Gram staining very ineffective. The presence of *M.tb* in sputum smears is determined using acid-fast staining, otherwise known as Ziehl-Neelson (ZN) staining. Sputum from infected patients will often identify acid-fast bacilli (AFB+) as red rods once stained. The limit of detection for acid-fast staining in an active TB patient sputum sample is between 5,000 - 10,000 bacilli / mL [27].

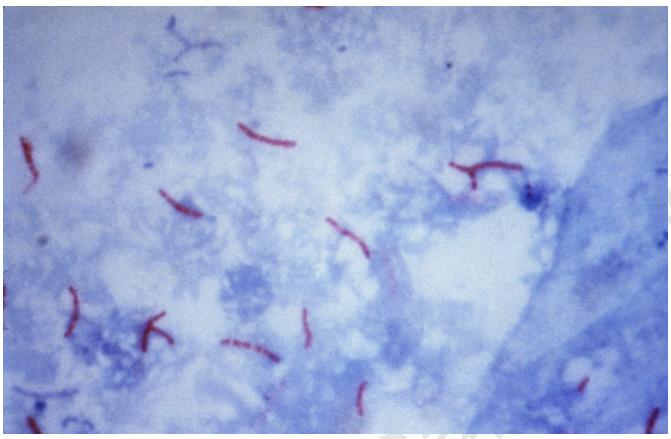

Figure 1.6: Ziehl-Neelson staining of *M.tb*
Acid-fast stained *M.tb* appear red when examined under a normal light microscope. Image obtained courtesy of Dr George Kubica, CDC [28].

Auramine staining with fluorescence microscopy is also routinely used for sputum smear microscopy.

1.1.4.3 *M.tb* culture

Fluids such as blood, serum or sputum can be used in cell culture techniques to detect the presence of *M.tb* bacilli within those fluids. The exact methodology differs depending on the fluid used but the basic concept is similar. The fluids are treated to remove other contaminants before being placed into culture using specific media. After six to 12 weeks of culture *M.tb* bacilli, if present, can be detected using ZN staining or by detecting the release of $^{14}CO_2$ in the case of the rapid radiometric culture system [29]. Newer culture techniques based on on mycobacterial growth in liquid culture (e.g. MGIT) can give quicker results, but can still take up to 7 - 14 days to confirm an *M.tb* infection.

1.1.4.4 Nucleic acid amplification testing

A relatively new diagnostic tool that has been implemented in the TB field is the use of nucleic acid amplification testing (NAAT). This technique uses PCR to amplify regions from *M.tb* specific genes of cultured patient samples. There are a number of possible targets for the PCR probes and as such a number of tests are commercially available. The most robust and automated system is the recently World Health Organisation (WHO) endorsed Gene Xpert Mtb/Rif test [30, 31], which test is capable of detecting Rifampicin resistant TB infections whilst concurrently detecting the presence of *M.tb*.

1.1.4.5 Interferon-γ release assays (IGRAs)

IGRAs make use of *in vitro* re-stimulation of lymphocytes using *M.tb* specific antigens such as early secreted antigenic target 6 KDa protein (ESAT-6) and culture filtrate protein-10 (CFP-10) [32, 33], both of which represent potent T and B-cell antigens that are secreted by *M.tb* [34]. Re-exposure to these antigens causes T cells to produce interferon-γ (IFN-γ) which is then measured using one of the *in vitro* assays: Enzyme-Linked Immunosorbent Assay (ELISA) based QuantiFERON-TB Gold; or the Enzyme-Linked Immunospot Assay (ELISpot) based TSPOT.TB. It should be noted however that these two tests are not inter-changeable as the former is a whole blood assay and the latter is a PBMC based assay, thus as CD4+ T cells decline (for example in patients dually infected with HIV) there may be a biased outcome in terms of a lack of sensitivity of the whole blood based QuantiFERON tests in comparison to the ELISpot.TB assay [35, 36].

1.1.5 Treatment

There are many *M.tb* strain types and disease pathology can vary from strain to strain. Since the 1940s and 50s treatment for an active infection has normally involved a combination of drugs to increase efficacy and to minimise the rate at which resistance to any single drug can be acquired. The most frequently recommended and effective combination for a primary TB infection is isoniazid (INH), rifampicin (Rif), pyrazinamide, and ethambutol for 2 months (termed the "intensive phase"), followed by isoniazid and rifampicin for 4 months (termed the "continuation phase") to theoretically induce complete eradication of all TB bacilli in the body [37]. Using multiple agents concurrently reduces the chances of selecting for a clone that is resistant to all of the drugs simultaneously; this is why using single drugs leads to resistant strains.

Name	Single letter abbreviation	Drug target
Isoniazid	H	InhA
Rifampicin	R	DNA-dependent RNA bacterial polymerase
Pyrazinamide	Z	Accumulation of pyrazinoic acid in bacterium
Ethambutol	E	Arabinosyl transferase

Table 1.3: First line drugs for TB treatment
The table above represents the first line drugs, and their single letter abbreviations, for treatment of active TB as well as the putative targets of these drugs in the *M.tb* organism itself.

A number of factors have combined to cause the emergence and proliferation of multi-drug resistant (MDR) *M.tb* strain types, spread across all *M.tb* lineages, within in the last decade. Primary among these factors has been the failure of many patients to complete their full course (6 months) of treatment and is characterised by many patients stopping treatment once their symptoms subside despite not having effectively cleared the infectious pathogen from their systems leading to acquired resistance over a period of time in the remaining bacilli. To combat this the World Health Organisation (WHO) has implemented the "Directly Observed Treatment, Short course" (DOTS) which is comprised of 5 key areas. These are: 1) government commitment to control TB, 2) diagnosis based on sputum-smear microscopy tests done on patients who actively report TB symptoms, 3) direct observation short-course chemotherapy treatments, 4) a definite supply of drugs, 5) standardized reporting and recording of cases and treatment outcomes.

1.1.5.1 Multi-drug resistant TB (MDR-TB)

MDR-TB strains are defined as resistant to at least INH or Rif [38–40]. Effective treatment of MDR-TB requires prior drug susceptibility testing (DST) in order to determine the appropriate second line drug combinations to use. The incidence of MDR-TB in South Africa has been estimated to be 1.8 % of new cases of TB and 6.7 % of re-treatment TB cases according to the *Global Tuberculosis Control: WHO report 2011* [4], although the incidence has been proven to increase drastically, when patients are co-infected with HIV, with some studies indicating an incidence rate as high as 39% of active TB infections [41].

Drug class	Examples	Drug target
Aminoglycosides	Amikacin	Bacterial 30S ribosomal subunit
	Kanamycin	
Polypeptides	Capreomycin	
	Viomycin	
	Enviomycin / Tuberactinomycin N	
Fluoroquinolones	Ciprofloxacin	DNA gyrase / Topoisomerase iv
	Levofloxacin	
	Moxifloxacin	
Thioamides	Ethionamide	
	Prothionamide	
Macrolide	Clarithromycin	

Table 1.4: Classes of second line drugs for TB treatment
This is not an exhaustive list but represents the main drug classes that are used in the treatment of MDR-TB [42].

A suspected MDR-TB patient will typically start on a course of treatment consisting of a combination of streptomycin, INH, Rif, ethambutol, pyrazinamide, moxifloxacin and cycloserine pending the result of a DST. Once the DST result has been received and the nature of the resistance is known an appropriate combination of five drugs should be used for a treatment course lasting 18 months.

Drug class or name	Example or additional information
Aminoglycoside or polypeptide antibiotic	Amikacin, kanamycin, capreomycin
Pyrazinamide	-
Ethambutol	-
Fluoroquinolone	Moxifloxacin
Rifabution	-
Cycloserine	-
Thiomide	Prothionamide
4-Aminosalicylic acid	Otherwise known as PAS
Macrolide	Clarithromycin
Linezolid	-
High-dose isoniazid	If low level resistance
Interferon γ	-
Thioridazine	-
Ampicillin	-

Table 1.5: List of drugs for MDR-TB treatment
The order in which the five drugs for the treatment of the case specific MDR-TB strains should be chosen is in descending order from top to bottom (based on known DST sensitivities). The isolate should also be confirmed as resistant to both isoniazid and rifampicin [43].

Interestingly most MDR-TB strains in South Africa appear to be derived from the Western Beijing strain [44]. Furthermore, it is thought that Rif mono-resistance in clinical isolates is a driver in the development of MDR-TB. The molecular basis of these observations however remains unknown.

1.1.5.2 Extensively drug resistant TB (XDR-TB)

Extensively drug-resistant tuberculosis is a TB isolate resistant to INH and Rif plus any fluoroquinolone and at least one of the three injectable second-line drugs (e.g. capreomycin, kanamycin, or amikacin) [45, 46]. The incidence of XDR-TB in Kwa-Zulu Natal, South Africa has been shown to be as high as 5 % [41]. Treatment of XDR-TB is similar in nature MDR-TB, allowing for the additional resistance in choice of second line drug cocktails, but it becomes exceptionally costly since the second line drugs are far more expensive. The treatment regime is normally two years long and can often lead to other complications such as hepatitis, depression and hallucinations due to the cytotoxicity of the chemotherapy. For both MDR- and XDR-TB the mortality rate is high despite optimal treatment regimes.

1.1.5.3 Totally drug resistant TB (TDR-TB)

Alarmingly, there is recent evidence to suggest the emergence of TDR-TB strains [47, 48]. Infection with these strains can not be effectively treated or brought under control using any of the current drugs available.

1.1.5.4 Isoniazid preventative therapy

There is an increase in the support for placing HIV+ patients, who do not have active TB, on isoniazid preventive therapy (IPT) due to the high risk of tuberculosis infection that these patients are subject to [49, 50] as well as the evidence that there is a 32 % decrease in the incidence of active TB cases in patients infected with HIV who receive IPT [51]. IPT monotherapy is administered to HIV+ patients for six to nine months, thus reducing the reactivation of latent *M.tb* infections and preventing a LTBI from propagating into an active disease state. There are two important factors to consider with regards to IPT. The first is the incidence of TB for the location in which the patient resides as initiating IPT in a high burden setting is likely to quicken the spread of drug resistance in the long run, but this risk is not as prevalent in low TB incidence settings [52, 53]. The second is that the benefit of IPT is only significant for patients who are TST positive (0.5 mm) and with a risk ratio of 0.38 compared patients who are TST negative and have a risk ratio of 0.89 [51].

1.2 HIV/AIDS

Human Immunodeficiency Virus (HIV) is a Lentivirus (*lenti* meaning "slow" in Latin), from the Retroviridae family [54]. Most lentiviruses have characteristically long periods of incubation in their hosts and normally do not cause immediate fatality of the host. There are two HIV subtypes, namely HIV-1 (the more wide spread and genetically diverse strain) and HIV-2 (largely restricted to West Africa and not nearly as genetically diverse) [55]. The virus itself is roughly spherical and approximately 120 nm in diameter. It contains 2 copies of positive single stranded genomic RNA (ssRNA), that code for 9 genes. These 9 genes encode for the all the proteins (approximately 20 in total depending on the strain type) that HIV is capable of producing [56], a summary of the proteins can be seen in Table 1.6. Retrovirus replication within a host cell is achieved using the virally-encoded enzyme reverse transcriptase.

Name	Size	Function	Localization
Gag			
MA	p17	membrane anchoring; env interaction; nuclear transport of viral core (myristylated protein)	virion
CA	p24	core capsid	virion
NC	p7	nucleocapsid, binds RNA	virion
	p6	binds Vpr	virion
Pol			
Protease (PR)	p15	Gag/Pol cleavage and maturation	virion
Reverse Transcriptase (RT)	p66, p51	reverse transcription, RNAse H activity	virion
RNase H	p15		virion
Integrase (IN)	p31	DNA provirus integration	virion
Env	gp120/gp41	external viral glycoproteins bind to CD4 and secondary receptors	plasma membrane, virion envelope
Tat	p15/p14	viral transcriptional transactivator	primarily in nucleolus/nucleus
Rev	p19	RNA transport, stability and utilization factor (phosphoprotein)	primarily in nucleolus/nucleus shuttling between nucleolus and cytoplasm
Vif	p23	promotes virion maturation and infectivity	cytoplasm (cytosol, membranes), virion
Vpr	p10-15	promotes nuclear localization of preintegration complex, inhibits cell division, arrests infected cells at G2/M	virion nucleus (nuclear membrane?)
Vpu	p16	promotes extracellular release of viral particles; degrades CD4 in the ER; (phosphoprotein only in HIV-1 and SIVcpz)	integral membrane protein
Nef	p27-p25	CD4 and class I downregulation (myristylated protein)	plasma membrane, cytoplasm, (virion?)
Tev	p28	tripartite tat-env-rev protein (also named Tnv)	primarily in nucleolus/nucleus

Table 1.6: List of HIV (poly)proteins, functions and locations

The list of HIV proteins, as well as the polyproteins, including brief description of the protein function and it's cellular location. Figure sourced from the *HIV Sequence Compendium*, 2009 [56].

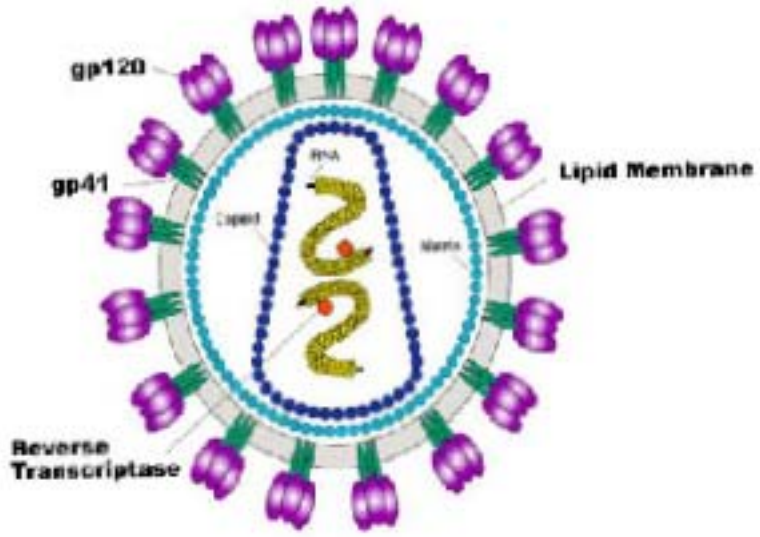

Figure 1.7: Human Immunodeficiency Virus
A simplified diagram of the HIV-1 virion [57].

1.2.1 Background

HIV is the causative agent of acquired immunodeficiency syndrome (AIDS) [58]. The first clinically observed AIDS patients appeared in the early 1980s on the East coast of the United States of America [59–63]. However the first literature to appear linking HIV and AIDS was published concurrently in 1983 by two separate research groups in the same issue of the journal *Science* [64, 65].

1.2.2 Distribution and burden of disease

Currently there are an estimated 33.3 million people globally who are infected with HIV, with sub-Saharan Africa being the worst affected. The estimated prevalence of HIV infections in sub-Saharan Africa is 22.5 million. Despite the global incidence of new HIV infections peaking at 3.2 million per annum in the late 90's there were still an estimated 2.6 million people who acquired a new HIV infection in 2009, with the majority (1.8 million) occurring in sub-Saharan Africa [66].

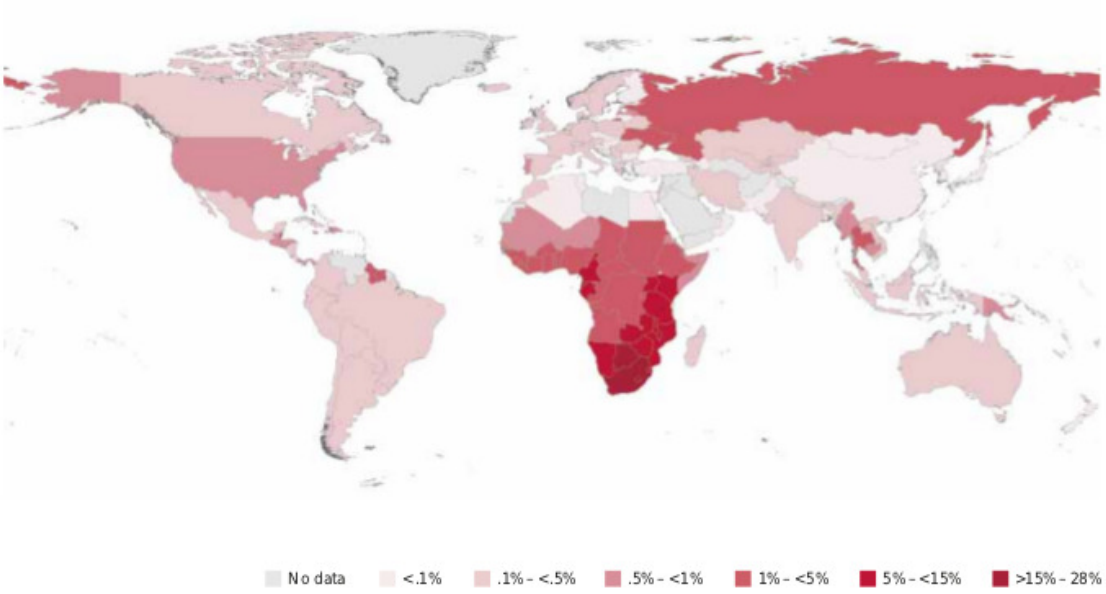

Figure 1.8: Estimated global prevalence of HIV in 2009
Figure 1.8 is the estimated prevalence as a percentage of HIV infected adults, between the ages of 15 and 49, per country in 2009 [66].

The number of HIV related deaths has decreased from it's peak in 2004 of an estimated 2.1 million deaths to the 2009 estimate of 1.8 million deaths (1.3 million in sub-Saharan Africa). This decrease is presumably due to the increase in the availability and distribution of ARVs globally. South Africa has one of the highest burdens of disease, in terms of absolute numbers, as well as one of the highest prevalence rates for HIV in the world, with approximately 10% of the adult population (5.6 million) infected with HIV [66]. In some informal settlements in South Africa, (e.g. Kayalitsha, Cape Town) the HIV prevalence is > 33 %.

1.2.3 Viral life cycle

1.2.3.1 Viral entry

The HI virus infects cells of the immune system, most notably CD4+ T cells, macrophages and dendritic cells. Viral entry into these cells is set in motion when the virion surface glycoprotein, GP120, binds to the cellular host cell receptor CD4. It is thought that this initial binding causes a conformational change in the GP120 protein allowing for binding to additional cellular chemokine receptors - generally either CXCR4 or CCR5. This more stable two pronged attachment allows the N-terminal fusion peptide, GP41, to penetrate the host cellular membrane.

Repeat sequences of GP41, HR1 and HR2 proteins interact, driving formation of a hairpin structure by collapsing the extracellular portion of the GP41 molecule. The resultant loop structure brings the virus and cell membranes together allowing them to fuse easily and the viral capsid to enter the cell [67, 68].

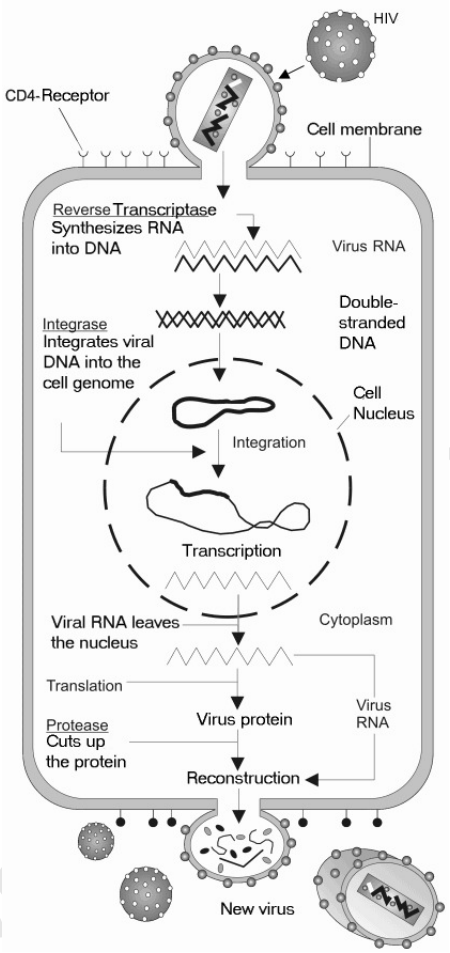

Figure 1.9: HIV life cycle

The simplistic life cycle of HIV from viral entry to reverse transcription, integration, production and budding. Source Wikimedia Commons [69].

Interestingly, a small percentage of the human population have a 32-bp deletion in the gene coding for the CCR5 receptor. Individuals with a homozygous deletion on both alleles for the gene have a fairly stringent resistance to HIV-1 viral entry into CD4 cells [70].

1.2.3.2 Viral Transcription

After gaining entry into the host cell, the positive single stranded genomic RNA is transcribed into a complimentary DNA (cDNA) molecule by virally-packaged reverse transcriptase. The

viral reverse transcriptase has ribonuclease activity (degrading the viral RNA) as well as DNA-dependent DNA polymerase activity. The sense cDNA strand is then copied into an anti-sense strand by the viral reverse transcriptase and the two strands combine to form a viral genomic DNA sequence. This viral DNA sequence is integrated into the host genome by the viral protein integrase [71], as depicted in the simplified graphic in Figure 1.9. The integrated DNA effectively becomes a pro-virus. The integrated viral DNA can lie dormant in the host genome until specific cellular transcription factors are present, most notably NF-κB [72]. The presence of these factors normally corresponds to the activation of the host T-cell response, normally due to an infection; thus cells actively fighting infections become machines for producing the virus they are carrying.

1.2.3.3 Viral Replication

Within an activated host cell, the integrated DNA pro-virus is transcribed into mRNA which is spliced into smaller pieces. The smaller pieces are transported to the cytoplasm where they are translated into the viral proteins Tat and Rev. The Tat protein encourages new virus production and the Rev protein accumulates in the nucleus and binds to viral mRNAs. The Rev-bound mRNAs leave the nucleus unspliced. These full length mRNA sequences produce the Gag and Env viral proteins. The Gag protein binds to the full length RNA (viral genome) and incorporates the complex into new viral particles [73].

1.2.3.4 Virion assembly and budding

New HIV-1 virions are assembled using the cleaved products of the Env polyprotein (GP160). GP160 is cleaved by protease into two units that are processed in the Golgi complex to form the envelope proteins GP41 and GP120. The envelope proteins are then transported to the host cell plasma membrane. The GP41 protein anchors the GP120 protein to the membrane, after which the Gag (p55) and Gag-Pol (P160) polyproteins follow suit, bringing the HIV genomic RNA along with them. The virion that forms begins to bud from the host cell. Maturation of the virion is achieved once HIV proteases cleave all the viral polyproteins into functional HIV proteins and enzymes which then assemble. This cleavage induced assembly can occur either during the formation of the virion bud that is still part of the host cell or once the immature virion has budded off from the cell. Once mature, the virus particles are capable of infecting other cells and perpetuating the life cycle of the virus itself. Figure 1.10 below is a scanning electron micrograph of HIV virions budding off from an infected lymphocyte.

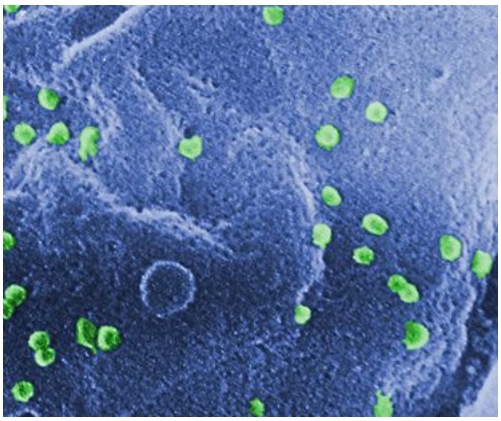

Figure 1.10: Virion budding
A scanning electron micrograph of HIV-1 budding (in green) from cultured lymphocytes. The multiple round bumps on cell surface represent sites of assembly and budding of virions. This image has been adapted from the original black and white picture by adding colour to highlight important features [74].

1.2.4 Transmission and pathogenesis

The HI virus is transmitted via body fluids from an infected person to an uninfected person. Post infection, the newly infected person undergoes a period of rapid viral replication. During this time there is a decline in the number of circulating CD4+ T cells and a concomitant increase in the activation of CD8+ T cells. During the acute phase of infection the circulating CD8+ T cells contain and even suppress the HIV viral load, inducing a rebound in the number of circulating CD4+ T cells [31].

The strong immune response that clears the viral load marks the start of the chronic stage of infection. This stage of the infection can vary greatly in length but is characterised by increased quantities of viral load in the lymph nodes. This could be attributed to the reservoir of virus that becomes prevalent in the follicular dendritic cells, which trap the virus and which reside close to the lymph nodes [75].

Although the population of activated CD4+ T cells is reduced by HIV infection, there remains a relatively high number of IFN-γ secreting CD4+ T cells, resulting in a bias towards one functional population of CD4+ T cells during an infection [76].

1.2.5 Treatment

Currently there are a number of different drugs that can be used to treat HIV positive individuals. Due to the rapid rate that the virus mutates and can acquire resistance, treatment is managed

using combinations of anti-retrovirals (ARVs). The three main classes of ARVs are Non-Nucleoside Reverse Transcriptase Inhibitors (NNRTIs), Nucleoside/Nucleotide Reverse Transcriptase Inhibitors (NRTIs), and Protease Inhibitors (PIs).

NRTIs are analogues of naturally occurring deoxynucleotides required for the formation of DNA strands. This class of drugs causes chain termination when the single stranded viral RNA is converted into dsDNA during the process of reverse transcription. This is achieved by virtue of the fact that DNA synthesis and elongation requires a free 3'-hydroxyl group on the deoxyribose moiety; during DNA strand formation the next incoming nucleotide forms a phosphodiester bond with this hydroxyl group in the 5' – 3' direction and without this 3'-hydroxyl group chain elongation can not occur. NRTIs lack this hydroxyl group and as such prevent further DNA strand synthesis or elongation. NRTIs are classed as competitive inhibitor drugs because they compete with host nucleotides for incorporation into the dsDNA molecules that the virus attempts to synthesize using its reverse transcriptase enzyme.

NNRTIs directly interfere with the viral reverse transcriptase protein itself by binding to the protein and inhibiting the movement of its domains. This class of drugs is classed as non-competitive inhibitors because they do not compete with substrate molecules (dNTPs) during catalysis.

Protease inhibitors (PI) prevent the progression of HIV infection by inhibiting the HIV-1 protease enzyme. This enzyme is responsible for the cleaving of nascent viral proteins for incorporation into new virion particles.

Highly active anti-retroviral therapy (HAART) involves using a combination of three ARVs.

1.2.5.1 Guidelines

HAART is not capable of realistically curing a patient infected with HIV or completely removing all virus particles from an infected host (projections estimate this would take as long as 60 years). The drugs used for treatment are cytotoxic, especially during prolonged exposure, and their side effects cannot be ignored. In light of this there is debate over the CD4 threshold at which a patient should initiate HAART. However patients with a low threshold CD4 count, 200 cells / mm^3 or less (350 cells / $mm^3$for pregnant women or children), should begin HAART immediately. This threshold should ideally be set at 350 cells / mm^3 for all groups to initiate HAART, however it is a massive expense.

In 2009 Dr Gero Hutter and colleagues successfully reduced the quantity of HIV in a previously infected patient to a level below any detectable limit. The patient had developed leukaemia and

was treated for this condition using a bone marrow transplant that had a homozygous deletion of the CCR5 gene [77]. That patient stopped ART after the transplant and has not had to start again since biopsies of tissue throughout his body have not yielded detectable HIV levels and his HIV anti-body titre continues to drop as time progresses. Although this isolated case has presented an interesting opportunity, there are a number of factors preventing it from being implemented universally, e.g. the complexity and high cost of the treatment, the risk of acquiring graft versus host disease, the difficulty in obtaining bone marrow for all HLA types that have the homozygous deletion of the CCR5 are some of the many reasons that this can not be considered a realistic option as a widely applicable cure for HIV infection.

1.2.6 Complications during HIV infection

HIV weakens the immune system by infecting and subsequently depleting CD4 lymphocytes and helper T cells. Thus providing the platform for an opportunistic infection (OI), such as an active TB infection, to manifest. The compromised immune system is incapable of effectively containing inhaled *M.tb* bacilli in granulomas, and infection can lead to rapid progression to disease symptoms [78, 79]. HIV infection can also lead to reactivation of a LTBI. Under normal circumstances, a healthy person has approximately a 10% risk of developing an active TB infection during their lifetime. This risk increases drastically to approximately 7 - 10 % per year for people who are infected with HIV [80, 81], with the risk of TB reactivation rising as the CD4 cell count drops [82–84]. The effective combination of these two converging pandemics has caused TB to become the leading cause of death in HIV infected individuals, with South Africa alone reporting an incidence of 134 deaths per 100 000 population from TB among HIV+ people in 2006 [85]. The synergistic effect of these two pathogens is of greater concern when considering that in South Africa in 2009 the incidence of new TB cases was approximately 1 % [4] of the population and of these more than 50 % were dually infected with HIV [4]. Today, as a result of this dual pandemic, approximately 21 % of all deaths in South Africa are associated with TB disease.

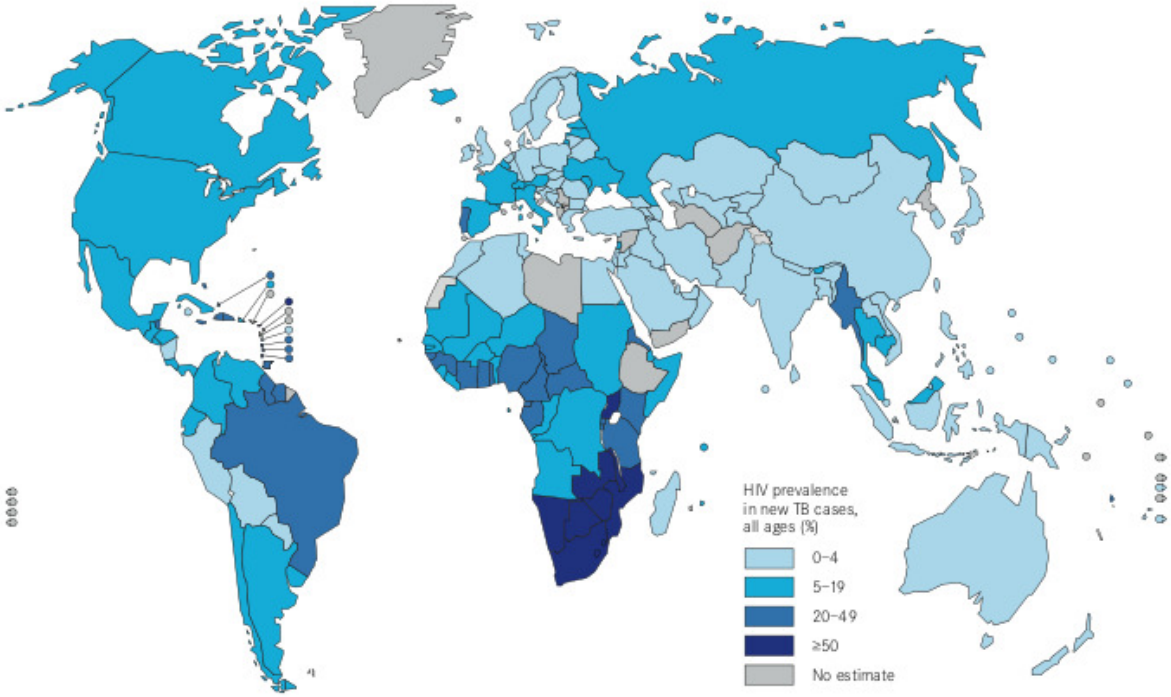

Figure 1.11: Prevalence of HIV in new TB cases
Estimated prevalence of HIV in new TB cases globally. The estimates are based on percentage of prevalence. Image sourced from the WHO [4].

HAART has been shown to play an effective role in preventing the development of active TB in HIV^+ patients, reducing the incidence of TB by up to 90% in patients receiving HAART when compared to those not receiving anti-retroviral drugs [80, 86, 87]. It appears however, that despite viral suppression with HAART, the risk of TB remains higher in HIV-infected persons than in HIV-uninfected persons, suggesting incomplete or a dysregulated immune restoration post HAART treatment [88]. The timing of HAART initiation needs to be considered carefully in terms of the risk factors for each patient, since premature therapy can lead to the onset of TB associated immune reconstitution inflammatory syndrome (IRIS), whilst delayed therapy increases the risk of other AIDS related illnesses occurring.

1.3 Immune reconstitution inflammatory syndrome (IRIS)

1.3.1 Background

IRIS has previously been referred to by numerous other names and acronyms such as immune restoration disease (IRD) [89], immune reconstitution disease, or immune reconstitution syndrome (IRS) [90–93]. It is possible for IRIS to be associated with a number of pathogens, of either a viral (cytomegalovirus, hepatitis B, herpes simplex and herpes zoster), fungal (cryptococcal meningitis and *Pneumocystis jirovecii*) or bacterial (*M.tb*, *M. xenopi*, *M. kansasii*, *M. avium* complex) nature [92, 94, 95]. The central and defining prerequisite for IRIS though, is that patients experience a relative immune defect that is then corrected whilst concurrently being infected with another pathogen. Most often this occurs in patients infected with HIV and who have initiated HAART, resulting in a severe inflammatory response to the infectious pathogen by the recovered, but apparently now dysregulated, immune system. However, by far the most commonly associated IRIS pathogen is *M.tb* and further references to or discussion of the IRIS condition hereafter will be to tuberculosis associated IRIS (TB-IRIS) unless otherwise stated.

Initially TB-IRIS was described as being the onset of a severe inflammatory response or "paradoxical worsening" of clinical symptoms in patients dually infected with TB and HIV, who had recently begun HAART - normally within the previous two weeks to one year. As the incidence of TB-IRIS increased however it became apparent that TB-IRIS had different and distinct forms. In 2006 at a conference in Kampala, Uganda, approximately 100 researchers from various fields around the world, debated and decided upon a standardised set of case definitions for TB-IRIS. These definitions are now used in both resource limited and resource rich settings alike, the aim behind standardising the definitions being to enable further insight into incidence rates, clinical symptoms and risk factors, as well as to make further research in this field more readily comparable [96]. The importance of having simple and practical case definitions for resource limited countries can not be overstated since these countries are generally afflicted with the highest incidences of both HIV and TB and yet in most cases do not have access to the same equipment and technologies to use when identifying cases of TB-IRIS.

Within TB-IRIS there are three case definitions that have been developed for the following clinically relevant and distinct TB-IRIS forms, namely:

1. Paradoxical tuberculosis-associated IRIS (already diagnosed with TB prior to HAART initiation)

2. ART-associated tuberculosis (develop a new TB infection post HAART initiation)

3. Unmasking tuberculosis-associated-IRIS (uncover a TB infection post HAART initiation)

The fundamental difference between "paradoxical TB-IRIS" and the other two forms of TB-IRIS is that they will have already been diagnosed with a TB infection prior to initiation of HAART. Whereas, patients from groups two and three will not have been diagnosed with TB before initiation of HAART but develop TB after the initiation HAART. The differential in the latter two groups, "ART-associated TB" and "unmasked TB-IRIS", is that patients from the former group develop TB from a new infection whereas patients from the latter group develop TB from a latent TB or sub-clinical TB infection.

1.3.2 Incidence and risk

The reported incidence of TB-IRIS has varied greatly, from anywhere below 10 % to above 40 %, across a broad range of locations and cohort sizes [97–107]. A recent meta-analysis was performed on data in the literature to determine the general incidence and mortality of TB-IRIS in relation to the degree of immunodeficiency [108], with the degree of immunodeficiency being determined by CD4 cell count. Based on this meta-analysis TB-IRIS develops globally in 15.7 % of patients dually infected with HIV and TB, with the mortality rate estimated to be 3.2 % [108]. Recent figures show that the prevalence of HIV co-infection in people with TB in South Africa is approximately 70 % [109] and the incidence of paradoxical TB-IRIS has been estimated to be approximately 20 % although different studies have found varied results regarding the precise incidence rate.

Some of the risk factors that have been identified so far for the development of TB-IRIS include: 1) disseminated and extrapulmonary tuberculosis [101, 104, 106]; 2) a shorter delay between the start of tuberculosis treatment and initiation of ART [107]; 3) a more vigorous immunological and virological response to ART [101]; and 4) more advanced HIV disease with lower CD4 cell count [103, 105].

CD4 counts (cells / μL)	Incidence Rates (%) [105]	Incidence Rates (%)[107]
< 50	63	36
>50	34	24

Table 1.7: Table of incidence rates of TB-IRIS stratified by CD4 counts
The table represents the incidence of TB-IRIS for patients within the first 30 days HAART initiation in studies from South Africa [105] and England [107].

In one study by Lawn *et al.* in South Africa, 12% of TB patients developed IRIS. However, the proportion of those who developed TB-IRIS was much higher (32%) among the subset who initiated ART in the first 2 months of TB treatment [105]. In an adjusted analysis, early initiation of ART (in the first month of TB treatment) was associated with a 70-fold higher risk of developing TB-IRIS when compared against patients who had a delayed initiation of ART (after at least 3 months of TB treatment). A separate study from the United States determined a rate of 15 % in a prospective cohort, but there was considerable morbidity and a frequent need for interventions. This study also highlighted the increased risk that is posed for early initiation of ARV treatment post TB treatment, with 69 % (75 / 109) of patients who registered an IRIS event having initiated HAART within 3 months of TB treatment [106].

1.3.3 Treatment challenges

1.3.3.1 HAART initiation

The treatment of both TB and HIV poses a number of challenges, of which perhaps the most important factor is the timing of the initiation of HAART relative to TB treatment. Patients with a low CD4 count and who could potentially undergo a rapid rise in their CD4 count post HAART as their viral load decreases are at an increased risk of developing TB-IRIS. The underlying mechanism associated to this increased risk factor are not entirely clear and may be due to the increased likelihood of disseminated TB as a result of a low CD4 count, or it could be indicative of the extent of an increased immune response related to the immune re-activation [102, 110–112]. However these patients do not have a strong enough immune system to afford an extensive delay in initiation of HAART to allow their TB treatment to clear the burden of TB antigen. Delaying HAART until after they have completed their TB treatment also has risks that must be considered, as the early initiation of HAART for HIV-infected patients has been shown to reduce the risk of AIDS progression as well as maintain a more effective immune system for a longer period [113].

Due to concerns that even brief delays in HAART initiation might lead to substantial increases in mortality in HIV-TB patients [114], a number of clinical trials have been conducted in an attempt to determine the best time point at which to initiate HAART. For example, Karim *et al.* conducted a three branch open label, randomized controlled trial through a large clinic Durban, South Africa. The three branches of this treatment study were: 1) sequential initiation of HAART treatment subsequent to completion of TB treatment; 2) early integration of HAART within four weeks of starting TB treatment; and 3) late integration of HAART four weeks after completing TB treatment [115]. The sequential therapy treatment branch was stopped early

as the integrated treatment branches had a significant, 56 %, combined decline in mortality in comparison, strongly suggesting integrated therapy would be better but this still does not fully answer the question of when is the best time to initiate HAART.

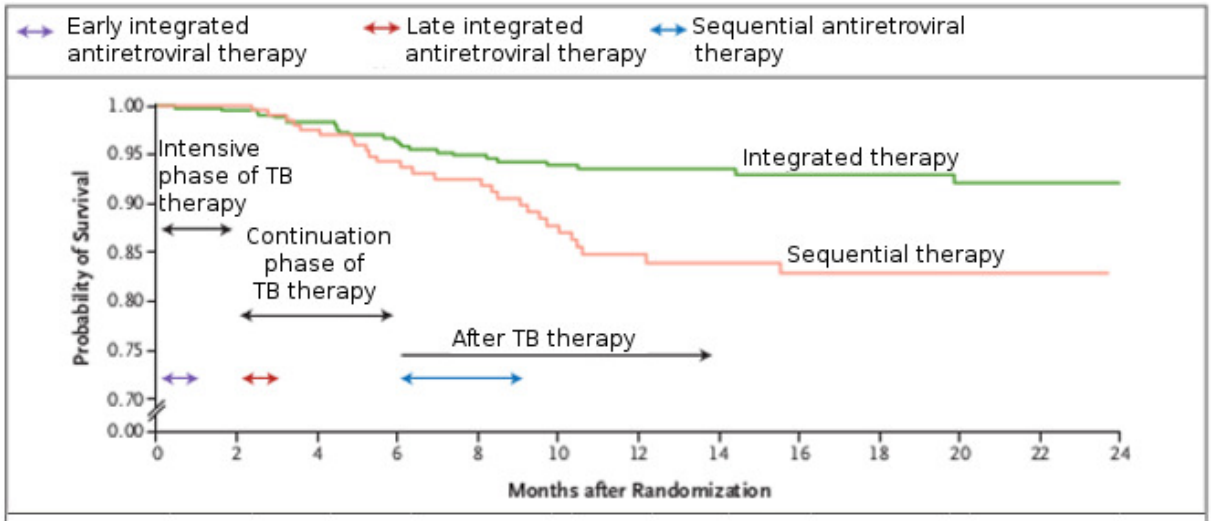

CD4+ Count	Integrated Therapy				Sequential Therapy				Hazard Ratio (95% CI)*	P Value
	No. of Patients	No. of Person-Yr	No. of Deaths	Death Rate/ 100 Person-Yr (95% CI)	No. of Patients	No. of Person-Yr	No. of Deaths	Death Rate/ 100 Person-Yr (95% CI)		
All patients	429	467	25	5.4 (3.5–7.9)	213	223	27	12.1 (8.0–17.7)	0.44 (0.25–0.79)	0.003
≤200 cells/mm³	273	281	23	8.2 (5.2–12.3)	138	137	21	15.3 (9.6–23.5)	0.54 (0.30–0.98)	0.04
>200 cells/mm³	156	186	2	1.1 (0.1–3.9)	75	86	6	7.0 (2.6–15.3)	0.16 (0.03–0.79)	0.02

* Hazard ratios are for the integrated-therapy group, as compared with the sequential-therapy group.

Figure 1.12: Kaplan–Meier survival curves for integrated and sequential HAART therapy
Image obtained from Abdool Karim *et al.* [115].

A separate open label, randomized control study performed in Cambodia by Blanc *et al.* has provided further insight in this regard. This trial involved 2 arms, an early arm where patients initiated HAART two weeks after starting their anti-TB treatment, and a late arm where patients initiated HAART eight weeks after starting their anti-TB treatment. The preliminary report from this trial indicated that mortality in the early arm was a significant 34 % lower than mortality in the late arm [116, 117].

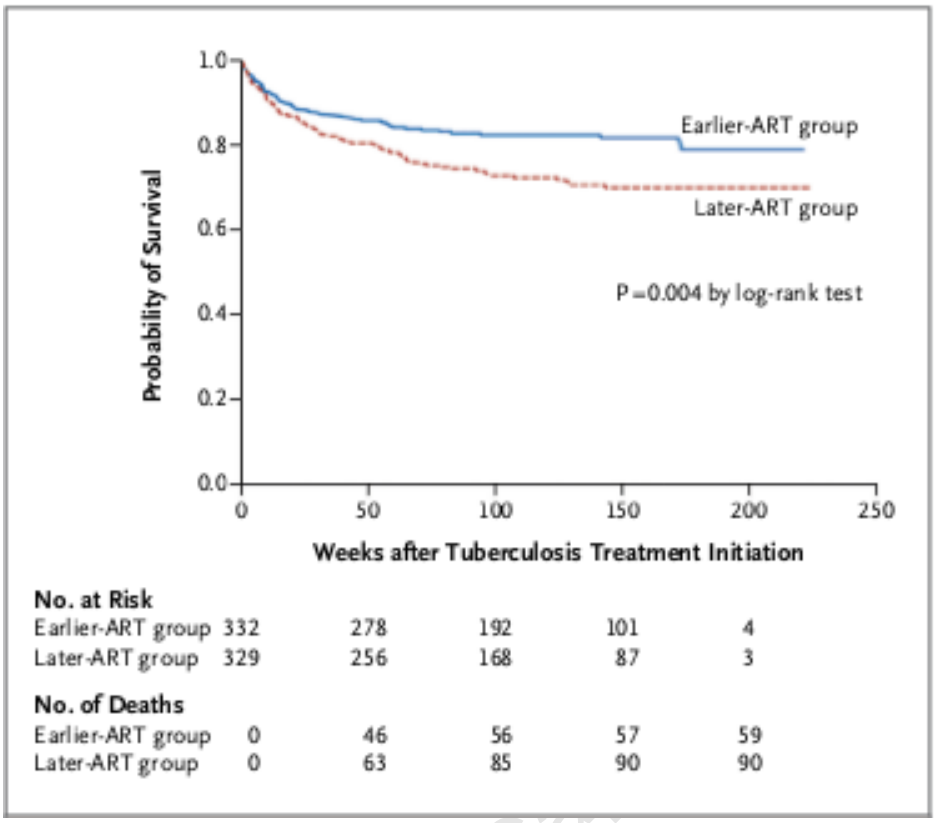

Figure 1.13: Kaplan–Meier survival estimates according to study group
Image obtained from Blanc *et al.* [117].

The findings of these trials as well as a number of other prospective trials suggest that early initiation of HAART would yield the best outcome in terms of mortality for patients co-infected with TB and HIV. WHO guidelines thus currently suggest initiation of HAART within two to eight weeks of starting anti-TB treatment for patients with a CD4 count of less than 200 cells / mm^3 [118], thereby effectively committing *circa* 20 % of HIV-TB patients on average to develop TB-IRIS and requiring concomitant management of those TB-IRIS patients.

1.3.3.2 Corticosteroid treatment

Prednisone - a broad spectrum immune suppressant - has been administered to TB-IRIS patients in an attempt to reduce the often severe inflammatory response that such patients produce if they initiate HAART too early. After anecdotal results appeared to favour this treatment regime it was decided to test this in a proper trial setting. The recent double blinded, randomized, placebo control study was performed by Meintjes *et al.* to test the effectiveness of prednisone therapy for paradoxical TB-IRIS patients [119]. The outcomes demonstrated that despite infection

occurring more often in the prednisone arm than the placebo arm for the trail, there was no difference in the incidence of severe infections. However, treatment with prednisone was found to "reduce the need for hospitalization and therapeutic procedures and hastened improvements in symptoms, performance, and quality of life" [119]. An important point to take note of is that prednisone helps to suppress the symptoms of IRIS but it does not treat the underlying cause. The most important factor to consider when treating paradoxical TB-IRIS in this manner, is that infection with drug resistant TB must be ruled out as well as any other causes of deterioration in the patient's health before administering corticosteroids [119].

Primary outcomes	Placebo Arm (n = 55)	Prednisone Arm (n = 55)	*P* value
Karnofsky performance score (wk 2, n = 92)	70 [50 - 90]	90 [80 -90]	<0.01
Karnofsky performance score (wk 4, n = 86)	80 [60 - 90]	90 [80 - 100]	<0.01
MOS-HIV Health Survey (wk 2, n = 98)	44.5 [36.7–52.4]	51.5 [44.5–54.5]	0.01
MOS-HIV Health Survey (wk 4, n = 94)	48.3 [39.7–55]	51.2 [46.6–56.8]	0.04
Infections while on study medication	17 [31%]	27 [49%]	0.05
Median hospital days	3 [0 - 9]	0 [0 - 3]	0.04
Severe infections	2	4	0.4

Table 1.8: Primary outcomes of prednisone vs placebo treatment
Values shown are medians (interquartile range) or numbers (%). ART, antiretroviral therapy; MOS, Medical Outcomes Study. Adapted from Meintjes *et al* [120].

1.3.4 Potential mechanisms of disease progression

The underlying mechanism of action in TB-IRIS disease progression is poorly understood. There are a number of theories that have been put forward on the possible mechanism behind disease aetiology and natural history but these are complicated by the fact that symptoms of TB-IRIS do not develop at a consistent period of time post HAART initiation. Instead, symptoms may develop anywhere from within the first week or two post HAART initiation up to a year after commencing HAART, indicating that there could be a number of mechanisms involved in its development, including *inter alia*:

Innate response. Research on the immunopathological mechanism has revealed that the innate immune response, driven by macrophages in particular, could be involved in TB-IRIS [121],

but no clear mechanism has yet been elucidated in this regard;

Adaptive T-cell mediated immunity. TB-IRIS has also been shown to be associated with a heightened Th1 response [122, 123], resulting in an increase in the number of circulating IFN-γ producing T cells and the restoration of delayed type hypersensitivity (DTH) responses to mycobacterial antigens [124, 125]. The regulation of the Th1 response is maintained by circulating T_{reg} cells and whilst the numbers of circulating T_{reg} cells for both TB-IRIS and HIV/TB co-infected patients who are on HAART and who do not develop TB-IRIS (otherwise referred to as "TBART" patients) are similar, the strength of the response is unbalanced in the case of TB-IRIS patients, perhaps suggesting that T_{reg} function as opposed to the absolute number of T_{reg} cells may underpin the dysregulation. HAART has been shown to restore the host granulomatous response to mycobacteria in HIV infected individuals [126–129], but the rapid rate at which this occurs and perhaps a lack of compensating immunoregulatory mechanisms may lead to the uncontrolled tissue-damaging responses that is a defining characteristic of TB-IRIS [92].

Another suggested mechanism could lie in a dysregulation of the Type 17 helper T cell (Th17) response: tissue suppuration of lymph nodes or other affected organs may occur in some TB-IRIS patients and, although the underlying immunopathology remains unclear, it may be indicative of a Th17 mediated immune response. Whilst both Th1 and Th17 responses tend to induce inflammation, the Th17 response is mediated by neutrophils [130, 131] and the Th1 response is mediated by macrophages;

Host genetic factors. It is also conceivable that host genetics may play a role in the underlying mechanism of the development of TB-IRIS, with individual patients having a genetic predisposition to the development of TB-IRIS [90, 132]. It is plausible for example that polymorphisms in cytokine genes may influence the rate of clearance of opportunistic pathogens or, alternately may cause dysregulation of the inflammatory response. The association of such polymorphisms with the development of TB-IRIS has been described for a number of associated organisms [132], but if there is a connection to an underlying mechanism it still needs to be elucidated. the association between certain polymorphisms in various cytokines and the development of IRIS is summarised in Figure 1.14.

	HIV-negative controls	HIV-positive controls without IRD	HIV patients who experienced herpes virus disease after HAART	HIV/HCV patients who experienced hepatotoxicity after HAART	HIV patients who experienced mycobacterial disease after ART
n	60	33	18	11	8
IL1A-889*2	45%	40%	53%	63%	75%
IL13+3953*2	47%	36%	53%	36%	50%
n	100–154	33	25	13	11
IL6-174*C	66%	64%	71%	61%	36%[c]
TNFA-308*2	34%	24%	52%[b]	23%	0%[b,c]
IL12-3'UTR*2	31%[a]	42%	8%[b,c]	54%	50%
IL12-promote-*2	83%[a]	85%	86%	54%[b,c]	62%

Figure 1.14: IRIS is associated with polymorphisms in the TNF-α, IL12B and IL6 genes
Results are presented as the percentage of individuals carrying the alleles shown. A| n = 100 HIV-negative controls. B| Significantly different from patients with no IRD (Fisher's exact test, P, 0.05). C| Significantly different from HIV- negative controls (Fishers exact test, P, 0.05) [132].

1.4 Aims of thesis

Immune responses to *M.tb* differ *in vivo* between TB-IRIS and control patients (dually infected with HIV and TB but do not develop IRIS symptoms, herewith referred to as TBART patients). This thesis describes proteomic research aimed at determining the molecular basis of these differences using an *in vitro* model of TB-IRIS, based on the use of cultured peripheral blood mononuclear cells (PBMCs) isolated from TB-IRIS and TBART patients, the goals being to:

1. Identify a potential protein biomarker for the IRIS condition

2. Provide the basis for a better understanding of the molecular origin of TB-IRIS

3. Serve as the basis for development of more targeted suppression of TB-IRIS.

As discussed earlier in this Chapter, it is possible that the mechanism that causes TB-IRIS could be due to a combination of innate immunity, adaptive T-cell mediated immunity and host genetic factors [133]. Consequently, the choice of sample with which to perform this study is important. Notably, the sites of TB infection in patients dually infected with TB and HIV are often extra-pulmonary and as such it is likely that the circulating lymphocytes will have been exposed to a number of TB specific antigens. Obtaining ethical clearance for tissue biopsies of sites of infection is extremely difficult and provides it's own unique difficulties when the issue of control samples is raised. Thus, the choice of using PBMCs which represent a well defined system that has fewer variables when compared with other easily obtainable samples (such as plasma) is an attractive one. Some may argue that sorting PBMCs into sub-populations would be a better approach in attempting to identify the differing immune

responses however it would be worthwhile to first establish what the differences for these two groups are utilising PBMCs before undertaking the vastly more technical and exhaustive approach of analysing where exactly these differences in signalling are generated. To date, analysis of the mechanism of TB-IRIS has been of a strictly immunological nature and it remains possible that further studies involving more diverse techniques could offer greater insight. Transcriptomic analysis may reveal differential patterns in mRNA expression pertaining to a number of interesting mechanisms however it has been well established that the correlation between mRNA levels and protein levels in a system is poor. Likewise, an epigenetic analysis would highlight those patients with different risk thresholds for developing TB-IRIS but would not ultimately result in a point of care diagnostic test. A more complete description of the differences between TB-IRIS and TBART patients at the protein level would extend our understanding beyond just the usual cytokines that have been previously studied to a more complete underlying set of proteins that are expressed. This would require using techniques that lie in the field of proteomics.

Proteomics is the large-scale study of proteins in a biological system during specific biological events [134]. Proteomic methodologies have been used to study a number of biological systems ranging in complexity from simple prokaryotes to complex organisms such as *Homo sapiens*. Discovery of disease-associated biomarkers or mechanisms of drug action are problems that can, in principle, be solved by modern mass-spectrometry-based proteomics since it is now possible to measure changes in expression levels of thousands of discrete proteins in a given biological system in response to, for example, bacterial challenge or drug perturbation. When considering the properties of what constitutes a good candidate biomarker the following three fundamental properties should be kept in mind: 1) it should be present in an easily accessible source material (e.g. blood, saliva, urine etc.), 2) it should be easy to detect and quantify in a robust and affordable manner, 3) it should be specifically associated with a disease state or tissue damage in a quantifiable manner [135].

2 Proteomics Review

2.1 Introduction

Proteomics has often been considered to be complementary to genomics or transcriptomics. However, proteomics research immediately encounters far greater difficulties that arise due to the fact that the complement of proteins expressed in any given sample has a far higher complexity and dynamic range and, moreover, different proteins typically do not share common physical or chemical properties or functions [136]. The sheer scale of protein variability can be estimated when considering that the human genome consisting of approximately 20 000 genes could produce up to 100 0000 proteins through differential splicing. Additionally, many proteins undergo dynamic post-translational modification (PTM) which further adds to the complexity of the target proteome, potentially producing millions of different proteins [137, 138]. Compounding this sheer complexity, protein quantities expressed in biological systems have been shown to have up to 12 orders of magnitude in difference of expression levels within a single biological sample [139].

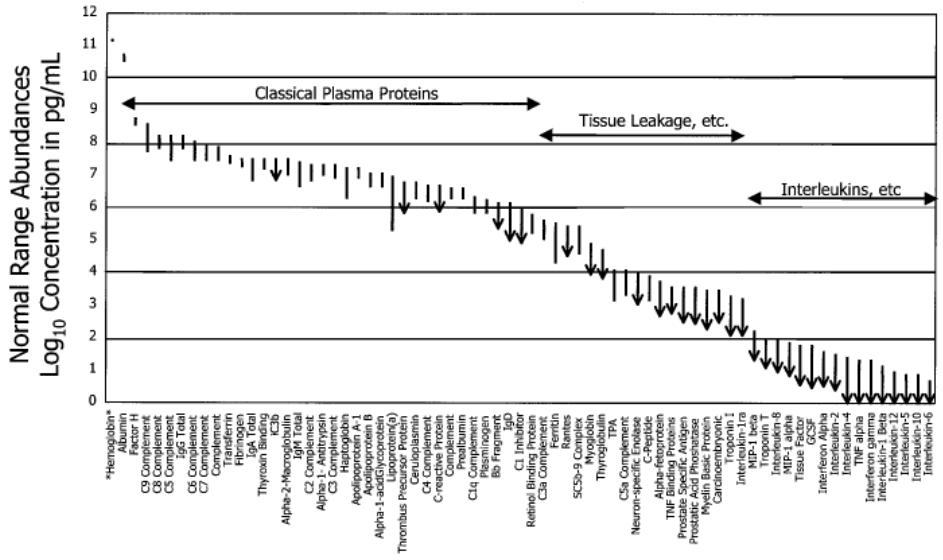

Figure 2.1: Plasma protein dynamic range

Abundance for 70 protein analytes in plasma is plotted on a log scale spanning 12 orders of magnitude. The classical plasma proteins are clustered to the left (high abundance), the tissue leakage markers (e.g. enzymes and troponins) are clustered in the center, and cytokines are clustered to the right (low abundance). Hemoglobin is included (far left) for comparison. Sourced from Anderson *et al.* 2002 [139]

Classically, the main techniques used for protein identification, such as western blotting or Edman degradation, were based on the isolation and characterisation of single proteins. The advent of Laemmli gels and, later, of 2D PAGE allowed for a broader, though still relatively crude, analysis of protein profiles to occur. However, the inherent low resolving power of 2D gels, coupled with the limiting sensitivity and poor gel-to-gel reproducibility has meant that 2D PAGE based technologies (including 2D DIGE) have increasingly been overtaken in recent years by direct liquid chromatography-mass spectrometry based approaches to high throughput protein identification and quantification. Thus, as technology has improved in general, and mass spectrometry (MS) instrumentation in particular, the study of proteins has gone from the study of an isolated protein or pathway to that of a global proteome within a biological system. MS has thus had a massive impact on making the field of proteomics a dynamic and rapidly evolving field of science.

2.2 Basics

A successful proteomics experiment requires an understanding of a number of intricacies, from the wet work bench leading all the way through to the *in silico* analysis. At each point along

the experimental pipeline there are a number of considerations and choices to be made and identifying the best approach, technique or piece of equipment to use often comes from an understanding of the strengths and weaknesses of each of these choices and how they relate to the fundamental experimental question that is being investigated.

2.2.1 Theory

The basic workflow that underpins any proteomic experiment can be broadly identified as follows: the generation or isolation of sample in a preparation step; the analysis of the sample using an appropriate mass spectrometer; and finally the output from the mass spectrometer is used in combination with search algorithms and databases to identify particular proteins.

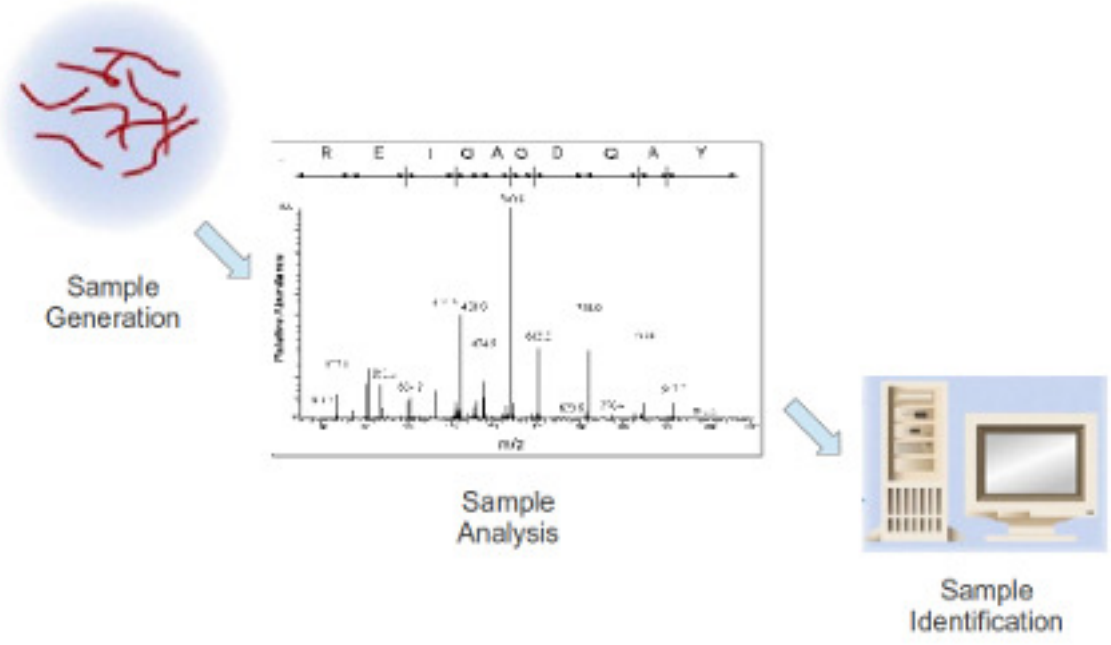

Figure 2.2: Basic proteomic workflow

Sample preparation is a broad topic of discussion and would be better served through specific analysis of the literature for protocols that have already been successfully identified for the sample concerned, a broad review of this topic will therefore not be given here. In order to perform mass spectrometric analysis of a sample, the sample must be ionised before being subjected to analysis within the mass spectrometer. Finally, mass spectra that are produced are then used to identify the compounds (either whole proteins, peptides, proteolytic peptides or fragmentation ions) in combination with search algorithms and databases.

2.2.2 Hardware

Mass spectrometers have 3 basic components, namely: an ionisation source, a mass analyser and a ion detector. There are several types of mass analyser that are currently in use today, each with specific strengths and weaknesses. There are two main types of ionisation source that are regularly used in proteomics to ionise the analytes.

2.2.2.1 Ion sources

Proteins and peptides have varying degrees of polarity, are non-volatile and are thermally unstable molecules that require an ionisation technique that transfers them into the gas phase (without extensive degradation) for further analysis using a mass analyser. There are two sources of ionisation for molecules that are to be analysed by mass spectrometry. The first is based on the sample being in a solid form and is known as matrix-assisted laser desorption/ ionisation (MALDI) ionisation [140–144]. Briefly, the MALDI matrix absorbs laser energy and transfers it to the acidified analyte that it encapsulates, the rapid laser heating causes desorption of the matrix and $[M+H]^+$ ions of analyte into the gas phase. The second ionisation technique that is regularly used is electrospray ionisation (ESI) [145]. ESI produces ions from a solution and the process is driven by high voltage (normally between 2 – 6 kilo volts) that is applied across the emitter at the end of the separation pipeline of the liquid chromatography (LC) instrument and the inlet of the mass spectrometer. This produces an electrically charged spray, known as a Taylor cone [146], that is followed by formation and desolvation of analyte-solvent droplets into a gas phase. Both sources produce ions that are then accelerated through an electric field before entering into the mass analyser. Interestingly, both Koichi Tanaka (MALDI ionisation of biological macromolecules) and John Fenn (ESI ionisation of biological macromolecules) received the Nobel Prize for Chemistry in 2002 - demonstrating the massive impact these technologies have had in the field of mass spectrometry.

2.2.2.2 Mass analysers

Mass analysers are the heart of any mass spectrometer and separate molecular ions based on their mass-to-charge (*m/z*) ratios. In addition, some analysers are capable of storing ions for short periods based on their *m/z* ratios. Analysers make use of either electrical or magnetic fields, or a combination of both, to move and select the ions from the source to the detector. As the motion and separation of ions is based on electrical and/or magnetic fields, the *m/z* ratio, and not only the mass, is of importance. The analyser is operated under high vacuum, preventing

ions from colliding with neutral gas atoms whilst travelling through the analyser, thus providing a clean environment and allowing the ions to reach the detector with a sufficient yield [147]. Mass spectrometers tend to be named based on the mass analyser they contain and there are a number of different models that are commonly used in the proteomic field. Ion trap (IT) and Orbitrap mass analysers separate ions based on their *m/z* radio frequency, quadrupoles (Q) use *m/z* stability, and time-of-flight (ToF) analysers use flight time through an evacuated tube [147]. Each mass analyser has unique properties, such as mass resolution, scanning speed, mass accuracy, sensitivity, and dynamic range.

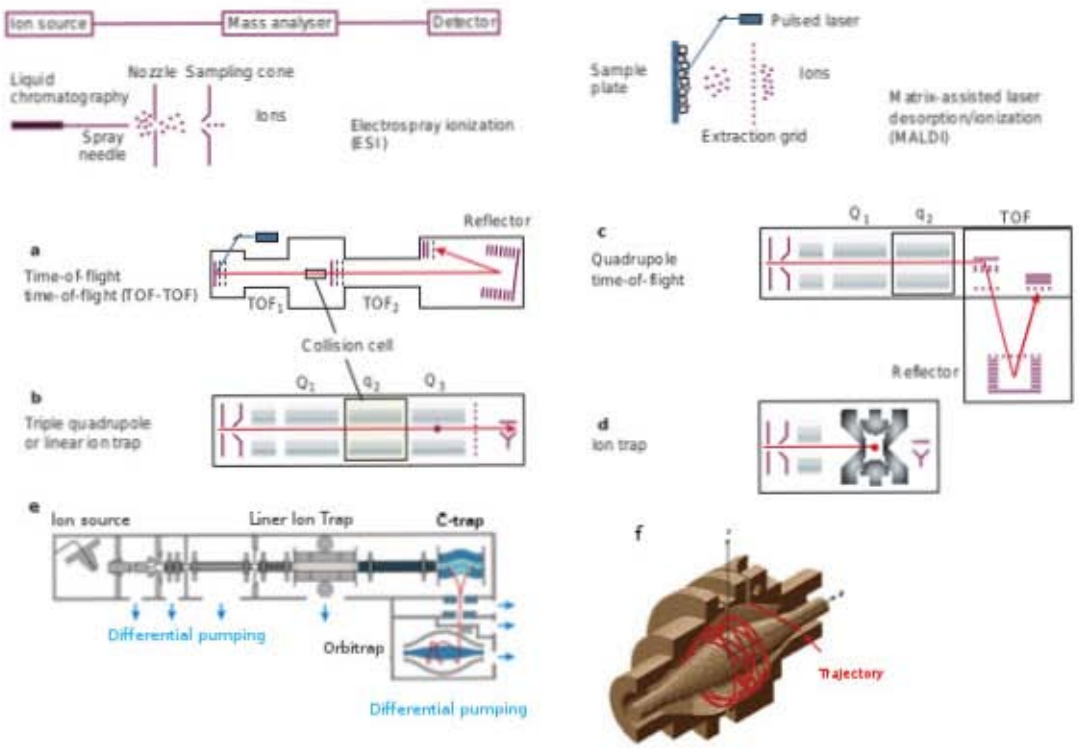

Figure 2.3: Popular mass analysers

The top most images depict two of the most common ion sources, ESI (top left) and MALDI (top right). Below that from A to F are schematics some of the more popularly distributed mass analysers and describes the movement of ionised molecules through them. A = a ToF-ToF instrument with a collision cell incorporated between the two ToF sections. Ions of a specific mass-to-charge (*m/z*) ratio are selected in the first ToF section and fragmented in the collision cell, after which the masses of the fragments are separated in the second ToF section. B = a quadrupole mass spectrometer, these machines select ions in the first quadrupole (Q1) by varying electric fields as a function of time between four parallel rods, allowing a stable trajectory for ions of a desired *m/z* ratio. These ions are then fragmented in a collision cell (q2) and the fragments are separated again in Q3. C = a Q-ToF mass analyser that has a quadrupole coupled to a ToF. The quadrupole allows highly sensitive selection of ions before they are fragmented in a collision cell and their fragment products are analysed by the ToF. D = a three-dimensional ion trap which captures ions using resonance of electric field frequencies (similar to how the Q3 functions in a triple quadrupole) which are subsequently scanned out creating tandem mass spectra. E = the orbitrap has two traps, of which the linear ion trap performs an initial scan of the *m/z* ratio of the ions before they undergo collision and their fragments are collected by the C-trap and then analysed by the orbitrap mass analyser (F) which identifies ions based on their cyclical trajectory in an electric field that is applied between two electrodes. Adapted from [148–150].

Depending on the combination of the different components used, a mass spectrometer can have a broad dynamic range, or high sensitivity, a high resolving power (resolution) or any of a number of other attributes. A basic comparison of some common mass spectrometers can be seen in Table 2.1. It is technically difficult to build a mass spectrometer that has all these attributes as the complexity of the physics that would be involved is prohibitive.

Analyser	Resolving power	Mass Accuracy	Sensitivity	Dynamic Range
ToF-ToF	20 000	5 - 10 ppm	Attomole	10^4
Q-ToF	60 000	5 - 10 ppm	Attomole	10^6
Orbitrap	150 000	2 - 5 ppm	Femtomole	10^4

Table 2.1: Comparison of characteristics of common mass spectrometers
Relative comparison of the resolution, mass accuracy, sensitivity, and dynamic range of the most popular instrument used in proteomic studies[147, 150].

The best mass spectrometers for specific applications will be discussed later in this review in connection to the experimental functions they are to perform.

2.2.2.3 Detectors

The most ubiquitous part of any mass spectrometer is the detector which, generally speaking, does not differ greatly between the various mass spectrometers currently on the market. The majority of mass spectrometers use an analogue ion detector, but there are a few exceptions that use a digital ion detector.

2.2.3 Software and algorithms

In proteomic experiments, a significant number of protein matches are incorrect due to a high rate of false positives. One reason for this is that a peptide mass does not uniquely define its sequence and a peptide sequence may not uniquely define a protein. Results from search engines should therefore be interpreted carefully in order to understand strengths and weaknesses of different search algorithms not least because the scoring functions of these engines are based on a number different algorithms.

Identifying proteins from a collection of tandem mass spectra involves assigning spectra to peptides, using either a *de novo* or database search strategy, and then inferring the protein set from the resulting collection of peptide-spectrum matches (PSMs). The peptide sequences in the database are generated by an *in silico* digest of the appropriate protein sample set according to the known cleavage pattern for the protease that was used for the *in vitro* digest. The normal experimental goal is to identify as many distinct proteins as possible at a specified false discovery rate (FDR). The majority of shotgun proteomic experiments to date have been analysed with a focus on controlling error rates at the peptide or level, rather than at the protein-level [151–157].

Most companies provide proprietary software for the analysis of mass spectra and identification of proteins from the data that the machine generates. Some of the more popular software suites include Protein Pilot (ABSciex), Spectrum Mill and MassHunter (Agilent), MASCOT (Matrix Science) and SEQUEST amongst many others. There have also been a significant number of open source software packages that have been developed for proteomic applications, most prominent amongst these being the Trans-Proteomic Pipeline (TPP).

2.2.3.1 Spectral matching

The spectral matching approach is based on algorithms that correlate experimental MS/MS spectra with theoretical spectra and count the number of peaks common to two spectra ("shared peak count"). Common search algorithms include SEQUEST, Spectrum Mill or X!Tandem [158]. Crux is an open source program that re-implements and extends the database search algorithm SEQUEST. However, Crux is quicker and returns a higher number of correct identifications than SEQUEST by using a peptide indexing scheme to rapidly retrieve candidate peptides for a given spectrum and then generating shuffled decoy peptides "on the fly" for each peptide in the target database. This approach ensures that each decoy peptide exhibits precisely the same amino acid composition and total mass as the corresponding target peptide [159]. Consequently, this provides a good null model and an accurate means of estimating the FDR [159]. The FDR is a measure of the percentage of PSMs that have been incorrectly accepted as true.

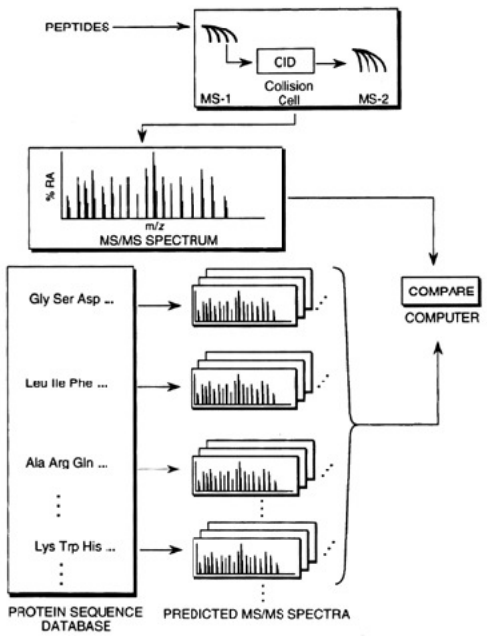

Figure 2.4: Spectral matching

2.2.3.2 Probability matching

Another approach is the use of a probabilistic algorithm that provides information about the probability that a particular peptide sequence produced the spectrum being analysed by chance. Popular probability based search algorithm engines are MASCOT, Andromeda and Peptide Prophet. The MASCOT algorithm itself is based on the probability that a match is a random event and is essentially evaluated using a MOWSE score. By adding the size of the database, an objective score is created, demonstrating the significance of a given hit [158].

2.2.3.3 Database filtering using sequence tags

A third approach makes use of sequence tags and database filtering. One algorithm that performs this function is InsPecT [160], which uses peptide sequence tags as efficient filters to reduce the size of the database by a few orders of magnitude while retaining the correct peptide with very high probability. In addition to filtering, InsPecT also uses novel algorithms for scoring and validating in the presence of modifications.

2.3 Databases

There are a number of protein sequence databases that are currently available to the scientific community. However, the vast majority of proteomics experiments make use of either the UniProt Knowledge Base (UnitProtKB) or the International Protein Index (IPI) databases - although the latter is quickly becoming obsolete due to the decision to stop updating IPI from late 2010. Both databases have extensive repositories of protein sequences although they do have subtle differences, the main difference being the level of annotation and curation for the UniProtKB database whereas the IPI database is essentially a meta-database formed from a number of other databases.

2.3.1 UniProtKB

The UniProtKB (`http://www.uniprot.org`) actually consists of 3 databases, namely the SwissProt, TrEMBL and PIR databases. The SwissProt database in particular is highly curated and has a high degree of annotation, containing data on protein sequences and associated experimental, biological or biomedical information. Within UniProtKB, there are a number of

species-dependent databases and within these there are subsets of the databases that allow for variables such as redundancy in the form of splice variants or isoforms as well as non-redundant database where one gene equals one protein: these 2 different databases are referred to as the *Homo sapiens* Reference Global Proteome and SwissProt Organism 9606 databases respectively. The Organism 9606 database contains protein sequences for only human proteins and excludes human like proteins that occur in other organisms, this database has approximately 20 000 proteins. The Reference Global Proteome database also contains only human proteins but allows for splice variants as well. This database contains approximately 100 000 proteins.

2.3.2 International Protein Index (IPI)

The IPI database (`http://www.ebi.ac.uk/IPI`) is a meta-database composed of a combination of other databases (including UniProtKB, Ensembl, RefSeq, HinvDB, and VEGA). IPI uses a complex algorithm to minimize sequence overlap while maintaining comprehensive proteome coverage for a given organism [161]. This database allows for splice variants as well, but curation of the database was recently terminated, thus new protein sequences will not be updated. This database contains close to 100 000 proteins.

2.4 Shotgun Proteomics

There are a number of strategies that can be employed to analyse proteins using mass spectrometry. The choice of which strategy to use is best informed by the biological question that is being investigated. Figure 2.5 provides a basic graphical overview of the different approaches that are currently employed in proteomics.

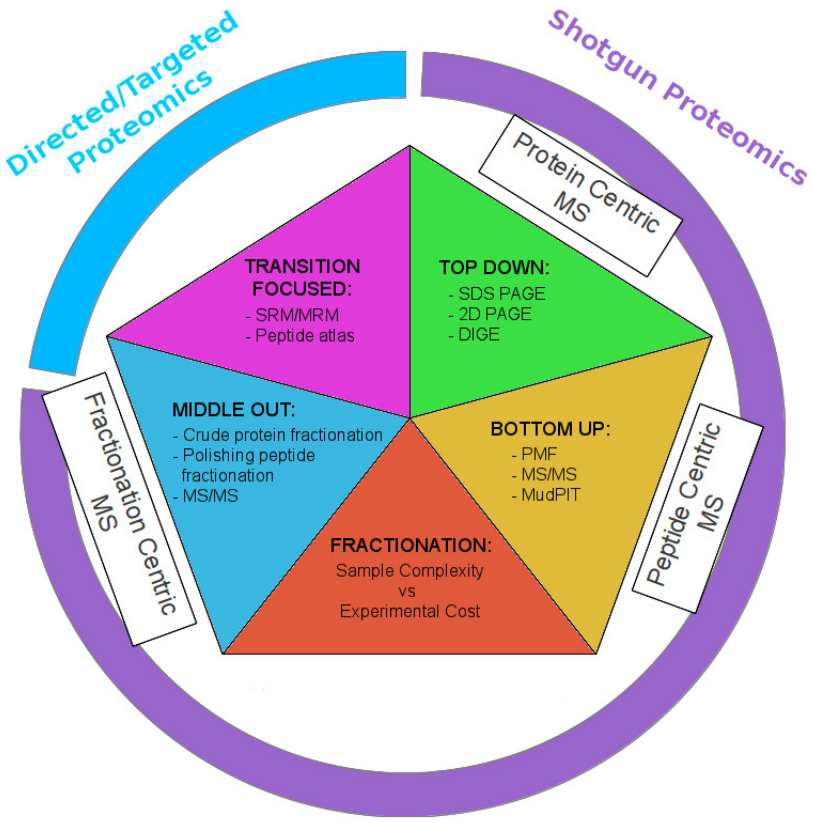

Figure 2.5: Overview of proteomic approaches

Each proteomics approach has an inherent advantage or potential disadvantage that should be considered prior to deciding which approach to use. Figure 2.6 describes a basic outline of top down and bottom up approaches as well as highlighting the strengths associated with each approach.

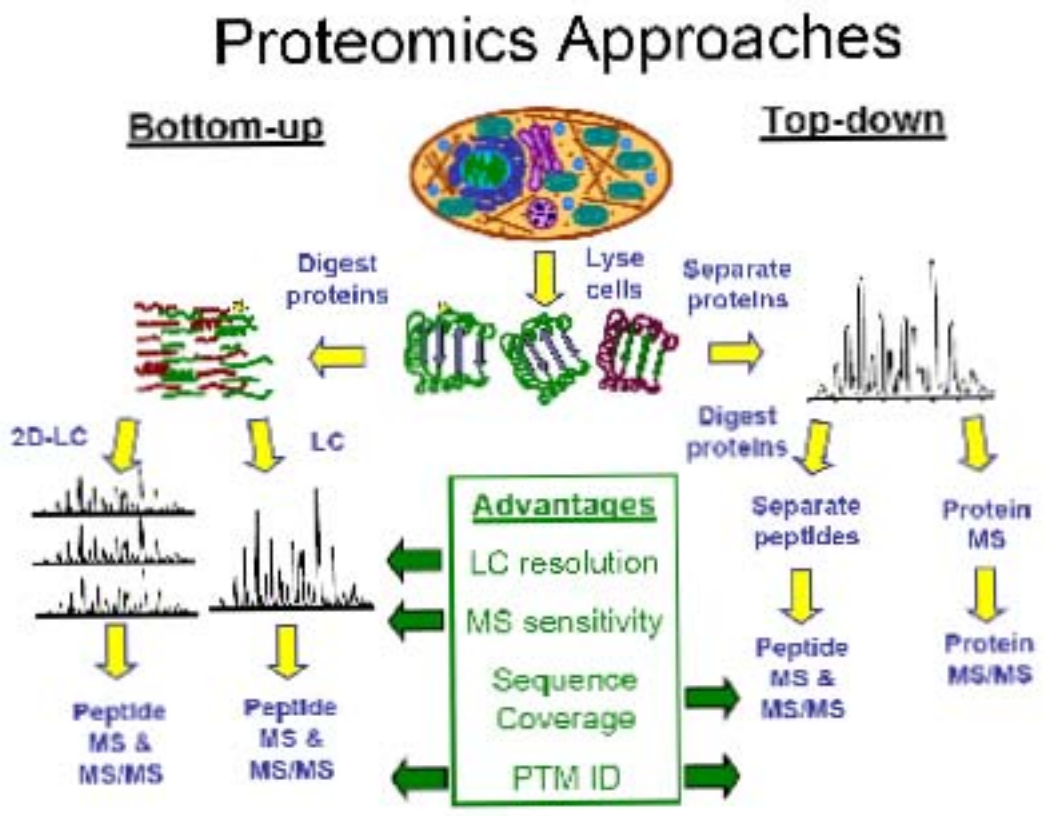

Figure 2.6: Comparison of proteomic approaches
The fundamental differences in top-down (right hand side) and bottom up (left hand side) proteomic approaches. LC = liquid chromatography, 2D = two-dimensional, PTM ID = Identification of post-translational modifications.

2.4.1 Protein-centric approaches (gel based)

The protein centric approaches are all based on identifying proteins from a sample using enzymatic digestion of the proteins and subsequent analysis of their proteolytic fragments and are often referred to as being a top-down approach. This technique was first published in the early 90's [162, 163], however the term used to describe the method, peptide mass fingerprinting (PMF), was first coined in 1993 [164].

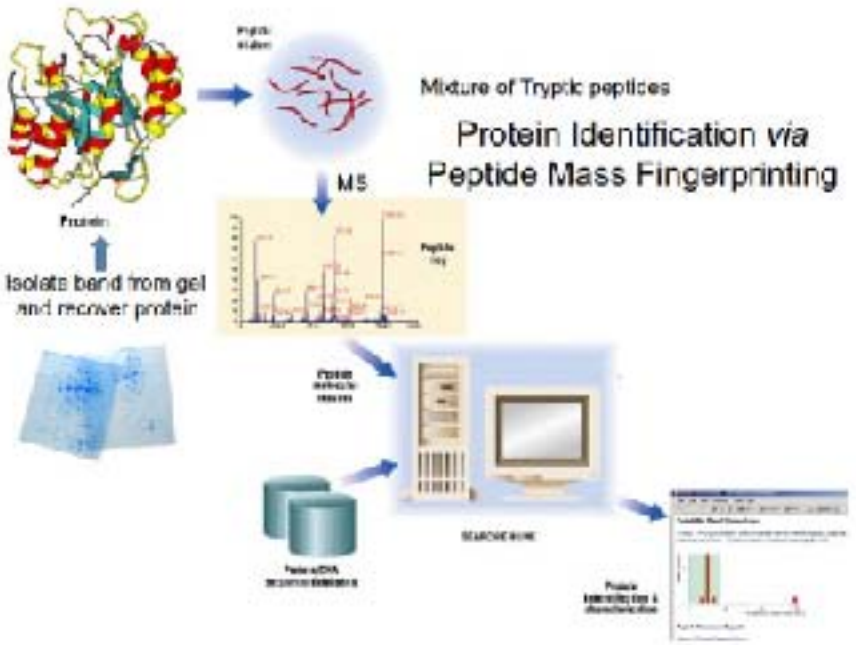

Figure 2.7: Peptide mass fingerprinting (PMF)

The most commonly used enzyme is trypsin however other there are a number of other enzymes that can be used such as chymotrypsin or endonuclease-Lys C. Trypsin is a well characterised protease that cleaves proteins on the C-terminus side of lysine and arginine residues, provided they are not followed by a proline, thus generating peptides that have a free N-terminal amine. This predictable cleavage pattern is integrated into subsequent data processing by generating *in silico* peptide fragments of each theoretically possible protein within the parameters of a given database.

The resultant proteolytic peptide fragment spectra of each digested protein can then be used to identify experimentally observed proteins by comparing the peptide-spectral-matches (PSMs) with the proteolytic peptides associated to an *in silico* digestion of the proteins. This was one of the earliest proteomic techniques that was widely employed and many of the PMF approaches rely on gel based separation of proteins, reviewed later in this Chapter, prior to enzymatic digestion. As mass spectrometers have evolved so to has the manner in which PSMs are determined, this term is now more commonly associated with MS/MS fragment data.

2.4.2 Peptide-centric approaches (gel free)

There are a number of peptide-centric approaches employed in proteomics and they are normally referred to as being a bottom up approach as they rely on the identification of proteins based on the fragmentation of their proteolytic peptides using MS/MS.

Protein identification using peptide-centric approaches is heavily reliant on having a database that exists whereby *in silico* enzymatic digestions of the proteins can be performed providing a reference set of spectra against which the experimentally observed MS/MS spectra can be analysed and peptides can be identified using PSM.

2.4.2.1 MS/MS

This approach has been further developed as mass spectrometers have developed the capacity for tandem MS analysis, providing a second dimension MS analysis of fragment ions. Peptide fragment fingerprinting (PFF) [147, 165, 166] is the analysis of proteolytic peptides that are scanned in the first MS dimension after which, selected precursor ions are then subjected to fragmentation and their subsequent fragment ions are then analysed in the second MS dimension. This approach significantly increases sample complexity as each protein is digested into a number proteolytic peptides, of which a selection are then fragmented further during MS/MS.

However most mass spectrometers can not perform scans on precursor ions and their subsequent fragmented ion products concurrently (with a few exceptions, such as an LTQ Orbitrap) and thus the machine cycles between MS and MS/MS scans - this is often referred to as the duty cycle or cycle rate of a mass spectrometer. Accurate MS scans are often used to provide quantitative data on precursor proteolytic peptide ions and MS/MS scans are used to confidently identify those ions. In order to increase the number of proteolytic peptides, and consequently their parent proteins, identified using MS/MS it has emerged that fractionation strategies are integral. One of the early strategies in this regard was the multi-dimensional protein identification technology (MudPIT)[167].

2.4.2.2 Peptide fragmentation strategies

As discussed in the previous sub-section, tandem mass spectrometry allows for specific parent ion species to be selected and fragmented and their subsequent ion fragments are then analysed in a second dimension. There are a number of possible techniques that can be employed to fragment the precursor ions.

The most broadly implemented approach is known as collision induced dissociation (CID). This approach involves accelerating the selected precursor ions through a collision chamber that is filled with an inert gas (normally nitrogen). The accelerated peptides collide with the inert gas molecules and fragment into component ion species. These component ion species (or "daughter ions") are then analysed in the second MS dimension. The majority of the fragment

ions produced by CID for peptides are *b* and *y* ion series. CID is the major fragmentation approach employed in mass spectrometers but is not the only approach employed for proteomic studies.

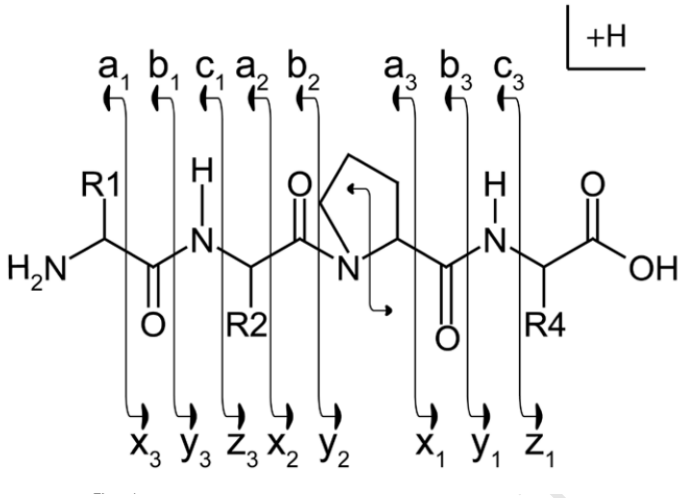

Figure 2.8: Roepstorff Nomenclature Scheme
Illustration of fragment ions formed from the backbone cleavage of protonated peptides. Fragment ions retaining the positive charge on the amino (N) terminus are termed *a*, *b*, or *c* type ions. Fragment ions retaining the positive charge on the carboxy (C) terminus are termed *x*, *y*, or *z* type ions. Adapted from Mikesh *et al.* 2006 [168].

Electron transfer dissociation (ETD) [169] provides an orthogonal alternative to CID for fragmentation analysis of peptide ion species [168] [170]. ETD forms unstable radical ions by using anions, commonly fluoranthene ions, to transfer electrons to the analyte that then fragment at sites that are the weakest bonds in the molecular structure. The resultant fragment ions produced are predominantly *c* and *z* ions from the parent peptides [169]. These radical-based fragmentations are very useful and powerful in the analysis of labile post-translational modifications, where sites of modification can be determined on peptides bearing modifications that are highly labile under CID conditions [171].

2.4.2.3 LC-MS/MS

In-line fractionation of proteolytic peptides using a liquid chromatography system that is coupled directly to the mass spectrometer (for ESI) or to a robotic spotter (for MALDI) form the basis for LC-MS/MS. As previously alluded to, MudPIT describes one of these in-line fractionation techniques. Essentially MudPIT is underpinned by a two dimensional orthogonal fractionation of peptides before analysis using a mass spectrometer. In the original experiment published by Washburn *et al.*[167], proteolytic peptides generated from a *Saccharomyces*

cerevisiae sample were solubilised and injected into an HPLC system coupled to a mass spectrometer. The peptide solution was separated by strong cation exchange in the first dimension and then subsequently by reverse phase in the second dimension before being analysed by MS/MS. Since then a number of methodologies have been developed to perform two dimensional orthogonal fractionation of peptides before subsequent MS/MS analysis. Not all of these methodologies are in-line, indeed some are off-line (the fractionation is performed on systems not directly connected to the mass spectrometer or spotter - a good example would be any of the gel based methods described earlier), however there are many different combinations of fractionation techniques and this will be discussed shortly hereafter.

2.4.2.4 *De novo* sequencing

In situations where a database does not exist or is incomplete/insufficient, it is possible to employ a different strategy in the bottom up approach whereby peptides undergo PFF and the subsequent ion fragments can be used to determine an amino acid sequence, in a similar manner to how Edman degradation works, by piecing together the component amino acid sequence within a given MS/MS spectrum. The amino acid sequence can then be used to perform a classical BLAST search to identify the protein that it belongs to. This strategy is referred to as *de novo* sequencing [172, 173].

The one constant that unites these three main forms of protein identification is the effect high mass accuracy mass spectrometers on the ability of algorithms to increase the number of proteins that are identified with a high confidence [174]. Higher mass accuracy machines have improved mass spectra resolution massively, contributing to the ability of algorithms to identify potential peptides and proteins. Another key development in improving the number of proteins that are routinely identified in modern shotgun proteomic experiments is sample fractionation. Simplifying complex samples has lead to a greater total number of ionised peptides as well as a greater number of PSMs and consequently a greater number of identified proteins.

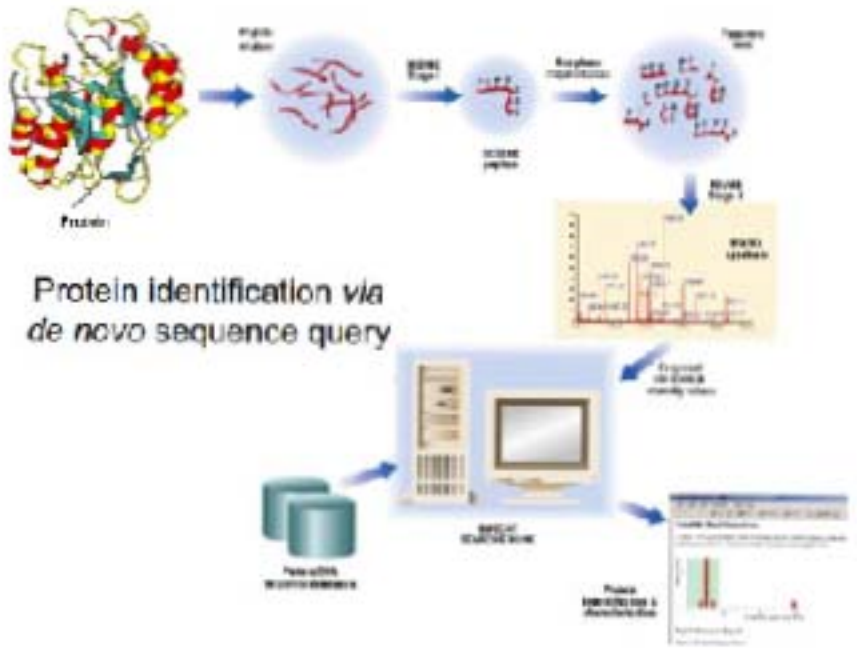

Figure 2.9: Protein identification using *de novo* sequencing

2.4.3 Fractionation strategies

A number of methods have been developed to try and delve deeper into the proteomes of complex samples. The uniting characteristic behind all these strategies is that they all involve fractionating a complex proteomic sample into a number of less complex fractions that can be run on a mass spectrometer without subsequently overburdening the capacity of the detector of the machine during any one experimental run. When deciding which method to use for fractionating a complex sample there are a number of key performance metrics that must be considered, namely: resolving power, orthogonality, and sample loss.

2.4.3.1 SDS PAGE

One of the first popular methods for identifying proteins using mass spectrometry involved separating the protein or proteins using sodium dodecyl sulfate (SDS) polyacrylamide gel electrophoresis (PAGE) also often referred to as one-dimensional electrophoresis (1DE). SDS PAGE is one of the simpler forms of fractionation that can be performed on a complex protein sample as it does not require expensive equipment or extensive training and has been in existence for a long time [175]. SDS PAGE separation of proteins is based on size exclusion as they migrate through a gel-like matrix when placed in an electric field. The sample protein mixture is

incubated in a buffer containing SDS and reducing agent, normally β-mercaptoethanol or dithiothreitol (DTT), to reduce any disulphide bonds. The reduced and denatured proteins bind SDS, a polar negatively charged molecule, causing the negatively unfolded proteins to migrate through an electric field. This fractionation technique is good for removing most buffer contaminants (the notable exception being guanidinium as it precipitates on contact with SDS) that would be incompatible with mass spectrometry and provides a robust manner in which to prepare complex protein samples whilst at the same time removing any incompatible buffer components. In the earlier days of proteomics this was a popular technique as stained SDS PAGE gels provided a means to visualise target bands of interest that could be excised and digested into proteolytic fragments, often using trypsin, for subsequent analysis using MALDI-ToF MS.

There are a few draw backs for this fractionation technique, chief amongst them being the limited resolving power in terms of separation of SDS PAGE, this technique is only effective for relatively simple protein mixtures or for pure proteins. Over and above the low resolving power of SDS PAGE, the quantity of protein required for visualisation using staining means that only high abundance proteins will be identified, making analysis of different gels inconsistent and difficult. It is also only applicable for whole intact proteins - it can not be used to separate out tryptic peptides effectively as they are too similar in size and would not separate with any great resolution before running off the bottom of the gel. Another issue to consider is the potentially variable nature of peptide extraction from gel slices which could have a serious effect on downstream label free quantification applications, however this can be negated (to a degree) through the use of a standardised protocol and loading comparable amounts of protein onto the SDS PAGE gels to begin with. SDS PAGE is highly orthogonal to other fractionation strategies as it is based on molecule size, however this technique does have a lower resolving power. Sample loss can be also be minimised by using robust in gel digestion protocols.

Figure 2.10: SDS PAGE gel (1DE PAGE)
An example of a typical SDS PAGE gel stained with colloidal Coomassie Blue.

2.4.3.2 2D PAGE

In an attempt to improve the resolving power of the fractionation strategy (SDS PAGE) employed in early proteomics, two-dimensional (2D) PAGE, also referred to as 2D electrophoresis (2DE), was used to allow for a two dimensional orthogonal separation of a protein mixture. In this technique, a sample is loaded onto an iso-electric focusing strip that separates/fractionates the proteins based on their iso-electric focusing point. The strip containing the separated proteins is then placed along the top of a PAGE gel, thus separating the proteins as if they were in a normal SDS PAGE gel in the second dimension. This two-step resolution allowed for the analysis of more complex samples, however there were still many issues that prevented this technique from being widely regarded as the best technique for proteomics. Chief amongst these is the difficulty associated with reproducing quality 2D PAGE gels as well as the inherent variation that occurs between any two gels making reliable analysis of differences in protein spots problematic. A number of software spot picking algorithms were developed to normalise gel images before robotic spot pickers excise spots of interest however these advancements still have limitations.

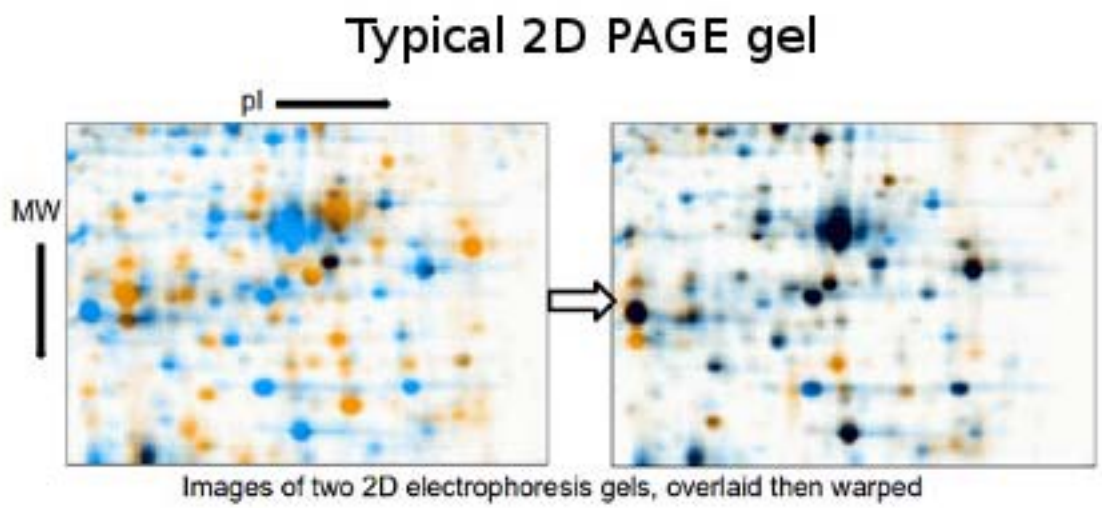

Figure 2.11: 2D PAGE gel (2DE PAGE)
An example of a typical 2D PAGE gel, in this case two gels have been overlaid (left) and then manipulated using software to align the spots better (right).

2.4.3.3 DIGE

In order to overcome these limitations as well as poor gel to gel reproducibility and to therefore improve the analysis of different samples using 2D PAGE, differential gel electrophoresis (DIGE) was developed [176] and has since been referred to as 2D DIGE. In this technique, the protein samples were labelled with different fluorescent dye probes before being combined and run on a single gel - thus eliminating the need to analyse different samples on different 2D PAGE gels using normalisation software to help align spots on different gels. With the cysteine-modifying DIGE labels a large quantity of a sample proteome may be visualised using as little as micrograms of starting material [177, 178]. Initially only Cy3 (red) and Cy5 (yellow) dyes were used, however a third dye - Cy2 (blue) - was also later introduced meaning that an internal standard could be run as well to provide quantitative information. It is worthwhile noting that the actual colours of these dyes differ between their physical appearance when compared to the colour that they appear to be when they fluoresce. This ability to multiplex samples, albeit in a limited capacity, resulted in 2D DIGE becoming a widely accepted and utilised tool in proteomics at the time. However the relatively low dynamic range of proteins that are visually identifiable using this technique means that analysis of low-abundance proteins using PMF is not possible as these proteins are often not present in large enough quantities. The relatively high cost of the reagents has also helped to hamper the spread of this technology in the proteomic fields. This has resulted in many other gel free techniques being developed for proteomic applications.

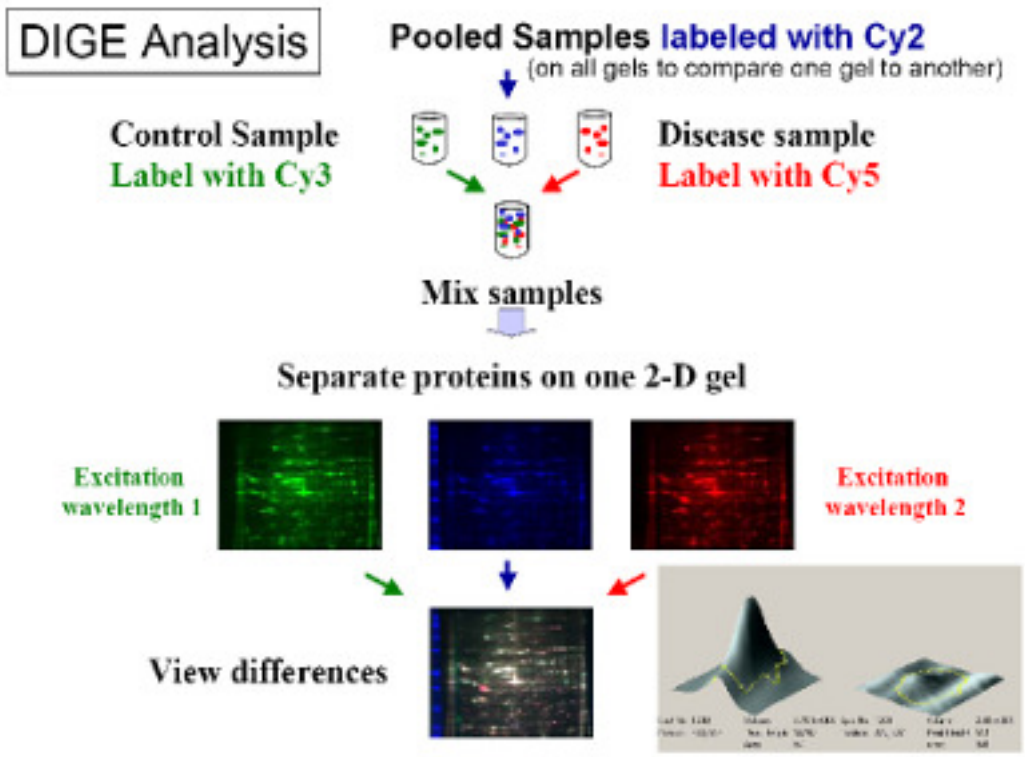

Figure 2.12: 2D DIGE gels

2.4.3.4 Ion Exchange Chromatography

Ion exchange chromatography relies on using a stationary phase (containing a charged functional group attached to the packing resin) and a polar aqueous mobile phase. The stationary phase forms ionic bonds with solute molecules, thus cationic columns (negatively charged) bind positively charged solute molecules and anionic columns (positively charged) bind negatively charged solute molecules. For this reason, the two forms of ion exchange chromatography are often referred to as strong cation exchange (SCX) or strong anion exchange (SAX) chromatography depending on the charge of the stationary phase that is being used. Anion exchange chromatography can also be performed, often by using the diethylaminoethyl (DEAE) functional group, and is known as weak anion exchange (WAX) . No matter the type of ion exchange utilised, the concept remains the same. Once the solute molecules have been bound they are stripped off the column through competitive binding using a similarly charged polar molecule in the mobile phase. Thus in cation exchange bound molecules are often released by increasing the Na^+, or some other positively charged molecule, concentration in the mobile phase and likewise a negatively charged molecule is used to competitively release solute molecules on SAX columns. Whilst peptides are fairly soluble and robust molecules, proteins

are prone to becoming insoluble in the presence of high salt concentrations, thus this fractionation strategy is often employed at the peptide level and not the protein level and due to it's downstream issues with mass spectrometry it is often used as the primary step in a two step fractionation strategy. Mass spectrometers do not tolerate high salt concentrations as the charged salts tend to ionise far more easily than bigger molecules such as peptides or proteins, and cause suppression these other molecules when ionisation occurs in the gaseous phase. A desalting step is required to clean up samples that have been fractionated using ion exchange chromatography. The strength of this technique lies in the resolving power of ion chromatography especially as it is highly orthogonal to reverse phase chromatography when it comes to separating molecules, the drawback of this technique is that it normally has a relatively high percentage of sample loss.

2.4.3.5 Reverse phase chromatography

Reverse phase (RP) chromatography makes use of a hydrophobic stationary phase (normally a long chain hydrocarbon attached to a resin) and an organic aqueous/mobile phase. Solute molecules, such as peptides, adsorb the hydrophobic matrix when in a polar solvent; as the solvent buffer increases in hydrophobicity, the peptides dissociate from the matrix at the point at which the interaction of the peptides with the solvent is more favourable than the interaction of the peptides with the stationary phase. The polar state of the mobile phase can be achieved using either an acid (such as formic acid) to create a low pH, or a base (such as tri-ethyl amine, or TEA) to create a high pH. Amino acids contain an amino group (-NH_2), a carboxyl group (-COOH) and in most cases, an R-group (except glycine) attached to the α-carbon. The R-groups of the amino acids have distinct chemical properties and these properties play a role in the formation of the chemical micro environment of the peptides that they belong to. The pK_a (the negative log of the dissociation constant, K_a) of the amino (~ pH 9 - 10) and carboxy groups (~ pH 1.8 - 2.4) are relatively constant across most amino acids, however the R-groups vary greatly, from ~ pH 4 for the acidic amino acids (aspartic and glutamic acid) all the way up to ~ pH 13 for the polar, hydrophilic amino acids serine and threonine. As these functionally different polar environments occur at distinctly different pH's they result in the overall polar environment for each peptide to be resolved differently under either a low pH (for conventional RP chromatography) or a high pH (for high pH RP chromatography). Consequently, it is possible to obtain two orthogonal means of separation on most peptide or protein species using a crude high pH RP fractionation step (involving specific quantities of organic solvent polarised using TEA to create the fractions) followed by the more conventional acidic pH RP LC fractionation, once the samples have been dried down to remove the original solvent. This technique has minimal sample loss and can be performed on whole proteins or

peptides.

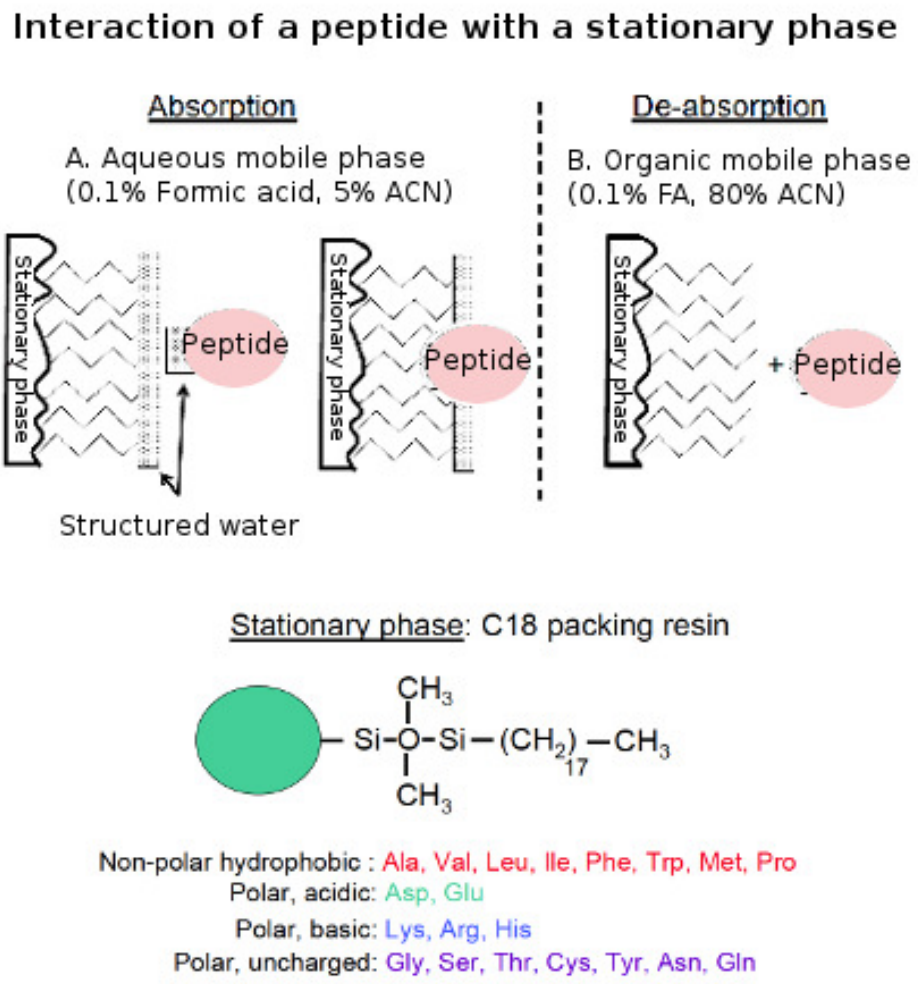

Figure 2.13: Reverse phase chromatography

Reverse phase chromatography separates molecules based on their hydrophobicity. Hydrophobic molecules adsorb to the hydrophobic column resin in the presence of a hydrophilic solute and gradually are stripped off the column resin as the hydrophobicity of the mobile phase increases. At the bottom of the figure is a breakdown of the chemical profiles of the various amino acids.

Where reverse phase chromatography has a more polar stationary phase compared to the mobile phase, there is another popular type of chromatography where the mobile phase is more polar than the stationary phase. This type of chromatography is referred to as hydrophilic interaction liquid chromatography (HILIC) [179]. This chromatography has number of uses but has been most widely applied in the field of glycoprotein analysis [180].

2.4.3.6 Affinity based chromatography

Due to the broad dynamic range of proteins in most complex biological samples it is conceivable that a depletion or enrichment step for a particular subset of proteins within that sample would be an attractive strategy. These techniques could be non-specific (for example, using precipitation [181, 182]), or targeted in nature (phytate-based rubisco depletion [183], antibody depletion of albumins [184, 185]). The concept behind these techniques is to either remove highly abundant proteins so that low abundant proteins will now fall within the dynamic range of analysis for the mass spectrometer, or to remove the proteins of interest for subsequent analysis by MS (this is often performed in phosphoproteomics [186–190]). Phosphoproteomics is focused on the identification and quantification of phosphorylated proteins as well as their phosphorylation sites (serine, threonine or tyrosine) [148, 191], and it is a field of proteomics that has seen a large amount of interest develop over the past decade. A common strategy for enrichment of phospho-serine or phospho-threonine based peptides or proteins is the use of affinity based chromatography techniques such as immobilized metal affinity chromatography (IMAC), metal oxide affinity chromatography (MOAC) and strong cation-exchange chromatography which have been shown to be complementary in nature [192].

IMAC makes use of fixed metal chelators with positively charged co-ordination sites that interact with the negatively charged groups of the phosphates and carboxylate moieties of the proteins or peptides of interest. The buffer pH will affect the specificity of the IMAC resin for phosphopeptides and proteins. IMAC phospho-enrichment can be used at the protein or peptide level [193–196] following strong cation exchange chromatography. MOAC however does not require a charging step as the metal ions are part of a solid bead instead of being linked to the chromatographic support. Consequently, materials such as titanium dioxide (TiO_2) are used widely for the enrichment of phosphopeptides [187, 197, 198]. A further level of control can be exerted using MOAC by using 2,5-dihydroxybenzoic acid (DHB) and aliphatic hydroxyl acids to increase the selectivity of TiO_2 for phosphopeptides [199, 200].

The analysis of phosphotyrosine based proteins or peptides is performed almost exclusively using immunoaffinity purification where antibodies that have been raised against specific motifs are used to enrich these residues from protein or peptide extracts [201–203].

There is a fourth approach that is neither depletion or enrichment specific, the ProteoMiner approach, which differs slightly in that it attempts to equalize protein populations by depleting high abundance proteins whilst concurrently enriching low abundance proteins using a diverse library of hexapeptides bound to chromatographic supports [182, 204]. It is worthwhile noting that despite manufacturers best attempts, these techniques are not always absolute in their capabilities and may introduce an unwanted bias into an MS based proteomics experiment.

That is not to say that these techniques should not be used, but the consequences of using these techniques should be fully understood before a decision is made.

2.4.3.7 Off-gel (iso-electric focussing)

Off-gel fractionation is based on iso-electric focusing. This technique can be performed on either proteins or peptides. Samples are loaded onto a pH focusing strip along with ampholytes to maintain the buffering of the system and then placed in an electric field. Sample separation occurs as a result of the samples having a charge at any pH other than their specific iso-electric point (pI). The charged samples migrate along the strip in the direction of the pH gradient at which they no longer have a charge and therefore are unaffected by the electric current. As each protein or peptide sample has a relatively unique pI, whose range in any particular sample can be quite broad, it is theoretically possible to fractionate the samples quite well. However, the degree of fractionation is not extremely high due to limitations in being able to have a large number of compartments in the off-gel strip and as a result this technique should be used as a primary fractionation step of a complex sample. Off-gel fractionation is not as compatible with sample preparation buffers as SDS PAGE is. The final fractions are left in a buffer with a high salt content and need to be de-salted before any further analysis can be performed on them, whether it is another fractionation step or analysis on a mass spectrometer.

2.4.3.8 Sub-cellular fractionation

There has been some interesting research into using novel fractionation strategies during the protein extraction process itself. The advantages behind these techniques is the inherent sub-cellular localisation information that can be associated with the protein fractions. Of the multitude of publications in this field, two in particular stand out for the simplicity of the concepts that they utilise: the first employs a sequential removal of proteins in layers from the cell itself using a combination of detergents to gradually gain access to the various cellular compartments [205]; the second makes use of density gradient centrifugation to separate sub-cellular compounds and vesicles apart into distinct fractions [206].

In the crude sub-cellular fractionation method (CSF), three to four fractions are generated consisting of 1) the cytosolic protein fraction, 2) the membranous organelles protein fraction, 3) the nuclear membrane protein fraction and 4) the insoluble proteins fraction. It is possible to combine fraction three and four during the extraction protocol to obtain three fractions in total. This technique uses different enzymes and detergents to sequentially remove the fractions of interest by centrifuging the remaining insoluble pellet at each step before re-solubilising the

pellet in the subsequent buffer. The advantage of this technique is a crude protein fractionation that also will provide sub-cellular localisation information. However, crossover of proteins does still occur across fractions and the reproducibility across differing cell types may be difficult to keep consistent. This approach may provide an excellent way to remove large subsets of proteins and in doing so shift the dynamic range of the remaining proteins to make another subset more easily visible - for instance removing the cytosolic proteins, and the consequent high abundance proteins contained therein, before analysing the nuclear protein subset.

The density gradient centrifugation is slightly more complex but has the added advantage of providing quantitative information using isotopic mass tags. This approach, known as the localisation of organelle proteins by isotope tagging (LOPIT), provides spatial information on identified proteins based on the density of the organelle or protein complex that the proteins are isolated from during a density gradient centrifugation step. This approach has been shown to increase the resolution and coverage of identified proteins when compared to other methods [207], as well as providing an adequate average snapshot of cells in *Drosophila melanogaster* [208]. The method relies heavily on developing density gradient organelle maps and an integrated bio-informatic approach and may require more resources than are available for every proteomics researcher. However the technique does provide a means of fractionating at the protein level before subsequent peptide-centric approaches are employed.

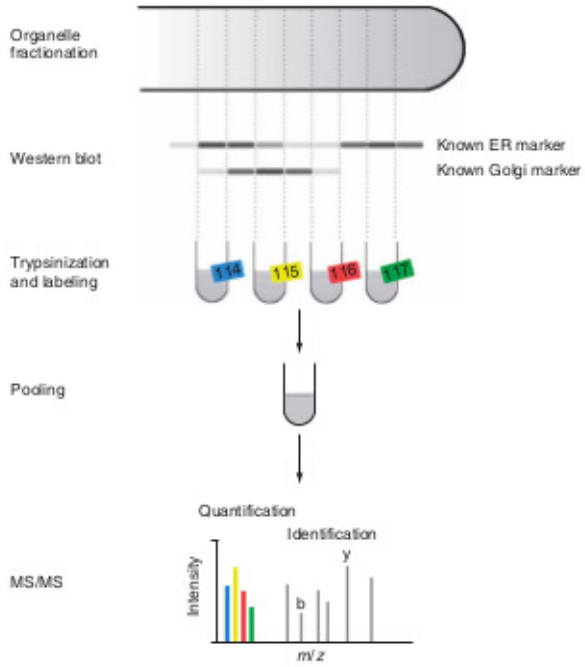

Figure 2.14: LOPIT organelle fractionation

The LOPIT approach allows for sub-cellular localisation and quantitative information to be extracted for proteins that are identified by MS/MS. In this example proteins from four fractions corresponding to different gradient fractions on a self generating iodixanol gradient are digested with trypsin before being labelled with separate iTRAQ labels and subsequently pooled. The pooled samples are then analysed using MS/MS where relative differences in quantitation across the four fractions are determined using the reporter element ions (114 - 117) that are detected. Proteins with a similar localisation on membranes will co-fractionate generating similar quantitation profiles, likewise it is possible to determine proteins are located amongst organelles of different densities [206].

2.4.4 Middle-out approach

The middle out approach lies somewhere between a protein-centric and a peptide-centric approach and is characterised by a crude primary fractionation of the sample at the protein level. The proteins in each of these fractions are then digested and the subsequent proteolytic peptides are subjected to a more thorough fractionation. The advantages of this mixed approach mean that highly abundant proteins can be restricted to certain subsets of fractions allowing for less abundant proteins to be identified. The peptide fractionation still provides a high degree of sample coverage allowing for the identification of a higher number of total proteins. The additional fractionation steps do however provide an additional set of opportunities for sample loss to occur.

2.4.4.1 Protein fractionation

There are a few protein fractionation strategies that are currently employed. The most common either employ IEF (using the off-gel technique), size exclusion (using 1D PAGE) or use biological localisation as part of the fractionation strategy (such as in crude sub-cellular fractionation). Ideally the choice of which protein fractionation technique to use should be decided based on the type, quantity and source of sample that is being worked upon. Samples that are difficult to re-solubilise may not combine well with the off-gel fractionator compared to 1D PAGE. Likewise, if the experimental question that is being considered is closely linked to cellular localisation of a protein then sub-cellular fractionation may be a more rewarding starting point that either IEF or 1D PAGE. Ideally the initial protein fractionation should not be exhaustive as this will exponentially increase the experimental cost as well as machine run time.

2.4.4.2 Peptide fractionation

The subsequent peptide fractionation strategy could be either a one- or two-step separation and this choice should be made after considering sample quantity, machine runtime and experimental cost. It is also worth considering that the higher the number of processing steps prior to MS/MS the greater the risk for sample loss or contamination. Peptides by their nature are more robust and soluble and thus should be able to withstand a broader variety of solubility constraints. It is also pertinent to use a peptide fractionation strategy that is orthogonal to the protein fractionation strategy.

The ultimate goal of the any shotgun proteomic work flow is to maximise protein coverage by maximising the number of identifiable peptides. This is achieved through a well thought out fractionation strategy that will reduce sample complexity during MS/MS. When designing a shotgun proteomic experiment it is thus important to consider the level of complexity of the sample, the quantity of sample available to work with and the cost of access to adequate resources (both financially and in terms of time) before deciding on a final work flow. There is no one-size fits all strategy and it is important to understand the repercussions of choices that are made regarding the design of the experiment and the subsequent handling of the sample prior to MS/MS analysis.

2.5 Quantitation strategies

2.5.1 Absolute and relative quantitation

Absolute quantitation strategies compare the quantities of individual peptides identified in a sample against the quantity of a labelled reference standard that has been spiked into the sample. The reference peptide(s) (usually a synthetic peptide) act as a known absolute value against which the sample peptides can be compared and their concentration back-calculated to an initial concentration via a standard curve.

Relative quantitation strategies compare the quantities of individual peptides identified in one sample with the quantities the same peptides in a separate sample or against other peptides within the same sample, however at no stage is the comparison normalised to a reference mass peptide that has been spiked into the sample. This strategy can be employed by using tags or labels, where a reference sample can be compared against an experimentally altered sample, or through label-free approaches, where the mass spectra are used to directly determine peptide abundance in one sample relative to another.

Labelling strategies are crucial for absolute quantitation, whereas relative quantitation can be performed using labelling or by label free methods. Both techniques have a number of possible strategies that can be employed.

2.5.2 Labelling strategies

Current label-based proteomic experiments generally employ a number of types of labelling strategy. The methods vary from integrating labels (either metabolically, chemically or enzymatically) to isotopic addition of an appropriate label.

2.5.2.1 Metabolically integrated labels

A powerful approach that has emerged in the last decade, employs differential stable isotope labelling by amino acids in cell culture (SILAC) [209]. This method commonly entails culturing cells in a medium that contains a stable isotopic form of arginine and lysine (e.g. arginine bearing six ^{13}C atoms) although there are other amino acids that may be utilised instead. Consequently, the "heavy" amino acid is incorporated into proteins during cell growth and development. A parallel set of cultures in a medium containing no replacement amino acids

produces a "light" set of proteins. SILAC allows "light" and "heavy" proteomes to be distinguished by MS while avoiding any chemical derivatisation during sample preparation. Arginine and lysine are used as the distinguishing amino acid as they are guaranteed to form part of all tryptic peptide fragments. Each peptide comprising a single lysine or arginine, providing there are no missed cleavages. The method allows for comparative analysis of proteome perturbations across two different culturing conditions. And furthermore allows the two cultures to be combined prior to any fractionation. The limiting factor for this strategy is that it requires cell culture for the label to be integrated and it can only be applied across a few different conditions and as such is not applicable for experiments that need to be multiplexed across a high number of conditions.

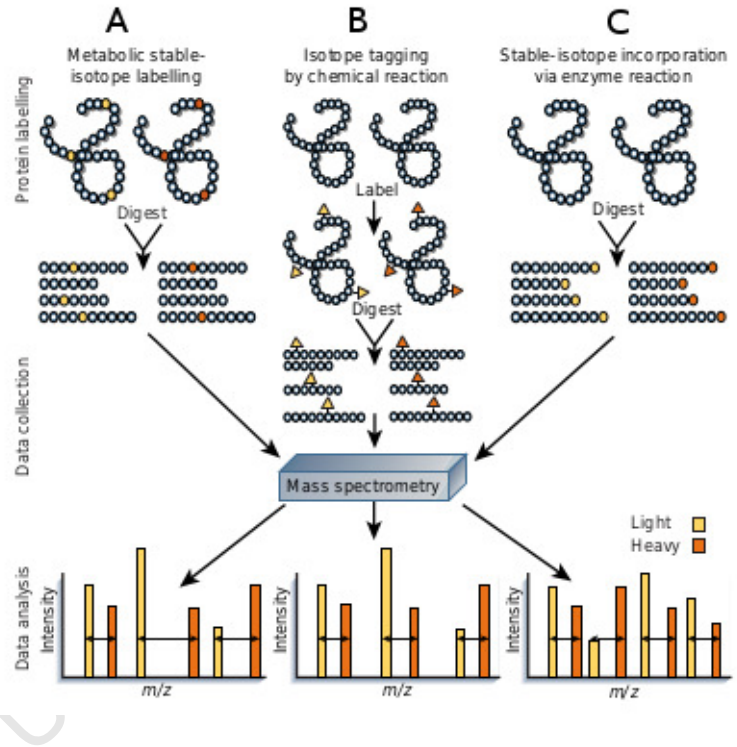

Figure 2.15: Comparison of stable isotope labelling workflows

The left hand column (A) is an example of a SILAC workflow where proteins are labelled metabolically by culturing cells in isotopically enriched media (for example, containing 15 N salts, or C-labelled amino acids). The resulting mass difference that is generated for peptide pairs using this method is variable as it depends on the amino acid composition. The middle column (B) is an example of an isotope-coded affinity tag (ICAT) workflow, where proteins are labelled at specific sites with isotopically encoded reagents. This method will generate a mass difference that is one or multiple times the difference in mass of the encoded reagent that was used. The right hand column (C) describes a typical enzyme based incorporation of an isotope label workflow whereby isotopic labelling is introduced using enzyme catalysis that incorporates ^{18}O during proteolysis in ^{18}O enriched water. The mass difference that is generated by this method is either 4 Da or 2 Da and can make subsequent bio-informatic processing for quantitation quite difficult [148].

2.5.2.2 Chemically added isotopic labels

Isotopic labelling typically involves the attachment of chemical tags that have different isotopic masses but identical structures to the reactive side chains of amino acids. Gygi *et al*. developed the isotope-coded affinity tag (ICAT) approach [210], whereby cysteine residues are specifically derivatised with a reagent containing either zero or eight deuterium atoms as well as a biotin group for affinity purification of cystein-derivatised peptides and subsequent MS analysis. Several variations on this chemical reagent class have since emerged to improve aspects such as recovery of labelled peptides or chromatographic properties [211–214]. A popular method that involves the use of cheaper reagents to incorporate a stable isotope dimethyl label has also been developed [215].

2.5.2.3 Enzymatic

It is possible to introduce a mass shift using serine proteases to catalyse the introduction two ^{18}O atoms into the carboxyl terminal of peptides in mixtures. Introducing labelled oxygen during the hydrolysis of proteins was reported more than 25 years ago and the ability of trypsin (and other serine proteases) to rebind the proteolytic peptides and introduce a second ^{18}O atom through micro-reverseability was reported in the mid 90s [216, 217]. This is a two-step procedure that requires proteins to be cleaved initially, before drying down the subsequent peptides. The dried peptides must then be incubated with trypsin in ^{18}O-enriched water for the label to be incorporated. This is a global labelling strategy and allows for comparison of two samples prepared in parallel against each other - similar to how a typical SILAC work flow would be performed[218, 219].

2.5.2.4 Isobaric approaches

Isobaric labels have identical chemical structures and identical masses - achieved through judicious placement of multiple isotopes of nitrogen and carbon - so they change the mass of the labelled product equally such that there is no shift in how the proteins or peptides are differentiated during MS; however the labels break apart in the collision cell prior to MS/MS analysis giving rise to different, quantifiable fragment ions, thus allowing for differential analysis. Most isobaric labels take advantage of the α- or ε-amino group of tryptic peptides and are activated as N-hydroxysuccinimide (NHS) esters. Two which are capable of multiplexing up to 8 and 6 samples respectively are the isotope tags for relative and absolute quantification (iTRAQ) and tandem mass tags (TMT) [220, 221]

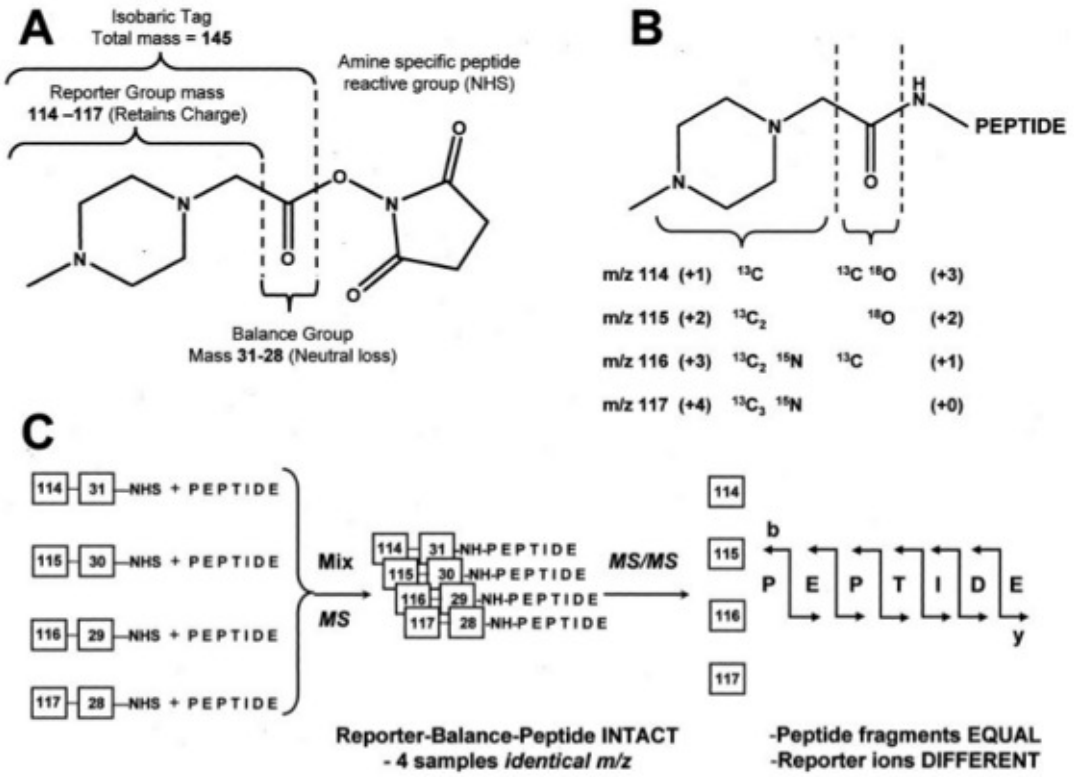

Figure 2.16: Structure of iTRAQ labels

The chemical structure of the four-plex iTRAQ label set is depicted (A) with the description of the distribution of the mass balance elements (B). The labels are amine reactive (C) and forms an amide linkage to any peptide amine (N-terminal or amino group of lysine). Each label has the same mass)145.1 Da) however the reporter elements are different for each label (114.1 to 117.1) and can be distinguished during MS/MS [220].

2.5.3 Label-free strategies

Label-free quantification approaches aim to correlate the mass spectrometric signal of intact proteolytic peptides or the number of peptide sequencing events with the relative or absolute protein quantity directly. The type of label free strategy that can be utilised is directly related to the mass resolution of the LC-MS data that is generated. Low to moderate mass resolution LC-MS data can be processed using spectral counting or extracted ion chromatograms. High mass resolution LC-MS data can use truly label free quantitation strategy that incorporates the detected *m/z* elution profile of a particular peptide ion, as detected at the MS1 level, as a function of LC retention time.

Method	MS acquisition mode	Method of quantitation
Spectral counting	Data-dependant acquisition (DDA)	Counting the number of times a peptide was identified
DDA-based ion counting	Data-dependant acquisition (DDA)	Ion intensity of intact peptides detected in the MS scans (survey scans)
MS survey scan based ion counting	MS survey scan	Ion intensity of intact peptides

Table 2.2: Differing types of label free quantitation using LC-MS/MS
A list of the broadly utilised quantitation methods that are currently employed, stratified in relation to how the data is acquired and what data is utilised to calculate the quantitation values. DDA = Data-dependant acquisition. Tabled sourced from [222].

Tables 2.2 displays the basic quantitation strategies that are currently employed in LC-MS/MS. Table 2.3 provides a more detailed analysis of the various factors that need to be considered when wanting to eploy a quantitation strategy. A more in depth description of various label free strategies follows below.

2.5.3.1 Spectral counting

Spectral counting is a semi-quantitative technique for determining the abundance of a detected peptide in proportion to the abundance of the total peptide sample. This is essentially achieved by determining the number of spectra per peptide as a proportion of the total number of peptide spectra recorded for a given sample. The drawbacks to this approach are that: 1) not all peptides in the sample ionise efficiently, 2) degenerate peptides can not be effectively counted, and 3) low numbers of spectral counts could be a function of low abundance, short protein length, erroneous identification, physicochemical properties affecting peptide observability or the sample complexity itself. There are a number of spectral counting algorithms that are currently available in the proteomics field, some of which have attempted to correct for as many of the listed issues as possible. The most widely utilised algorithms are; the normalised spectral abundance factor (NSAF), the absolute protein expression method (APEX), the exponentially modified protein abundance index (emPAI) and the spectral index quantitation (SINQ) method [224–228]. The NSAF algorithm attempts to adjust the abundance values that are calculated for a specific peptide according to the length of the protein from which it is derived. The emPAI, APEX and SINQ methods make use of various ways to utilise a derived index for calculating abundance values based upon the premise that the empirical relationship between the number

	Dynamic range	Proteome coverage	Quantitative accuracy	Nature of quantitation	Number of samples to compare	Quantification level
Metabolic labeling						
^{15}N	1–2	Medium	Precise (<10% rsd) (114)	Relative	2	MS
SILAC	1–2	Medium	Precise (<10% rsd) (82)	Relative	2 or 3	MS
Chemical labeling						
ICAT	1–2	Poor	Precise (<10% rsd) (36)	Relative	2	MS
ITRAQ, TMT	2	Medium	Medium (10–30%) (6)	Relative	2–8	MS2
Standard peptide	2	Poor (There are few target proteins that can be selected efficiently in a single LC-MS/MS experiment.)	Precise/Good	Relative/ Absolute[1]	2–many	MS or MS2
Label-free						
Ion intensities (iBAQ, Top3)	3	Good	Medium (10–30% rsd) (3)	Relative	Many (depends on reproducibility of chromatography)	MS
Spectrum count	3	Good	Poor (>30% rsd)	Relative	Within sample/many	MS2
Derived indices (APEX, emPAI)	3 or 4	Good	Poor (>30% rsd)	Relative/ Absolute[2]	Within sample/many samples	MS
Gels						
2D gels	1 to 4, depending on dye	Medium	Medium (10–30% rsd) (29)	Relative/ Absolute[1]	Many (depends on reproducibility of gels)	Image analysis

Table 2.3: Technical parameters of the different quantitation strategies for LC-MS/MS

An overview of the various parameters for label free and labelling workflows currently employed in quantitative LC-MS/MS experiments. 1 = Absolute quantitation is possible only through relative comparison to a spiked "known" standard. 2 = Absolute quantitation is possible only through empirical features and back-calculation using the molecular weight of the protein and total protein amount in the sample. Adapted from [223].

of spectra or peptides identified for a given protein and overall protein abundance in the sample is used as a basis to calculate the absolute concentration of each protein within the sample.

2.5.3.2 Extracted ion chromatograms (XIC)

When using XICs for semi-quantitatively tracking peptide abundance in a sample, a peptide must be identified at least once. The the *m/z* ratio and retention time (T_R) of the identified peptide is then used to extract an ion chromatogram of the MS precursor ion. The ion chromatogram can be integrated to ascertain a measure of quantitation [229, 230]. The drawback to this method is the reproducibility of chromatography across multiple runs which will directly affect the T_R of the peptide being used for extraction of the ion chromatogram [231]. For both spectral counting and XICs there is no estimation for error rates. The quantitation is also complicated by the stochastic nature of the MS/MS sampling process, especially when it comes to low abundance peptides.

2.5.3.3 Label-Free Quantification of Multidimensional LC-MS Data

For more accurate label free quantification, the LC-MS data needs to be acquired at a high mass resolution at the MS1 level. Machines equipped with the new generation of ToF or OrbiTrap mass analysers are normally used for this method as they have high resolution power and mass precision - often in the low parts per million (ppm) mass unit range. Peptide signals are detected at the MS1 level and distinguished from noise by their characteristic isotopic pattern. These patterns are then tracked across the T_R dimension and used to construct a chromatographic elution profile of the monoisotopic peptide mass. The total ion current of the peptide signal is then integrated and used as a quantitative measurement of the original peptide mass. Extracted peptide signals can be mapped across multiple LC-MS runs using co-ordinates on the *m/z* and T_R dimension. The efficiency of the tracking is dependant on the mass resolution of the MS1 level. It has been shown that this process can be linear across three to four orders of magnitude after normalising the data concerned to remove any systematic artefacts in the peptide intensity values between LC-MS measurements.

An algorithm that is often used to estimate protein abundances across a number of samples in either a label free or SILAC dependent manner for LC-MS/MS experiments is the intensity based absolute quantification (iBAQ), this algorithm is often utilised in the MaxQuant software suite [232]. In this algorithm, absolute protein amounts are calculated as the sum of all peptide peak intensities divided by the number of theoretically observable tryptic peptides [233].

The Top3 algorithm was proposed by Silva *et al.* and is essentially an algorithm that calculates the abundance of each protein based upon the average intensity of its three best ionizing peptides [234]. This algorithm can theoretically be applied to any number of the best ionising peptides and is therefore sometimes referred to as the TopN method. A recent comparison of various label free quantitative algorithms showed that only the Top3 method is directly proportional to protein abundance over the full quantification range and consequently is the preferred method in the absence of reference protein [235].

2.6 Targeted proteomics

Targeted proteomics differs from shotgun proteomics in that the mass spectrometer is programmed to analyse precursor ion sequences in MS until a precursor ion which has been included on a list of watched peptides is identified at which point the precursor ion is selected for fragmentation and further analysis by MS/MS. This approach can be performed using two major techniques, the first involves building a peptide atlas of candidate precursor ions so that subsequent machine run time may be minimised without lowering the number of identifiable peptides significantly and the second utilises already existing repositories, such as PeptideAtlas, to provide these precursor ions and their expected transition masses.

2.6.1 Directed approaches

The directed approach has been developed so that large scale quantitative analysis of relatively complex samples can be performed, especially with respect to longitudinal time course studies, without the associated extended machine run time and resources that would be required in order to achieve this intensive analysis. This technique is often performed on LTQ-Orbitrap instruments as they have the capacity to trap precursor ions before selecting appropriate ions for subsequent MS/MS analysis. Essentially this process requires an initial set of runs to be performed to acquire a set of precursor ions that can be used to effectively identify proteins likely to be in the sample of interest. Once the atlas database is sufficient in size, a limited number of unique precursor ions, as well as their subsequent transition ions, can be identified per protein and an inclusion list can be formed. The inclusion list ensures that the mass spectrometer does not waste duty time analysing potentially redundant peptides and does not waste time analysing vast numbers of peptides belonging to only one protein but instead will analyse peptides that form part of the inclusion list before analysing other peptides that are available. Although costly in terms of machine time to create an effective transition database,

this approach can prove to be hugely effective for long term experiments involving very specific samples from the same source organism. The power of this technique has been rather elegantly used to track drug perturbations in moderately complex organisms over multiple time points with some fascinating results [236]. By reducing machine runtime without compromising the number of proteins that can be identified and quantified, this technique provides the opportunity to analyse many more time points to delve deeper into longitudinal changes in proteomic profiles. An added strength is that every run can be used to further develop the size of the atlas database and potentially increase the number of proteins that can be identified using less machine time.

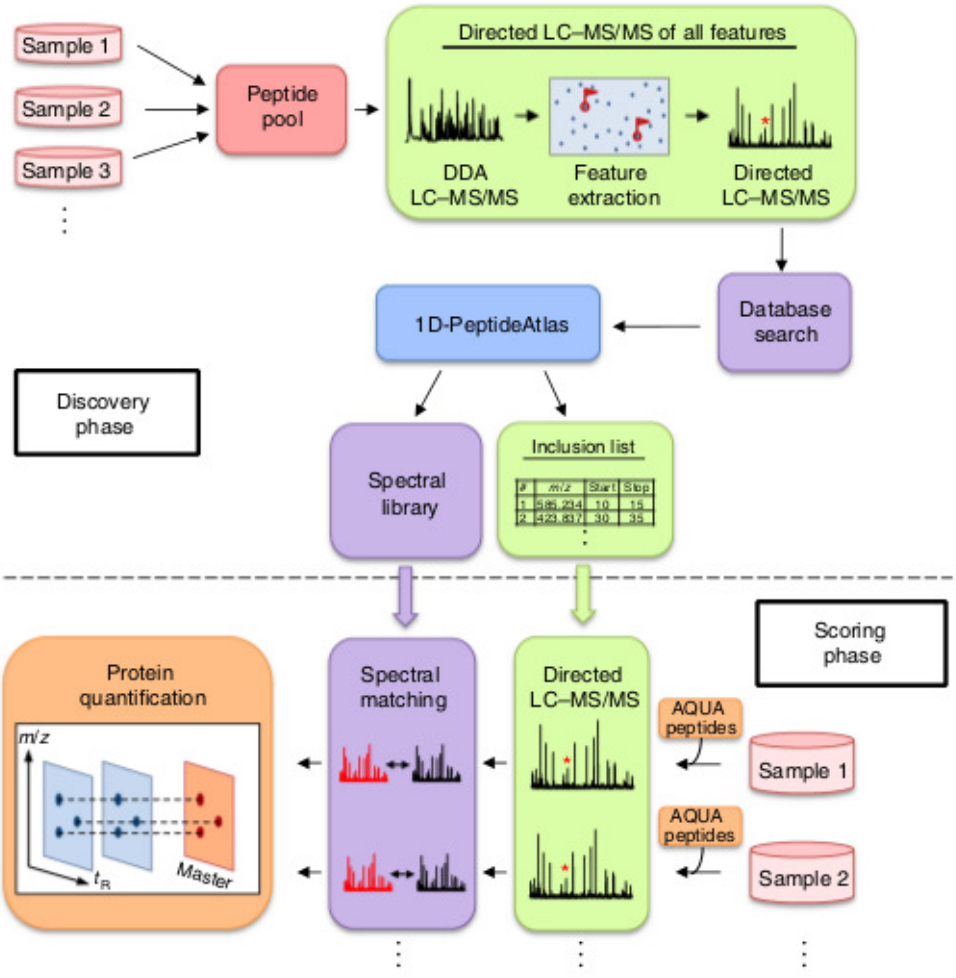

Figure 2.17: Outline of a directed proteomic approach

The directed approach involves two phases, an initial discovery phase and a secondary scoring phase. In the discovery phase the peptide samples from the different cell states are mixed together and analysed using data-dependent acquisition 1D LC-MS/MS. Comprehensive proteome coverage is achieved by sequential sequencing of all detectable pre-cursor ions using directed LC-MS/MS analysis coupled to database searching. The resultant identified peptide sequences are then stored in a 1D Peptide Atlas database along with some other key features (ion signal intensity, retention time and *m/z* ratio). The best five proteotypic peptides (PTPs) are then identified for each protein and stored in an inclusion list. In the second phase the LC-MS/MS is focused on the PTPs that are in the inclusion list as well as a set of heavy labelled reference peptides which can be used to calculate quantitation values using label-free approaches [236, 237].

2.6.2 Selected reaction monitoring

Selected reaction monitoring (SRM), also often referred to as multiple reaction monitoring (MRM), is normally performed on a triple quadrupole machine as it requires three phases. In the first phase, the first quadrupole scans the available precursor ions and very specifically selects

candidate peptides that have already been identified by the researcher running the experiment to be of value. These candidate peptides must conform to a few rules such as they should ionise easily, be specific to the protein of interest and should be reproducible through sample preparation. The second phase occurs when the selected precursor ion is subjected to fragmentation in the second quadrupole producing a series of fragment ions. The third phase makes use of specific fragment ions, once again that the researcher has deemed to be of interest, that are unique to the precursor ion to confirm the identity of the precursor ion and thus the identity of the protein that the precursor ion belongs to. This technique contains two selection steps and for this reason has a higher dynamic range (normally in the order of five magnitudes) compared to shotgun proteomic techniques (normally in the region of four orders of magnitude). It is sensitive due to the non-scanning mode and has a wide dynamic range, all of which combine to make this an excellent technique for quantitative proteomics.

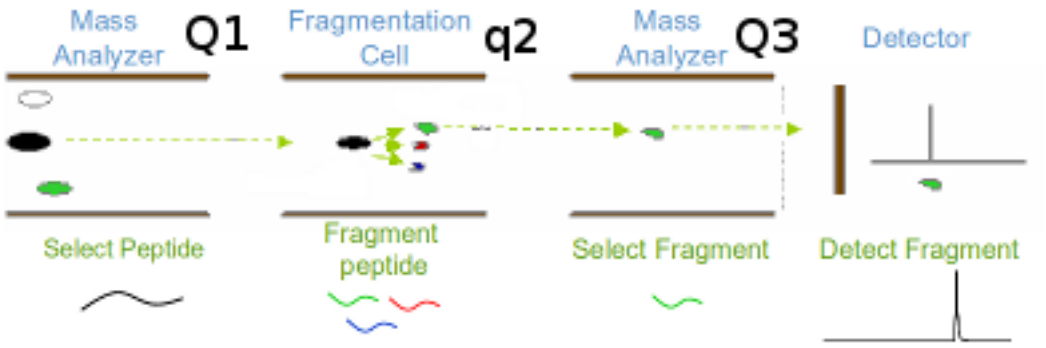

Figure 2.18: A basic SRM analogy
In a typical SRM experiment, the first quadrupole (Q1) will select a peptide which will then be fragmented in the second quadrupole (q2). The third quadrupole (Q3) then selects a specific fragment of the fragmented precursor ion.

Absolute quantitation in proteomics requires internal standards against which a comparison of the measured component of interest can be performed. This is often achieved in SRM analysis using isotopically labelled synthetic peptides that are added to the sample prior to the LC-MS. Alternatively label-free relative quantitation can be achieved through comparison of the normalised peak intensities between different samples (e.g. disease and control). However the limiting factor is the sample complexity as only a few hundred, at the most, transitions can be monitored for any given LC-MS run and given the dynamic range of these instruments compared (10^5) to the dynamic range that exists in biologically complex samples (10^{12}) it is clear that sample preparation is crucial for a successful analysis.

A couple of the key specifics of this technique when applied to proteomics, as opposed to small molecules where this technique has been used for considerably longer, are: 1) multiply charged

precursor ions produce fragments with higher *m/z* values than the precursor ions, requiring the instrument to have an extended mass range; 2) the experimental design needs to be performed prior to SRM analysis in order to be able to identify proteotypic peptides of interest (from which protein identification can be inferred) as well as their fragment ions, this process needs to take into account the complex nature of the sample being analysed.

2.7 Discovery to validation

As has been discussed in this review it is clear that proteomics is a diverse field of study and has many techniques that will be used when a specific task needs to be performed, covering everything from discovery to validation of candidate biomarkers.

2.7.1 Proteomics pipeline

There have been many discussions and demonstrations regarding the application of proteomics to drug discovery for big pharma companies. Invariably the discovery phase requires the identification of as many proteins as possible using a minimal number of biological samples and ultimately leads to the validation phase where a small number of proteins are monitored across a larger number of biological samples.

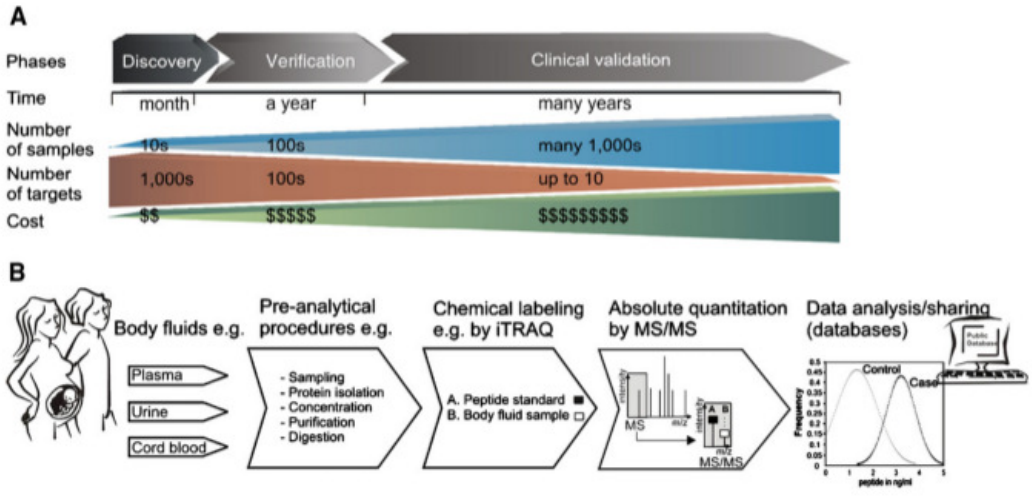

Figure 2.19: Typical proteomics pipeline

Row A describes the current pipeline from discovery to validation that has been implemented for many drugs in big pharma companies to date. Row B describes a possible alternative workflow as well as the application proteomics can play within this workflow [238].

The advantages of proteomics are the high throughput manner of the techniques and the relative cost per data point, especially when compared to other non ”omic” based biological assays.

2.7.2 Proteomics question

With the varied proteomic techniques and applications that have been developed it is crucial to understand which techniques should be used for the proteomic question that is to be interrogated. Thus having a clear understanding of the key differences in shotgun and directed approaches is fundamental for any keen proteomic researcher. If the biological question involves attempting to understand how drugs can perturb a biological pathway for a particular system, then a discovery approach would be best suited. However if the biological question is to validate whether a particular protein can be used as a biomarker for identifying a disease outcome then a directed approach would be a better solution. As technology develops and mass spectrometers improve the need for quality sample preparation in order to maximise the dynamic range that is analysed will diminish slightly, however currently sample preparation is one of the most critical steps in performing a successful proteomic experiment - provided the correct technique is chosen for the biological question concerned.

The aim for this thesis was to determine *ex vivo*, using PBMCs, the molecular basis of the differences in the immune responses to *M.tb* that occur *in vivo* between TB-IRIS and TBART patients. The main outcomes being to:

1. Identify a potential protein biomarker for the IRIS condition
2. Provide the basis for a better understanding of the molecular origin of TB-IRIS
3. Serve as the basis for development of more targeted suppression of TB-IRIS.

Thus, a high throughput proteomic approach was utilised as this approach provides the best opportunity to analyse the changes in the proteomic profile at the broadest possible level that occur within these PBMCs when challenged by H37Rv antigen and/or treated with dexamethasone. In order to increase proteomic coverage in the most cost effective manner, a middle out fractionation strategy has been employed in conjunction with a quantitative label free LC-MS/MS approach. Due to cost and sample scarcity considerations patient samples have been pooled for this analysis. Further details on the exact methodology follows in the following Chapter.

3 Materials and Methods

3.1 Patient recruitment

Blood samples were drawn from patients that were admitted to Brooklyn Chest Hospital in Stanberry Road, Ysterplaat, Cape Town after informed consent was obtained. Patients were enrolled into a broad ranging study and assessed at defined intervals for the development of paradoxical TB-IRIS and other clinical events using the consensus clinical case definition [96]. Within this study, bloods were drawn from enrolled patients pre-ART initiation, on the day of ART initiation, within three days of enrollment, and then subsequently at one, two, three, four, eight and 12 weeks after initiation of ART. Patients were then clinically diagnosed as either having developed paradoxical TB-IRIS or as TBART responders by Dr Graeme Meintjes. Dr Meintjes was in charge of patient recruitment as well as determining if a patient satisfied the criteria required to participate in the study (listed below), Rene Goliath was the nurse in charge of securing patient blood samples. The experimental analyses undertaken for this thesis was performed on bloods obtained in week three of this process, Figure 3.1. This study was nested within a larger study entitled "Prospective cohort study of hospitalised HIV-TB co-infected patients at Brooklyn Chest Hospital" that has been granted ethical clearance by the University of Cape Town Research Ethics Committee (REC 049/2009)). Recruitment criteria for the study were as follows; all the inclusion criteria are required and if any of the exclusion criteria are met then the patients were excluded.

Inclusion criteria:

1. Patients diagnosed with TB on the basis of microbiological investigation or highly suggestive clinical and radiological features
2. Patients who reported symptomatic improvement after commencement of TB treatment
3. Patients who were HIV-infected and qualified for anti-retroviral treatment (ART), as defined within South African Department of Health guidelines
4. Patients who were willing and able to sign the informed consent form (ICF)

Exclusion criteria:

1. Patients with previous ART experience (excluding anti-retroviral for PMTCT)
2. Patients infected with rifampicin resistant TB
3. Patients younger than 18 years old
4. Pregnant patients
5. Patients who were confused or unable to understand the ICF
6. Patients with a haemoglobin count of less than 6.5 g / dL

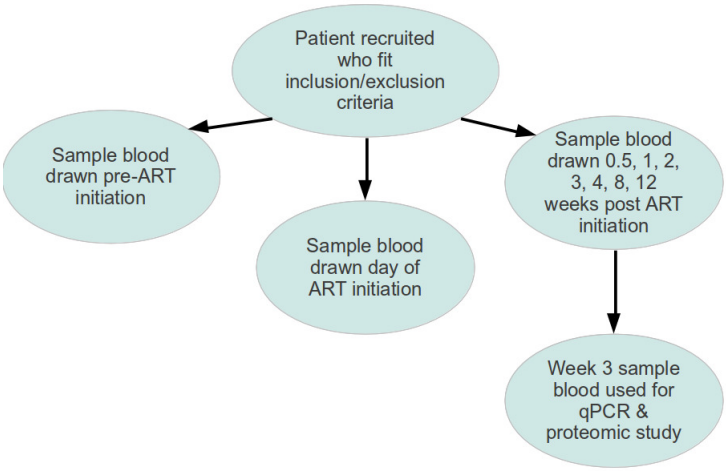

Figure 3.1: Cohort recruitment

3.2 PBMC preparation

Blood samples were drawn into Sodium-heparin vacutainers and were processed in a Bio-safety Level 2 (BSL 2) facility within 8 hours of being drawn, using a standard Ficoll/Histopaque density gradient centrifugation protocol, briefly described below:

Between 10 mL and 15 mL of patient sample blood was mixed with an equal volume of Dulbecco's Phosphate Buffered Saline (PBS, Sigma cat. no. D8537) in a 50 mL Falcon tube. The resultant PBS/blood mixture (between 20 mL and 30 mL) was carefully layered onto 10 mL of Ficoll-Paque™ (GE Healthcare cat. no. 17-1440-03) in a new Falcon tube. The mixture was

centrifuged at 700 x g for 20 minutes at room temperature (brakes off). The characteristically thin and milky white middle phase (normally approximately 5mL in volume), containing the PBMCs, was removed and added to 10 mL of RPMI-1640 (Sigma cat. no. R8758) in a new Falcon tube. Once completed this volume was topped up to 30 mL using RPMI-1640. The cells were then pelleted at 600 x g for 10 minutes at room temperature (brakes on). The supernatant was discarded and the cells were re-suspended in 10 mL RPMI-1640 and a 20 µL aliquot was removed for cell counting (described in section 3.2.1). The cells were spun down at 600 x g for 10 minutes at room temperature (brakes on) and the pellet was re-suspended in 400 µL of RPMI-1640, after which, 500 µL of cell freeze solution, comprised of 20 % DMSO and 80 % FCS, was added dropwise. The solution was then transferred to a Nunc vial and placed in a Mr Frosty™ (Thermo Scientific cat. no. 5100-0001) at -80 °C overnight, before being transferred to a liquid nitrogen tank for long term storage.

3.2.1 Cell counting

Cell counting was performed using a standard Fast-Read 102™ counting chamber microscope slide (Hycor Biomedical cat. no. 1482207):

These standard counting chamber slides consist of 10 counting chambers per slide. Each chamber contains ten 4 x 4 grids which are used to count the number of cells within each block's perimeter. The volume above each 4 x 4 grid is 0.1 μL. Cells counts were performed using the 20 µL aliquot that was removed in the PBMC extraction described above which was added to 20 µL of 0.4 % trypan blue (Sigma cat. no. T8154), forming a 1:1 dilution. The counting chamber in the slide was loaded using 10 µL of this solution. Counts were determined using two rows of the chamber, containing eight blocks per row. The total number of cells, in the 10 mL RPMI-1640 PBMC solution from which they were removed, is obtained by multiplying the total number of cells counted across two rows by the dilution factor when using the trypan blue and then working back from the volume above the blocks counted (0.1 μL) to the volume of the RPMI-1640 PBMC sample solution (10 mL). Formula 3.1 was used to determine the concentration of PBMCs in the sample solution.

Algorithm 3.1 Number of cells in RPMI-1640 PBMC solution

Number of PBMCs solution = [Total cells counted across two rows of four blocks] x 2 x 10^5

3.3 PBMC culture: general conditions

The frozen PBMCs were processed in batches of no more than four samples at a time. Cells were defrosted from liquid nitrogen storage by rapidly bringing their temperature to 37 °C using an incubator. The media was then exchanged for one that was dimethylsulfoxide (DMSO) free by centrifuging and replacing the supernatant with RPMI-1640 containing 10 % fetal calf serum (FCS), otherwise referred to as R-10. The cells were placed an incubator at 37 °C overnight under 5 % CO_2 atmosphere. The following day the cells were pelleted (600 x g, 10 minutes, room temperature), re-suspended in R-10 and counted (as previously described in Section 3.2.1). Post counting, the cells were pelleted and re-suspended in R-10 to a final concentration of 2 x 10^6 PBMCs/mL, then plated at a final quantity of 100 000 PBMCs / well in sterile 96 well round bottom cell culture plates with lids (Costar, Corning, Cambridge, MA, USA - Cat no. 3595). This was done in order to minimise sample loss during protein and RNA extraction protocols. All PBMC cultures for this study were performed in the presence of HAART. The HAART cocktail used for cell culture was a combination of three anti-retrovirals, namely; lamivudine (3TC), efavirenz and zidovudine (AZT), all of which were solubilised appropriately and combined into a stock solution. The various cell culture conditions are shown below in Table 3.3 for the qPCR work and in Table 3.7 for the proteomics work.

ARV concentrations were selected based on two previous publications specifically dealing with these three drugs, either in various combinations with one another, or individually [239, 240]. Based on these publications it was decided to use the following culture concentrations for efavirenz, 3TC and AZT respectively: 115 nM, 9 μM and 5 μM,which are considered close approximations to the maximum serum concentrations of these drugs *in vivo*.

Culture Reagent		**Final concentration**
ARVs	3TC	9 μM
	Efavirenz	115 nM
	AZT	5 μM
Dexamethasone		15 ng/mL
H37Rv		250 000 CFUs/mL

Table 3.1: Final condition-specific reagent concentrations per well

The concentration of dexamethasone was determined as follows. It has been shown that rifampicin affects the bioavailibility of prednisolone *in vivo* [241] and the C_{max} for prednisolone in the presence of rifampicin was found to be in a range of between 100 ng/mL to 1000 ng/mL [241]. Rifampicin reduces the effectiveness of certain p450 enzymes, most notable CYP3A4, to

metabolise drugs in the body - either through increased clearance of co-administered drugs or by inhibition of interaction with the p450 enzymes [242, 243]. Dexamethasone is metabolised by CYP3A4 and as such dosage for patients receiving dexamethasone whilst being treated with rifampicin should be increased [244]. Dexamethasone is the stable analogue of prednisolone, which is the pro-drug of prednisone. According to the South African Medicines Formulary dexamethasone is thought to be approximately 6.7 times stronger than prednisone or prednisolone [245]. Thus, mathematically, the comparative effective range for dexamethasone is between 14.9 ng/mL and 149.25 ng/mL as described in the study by McAllister [241]. A separate study specifically involving the effects of dexamethasone on PBMCs *ex vivo* was performed using a concentration of 13 ng/mL [246]. It was therefore decided to use a concentration of 15 ng/mL of dexamethasone for the *ex vivo* PBMC cell culture work in order to mimic as closely as possible the expected *in vivo* concentrations in TB-IRIS and TBART patients who by definition are on rifampicin treatment.

When determining the antigen load for re-stimulation of the cultured PBMCs it was decided to use a theoretical multiplicity of infection (MOI) for the *M.tb* antigen (strain H37Rv). It was decided to use a theoretical MOI of 5:1 (antigen:target) as this would ensure that most of the macrophages would be exposed to at least one bacilli whilst concurrently ensuring that the system was not overwhelmed with too much antigen. The base assumption being that of the 100 000 PBMCs per well, approximately 10 000, or 10 %, of the population could be expected to be macrophages. Thus with an MOI of 5:1 it was decided to use 50 000 colony forming units (CFUs) of heat killed H37Rv for this study. Heat killed H37Rv was obtained by heating a solution of a known concentration of *M.tb* to 80 °C for 4 hours.

Cells were cultured in a final volume of 200 μL in R-10. Each well contained 100 000 PBMCs as well as appropriate concentrations of anti-retrovirals (ARVs) and if required Dexamethasone and/or heat-killed H37Rv. Individual stock solutions (Table 3.2) for the different conditions were prepared such that each well contained 50 μL PBMC stock solution, 50 μL condition specific stock solution and 100 μL of R-10. The final culture concentrations in each well for the individual reagents can be seen in Table 3.1.

Condition	**Conditional stock solution volumes (μL)**				
	ARVs	**Dexamethasone**	**H37Rv**	**R-10**	**Total vol.**
+ Dex / + H37Rv	3	20	20	7	50
+ Dex / - H37Rv	3	20	-	27	50
- Dex / +H37Rv	3	-	20	27	50
- Dex / - H37Rv	3	-	-	47	50

Table 3.2: Condition-specific stock solution volumes

After culturing, viable cells were counted (as per Section 3.2.1) to ensure no bias in cell quantities per sample in downstream analysis. An analysis was also performed to determine the potential for selective depletion of monocytes through adhesion to the cell wall. Cell recoveries were compared testing the effectiveness of using ice cold 5 mM EDTA versus ice cold PBS. There were no measurable differences (using cell counts of recovered cells compared to seeding amounts) for either so it was decided to use ice cold PBS when rinsing out culture wells.

3.4 Quantitative real-time PCR range-finding experiment

Before the proteomic experiment could be performed, the optimal culture time for proteomic analysis needed to be determined. However it was deemed too costly to determine the optimal time point by LC-MS/MS so it was decided that the best method to use would be quantitative real-time PCR (qPCR), specifically looking at the variation in expression profiles of a number of genes across four pre-determined time points. qPCR is a robust technique that allows for the quantitation of a gene product based on the cycle time required for that gene product to be detected at a particular threshold. qPCR can be used to determine either relative or absolute expression levels particular target genes, depending on the experimental design. The basis for determining the quantity of the gene copy number is based on the principle that each PCR cycle doubles the quantity of a particular gene product and so at any given cycle number, the amount of product formed is directly related to the quantity of the gene available for replication at the start of the PCR experiment. The changes in expression levels can therefore be empirically determined as an absolute value (providing a standard curve for a known product is used) or in relative terms across samples (e.g. the same sample but at differing time points). For the purposes of this work, relative quantitation of a set of target gene expression levels was sufficient as the purpose of the experiment was to determine which of the four potential culture time points would be best suited for the proteomic work flow.

The first set of cell cultures were set up for a qPCR range-finding experiment (Table 3.3) to determine the optimal time point for a proteomic investigation. The qPCR experiment involved using five TB-IRIS patient samples and five TBART patient samples cultured individually under four conditions (plus and minus re-stimulation with heat-killed *M.tb* H37Rv; plus and minus treatment with Dexamethasone) across four separate time points (0, 6, 20 and 44 hours) post restimulation.

Condition	0 hours	6 hours	20 hours	44 hours
+ Dex / + H37Rv				
+ Dex / - H37Rv				
- Dex / + H37Rv				
- Dex / - H37Rv				

Table 3.3: Culture conditions for qPCR experiment.
Five TB-IRIS samples and five TBART samples were cultured individually in the presence (+ H37Rv) and absence (- H37Rv) of restimulation with heat-killed TB antigens (H37Rv) as well as in the presence (+ Dex) and absence (- Dex) of Dexamethasone.

For clarity, Table 3.4 defines what culture conditions have been used and how they have been abbreviated when referenced in this thesis.

Patient label	Dataset labels	Culture conditions
TB-IRIS or TBART	MM (minus / minus)	Minus dexamethasone / Minus re-stimulation with H37RV
	MP (minus / plus)	Minus dexamethasone / Plus re-stimulation with H37RV
	PP (plus / plus)	Plus dexamethasone / Plus re-stimulation with H37RV

Table 3.4: Culture conditions and corresponding data labels

3.4.1 RNA extraction

PBMCs cultured under each condition and for each length of time were processed individually in parallel. The cells were washed twice in PBS (volume times) and then pooled post culturing according to common time point and condition and TB-IRIS or TBART origin, yielding a total of 32 pools. Each pool contained approximately 500 000 cells from which RNA was extracted immediately. A pooling strategy was adopted for both the qPCR and the subsequent proteomic work as a combination of the scarcity in available sample as well as the exponential increase in machine run time for mass spectrometry that would be incurred using non-pooled samples necessitated this.

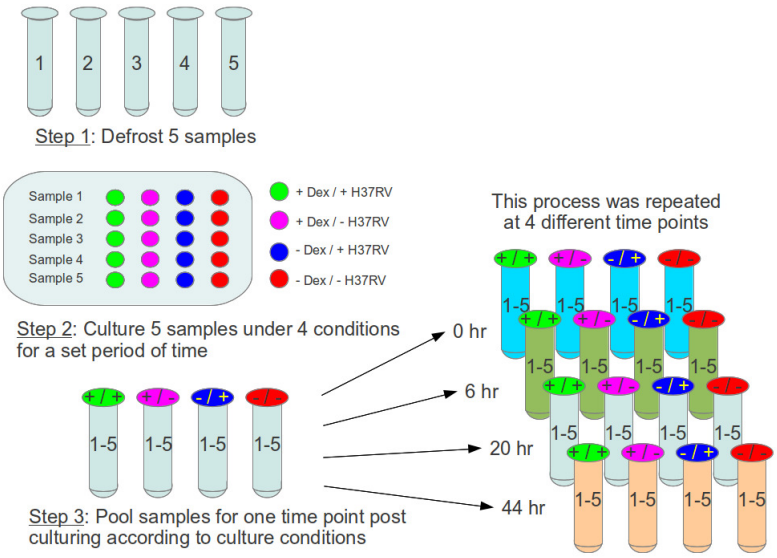

Figure 3.2: Basic workflow of sample culturing for qPCR experiment

The culture workflow indicated above was conducted for five TB-IRIS patient samples and five TBART patient samples, resulting in 32 pooled samples (16 TB-IRIS and 16 TBART) across 4 time points that were then used to extract RNA for the qPCR time-ranging experiment.

RNA was extracted from the pooled cells using a standard QIAzol (Qiagen, Hilden, Germany - Cat. no. 79306) extraction protocol as described by the guidelines provided with the reagent (`http://www.qiagen.com/literature/render.aspx?id=375`). As per the reagent protocol: 5 - 10 x 10^6 cells can be extracted in 1 mL QIAzol. Previous cell cultures resulted in 500 000 PBMCs per condition being generated for RNA extraction. Thus 200 µL QIAzol was added to each pool of 500 000 PBMCs in a 1,5 mL tube and gently triturated. To this, 40 µL of chloroform was added and the eppendorf was gently inverted to mix before being incubated on ice for 10 minutes. Insoluble debris was removed by centrifuging the sample at 10 000 x g at 4 °C for 10 minutes. The aqueous phase was transferred to a new 1.5 mL tube before adding 100 µL isopropanol, to precipitate the RNA, and was incubated at -20 °C overnight. The following day the RNA was pelleted at 8 000 x g at 4 °C for 30 minutes. The supernatant was discarded and the RNA pellet was washed in 200 µL 75 % ethanol. The RNA was pelleted once more by centrifuging at 8 000 x g at 4 °C for 20 minutes before being re-suspended in 30 µL RNAse free water. The RNA was quantified using a Nanodrop™ (A_{260} / A_{230} and A_{260} / A_{280}) and then stored at -80 °C. To improve the yield and stability of RNA during the extraction protocol, the area and equipment that where utilised for the extractions were cleaned using RNAse AWAY™ (Sigma cat. no. 83931).

3.4.2 Quantitative real-time PCR

Quantitative real-time PCR, sometimes referred to as RT-PCR, was performed on the extracted RNA using a one step RNA-Ct kit (Applied Biosystems, Foster City, CA, USA - Cat. no. 4393463) on a Roche LightCycler™ 400 qPCR machine. The RNA was defrosted and diluted to a final concentration of approximately 2.4 ng/mL ensuring that each well in the 384 well qPCR plate contained 10 µg of RNA. The basic components of each well per plate was based on Table 3.5.

Reaction component	**Volume (µL) / Reaction**
TaqMan® RT enzyme mix (40x)	0.25
TaqMan® RT-PCR mix (2x)	5
TaqMan® PDAR probe (20x)	0.5
Sample RNA template	4.25
Total	10

Table 3.5: Reagent volumes per well for each qPCR plate

The qPCR plates were prepared using a QIAgility robotic plater (Qiagen, Hilden, Germany) and the corresponding software (Version 4.11.0). For each mRNA to be quantified, total RNA was plated in triplicate for each time point, condition and sample type (TB-IRIS and TBART). The expression of the following genes were successfully analysed: IL 8, IL 12, IFN-γ and TNF-α. The qPCR machine cycling conditions were as per Table 3.6. The constitutively expressed GAPDH gene was used as a reference house-keeping gene for this study and expression of the target gene was normalised to this reference gene in all the samples studied [247].

Step	**Temp (°C)**	**Duration**	**Cycles**
Reverse transcription step	48	15 min	Hold
Enzyme activation	95	10 min	Hold
Denature	95	15 sec	40
Anneal / Extend	60	1 min	

Table 3.6: qPCR machine cycling conditions

The qPCR plate was laid out as per Figure 3.3, the probes were donated from the Wilkinson lab based at the Institute for Infectious Diseases and Molecular Medicine (IIDMM). Probes for the following genes were obtained: IL 2, IL 6, IL 8, IL 12, IFN-γ, TNF-α and GAPDH. The genes were spread across 2 consecutive plates that were plated and run on the LightCycler™ consecutively on the same day. A repeat qPCR experiment (technical replicate) was performed

on a separate plate for the 20 hour time point for IL 2, IL 6, IL 8, IL 12, TNF-α, IFN-γ and GAPDH after analysis of the first qPCR run showed inconsistent results for this time point.

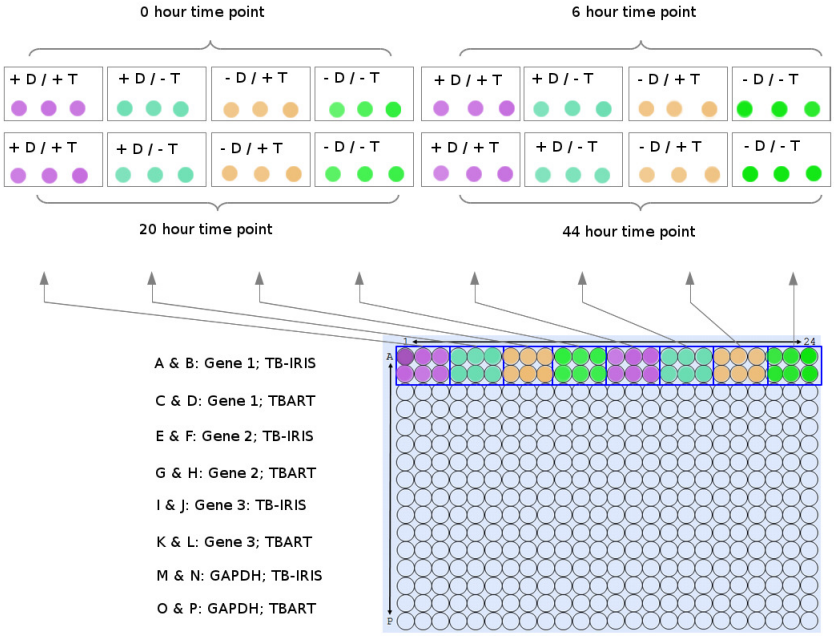

Figure 3.3: Basic setup for qPCR plate

The basic plate setup for the qPCR experiment. Rows A to N contained gene probes for test genes and the final two rows (O &P) contained gene probes for a reference house keeping gene (GAPDH). Each gene was tested using RNA isolated from four distinct time point samples. Each time point was further broken down into four culture conditions. D = Dexamethasone, T = H37Rv, + = cultured in the presence of, - = cultured in the absence of.

3.4.3 qPCR data analysis

The threshold cycle (Ct) required to reach a specified, common PCR product yield was determined in triplicate for each target gene (IL 8, IL 12, IFN-γ, TNF-α) as well as for the reference gene (GAPDH) in each of the 32 samples. For each pooled sample the target gene triplicate Ct data was normalised for total RNA quantity by subtracting the mean Ct number for GAPDH from the mean Ct number for the specific target gene (Ct 'target gene' - Ct GAPDH), giving a normalised mean Ct value (ΔCt) for all the target genes.

Before comparing external perturbation induced variation in gene transcription levels per time point across TB-IRIS and TBART groups, genes were standardised against their non-perturbed baseline condition (- Dex / - H37Rv); at the same time point. This was achieved by subtracting the normalised ΔCt target gene for the baseline condition (- Dex / - H37Rv) from the normalised ΔCt of the target gene for the target condition (one of + / +, + / - or - / +). Thus for example,

ΔΔCt (TB-IRIS; 6 hour; IFN-γ; + / +) is obtained by subtracting ΔCt (TB-IRIS; 6 hour; IFN-γ; - / -) from ΔCt (TB-IRIS; 6 hour; IFN-γ; + / +).

After normalisation and baseline subtraction was performed, the difference in expression levels between the TB-IRIS and TBART groups was determined for each of the three non-baseline conditions (+ Dex / + H37Rv, + Dex / - H37Rv and - Dex / + H37Rv) at a given time point by subtracting ΔΔCt TBART sample target gene from the corresponding ΔΔCt TB-IRIS sample target gene for each time point resulting in a ΔΔΔCt value for the target gene at a specific time point for a specific condition.

Due to the exponential nature of PCR amplification, the ΔΔCt values relate to the difference in absolute mRNA quantities according to the relationship $2^{-\Delta\Delta Ct}$. For simplicity, the analysis of trends was performed using the ΔΔCt values themselves, however it should be noted that a negative ΔΔCt value indicates an increase in transcription levels and a positive ΔΔCt value indicates a decrease in transcription levels.

3.5 Proteomic experiment

3.5.1 Method development

Prior to defrosting TB-IRIS and TBART patient PBMCs for culturing in preparation for the drug and re-stimulation perturbation experiment illustrated in Figure 3.5, freshly isolated PBMCs obtained from volunteers were used to test method development as outlined below. A number of cell lysis and protein extraction buffers were tested to determine which buffer would provide the highest and most diverse yield of proteins from a sample of PBMCs. There were three broad passages of method development, each of which was directly related to the type of mass spectrometer that was used for that passage of work.

3.5.1.1 MALDI ToF/ToF workflow

Extraction optimisation: The original mass spectrometer that was available for this study was a 4800 MALDI-ToF/ToF (Applied Biosystems) that was available through the Centre for Proteomic and Genomic Research (CPGR). The original approach that was used involved iTRAQ reagents. Consequently there was a need to ensure that buffers containing primary amines (the most common primary amine based buffers being Tris base and ammonium bicarbonate) were excluded or adapted to accommodate the iTRAQ chemistry.

The initial extraction protocol that was used, was derived from the work of Skopeliti *et al.* [248]. This involved cell lysis using a 3-[(3-cholamidopropyl)dimethylammonio]-1-propanesulfonate (CHAPS) based lysis buffer adapted by replacing 50 mM Tris-Cl pH 8 with 100 mM tri-ethyl ammonium bicarbonate (TEAB) as the buffering solvent. Figure 3.4 is a simplified outline of the protocol and brief description of the workflow described by Skopeliti *et al*.

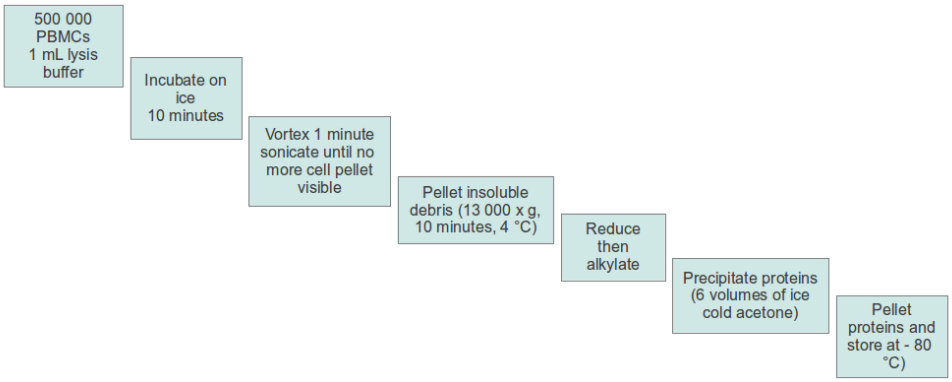

Figure 3.4: Simplified protein extraction protocol described by Skopeliti et al.

The altered lysis buffer used for initial protein extractions consisted of 100 mM TEAB containing 2 % CHAPS, 15 mg/mL DTT, 2 mM $MgCl_2$, 200 U/mL benzonase and a protease inhibitor cocktail (Roche cat. no. 05892970001). Proteins were extracted in 100 μL lysis buffer as per the protocol in figure 3.4. Protein yields from 1 x 10^6 PBMCs were typically between 60 - 80 μg. A number of extractions were performed and the protein pelleted however, based on the standard operating procedures implemented by the CPGR, tryptic digest had to be performed by employees only. Consequently, pelleted proteins were transferred to the CPGR for re-solubilisation, tryptic digestion and MS analysis. The issue of protein re-solubilisation for tryptic digestion led the CPGR to develop a new extraction protocol.

Briefly: Between 5 x 10^5 and 2 x 10^6cells were lysed in 50 μL lysis buffer consisting of 500 mM TEAB containing 0.05 % deoxycholate (DOC), 1 % *n*-octyl 3-D glucopyranoside (OGP) and 4 M guanidine-HCl. The lysate was sonicated in a sonicating water bath until the cells dissolved, insoluble debris was removed by centrifugation. The proteins were precipitated out of the supernatant using 4 volumes of ice cold acetone at - 20 °C overnight. The protein precipitate was pelleted and the supernatant removed. The pelleted proteins were then dissolved in 20 μL of dissolution buffer consisting of 500 mM TEAB, 6 M guanidine-HCl. The DOC protocol led to an increase in the amount of total protein extracted. Using the DOC extraction protocol on 5 x 10^5 PBMCs resulted in protein extraction yields of approximately 60 - 80 μg of crude total protein.

Tryptic digestion: The protocol for tryptic digestion that was performed by the CPGR is as follows. An aliquot of 5 μL of sample at a concentration of 20 µg / μL was placed into 1,5 ml centrifuge tube. The volume was adjusted to 10 µl by adding 5 μL 50 mM TEAB. The sample was reduced by adding in 1 μL 100 mM TCEP and incubated for 1 hour at 60˚C. The sample was allowed to cool down to room temperature before alkylating by adding 1 μL of 100 mM S-methylmethanethiosulphonate (MMTS) - prepared in 2-propanol - and incubated for 15 min at room temperature. The sample volume was adjusted to 45 µl using 50 mM TEAB. Digestion was performed by adding 5 µl 50 mM TEAB containing 5 µg of trypsin to the sample which was incubated at 37˚C for 18 hours. After incubation, samples were dried down by speedivac in preparation for MS analysis using the MALDI-ToF/ToF.

Nano-LC and plate spotting: All nLC mass spectrometry experiments were performed on a Dionex Ultimate 3000 connected to a robotic plate. For liquid chromatography, separation was performed on a LC Packings column (15 cm, 75 μm ID, 3 μm, C18) that was fitted with a C18 trap column (5 mm, ID 300 μm) at a flow rate of 300 nL / min. The gradient used was as follows: 5 % solvent B for 5 minutes, followed by 5-15 % solvent B in 5 minutes, followed by 15 - 60 % solvent B in 85 minutes, followed by 60 - 90 % solvent B in 10 minutes and kept at 90% solvent B for 10 minutes. Solvent A was 0.15 % tri-fluroacetic acid (TFA) in 98 % water, and solvent B was 0.12 % TFA in 80 % acetonitrile (ACN).

MALDI-ToF analysis: The mass spectrometer was operated in data-dependent mode to automatically switch between MALDI-ToF-MS and ToF/ToF-MS/MS acquisition. Data was acquired using the 4000 Series Explorer software package. The matrix used for the MALDI plates was α-Cyano-4-hydroxycinnamic acid. A fixed laser intensity of 4500 Hz was used and a total of 600 shots per spectrum was set for MS mode. The number of sub-shots per spectrum was set to 60 in MS mode. The laser search pattern was set to random with no bias towards the centre or edge of the spots. Timed ion selection was enabled and the precursor ion scan MS spectra (m/z 800 – 3000) were acquired in the MALDI-ToF with resolution R = 17 000 - 22 000. The weakest pre-cursors were selected first, with a minimum signal to noise (S/N) threshold of 35, for collision induced dissociation. Fraction-to-fraction precursor mass tolerance was set at 100 ppm. Internal calibrants (angiotensin 1, *m/z* 1296.685; glu-1-fibrinopeptide, *m/z* 1570.677; neurotensin, *m/z* 1672.925; ACTH clip 19-39, *m/z* 2465.198) enabled accurate mass measurement in both the MS and MS/MS modes. The MS reflector was operated in positive mode. For MS/MS, 800 shots per spectrum and 40 shots per sub-spectrum were set. Ion selection threshold was set such that at least 5 peaks appeared above an estimated S/N ratio of 100.

However the results obtained from the MALDI-ToF/ToF remained unsatisfactory despite the improved extraction protocol.

3.5.1.2 Q-ToF workflow

At this point in time, an opportunity for hands on experience with an Agilent 6530 Q-ToF, acquired by the Department of Molecular and Cellular Biology at the University of Cape Town, arose. This led to the development of a workflow directed towards this instrument. The DOC extraction was utilised but tryptic digestion and peptide fractionation required optimisation.

Trypsin digestion: Proteins extracted using the DOC protocol were reduced by adding 1 μL 105 mM and incubating at 60 °C for 1 hour. The sample was gently mixed and quickly spun down before alkylation using 1 μL of 84 mM tris(2-carboxyethyl)phosphine (TCEP) for 30 minutes at room temperature in the dark. After reduction and alkylation 38 μL of 500 mM TEAB was added, to reduce the guanidine concentration, and briefly mixed and spun down before adding in trypsin at a ratio of 25:1 (protein:trypsin). The sample was then left in a wet chamber at 37 °C overnight. The tryptic digest was stopped the after 18 hours by adjusting the pH to below pH 4 using an appropriate volume of dilute formic acid (FA). The tryptic digest was desalted using PepClean™ C-18 spin columns (Thermo Scientific, cat. no. 89870) as per the manufacturer's instructions. The desalted peptides were dried down in a speedivac and stored at - 80 °C.

A second method of sample preparation and specifically trypsin digestion was also tested. The second method of sample preparation involved using filter aided sample preparation (FASP). Proteins extracted using the DOC method and pelleted by acetone precipitation were re-solubilised in 4 % sodium do-decyl sulfonate (SDS), 100 mM di-thiothreitol (DTT - Sigma cat. no. D9779) in water. The protein suspension was incubated at 95 °C for 20 minutes [249]. A 200 µg fraction, as quantified by Bradford reagent (Fermentas cat. no. R1271), of reduced total protein was then added to a 30 kDa molecular weight cut-off (MWCO) spin filter (Nanosep cat. no. OD030C33) and concentrated down to approximately 30 µL by centrifugation. The decision to use the 30 kDa MWCO spin filters instead of a smaller cut-off size spin filter was based on the elegant work performed by Wiśniewski *et al* [249], which showed that the slightly higher MWCO filters were better for washing off detergent but did not negatively affect the number of small molecular weight proteins (less than 30 kDa) that were identified. The 30 μL retentate was alkylated by adding 500 µL of UA buffer (8 M urea, 0.1 M Tris-Cl pH 8.5) containing 50 mM iodoacetamide (hereafter referred to as IAA), and incubated at 20 °C for 20 minutes. Unreacted IAA was then removed by buffer exchange by adding in 500 µL of UA buffer to the spin filter

retentate and reducing the volume by centrifugation; this was repeated three times. The urea concentration was then reduced to a trypsin compatible level by diluting the spin filter retentate with 500 µL ABC (50 mM Ammonium Bicarbonate) and then re-concentrating the protein, by centrifugation to a final retentate volume of approximately 30 μL; this was repeated three times. Two micrograms (2 μg) of sequencing grade trypsin (Promega cat. no. V5111) was dissolved in 40 µL of ABC and was then added to the retentate, giving a final protein:trypsin ratio of 100:1. The spin filter was incubated in a wet chamber at 37 °C overnight, then transferred to a new 1.5 mL tube and the tryptic peptides were separated from undigested protein and trypsin by centrifugation at 10 000 x *g* at 20 °C for 10 minutes through the 30 kDa MWCO membrane.

Peptide fractionation: To increase proteome coverage, fractionation strategies at the peptide level were tested to see which strategy would yield the highest number of protein identifications.

The first fractionation technique employed was the 3100 OFFGEL Fractionator (Agilent Technologies, Santa Clara, California, Illinois, U.S.A). Optimisation of this technique was performed using the smaller 12 cm strip with a focusing range of pH 4 - 7. Approximately 300 μg of protein was obtained from 3 x 10^6 PBMCs using the DOC protein extraction method and digested using the first trypsin protocol described above. The desalted peptides were then loaded onto the 3100 OFFGEL apparatus as per the manufacturers protocol (`http://www.chem.agilent.com/Library/usermanuals/Public/G3100-90113_OFFGEL_Fractionator.pdf`), and run overnight using the standard "OG12PE01" program.

The second fractionation technique that was tested was high pH reverse phase chromatography. This strategy was optimised using a DOC extraction performed on 1.6 x 10^6 PBMCs resulting in approximately 130 μg of protein. The resultant protein pellet was run through the FASP process and digested with trypsin, as described above, before being desalted on a C-18 spin column and dried down in a speedivac. The peptides were then solubilised in 5 % ACN, 1.25 % TEA (~ pH 10) and run through a purpose manufactured C-18 micro-column. This column was manufactured from a typical SDS PAGE gel loading pipette tip that was twisted to form a fret and then packed with C-18 resin obtained from a Supelco C-18 Discovery column (Supelco cat no. 52601-U). The micro column was prepared for the peptide sample by washing it with approximately 15 column volumes (CV) of 50 % ACN,1.25 % TEA, before being conditioned with approximately 15 CVs of 5 % ACN, 1.25 % TEA. The peptide sample was re-suspended in 40 L of 5 % ACN, 1.25 % TEA and loaded onto the column. The flow through was kept and reloaded onto the column. The column was washed with approximately 5 - 8 CVs of 5 % ACN, 1.25 % TEA. Five stepwise fractions of increasing organic solvent concentration (10 %, 15 %, 20 %, 25 % and 80 % ACN at a constant 1.25 % TEA) were sequentially loaded

onto the column and the flow through collected. The flow through from the sample loading was combined with the 80% ACN fraction, the samples were dried down in a speedivac.

Q-ToF analysis: The 12 p*I* fractions from the OFFGEL Fractionator were collected and desalted before being run on an Agilent 6530 Q-ToF mass spectrometer (Agilent Technologies, Santa Clara, California, Illinois, U.S.A). The Agilent Q-ToF incorporates a n-LC chip-cube system where the LC column is contained on a chip that also contains the ESI needle for the mass spectrometer. All nLC mass spectrometry experiments was performed on an Agilent 1290 Infinity nLC CHIP-cube system connected to an Agilent 6530 Q-ToF mass spectrometer (Agilent Technologies, Santa Clara, California, Illinois, U.S.A) equipped with a nanospray ESI source. Liquid chromatography was performed on a Zorbax 300 SB-C18 column housed in a 0.075 x 150 mm chip, containing a 160 nL enrichment column and with a 5 μm particle size (Agilent Technologies cat. no. G4240-62010), at a flow rate of 300 nL / min. The gradient used was as follows: 3 % solvent B at 0 minutes, followed by 5 % in 0.1 minutes, followed by 8 % in 2 minutes, followed by 35 % solvent B in 60 minutes, followed by 40 % in 67 minutes, followed by 90 % in 67.1 minutes and 90 % solvent B for 4 minutes, before dropping to 3 % solvent B for 20 minutes. Solvent A was 0.1 % FA, 3 % ACN in water, and solvent B was 0.1% FA, 3 % water in ACN.

The mass spectrometer was operated in data-dependent mode. Ionization mode was set to positive electrospray and the scanning range for MS spectra was set at 275 - 2000 *m/z* (MS) and 50 - 2000 *m/z* (MS/MS). A maximum of 10 precursors per cycle was allowed and the rate of acquisition was set to 8 Hz (MS) and 3 Hz (MS/MS). The collision energy for the CID was set at -4.8+3.6 V (precursor *m/z* / 100). In data-dependent LC-MS/MS experiments, dynamic exclusion was used with a 60 s exclusion duration excluded after 1 spectra, the isolation width was set to medium(4m/z) in MS/MS mode. Mass spectrometry conditions were 1.85 kV, with the drying gas temperature set to 325 °C. A reference mass of trace amounts of the calibrant HP-922 (922.0097 *m/z*) were continuously inserted into the ionisation region.

Despite the number of protein identifications increasing in comparison to the MALDI-ToF/ToF results, the number of proteins identified were still very low. The stability of the ESI nanospray appeared to be inconsistent. Agilent has recently replaced the CHIP-cube system and the majority of the ESI source aperture components, at their own cost, in an attempt to increase the stability of the nanospray ESI source.

3.5.1.3 LTQ-Orbitrap workflow

An LTQ-OrbiTrap became available and it was decided to test the high pH fractions that were originally intended for the Q-ToF on the OrbiTrap instead. The desalted and dried down peptide fractions were sent to Dr Salome Smit in the Central Analytical Facility, at the University of Stellenbosch. All nLC mass spectrometry experiments were performed on a Thermo Scientific EASY-nLC II connected to an LTQ Orbitrap Velos mass spectrometer (Thermo Scientific, Bremen, Germany) equipped with a ESI source. For liquid chromatography, separation was performed on a EASY-pre-column (2 cm, ID 100 μm, 5 μm, C18), followed by an EASY-column (10 cm, ID 75 μm, 3 μm, C18) at a flow rate of 300 nL / min. The gradient used was as follows: 5-15 % solvent B in 5 minutes, followed by 15 - 40 % solvent B in 80 minutes, followed by 40 - 60 % solvent B in 10 minutes, followed by 60 - 80 % solvent B in 5 minutes and kept at 80 % solvent B for 10 minutes. Solvent A was 0.1 % FA in water, and solvent B was 0.1% FA in ACN.

The mass spectrometer was operated in data-dependent mode to automatically switch between Orbitrap-MS and LTQ-MS/MS acquisition. Data was acquired using the Xcaliber software package. The precursor ion scan MS spectra (m/z 400 – 2000) were acquired in the Orbitrap with resolution R = 60 000 with the number of accumulated ions being 1 x 10^6. The 20 most intense ions were isolated and fragmented in the linear ion trap (number of accumulated ions 1.5 x 10^4) using collision induced dissociation. The lock mass option (polydimethylcyclosiloxane; *m/z* 445.120025) enabled accurate mass measurement in both the MS and MS/MS modes. In data-dependent LC-MS/MS experiments, dynamic exclusion was used with a 60 s exclusion duration. Mass spectrometry conditions were 1.8 kV, capillary temperature of 250 °C, with no sheath and auxiliary gas flow. The ion selection threshold was 500 counts for MS/MS and an activation Q-value of 0.25 and activation time of 10 ms were also applied for MS/MS.

Middle out optimisation: Based on the positive results obtained using the bottom up method, it was decided to try and improve proteomic coverage by introducing an initial crude protein fractionation step followed by individual and parallel trypsin digestion of the protein fractions and subsequent separate fractionation of the resultant peptides. Two protein fractionation methods were tested. The first was crude sub-cellular fractionation and the second was phosphoprotein enrichment.

Crude sub-cellular fractionation (CSF) involves sequentially extracting location specific proteins from cells using a series of detergent based buffers that gradually strip the various membrane layers off of animal cells and was performed as described by Holden *et al*. [205]. This protocol was performed on duplicate samples containing 3 x 10^6 PBMCs. Each fraction was processed

individually and in parallel and run on a standard 10 % glycine-SDS-PAGE Laemmli. The cytosolic fraction was obtained by lysing 3 x 10^6 cells in a 1.5 mL tube using 400 μL buffer 1 containing 50 mM HEPES pH 7.4, 150 mM NaCl, 25 μg / mL digitonin (Sigma cat. no. D141) and incubated at 4 °C for 10 minutes whilst gently being rotated end over end. The insoluble material was pelleted by centrifugation at 2 000 x *g* at 4 °C for 10 minutes. The supernatant containing cytosolic proteins was removed and the pellet was washed with 1 mL ice cold PBS and pelleted again and the PBS removed. The pellet was re-suspended in 400μL of buffer 2 containing 150 mM NaCl, 50 mM HEPES pH 7.4, 1 % NP40 and incubated for 30 minutes on ice (the suspension was gently agitated every 10 minutes). Insoluble debris was pelleted by centrifugation at 7 000 x *g* at 4 °C for 10 minutes, before the supernatant was removed and kept aside as the membranous organelle fraction. The remaining pellet was washed with PBS and re-pelleted by centrifuging at 7 000 x *g* at 4 °C for 10 minutes. The insoluble debris was re-suspended in 320 μL ice cold buffer 3 containing 150 mM NaCl, 50 mM HEPES pH 7.4, 0.5 % DOC, 0.1 % SDS, benzonase (1 U / mL) and incubated at 4 °C for 1 hour whilst gently being rotated end over end. Post incubation, 40 μL of 10 % SDS and 40 μL of 1 M DTT were added to the suspension. The tube was vortexed and placed in a heating block for 20 minutes at 95 °C. Any insoluble debris was pelleted by centrifugation at 10 000 x g at 4 °C for 10 minutes. The supernatant was removed and kept as the third nuclear membrane and insoluble protein fraction. The 3 separate fractions (cytosolic, membranous orgenelles and nuclear membrane/insoluble proteins) that were obtained were aliquoted into 4 fractions as soon as they were isolated. The first was used for quantitation by Bradford assay, the second was tested for compatibility with the FASP process, the third was run on a gel and the fourth was stored at - 80 °C.

The complexity of any protein sample can be derived from numerous factors, including the number of unique proteins in the sample as well as any post-translational modifications of those proteins. One of the most common PTMs that occurs to proteins is the phosphorylation at either the serine, threonine or tyrosine residues. Phosphorylation has been shown to play a key role in cellular signalling in a number of pathways, from apoptosis to immune mediated cellular signalling. Phosphorylation is among the most widespread post-translational modifications in nature, and it has been estimated that more than 30% of the proteins in a given mammalian cell at some point during their expression are phosphorylated [250]. However due to their charged nature and relatively low abundance, phosphoprotein derived peptides are very difficult to detect in a complex peptide sample. For this reason a phosphoprotein enrichment could be very useful as it would allow a focus in subsequent analysis on phosphoproteins. Phosphoproteins can be isolated from a complex protein mixture via the negatively charged phosphate groups (PO_4^{2-}). Phospho-enrichment was performed, using a CHAPS based buffer, as per the protocol provided (http://www.qiagen.com/literature/render.aspx? id=23717) in the Phosphoprotein Purification Kit (Qiagen, cat. no. 37101). Proteins were extracted from 3 x 10^6 PBMCs, the frozen cells

were defrosted and re-suspended in 3 mL of phosphoprotein lysis buffer (0.25 % CHAPS, benzonase, 25 mM MES pH 6.0, 1 M NaCl) and incubated at 4 °C for 30 minutes. Post-incubation, insoluble debris was pelleted by centrifugation at 10 000 x *g* for 30 minutes at 4 °C. The supernatant was loaded onto the pre-prepared phospho-enrichment column and the flow through was re-loaded onto the column. This step and the subsequent steps were performed at room temperature. After re-loading, the flow through was reserved as a phospho-depleted fraction. The column was washed using 6 mL of phosphoprotein lysis buffer. The phospho-enriched fraction was eluted by adding 2 mL of phosphoprotein elution buffer (50 mM K_2PO_4 pH 7.5 , 50 mM NaCl) to the column and collecting the flow through. The 2 separate fractions (phospho-enriched and phospho-depleted) that were obtained were aliquoted into 4 fractions as soon as they were isolated. The first was used for quantitation by Bradford assay, the second was tested for compatibility with the FASP process, the third was run on a gel and the fourth was stored at - 80 °C.

3.5.2 Cell culture and pooling strategy

Once the proteomic method development yielded positive results using the OrbiTrap, the second cell culture experiment for the proteomic study of TB-IRIS and TBART PBMCs was conducted (Table 3.7). The culturing involved 30 TB-IRIS and 30 TBART patient samples. These samples were cultured, as described in table 3.7, at one time point using the same four conditions as those used for the qPCR time-ranging experiment. The time point was determined by the outcome of the qPCR time-ranging experiment.

Condition	Time point
+ Dex / + H37Rv (+ / +)	20 hour
+ Dex / - H37Rv (+ / -)	20 hour
- Dex / + H37Rv (- / +)	20 hour
- Dex / - H37Rv (- / -)	20 hour

Table 3.7: Culture conditions for proteomics workflow

Samples were defrosted in batches of four, from either TB-IRIS or TBART samples. The cultured PBMCs were processed sequentially in batches of four from their removal from liquid nitrogen storage through to culturing and pooled during PBS washing post culturing. Each condition at the single time point was pooled, i.e. four TBART samples were defrosted and cultured under four separate conditions. The samples were pooled for each condition post-culturing, leaving four pooled patient samples per condition (Table 3.7) that were then stored at - 80 °C.

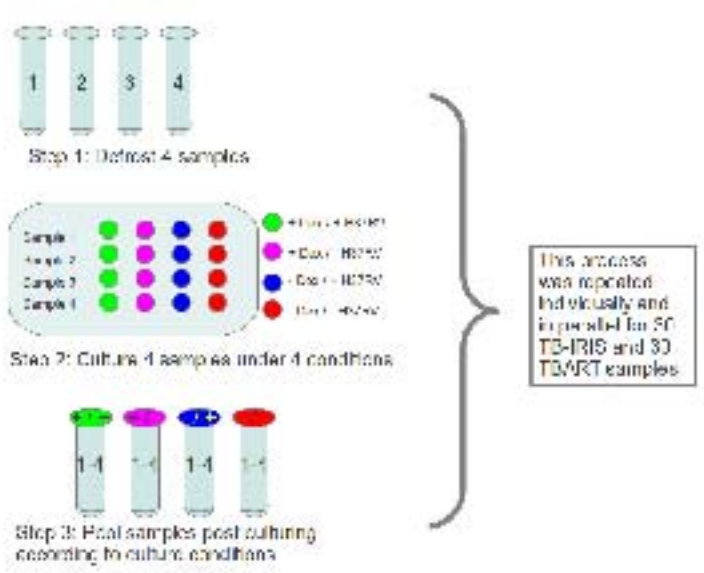

Figure 3.5: Basic workflow for sample culturing for proteomic experiment

A second biological repeat of 6 TB-IRIS patient samples was performed after the insoluble pellets for the 30 TB-IRIS pooled patient samples were misplaced. This meant that subsequent proteomic analysis was performed using the pooled sample of 6 TB-IRIS patients and the pooled sample of 30 TBART patients.

3.5.3 Protein extraction and fractionation

Both the TB-IRIS and TBART samples were processed individually and in parallel to produce two crude fractions during protein extraction. Due to resource restrictions (notably access to enough machine time and the high cost of machine time), it was decided to perform protein extraction and subsequent mass spectrometry analysis on 3 of the 4 TB-IRIS samples (+ Dex / + H37Rv; - Dex / + H37Rv; - Dex / - H37Rv), and on 2 of the 4 TBART samples (- Dex / + H37Rv; - Dex / - H37Rv).

3.5.3.1 Phospho-enrichment:

Phospho-enriched and phospho-depleted protein fractions were obtained from pooled samples of 30 TB-IRIS and 30 TBART patients using the protocol described in subsection 3.5.1.3. The pooled sample of PBMCs, containing approximately 3 x 10^6 cells, for both TB-IRIS and TBART patient were processed individually and in parallel.

3.5.3.2 SDS PAGE

A third protein fraction was obtained by re-solubilising the insoluble cellular debris that was pelleted after the phospho-enrichment extraction, described in subsection 3.5.1.3, using standard 1 x sample application (SAB) buffer - commonly used in Laemmli gels [175] - composed of 40 mM Tris-HCl (pH 6.8), 2 % SDS, 2 mM β-mercaptoethanol, 4 % glycerol, 0.01 % w/v bromophenol blue. This was performed on the pellets of the pooled sample of 30 TBART patient samples and on a biological repeat of 6 pooled TB-IRIS patient samples. The SDS re-solubilisation was performed using 100 μL , for the pooled TBART samples and 20 μL 1 x SAB for the pooled TB-IRIS samples. Re-solubilised samples were heated to 95 °C for 10 minutes before being spun down and loaded onto a standard 10 % glycine-SDS-PAGE Laemmli gel. The TBART samples were loaded in duplicate lanes on a 1 mm thick 10 % glycine-SDS-PAGE Laemmli and the TB-IRIS samples were loaded onto a separate 1 mm thick 10 % glycine-SDS-PAGE Laemmli gel. Both gels were prepared from the same stock solutions in parallel and run separately at 20 mA for 90 minutes.

3.5.4 Protein digestion

Peptides for the phospho-enriched extractions were obtained by using an adaption of the filter aided sample preparation (FASP) method[251]. The FASP process was performed on only the phospho-enriched fractions for both the TB-IRIS and TBART patient samples. The phospho-enriched samples were reduced by adding DTT to a final concentration of 100 mM and boiling at 95 °C for 20 minutes, before being loaded onto the 30 kDa MWCO spin filters and the protocol was continued as described in sub-section 3.5.1.2.

In gel trypsin digestion: The individual lanes from the glycine-SDS PAGE gels were cut into 5 separate equal sized slices. Each gel slice was cut into smaller cubes. The cubes from each gel slice were pooled into 5 separate fractions that were processed individually in parallel. The fractions were washed twice with 300 μL water followed by 300 μL of a 50% (v/v) acetonitrile solution for 10 min. The acetonitrile was replaced with 300 μL 50 mM ammonium bicarbonate and incubated for 10 minutes, and repeated twice more. All the gel fractions were then incubated in 300 μL 100% acetonitrile until they turned white, after which the gel pieces were dried *in vacuo*. The proteins were reduced with 120 μL 10 mM DTT for 1 hour at 57 °C. This was followed by brief washing steps with 300μL 50 mM ammonium bicarbonate,

followed by 300 μL 50% acetonitrile, before the proteins were alkylated in 120 μL 55 mM iodoacetamide for 1 hour in the dark at room temperature. Following alkylation the gel pieces were washed with 300μL 50 mM ammonium bicarbonate for 10 minutes followed by 300μL 50% acetonitrile for 20 minutes, before being dried *in vacuo*. In-gel protein digestion was then carried out by immersing the gel slices in 100 µL of a 10 ng/µL trypsin solution and incubating at 37 °C overnight. The resulting tryptic peptides were extracted from the gel slices twice with 100μL 70% acetonitrile, 0.1% FA for 30 minutes, and then dried in a speedivac and stored at -20 °C. The dried peptides were re-solubilised in 5% acetonitrile, 0.1% formic acid in preparation for mass spectrometry.

3.6 Mass spectrometry

Mass spectrometry was outsourced to the Central Analytical Facility based at Stellenbosch University in the Western Cape, South Africa. In the case of the phospho-enriched and phospho-depleted fractions, the samples were prepared to the point of a purified and desalted peptide digest that was dried down before being transferred to the facility. The insoluble debris fraction samples were transferred to the facility as complete Laemmli gels that had already been stained with colloidal Coomasie Blue (CCB). The Laemmli gels were processed as described in Subsection 3.5.4.

3.7 Data analysis

The RAW data files generated by the mass spectrometer were converted into MS2 files using the MakeMS2 program (`http://proteome.gs.washington.edu/software/makems2/`). Once converted the MS2 files were then analysed using Crux [159]. The main parameters for this particular study were firstly, an FDR of 5 % as determined by Crux using a q-value score of 0.05 or less. The q-value of an individual hypothesis test is the minimum FDR at which the test may be called significant. Secondly, only uniquely mapped peptides (one peptide mapping to one protein only) for protein identifications were used. Crux is not proficient at assigning proteins from degenerate peptides (one peptide mapping to multiple proteins) with high confidence. Other than these two parameters, the standard default settings for the Crux algorithm were used (the parameter file is attached in the Appendix section). Due to the difficulties that Crux has pertaining to degenerate peptides, the final protein assignments based on the identified peptides from the Crux algorithm was performed using the Trans-Proteomic Pipeline (TPP). The TPP algorithm performs far better at assigning proteins from degenerate peptides. The databases that were used for the Crux and TPP searches were: Firstly, SwissProt Human 9606 database - this

database contains no splice variants; secondly, SwissProt Global Proteome Human Organism 9606 - this database contains splice variants; and thirdly, the IPI database (version 3.5).

The Crux search was performed using was the University of Cape Town ICTS-HPC cluster. The output from Crux was then parsed through TPP for protein assignment of the identified peptides using Protein Prophet. The basic data processing workflow can be seen in Figure 3.6.

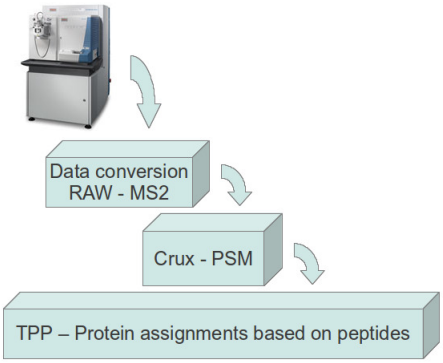

Figure 3.6: Proteomic data processing pipeline

Data processing for proteomic analysis: the RAW data file output of the mass spectrometer was converted into an MS2 file which was then used by Crux to undergo PSM. The identified peptide lists that are generated are then parsed through the TPP for protein assignment from the peptides.

4 Quantitative Results

4.1 PBMC culture optimisation

Prior to any proteomic or qPCR experiments being performed, it was important to verify whether or not any of the *M.tb* antigen (H37Rv) or the drugs (ARVs or dexamethasone) that were used during the *ex vivo* culturing process resulted in any negative or abnormal side effects such as induced cellular apoptosis or decreased cell viability amongst others. To confirm this, PBMCs from three healthy donors were isolated and cultured in the presence and absence of ARVs. The cultures were performed in duplicate and the mean PBMC numbers were compared as the percentage of living cells remaining versus the increasing length of exposure to the ARVs (Figure 4.1). The ARVs were tested on their own and as a combination in conjunction with a negative control (water).

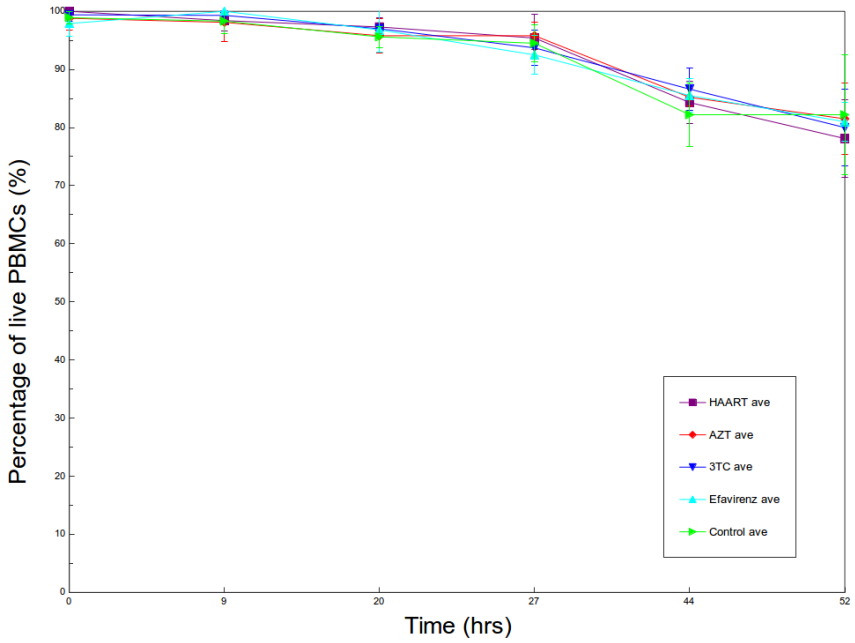

Figure 4.1: ARV cytotoxicity study

The average percentage viability of PBMCs from three healthy donors, cultured in duplicate. The averages are for PBMC viability cultured in the presence of: 115 nM Efavirenz (turquoise), 5 μM AZT (red), 9 μM 3TC (blue), all three ARVs combined (purple) and a control of de-ionised H_2O.

Cellular viability was not significantly affected by any of the individual ARVs or any administered combinations, as the cell viability remained above 80 % for up to 44 hours culturing and dipped nominally below 80 % at 52 hours of culturing, Figure 4.1.

A similar experiment was repeated to test the effect of dexamethasone and H37Rv on their own and in combination with ARVs (Figure 4.2). This experiment was performed on PBMCs isolated from the same three healthy donors previously used for the ARV cytotoxicity experiment, in duplicate with the mean of these repeats being plotted in Figure 4.2. The cell culture time point was not extended beyond 49 hours as a result of the cellular viability dropping below 80 % at the 52 hour time point in the previous ARV cytotoxicity experiment.

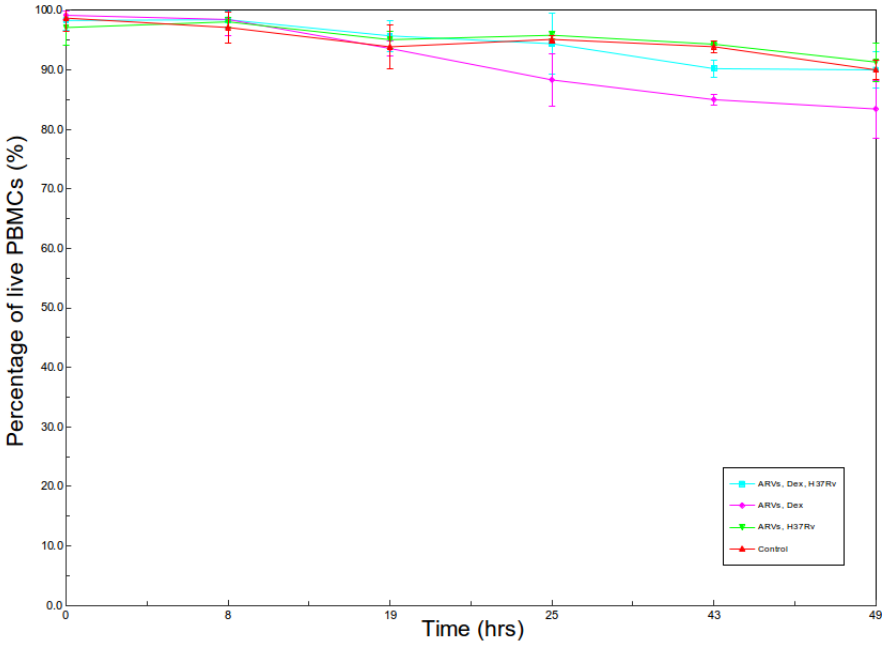

Figure 4.2: Dexamethasone and heat killed H37Rv cytotoxicity study
The average percentage viability of PBMCs from three healthy donors, cultured in duplicate. The averages are for PBMC viability cultured in the presence of: HAART combination and 15 ng / mL dexamethasone and 50 000 CFUs heat killed H37Rv (red), HAART combination and 15 ng / mL dexamethasone (green), HAART combination and 50 000 CFUs heat killed H37Rv (turquoise), and a control of de-ionised H_2O (cyan).

Culturing PBMCs in the presence of various combinations of the drugs (ARVs or dexamethasone) or antigen (H37Rv) had a negligible effect in terms of cell viability in comparison to the control and therefore should not cause any significant changes in a global proteomic comparison since there is no intrinsic bias associated with decreased cell viability on addition of drug or antigen to the culture wells (Figure 4.2).

4.2 qPCR work

Given that TB-IRIS is known to be an inflammatory syndrome characterised by hyper-cytokinemia [252], it was decided to analyse the quantities of the following genes: IL 8, IL 12, IFN-γ and TNF-α, as a simplistic indicator of differences in inflammatory protein expression patterns within each time point for each condition. The analysis was performed in triplicate for each gene at each of the four chosen time points (0, 6, 20 44 hours). The changes in the expression levels were determined as per the $\Delta\Delta$Ct method described in the Methods chapter (Subsection 3.4.3). The difference in gene expression profiles were plotted per time point and the inter-conditional trends were analysed.

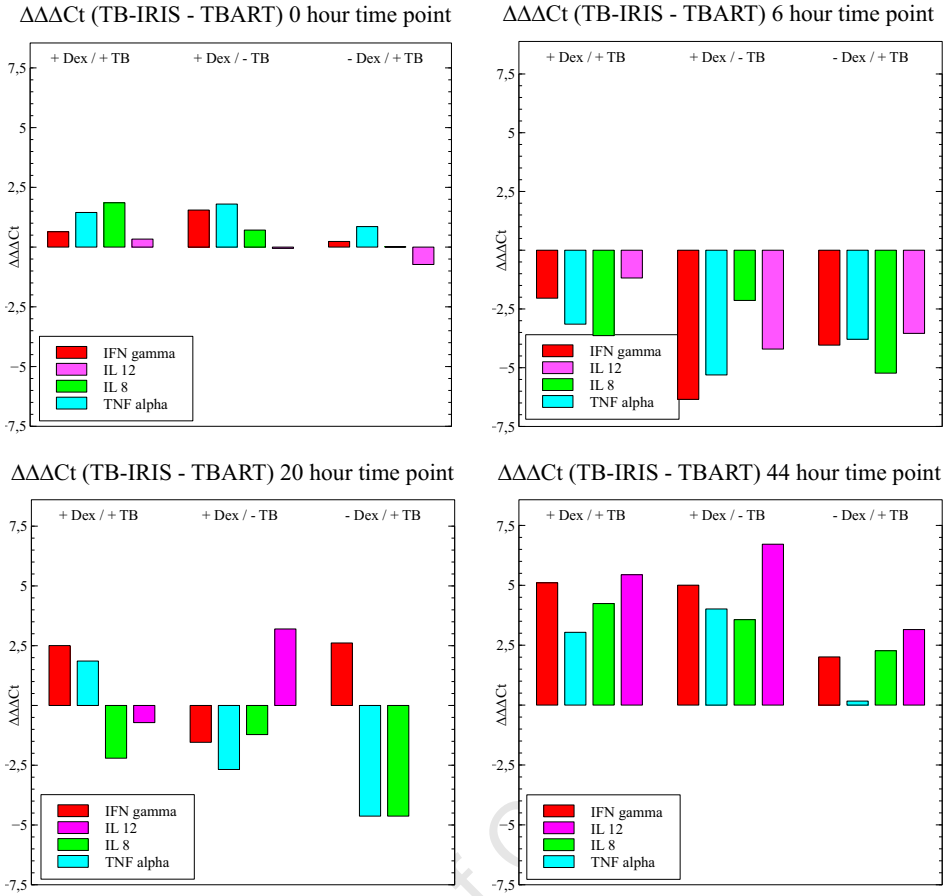

Figure 4.3: qPCR results - intra-condition analysis
Four time points (0, 6, 20 and 44 hours) were analysed for the difference in expression of four genes (IFN γ, TNF α, IL 8 and IL 12) according to the ΔΔΔCt method described in the Methods chapter (Subsection 3.4.3).

The selection criteria for the optimal time point to utilise for the LC-MS/MS based proteomics analysis were based on the following: 1) The expression profile of the analysed genes needed to display high levels of variation - as an indication of an inflammatory response that was not biased one way or another (e.g. a skewed Th1 or Th2 response), 2) A high level of expression of the genes - thus likely indicating a measurable response for this time point. In Figure 4.3 the 0 hour time point is the baseline effect against which the other time points were analysed. The 6 and 44 hour time points both have strong intra-time point trends, with the 6 and 44 hour time points having relatively higher levels of expression (in terms of scale of expression), although the expression profiles are biased in one direction for each time point respectively. The 20 hour time point has a mixed expression profile with a relatively strong scale of expression for the analysed genes, thus being the likely time point to best study the apparent dysregulation of the immune response in TB-IRIS patients.

4.3 Protein extraction method development:

4.3.1 MALDI-ToF/ToF workflow:

In order to establish a viable sample preparation method for MALDI ToF/ToF analysis, initial focus was on a CHAPS based protocol (Methods chapter, Subsection 3.5.1.1). An extraction volume of 100 μL of a 2 % CHAPS based lysis buffer was used for 1 x 10^6 PBMCs after initial attempts using larger volumes of this lysis buffer (up to 1 mL) yielded poor recovery results (the concentration of extracted proteins in the larger extraction volumes was too low and was close to the lower limits of detection for the Bradford assay). The efficiency of the smaller volumes of the extraction buffer were then visually inspected using a standard 10 % glycine-SDS-PAGE Laemmli gel (Figure 4.4). Yields using this extraction protocol were generally consistent and extractions from 500 000 PBMCs resulted in approximately 60 - 80 μg of crude total protein, as quantified by the Bradford assay, and was consistent with previously published yields [248].

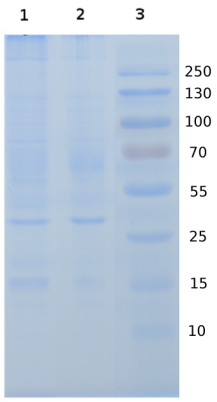

Figure 4.4: Initial iTRAQ compatible protein extractions
The gel pictured was used to run extracts from two different donor samples (lanes 1 and 2) that were extracted using the CHAPS based protocol described by Skopeliti *et al.* [248], both lanes contain approximately 10 μg as determined by Bradford reagent. Lane 3 is a molecular weight marker.

4.3.2 ESI Q-ToF workflow:

The 2 % CHAPS based lysis buffer that was initially used in the MALDI ToF/ToF workflow was carried over to the ESI-MS workflow. However, the 2 % CHAPS based lysis buffer was incompatible with downstream iTRAQ labelling - due to it containing Tris which is effectively a primary amine and interferes with the iTRAQ chemistry - thus the proteins had to be precipitated and re-suspended in an iTRAQ suitable buffer. The iTRAQ compatible buffer also needed to

be compatible with trypsin for efficient enzymatic digestion prior to labelling. The following iTRAQ compatible re-solubilisation buffers were attempted:

The first buffer tried was 500 mM TEAB as this is an ideal buffer for trypsin digestion (~ pH 8.5) and is compatible with the iTRAQ chemistry. However, this buffer failed to re-solubilise a large number of proteins, leaving behind a large protein pellet.

The second buffer evaluated was 8 M urea in 500 mM TEAB. Post-resuspension, the urea concentration was then diluted to 2 M using 500 mM TEAB. This approach still left behind a small insoluble pellet and also increased the risk of carbamylated proteins being generated during the workflow. A similar approach was attempted using 6 M guanidine-HCl in 500 mM TEAB which was subsequently diluted down to 1 M using 500 mM TEAB. Although removing the risk of carbamination, this approach did not perform better in terms of protein re-solubilisation.

We then hypothesised that the 2 % CHAPS (Methods chapter, Subsection 3.5.1.1) based buffer used for the protein extraction may be selective (not producing a complete and representative protein extraction) and that difficulties with downstream re-solubilisation may be attributable to its properties. A new method was tested, substituting a DOC (Methods chapter, Subsection 3.5.1.1) based buffer for the CHAPS based buffer.

To test whether or not the DOC extraction was selective it was tested against lysing a PBMC pellet in standard 1 x Laemmli SAB. The two extractions were performed on 500 000 PBMCs, each isolated from the same donor: the first set was processed using the DOC extraction method and the second set was processed by lysing the cells directly in a 1 x Laemmli SAB. Insoluble debris was removed from both samples and the supernatant from both extractions were then run on a 10 % glycine-SDS-PAGE Laemmli gel (20 mA, 1 hour 30 minutes) , Figure 4.5.

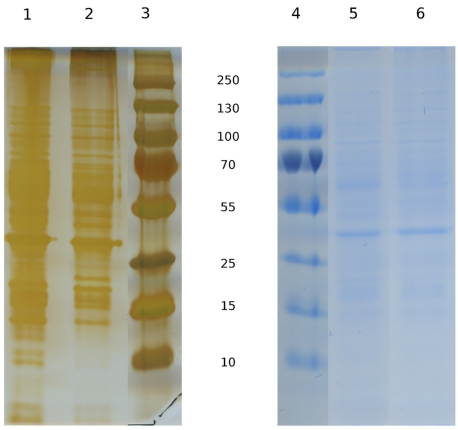

Figure 4.5: Comparison of completeness of extraction
The gel was run and first stained in colloidal Coomassie Blue (lanes 4 - 6) and then stained using the more sensitive silver stain (lanes 1 -3). Each lane contains the following: 1 and 6) Approximately 10 μg of DOC extract, 2 and 5) Approximately 10 μg of SDS/Laemmli extract, 3 and 4) Molecular weight marker - lanes 1 - 3 have been silver stained, lanes 4 - 6 have been stained using Colloidal Coomassie Blue.

It was then decided to evaluate whether the DOC protein extraction protocol was compatible with a standard trypsin digestion protocol for iTRAQ labelling and was capable of producing a large number of well digested peptides that could be easily detected along a broad range when run on a simple gradient through a C-18 reverse phase column on a n-LC system. This was done by performing a test DOC extraction on approximately 1 x 10^6 PBMCs, followed by acetone precipitation of the extracted soluble proteins.

Once precipitated the protein pellet was transferred to the CPGR for tryptic digest and n-LC analysis. This was performed as follows: the protein pellet was re-suspended as per Methods chapter (Subsection 3.5.1.1), for the DOC protocol and reduced in 5 mM TCEP at 57 °C for 1 hour, then alkylated (20 mM iodoacetamide, room temperature, 45 minutes in the dark) and finally digested by adding in trypsin at a ratio of 1:50 (trypsin:total protein) and incubated at 48 °C overnight. The following day the solution was desalted before being analysed on the n-LC.

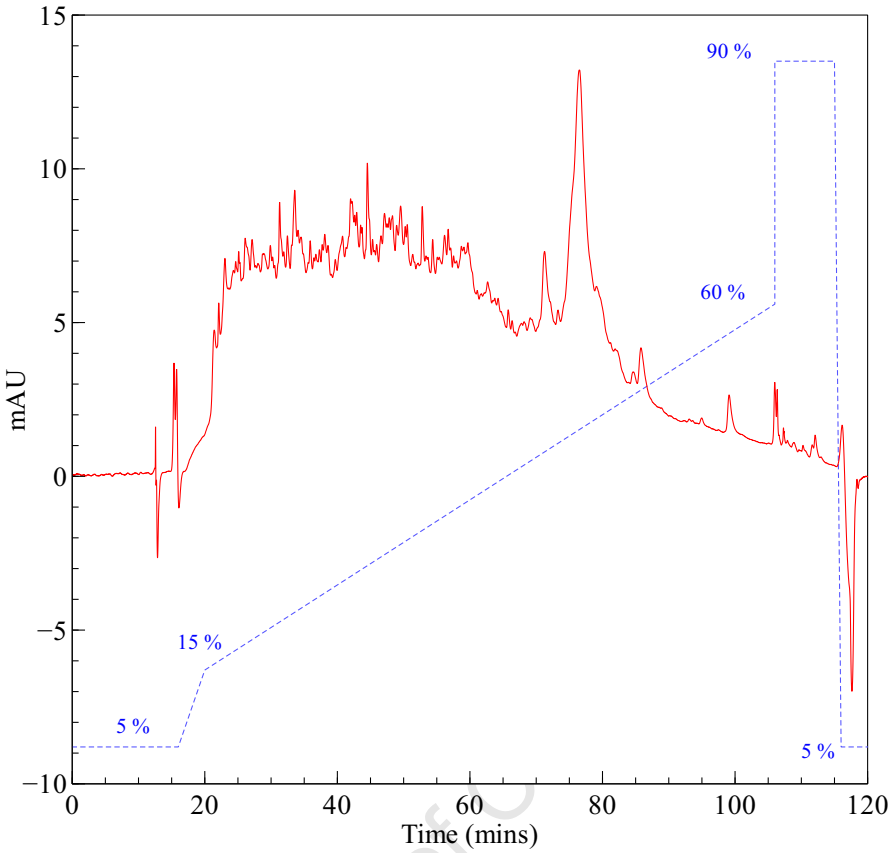

Figure 4.6: Nano-LC digest trace

The UV 214 trace (red line) of a typical protein digest from the DOC method. In this particular instance approximately 5 μg of peptide was loaded onto a Dionex UltiMate® 3000 Nano LC system and run over 120 minutes at a flow rate of 0.300 μL / minute. The solvent gradient (blue line) is for the percentage of solvent buffer B. Solvent buffer B was 95 % ACN, 0.125 % tri-fluoro-acetic acid (TFA) in H_2O.

The success of the tryptic digestion in the protein product extracted using the DOC method led to further method development and optimisation on the fractionation strategies that would be employed on these samples.

4.4 Peptide Fractionation strategies:

In order to tease apart complex proteomic samples for more comprehensive LC-MS/MS analysis, a number of fractionation strategies were tested.

4.4.1 Off-gel fractionation:

Protein extracted from PBMCs via the DOC protocol was digested with trypsin and desalted as above. An aliquot of the tryptic peptides was removed before loading 300 μg onto the Agilent 3100 OFFGEL fractionator. The resultant MS spectra of the whole peptide lysate can be seen in comparison to two of the OFFGEL fractions in Figure 4.7.

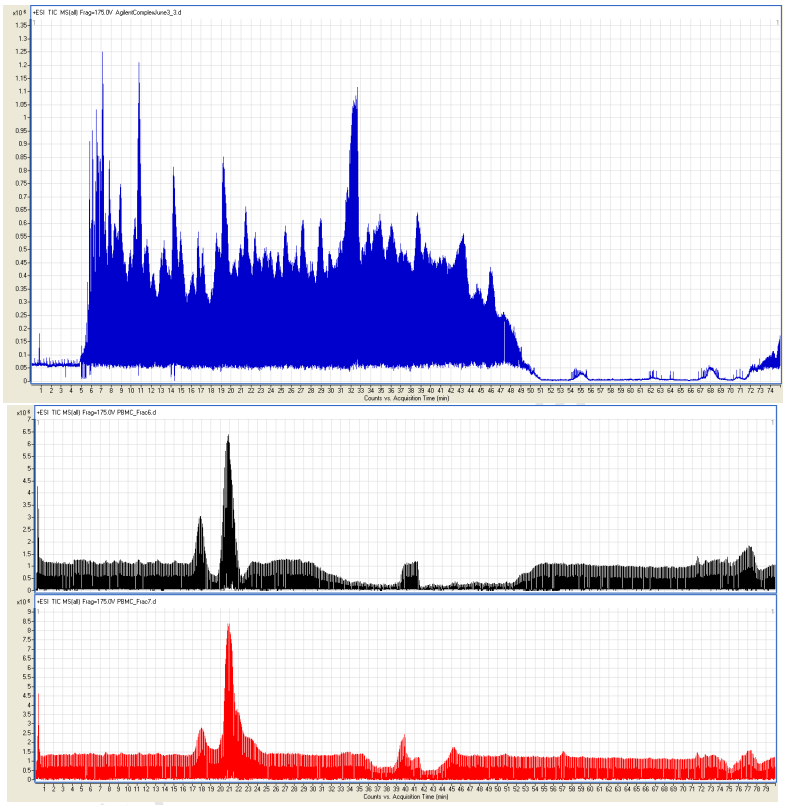

Figure 4.7: Effectiveness of Off-gel fractionation on crude PBMC protein extract
The effectiveness of Off-gel fractionation of proteins extracted from PBMCs was tested using an Agilent 3100 Off-gel Fractionator. Approximately 300 μg of protein was digested using trypsin, the peptide mixture was desalted before being run on the fractionator. The resultant fractions were desalted and then run on a Agilent 6530 Q-ToF (two of these Off-gel fractions are displayed as the red and black total ion current chromatograms - bottom and middle respectively). An aliquot of the original protein extraction was removed prior to Off-gel fractionation and the whole peptide mixture was run as a control on the same mass spectrometer (blue total ion current - top).

The lack of protein identifications in the combined Off-gel fractionated samples (less than 20) when compared to the whole peptide mixture (over 100) and the apparent overall loss of complexity in the recovered fractions excluded this method from further experimental optimisation in this project.

4.4.2 High pH C-18 reverse phase fractionation:

Given the poor performance of the Off-gel fractionation, it was decided to evaluate high pH reverse phase separation as an alternative. Approximately 50 μg of tryptic peptide was loaded onto a self-manufactured reverse phase tip column containing approximately 8 μg of C-18 resin. A manual step gradient (10, 15, 20, 25, 80 %) was applied and individual fractions collected and analysed by LC-MS/MS at Stellenbosch University where Dr Salome Smit performed the subsequent MS analysis (described in the Methods chapter, Subsection 3.5.1.3). The fractions were run using a 90 minute n-LC gradient and the results were processed using Crux version 1.37. The parameters for the search were a q-value of 0.05 and degenerate peptides were included in the identification of the protein numbers. The results are listed in Table 4.1.

Sample	**UniProt Organism 9606**	**UniProt Organism 9606 GP**	**IPI v3.85 HUMAN**
F1: 5 % ACN	170	492	611
F2: 10 % ACN	211	266	758
F3: 15 %ACN	162	365	589
F4: 20 % ACN	178	375	393
F5: 80 % ACN	107	204	293
Total non-redundant proteins	447	1011	1591
Total redundant proteins	828	1763	2645
% Redundancy	53.99	57.35	60.15

Table 4.1: Initial high pH RP protein numbers

The total number of proteins identified in each fraction (F1 - F5) are shown per database from which they were obtained. The total number of non-redundant proteins is the total number of unique proteins summed across all fractions. The total redundant proteins is the sum of each fraction together, including overlapping proteins. The percentage redundancy is a measure of the percentage of proteins that are unique and do not overlap across the different fractions. Organism 9606 in the UniProt databases is *Homo sapiens*. The difference between the two UniProt database in Table 4.1 is that the GP database is the global proteome and contains splice variants and other protein modifications, whereas the non-GP database essentially contains one protein per gene. The IPI database is a meta-database that is formed from a number of other databases including UniProtKB, Ensembl, RefSeq, HinvDB and VEGA and contains splice variants and isoforms although it has recently ceased curation.

Although results varied greatly depending on the database used, they indicated that the high pH reverse phase separation protocol combined with the DOC extraction method was successful and that the next step in the project could begin.

4.5 Protein fractionation strategies:

Concurrent work by other members of our lab showed promising results using a "middle out" approach (a limited protein fractionation step followed by a more extensive peptide fractionation of the protein fraction-derived proteolytic peptides before MS analysis). This led to the testing of two approaches for protein fractionation that could then be processed using the FASP protocol described in the Methods chapter (Subsection 3.5.1.2). For ease of comparison, the fractionated proteins were analysed on a standard 10 % glycine-SDS-PAGE Laemmli gel.

4.5.1 Crude sub-cellular fractionation:

Briefly, cytoplasmic proteins (fraction 1) were extracted after permeabilising the cell membrane using digitonin, allowing the cytoplasmic proteins to diffuse out into the supernatant. Following centrifugation, the supernatant was remove and the pellet was then re-suspended in an NP40 based buffer which solubilised the membranous organelles and their proteins (fraction 2). The remaining cellular debris was pelleted by centrifugation and re-suspended in E-RIPA buffer (containing 1 % SDS) to give the nuclear/insoluble protein fraction (fraction 3). An SDS-PAGE gel was then used to compare the differences and similarities of the protein complement in each fraction, Figure 4.8, as well as to determine the reproducibility of the method for multiple extractions.

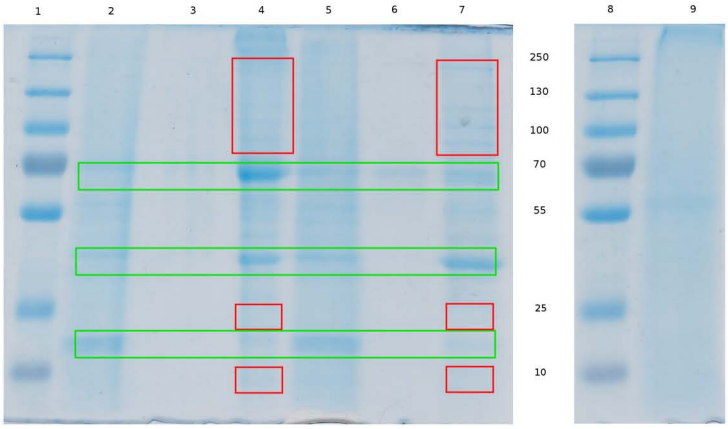

Figure 4.8: Crude sub-cellular fractionation
The gel above contains the CSF fractions (lanes 2 -7) extracted from two separate aliquots of 3 x 10^6 PBMCs, as well as a DOC extraction (lane 9) from 1.6 x 10^6 PBMCs. All PBMCs were from the same donor. The individual lanes contain: Molecular weight marker (1 & 8), cytoplasmic proteins fraction (lanes 2 & 5), membranous-organelle protein fraction (lanes 3 & 6), nuclear & insoluble protein fraction (lanes 4 & 7) and the DOC extraction (lane 9). The CSF samples from the first extraction (lanes 2 - 4) were processed using the FASP protocol using a starting volume of 400 μL of starting material for all three fractions. The CSF samples from the second extraction (lanes 5 - 7) were processed using the FASP protocol from a starting volume of 225 μL of starting material for all three fractions. These volumes equated to approximately equal quantities of protein for each fraction being loaded onto a 30 kDa MWCO spin filter at the initiation of FASP (~ 200 μg - as determined by Bradford reagent). After the FASP process was completed up to the step prior to trypsin digestion, an equal volume aliquot (~ 20 μL) was removed from the spin filter retentate and run on a gel. The DOC extraction was not processed using the FASP protocol and approximately 10 μg of protein was loaded as determined by Bradford reagent. The gel was then stained using colloidal Coomassie Blue.

4.5.2 Phosphoprotein enrichment:

Phosphoproteins are often enriched using chromatography based on IMAC or TiO_2 resins. To test the effectiveness of this method, an extraction was performed on a duplicate set of 3 x 10^6 PBMCs: one set was extracted in 1.5 mL 0.25 % CHAPS based lysis buffer and the other in 3 mL 0.25 % CHAPS based lysis buffer (Methods chapter, Subsection 3.5.1.3), both samples were then enriched for phosphoproteins on a proprietary column according to the manufacturers guidelines (`http://www.qiagen.com/literature/render.aspx?id=23717`). The phospho-enriched and phospho-depleted fractions were then processed using the FASP protocol described in the Methods chapter (subsection 3.5.1.2). An aliquot was removed prior to tryptic digestion and run on a 10 % glycine-SDS-PAGE gel (Figure 4.9) to estimate the amount of overlap between the two fractions, as well as compare them to the DOC extraction protocol that had been employed in previous extractions.

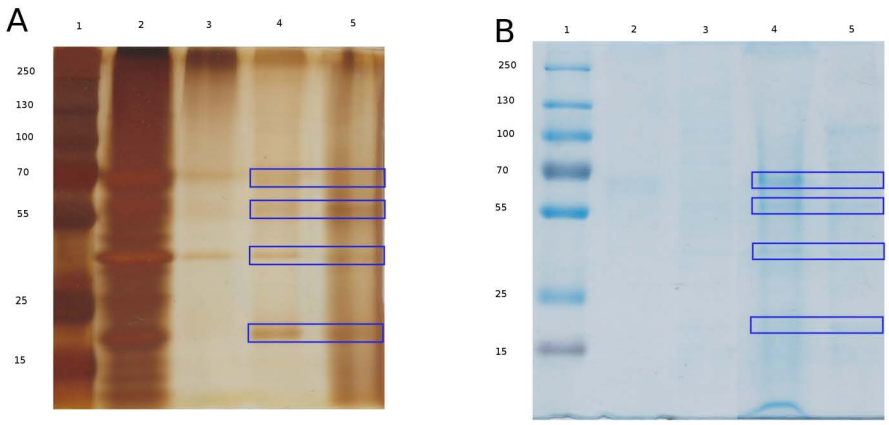

Figure 4.9: Phospho-protein extraction (Silver stained and CCB)
In Figure 4.9, Gel A contains the phospho-depleted (PD) fractions and the phospho-enriched (PE) that were extracted from two separate aliquots of 3 x 10^6 PBMCs. All PBMCs were extracted from the same donor. The extractions were performed as per the kit protocol with the only difference being that the first extraction was performed in 3 mL CHAPS extraction buffer and the second extraction was performed in 1.5 mL CHAPS extraction buffer. The individual lanes contain: Molecular weight marker (1), PD 1.5 mL (2) PD 3 mL (3) PE 1.5 mL (4) PE 3 mL (5). The 3 mL sample (PD and PE) was processed for FASP using a total volume of 250 μL of starting material. The 1.5 mL sample (PD and PE) was processed using a starting volume of 450 μL of starting material. These volumes equated to approximately equal quantities of protein for each fraction being loaded onto a 30 kDa MWCO spin filter at the initiation of FASP (~ 200 μg - as determined by Bradford reagent). After the FASP process was completed up to the step prior to trypsin digestion, an equal volume aliquot (~ 20 μL) was removed from the spin filter retentate and run on an SDS-PAGE gel. Staining was performed using a silver stain kit. Gel B, contains exactly the same samples as gel A in the same lanes but was stained using colloidal Coomassie Blue.

4.5.3 Improved discovery strategy for shotgun proteomics:

A closer inspection of Figures 4.8 and 4.9 show some interesting details and characteristics. In Figure 4.8 it can be seen that the reproducibility of the extraction is inconsistent across the two extractions (green boxes) as well between the individual fractions of the two extractions (red boxes): for example, high abundant proteins occur in all the fractions and certain bands are present in one fraction but not in the same fraction for the repeat extraction. It appears that the membranous-organelle protein fraction (fraction 2) had a far lower total protein quantity than fractions 1 and 3 (cytoplasmic and nuclear/insoluble respectively). This would introduce another variable in terms of workflow processing as this fraction would probably not need peptide fractionation post tryptic digest, whereas the other two fractions would. By contrast, from Figure 4.9 it appears that the volume used for the extraction has a bearing on the outcome of the subsequent phospho-enrichment. A lower extraction volume (1.5 mL) appears to favour an increase in the PD fraction complexity, whereas a higher extraction volume (3 mL) seems to

favour enrichment of the phosphoproteins (PE fraction). The 3 mL PE fraction also appeared to have a high number of proteins across a large molecular weight range, with only four highly abundant proteins visible (blue boxes). Based on these observations, as well as the fact that it would be inherently appealing to enrich for proteins that are involved in signalling pathways in order to gain insight regarding the differential response of the TB-IRIS and TBART samples to the various experimental conditions, it was decided that the best option would be to use the phosphoprotein enrichment rather than of the crude sub-cellular fractionation.

4.5.3.1 Protocol finalisation

Following on from the decision to use phospho-enrichment, the subsequent proteomic work was performed on TB-IRIS and TBART samples as opposed to healthy donors as the need to optimise a protocol or workflow had now been completed. Pooled culture samples for the relevant time point and culture conditions for both TB-IRIS and TBART samples were extracted using the phospho-enrichment 0.25 % CHAPS based lysis buffer. The insoluble proteins were pelleted by centrifugation and the soluble proteins were loaded onto the phospho-enrichment column, whilst the flow through was collected and kept aside for analysis as the phospho-depleted fraction. The phospho-enriched fraction was obtained by eluting the bound phosphoproteins.

4.5.3.2 Initial phospho-depleted results

As part of this phospho-enrichment approach, the phospho-depleted fraction could be further fractionated to tease apart the higher quantity and complexity of the non-phosphorylated. Initially, this was attempted by performing a manual high pH RP fractionation on the flow through of the phospho-enrichment column. The flow through from the phospho-enrichment column was thus collected and concentrated on a 10 kDa MWCO spin filter before being processed as before (Sub-section 4.4.2). The crude fractions from the high pH reverse phase column (five per sample) were collected and analysed by LC-MS/MS an Orbitrap Velos mass spectrometer. Disappointingly, four out of five fractions identified between five and 25 proteins per fraction, with the fifth fraction identifying 88 proteins. Based on this outcome, it was decided to examine the selectivity of the CHAPS extraction of the phospho-protein enrichment kit.

4.5.3.3 Secondary phospho-depleted results

Previous high pH reverse phase fractionation (Subsection 4.4.2) had been shown to be robust and provide high recovery of sample. However, based on the low numbers seen in the initial phospho-depleted results using the flow though from the column during the phospho-enrichment protocol, it was decided to determine how much protein remained as part of the insoluble pellet that was recovered during the phospho-protein extraction after the lysis of the PBMCs using the 0.25 % CHAPS based buffer. The insoluble protein pellets from the various samples during the phospho-protein extraction were re-solubilised in 50 μL 1 x SAB buffer and incubated at 95 °C for 20 minutes. A 10 μL aliquot was then run on a standard 10 % glycine-SDS-PAGE Laemmli gel. A large number of proteins were visible on this gel so a second gel was then run maximising sample loading.

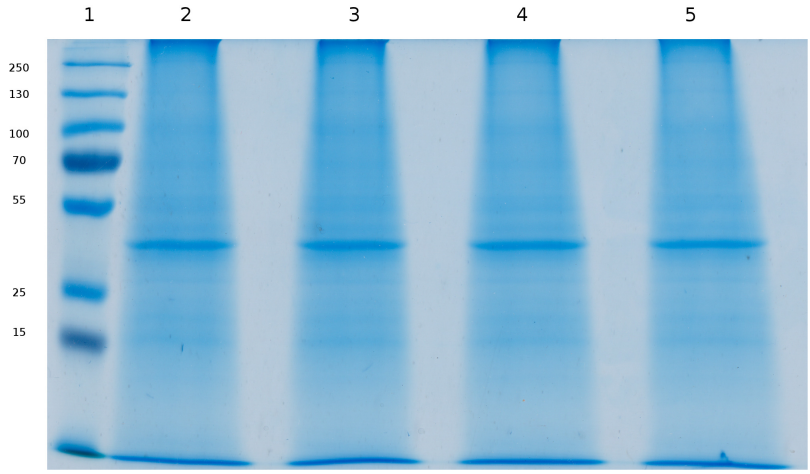

Figure 4.10: TBART phospho-depleted gel

Figure 4.10 above, is of the insoluble protein pellets from the phospho-protein extraction of the TBART samples, run on a standard 10 % glycine-SDS-PAGE gel. The 1mm thick gel was run for 90 minutes at 20 mA and stained using CCB. Lane 1 was the molecular weight marker. Lanes 2 and 3 were duplicates of the TBART - Dex / - heat killed H37Rv (MM), lanes 3 and 4 were duplicates of the TBART - Dex / + heat killed H37Rv (MP) samples. All lanes were loaded using 20 μL aliquots of the insoluble protein pellet re-solubilised in 50 μL 1 x SAB and heated to 95 °C for 20 minutes.

An identical gel was run as a biological replicate of the TB-IRIS samples, Figure 4.11.

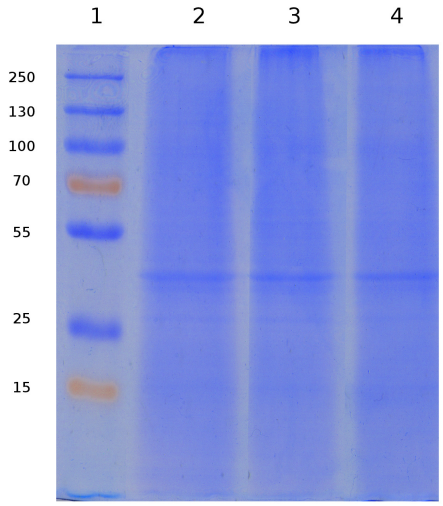

Figure 4.11: TB-IRIS phospho-depleted gel
Insoluble protein pellets from the phospho-protein extraction of the TB-IRIS samples, run on a 10 % glycine-SDS-PAGE gel. The 1mm thick gel was run for 90 minutes at 20 mA and stained using aquastain (AcquaScience, cat. no. AS0001000) . Lane 1 was the molecular weight marker. Lane 2 was the TB-IRIS + Dex / + heat killed H37Rv (PP) sample, lane 3 was the TB-IRIS - Dex / + heat killed H37Rv (MP) sample and lane 4 was the TB-IRIS - Dex / - heat killed H37Rv (MM) sample. All lanes were loaded using the 20 μL aliquot of 1 x SAB that was used to re-solubilise the pellet by heating to 95 °C for 20 minutes.

Each lane of each gel was cut into five fractions and each gel slice was then subjected to in-gel tryptic digestion according to the method described in the Methods chapter (Subsection 3.5.4). The TBART samples, Figure 4.10, had enough sample for duplicate lanes to be combined together. The TB-IRIS samples, Figure 4.11, had enough sample for one lane per sample to be run. Following extraction of the resultant tryptic peptides from the gel slices, each set of peptides were analysed by LC-MS/MS on an Orbitrap Velos mass spectrometer.

4.6 Data processing for downstream software analysis

The RAW data for each proteomic experiment described above was processed at the time of acquisition using the basic workflow outlined in the Methods chapter (Section 3.7). However, in order to obtain an accurate measure of the protein numbers for each method and to obtain a relative perspective on the number of proteins identified in each method, whilst allowing for updates in software and databases the RAW data for each method was subsequently re-processed using an identical workflow and parameters (algorithm version, databases, thresholds etc.). The outcomes of this can be seen in Table 4.2.

4.6.1 Barista identification

The Barista algorithm was used to identify proteins from the various experiments [253]. Due to the nature of the pairwise analysis it was decided to use a q-value of ≤ 0.05 as the threshold in downstream analysis since the probability of specific proteins being false positives in *both* sets of data would be lower than the q-value for a single dataset and could thus be included in the analysis.

Sample Group	Culture condition	UniProt Organism 9606 Global Proteome $q \leq 0.05$	UniProt Organism 9606 Global Proteome $q \leq 0.05$
TB-IRIS PD	MM	299	206
	MP	631	484
	PP	602	470
TB-IRIS PE	MM	283	214
	MP	129	76
	PP	258	211
TB-IRIS PDE	MM	467	395
	MP	692	573
	PP	695	586
TBART PD	MM	595	450
	MP	535	406
TBART PE	MM	262	186
	MP	246	151
TBART PDE	MM	698	606
	MP	635	481

Table 4.2: Non-redundant protein numbers per sample group

Protein numbers indicated above are the total number of non-redundant proteins identified per sample group. The "ALL" groups are the non-redundant numbers for the constituent culture condition protein lists. All protein numbers are calculated with a Barista q-value ≤ 0.05 (column one) and ≤ 0.01 (column two) . PD = phospho-depleted, PE = phospho-enriched, PDE = phospho-depleted + phospho-enriched.

In Table 4.2, the phospho-enriched (PE) data is from the 0.25 % CHAPS lysis followed by on-column phospho-enrichment, followed by tryptic digestion and analysis by LC-MS/MS. The phospho-depleted (PD) data is from the re-solubilisation of the insoluble protein pellet that remained after the CHAPS based lysis for the phospho-enrichment protocol that was subsequently fractionated using SDS PAGE before undergoing in-gel tryptic digestion and then analysed by LC-MS/MS. The different fractions were merged at the spectra level using the Barista algorithm. These two datasets were then combined at the protein level into a non-redundant list resulting in the final PDE numbers observed in Table 4.2. The data from

the analysis of the flow through from the phospho-enrichment column was excluded due to the poor number of identifications and inconsistent quality.

4.6.2 Protein quantification

Protein quantification was performed using normalised spectral abundance factor (NSAF) values that were obtained from the spectral data during protein identification. It has been shown that the the number of spectra that identify a protein correlate to the quantity of the protein that is present in the sample [254], and since small proteins tend to have fewer spectral counts than large proteins, spectral count normalisation is often used to minimise quantitative errors. A normalisation approach using NSAF values was proposed by Zybailov *et al*. [224], whereby the NSAF for a protein k is a normalised spectral count taking into consideration the spectral counts and protein length of all proteins identified in the experiment. The relative abundance of proteins within an experiment can thus be compared by using the NSAF of each protein that is identified.

5 Qualitative Results

5.1 Data set pairing

Datasets were analysed in a pairwise manner to increase the overall number of identified proteins that were used for further downstream analysis. Datasets were paired within their corresponding patient groups (TB-IRIS or TBART) and contained one test condition (MP or PP) paired against the baseline condition (MM) for that respective patient group, giving a ratio fold change representing the paired dataset. Protein identifications were performed using a q-value of $\leq$ 0.05 as the cost/benefit ratio for using this slightly less stringent q-value was such that there was just under a 20 % gain in protein identifications for both the TB-IRIS and TBART data at a cost of the number of false positives increasing by four percent. The probability that any specific false positives would be found by chance in both paired datasets also serves to reduce the number of false positives that would likely be seen in the common proteins in each paired datasets. The lack of replicates also means that there is not enough power behind the statistics when analysing changes in protein expression profiles at the protein level and consequently the majority of the analysis is performed at the pathway level. This is not to say that potentially interesting trends may be identified at the protein level, however it is not possible to state with confidence if these trends are significant or not.

The paired groups and their corresponding number of proteins (based on the quantified proteins common to both datasets in Table 4.2) are listed in Table 5.1.

Paired conditions		Common proteins
TB-IRIS MP	TB-IRIS MM	320
TB-IRIS PP	TB-IRIS MM	337
TBART MP	TBART MM	391

Table 5.1: Pairwise protein datasets for downstream IPA analysis
For each paired condition, commonly identified proteins with NSAF values (Barista quantitation values) were quantile normalised and their ratios of expression (test / baseline) were then used in further analysis in the IPA software.

Despite there being a noticeable difference in the numbers of proteins identified in the TB-IRIS PDE MM dataset compared to the TBART PDE MM dataset - 467 versus 698 - (Table 4.2), it appears from the subsequent qualitative data analysis that this has not skewed the results by limiting one of the baseline datasets in the IPA analysis. Indeed, looking at Table 5.1 shows that the number of paired proteins per dataset is approximately similar. A further analysis of the distribution of canonical pathways, Figure 5.12, indicates that only 12 % (15 / 125) of the identified canonical pathways are unique to the to the TBART MP-MM paired dataset.

5.2 Systems analysis using Ingenuity Pathway Analysis data

Ratios for the fold change of the common proteins found in each individual paired datasets were uploaded into Ingenuity Pathway Analysis (IPA) software where they were analysed using default program parameters after being log transformed. The only changes to the default conditions were to limit the analysis to *Homo sapiens* based parameters, excluding mouse and rat parameters. A Core Analysis and a Biomarker Analysis were performed as standard for each paired dataset that was uploaded. Comparison of Core and Biomarker analyses for certain combinations of the paired datasets were also performed. The level of analysis can broadly be interpreted at the protein level as well as at the pathway level and the results of these are presented hereafter.

5.2.1 Intra-condition protein level analysis

In IPA, the Core analysis function ranks the top candidates that have been identified across a number of fields. Table 5.2 shows the predicted fold changes in protein abundance for the highest ranked candidates (by degree of change) across the paired datasets described in Table 5.1. Fold changes were obtained from the ratio, x, of the normalised spectral abundance factor (NSAF) values for proteins common to both datasets where if $x < 1$ then it is converted by the formula $-1 / x$ but if $x > 1$ then there is no need to convert.

Rank	TBART MP/MM		TB-IRIS MP/MM		TB-IRIS PP/MM	
	Protein	Fold Change	Protein	Fold Change	Protein	Fold Change
1	APOB / P04114	7.080	FASN / P49327	11.269	MPST / P25325	16.228
2	ACADM / P11310-2	5.270	ESYT1 / Q9BSJ8-2	8.118	PSMD11 / O00231	12.200
3	DHX15 / O43143	4.697	PYGB / P11216	6.235	ILK / Q13418	10.660
4	SEPT9 / Q9UHD8-2	4.663	MYO1F / O00160	6.053	RTN4 / Q9NQC3-2	6.640
5	CSTA / P01040	3.624	LTBP1 / Q14766	5.798	ESYT1 / Q9BSJ8-2	5.037
6	TXNDC5 / Q8NBS9	3.354	INF2 / Q27J81-2	5.562	ARRB1 / P49407-2	4.802
7	TMEM109 / Q9BVC6	3.326	PDE5A / O76074-2	4.694	CDC42 / P60953	4.276
8	RAC2 / P15153	3.319	CORO1C / Q9ULV4 *	4.301	ARHGAP1 / Q07960	4.183
9	RAP2B / P61225	3.258	NONO* / Q15233	4.288	PYGB / P11216	4.135
10	HBB / P68871	2.887	DAAM1* / Q9Y4D1-2	4.259	INF2 / Q27J81-2	4.069

Table 5.2: IPA core analysis predicted protein changes: up-regulated

The values represent the predicted up-regulation fold change in the corresponding proteins. TBART MP/MM = the ratio of the fold change values determined by the NSAF values for specific proteins from the TBART MP dataset divided by the NSAF values for the corresponding proteins in the TBART MM dataset, TB-IRIS MP/MM = the ratio of the fold change values determined by the NSAF values for specific proteins from the TB-IRIS MP dataset divided by the NSAF values for the corresponding proteins in the TB-IRIS MM dataset, TB-IRIS PP/MM = the ratio of the fold change values determined by the NSAF values for specific proteins from the TB-IRIS PP dataset divided by the NSAF values for the corresponding proteins in the TB-IRIS MM dataset. * indicates proteins that do not exceed the threshold limit in Figure 5.2 and Figure 5.2.

Rank	TBART MP/MM		TB-IRIS MP/MM		TB-IRIS PP/MM	
	IPA / UniProt	Fold Change	IPA / UniProt	Fold Change	IPA / UniProt	Fold Change
1	ECHS1 / P30084	-4.664	IFI16 / Q16666-2	-7.450	F5 / P12259	-9.885
2	YWHAB / P31946-2	-3.760	PRKCSH / P14314	-6.531	PIP4K2A / P48426	-6.329
3	CCT4 / P50991	-3.672	PDIA4 / P13667	-5.685	PDIA4 / P13667	-6.061
4	PSME1 / Q06323	-3.619	RAB33B / Q9H082	-5.651	OLFM4 / Q6UX06	-5.265
5	PRDX6 / P30041	-3.570	TXNDC5 / Q8NBS9	-5.049	ETFA / P13804	-5.114
6	ARHGEF1 / Q92888-3	-3.426	ANXA6 / P08133	-4.981	HNRNPD / D6RF44	-5.082
7	OGDH / Q02218	-3.340	GP1BA / P07359	-4.856	RUVBL2 / Q9Y230	-4.957
8	ANK1 / E7EVX7	-2.855	TPM3 / P06753	-4.733	PSMA7 / O14818	-4.839
9	UQCRC2 / P22695 *	-2.777	APOC3 / P02656	-4.662	HSPA4 / P34932	-4.155
10	BCAP31 / P04908 *	-2.698	ARHGDIB / F5H2R5 *	-4.312	UBR4 / Q5T4S7-2	-3.907

Table 5.3: IPA core analysis predicted protein changes: down-regulated

The values represent the predicted down-regulation fold change in the corresponding proteins. TBART MP/MM = the ratio of the fold change values determined by the NSAF values for specific proteins from the TBART MP dataset divided by the NSAF values for the corresponding proteins in the TBART MM dataset, TB-IRIS MP/MM = the ratio of the fold change values determined by the NSAF values for specific proteins from the TB-IRIS MP dataset divided by the NSAF values for the corresponding proteins in the TB-IRIS MM dataset, TB-IRIS PP/MM = the ratio of the fold change values determined by the NSAF values for specific proteins from the TB-IRIS PP dataset divided by the NSAF values for the corresponding proteins in the TB-IRIS MM dataset. * indicates proteins that do not exceed the threshold limit in Figure 5.1 and Figure 5.2.

A second, more visual analysis of the changes in the protein expression profiles of the two disease states (TBART and TB-IRIS) was performed using the log of the ratios of the changes in individual protein NSAF expression values that were plotted using the R scripting language on a Cartesian plane. A threshold of two times the standard deviation was employed to eliminate normal random error or variation in the measurements and hence distinguish them from causal variation. Standard deviation represents how much variation exists from the average mean, or expected value in a dataset. A low standard deviation indicates that the data points tend to be very close to the mean; whereas, a high standard deviation indicates that the data points are

spread out over a large range of values.

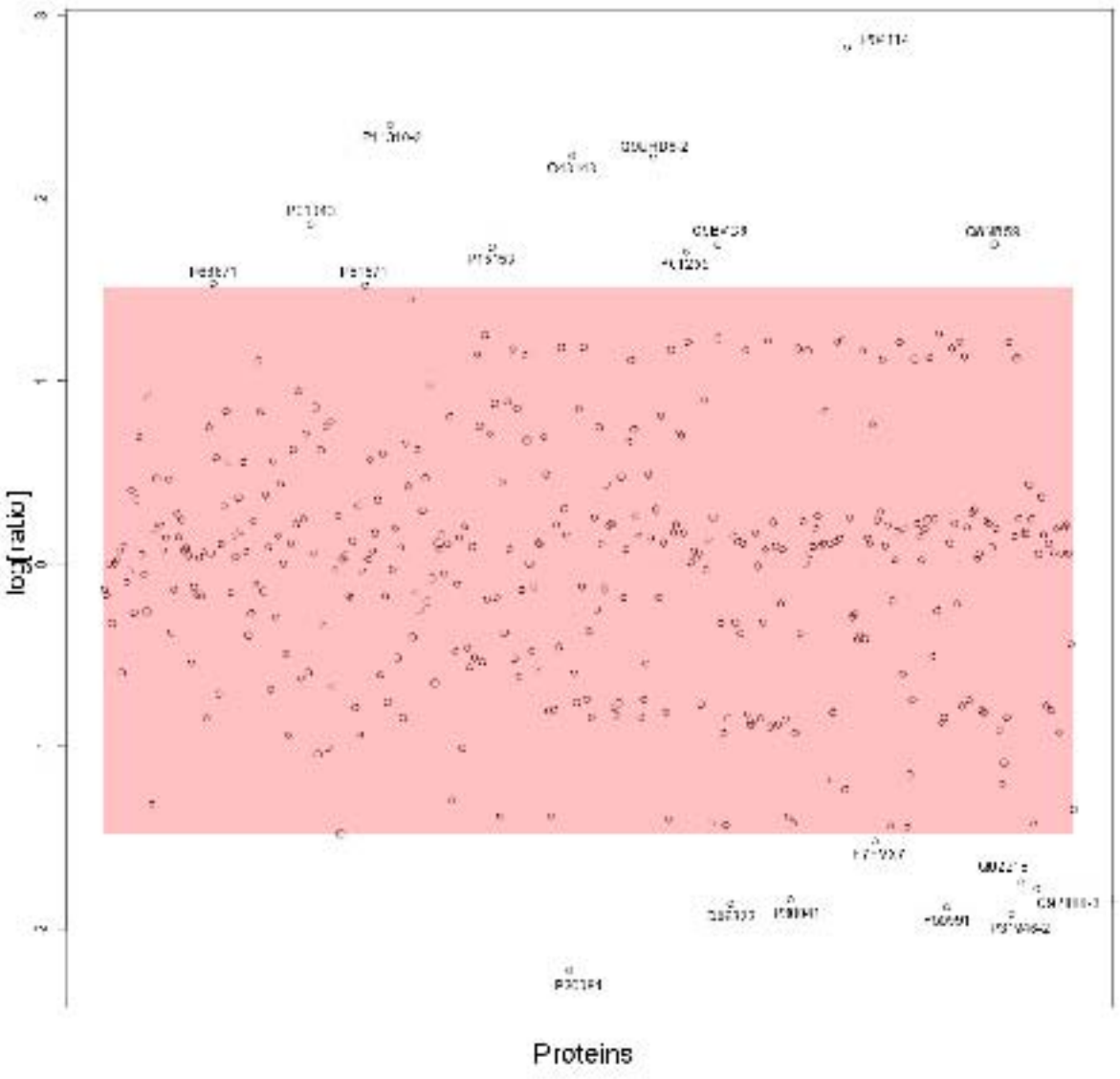

Figure 5.1: Protein expression profile distribution of TBART MP samples
The ratios of the quantile-normalised quantitation values for the TBART MP and TBART MM datasets were $\log_2$ transformed and plotted on a set of axis. Proteins that did not have significant (more than two times the standard deviation of the mean) changes in their ratios were excluded (pink band) leaving only proteins of interest labelled.

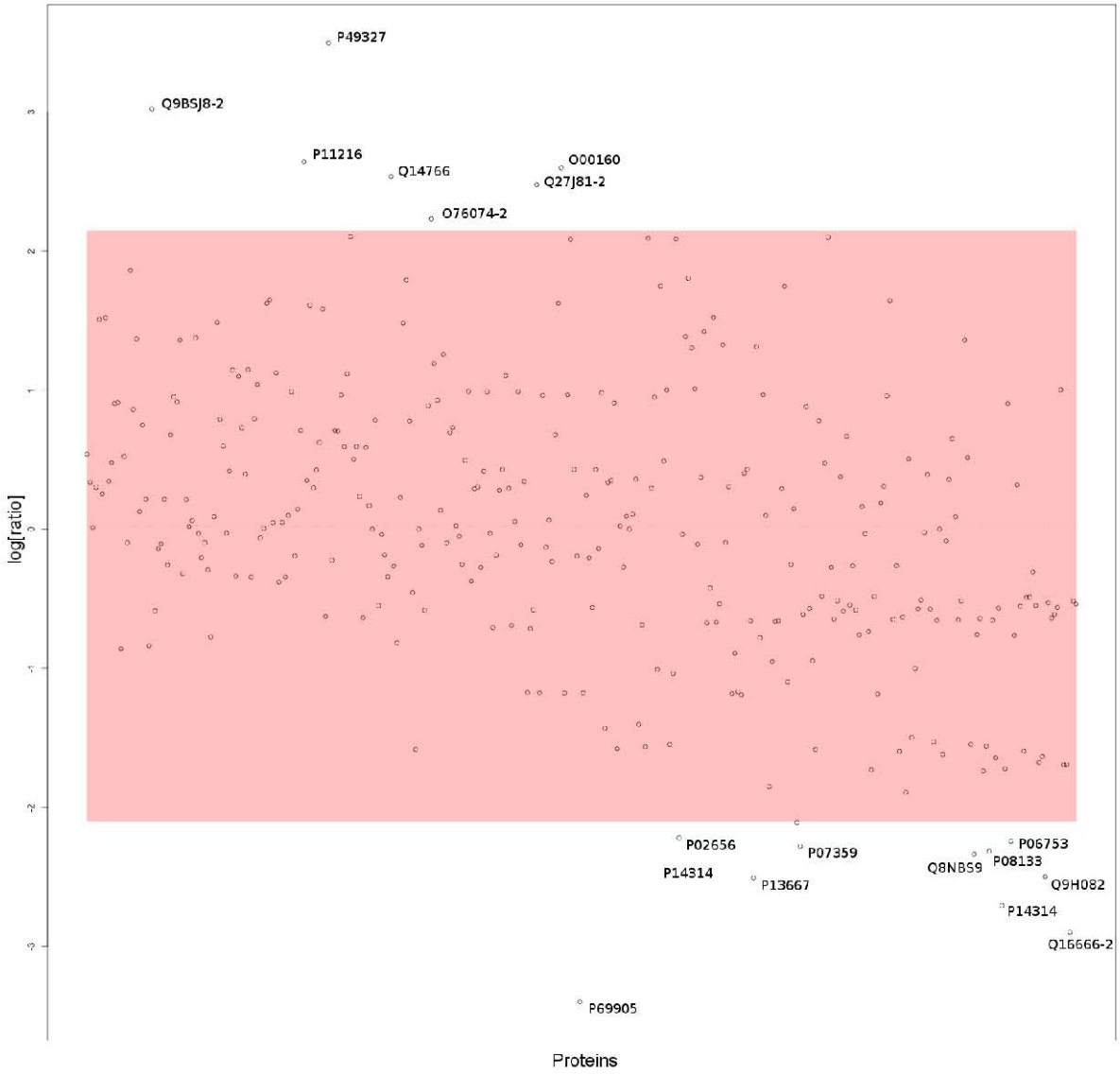

Figure 5.2: Protein expression profile distribution of TB-IRIS MP samples
The ratios of the quantile-normalised quantitation values for the IRIS MP and IRIS MM datasets were $\log_2$ transformed and plotted on a set of axis. Proteins that did not have significant (more than two times the standard deviation of the mean) changes in their ratios were excluded (pink band) leaving only proteins of interest labelled.

The effect of dexamethasone on the protein expression profile of TB-IRIS patient derived PBMCs in the presence of H37Rv antigen was also plotted.

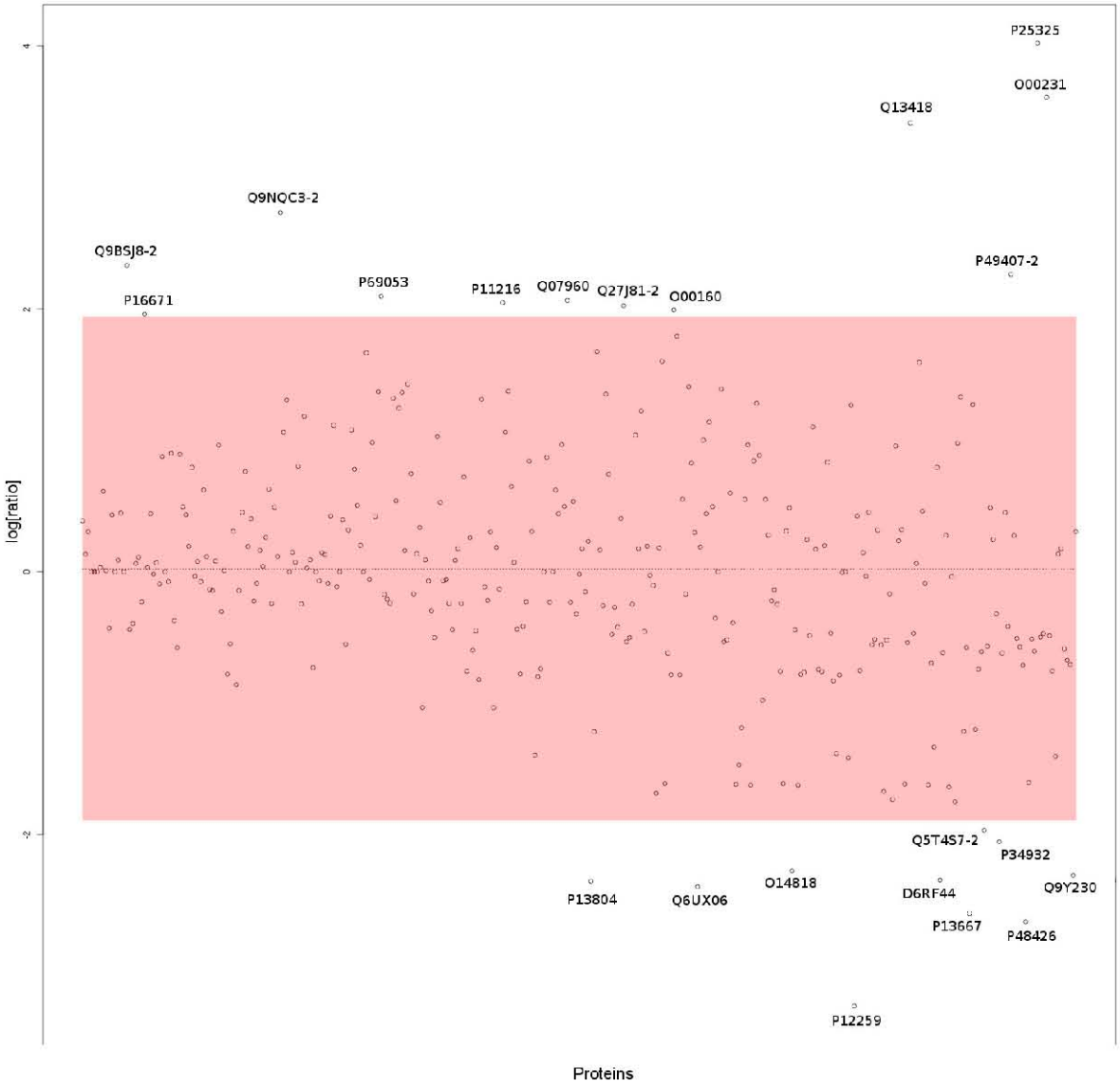

Figure 5.3: Protein expression profile distribution of TB-IRIS PP samples
The ratios of the quantile-normalised quantitation values for the IRIS PP and IRIS MM datasets were $\log_2$ transformed and plotted on a Cartesian plane. Proteins that did not have significant (more than two times the standard deviation of the mean) changes in their ratios were excluded (pink band) leaving only proteins of interest labelled.

There are a number of interesting proteins that apparently have significant changes in abundance but without repeat measurements of expression values it is difficult to maintain statistical confidence in these absolute values. Regardless, this analysis does provide a few proteins of interest that may prove worthwhile for analysis in future studies.

An inspection of the top three ranked identified proteins for the three pairs of data shown in

Table 5.2 and Table 5.3 does not reveal any significant involvement of these proteins in any inflammatory based pathways. The exception being that of integrin linked kinase (ILK), a plasma-membrane protein that plays a key role in integrin signalling that is up-regulated in the TB-IRIS PP/MM dataset. Although the lack of any other proteins relating to inflammatory responses or cell-to-cell communications makes it difficult to ascertain the significance of this finding. In fact, the vast majority of the proteins from those tables have very little if any overlap in related pathways to which they belong.

IPA has the capacity to interrogate data against known or putative biomarkers as well as to identify potential biomarkers through their presence or absence across directly compared datasets. A biomarker analysis using IPA was performed for all three conditions and Table 5.4 shows the outcome.

Condition	Gene Name	Protein details
TBART MP/MM	HLA-DRB1	MHC II, DR beta 1
	ITGB	Integrin beta 2, complement component receptor 3 and 4 subunit
	PRKCD	Protein kinase C, delta
	PTPN6	Protein tyrosine phosphatase, non-receptor type 6
TB-IRIS PP/MM	ARRB1	Arrestin, beta 1
	CD36	CD36 molecule, thrombospondin receptor
All three	MPO	Myeloperoxidase
	STAT1	Signal transducer and activator oftranscription 1, 91 kDa

Table 5.4: IPA biomarker analysis

Biomarker analysis using IPA software for the three patient derived PBMC datasets was performed, specifically looking for biomarkers within human cells related to inflammatory or immunological dysfunction. No unique biomarkers were found for the TB-IRIS MP/MM datasets, however there were two biomarkers common to all three datasets that were observed.

5.2.2 Intra-condition biological pathway level analysis

Analysis of the distribution of *p*-values for the datasets across various biological functions provides an overview of the differences or similarities that exist across these samples.

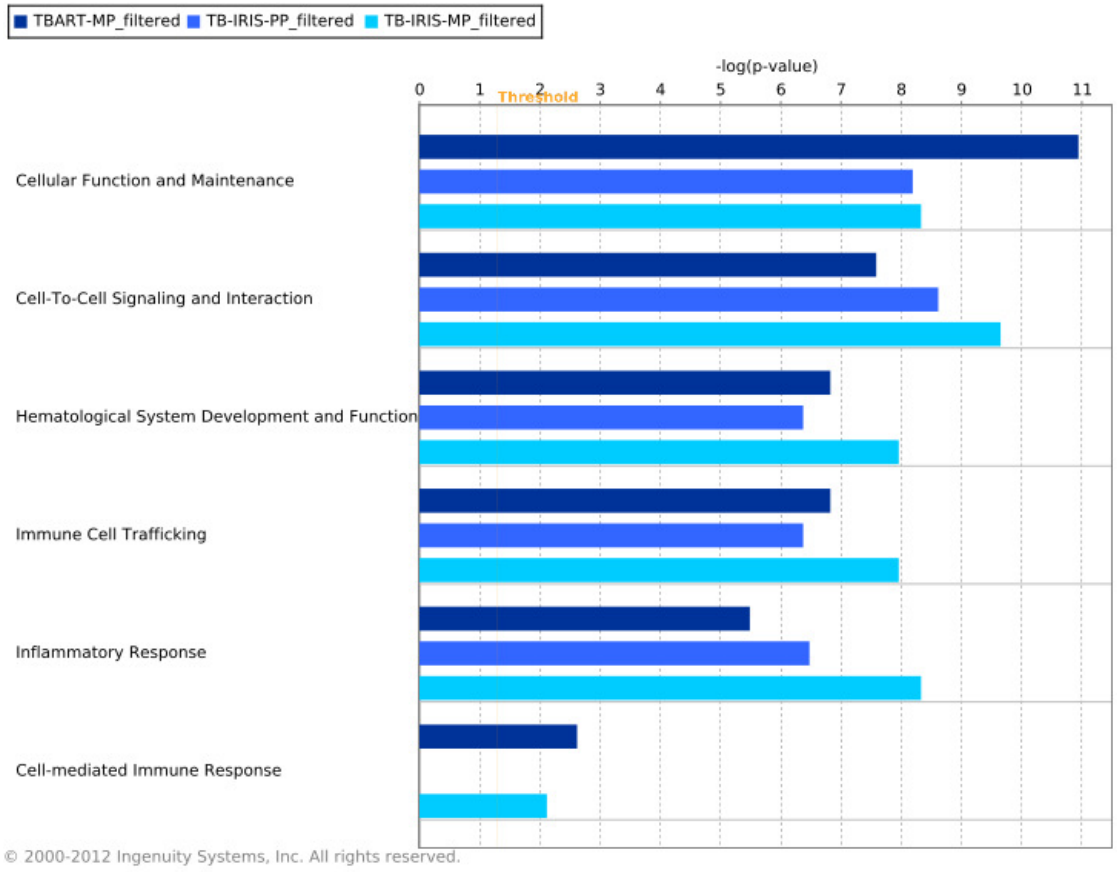

Figure 5.4: Overview of differences in biological functions

It is immediately clear from Figure 5.4 that major differences in the biological functions exist between each of the three conditions that were analysed. For example, it seems intuitive that inflammatory responses should be more highly represented in the TB-IRIS than TBART samples and that the dexamethasone treated TB-IRIS samples should be intermediate between the two. It is less obvious though why differences might exist between TB-IRIS and TBART samples in "cell function and maintenance" or "cell-to-cell signalling and interaction". A more probing analysis of the composition of the differences in these biological functions and their composite pathways, using the activation z-score values, reveals some interesting differences between the TB-IRIS MP/MM, TB-IRIS PP/MM and TBART MP/MM datasets. These differences have been tabulated in Figure 5.6.

Within IPA, the z-score algorithm is used as a means to calculate the activation state of a pathway. The z-score prediction is based on relationships, referred to as edges, in the molecular pathway. The edges must; 1) Represent experimentally observed gene expression or Upstream events, 2) Be associated with a direction of change that is either activating or inhibiting (as derived from the literature compiled in the Ingenuity Knowledge Base). As depicted in Figure

5.5, given the observed differential regulation of a gene (up or down), the z-score determines the activation state of an upstream regulator by the regulation direction associated with the relationship from the upstream regulator to the gene. If the z-score is ≥ 2 then the pathway activity is predicted to increase, while if the z-score is $\leq$ - 2 then the pathway activity is predicted to decrease, with values between 2 and -2 are not assigned predictions in activation state.

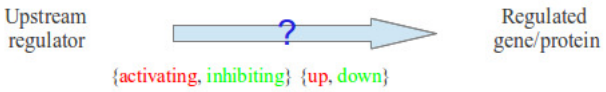

Given the observed differential regulation of a gene (up or down), the z-score determines the activation state of an upstream regulator by the regulation direction associated with the relationship from the Upstreamregulatorto the gene:

Regulation direction associated with the edge	Observed gene regulation	Predicted activation state of the upstream Upstream regulator
Activating	Up	Activated
Activating	Down	Inhibited
Inhibiting	Up	Activated
Inhibiting	Down	Inhibited

Figure 5.5: How the z-score is calculated

The activation z-score identifies upstream regulators that can explain changes in expression of the gene or protein for the observed dataset, and predicts the activation state of the upstream regulators. IPA assigns the red colour to up-regulated products and green to down-regulated products.

A biological function is only predicted to increase or decrease if the z-score meets the minimum statistically relevant thresholds described. The z-score is thus notably different from a *p*-value in that it used to predict activity of a pathway and not just identify pathways that show enrichment in the test data sets.

A

TB-IRIS MP

Focused Biological Pathway	Z-score	*p*-value	# Molecules	Biological function
Adhesion of blood platelets	2.183	3.74E-03	6	
Cell movement of PBMCs	2.000	1.27E-03	4	
Formation of cellular protrusions	2.384	4.96E-03	12	
Interaction of blood cells	-2.000	1.66E-02	5	

B

TB-IRIS PP

Focused Biological Pathway	Z-score	*p*-value	# Molecules	Biological function
Activation of APCs	2.155	1.58E-02	9	
Activation of myeloid cells	2.762	1.02E-03	13	
Activation of neutrophils	2.213	2.03E-02	5	
Activation of phagocytes	2.762	1.36E-04	16	
Adhesion of blood platelets	2.400	3.46E-06	7	
Adhesion of granulocytes	2.234	4.48E-05	8	
Adhesion of neutrophils	2.013	1.74E-05	8	
Aggregation of blood cells	2.220	8.49E-04	10	
Cell movement of phagocytes	2.141	1.73E-03	17	
Inflammatory response	2.616	7.44E-03	21	
Migration of neutrophils	2.190	1.86E-03	6	
Stimulation of cells	2.111	1.86E-02	11	
Transmigration of phagocytes	2.213	1.48E-02	5	

C

TBART MP

Focused Biological Pathway	Z-score	*p*-value	# Molecules	Biological function
Adhesion of monocytes	2.083	1.41E-03	6	
Proliferation of T-lymphocytes	2.098	1.03E-03	18	
Organisation of cytoplasm	2.271	1.14E-11	51	
Organisation of cytoskeleton	2.282	5.57E-10	43	
Microtubule dynamics	2.341	7.23E-04	23	
Engulfment of leukocytes	2.000	1.84E-02	5	

D

Figure 5.6: Delving deeper into biological functions

Significant z-score values for specific biological functions belonging to multiple biological pathways (highlighted in the key provided as part D). The number of molecules refers to the number of molecules in this dataset that are being used to categorise the the specific biological function as well as determine the z-score. The *p*-value is the significance level of over-representation of the molecules associated with the specific biological function.

An assessment of the differences in biological functions (using the z-score) is one of many macro-level analyses that can be performed to analyse differences in biological dataset trends. The second macro-level analysis that was performed entailed the analysis of the canonical pathways of the three datasets using the *p*-value as a measure of over-representation. The *p*-value is a measure of the likelihood that the association between a set of genes in a target

dataset and a related function is due to random association. The smaller the p-value, the less likely that the association is random and the more significant the association. In general, p-values < 0.05 indicate a statistically significant, non-random association. The p-value of overlap is calculated in IPA by the Fisher's Exact Test.

An analysis of non-significant activation scores for the TB-IRIS MP/MM dataset also revels a number of biological functions that have been activated, Table 5.5.

TB-IRIS MP/MM			
Focused Biological Pathway	Z-score	p-value	# Proteins
Activation of blood cells	0.649	3.97E-06	30
Activation of phagocytes	0.856	2.98E-04	15
Activation of T lymphocytes	0.941	1.51E-02	11
Activation of mononuclear leukocytes	1.056	1.07E-02	15
Phagocytosis of granulocytes	1.000	2.13E-03	4
Phagocytosis of myeloid cells	1.067	1.78E-03	5

Table 5.5: Non-significant TB-IRIS analysis

Activation scores of other immunological and inflammatory based biological functions for the TB-IRIS MP/MM dataset that did not achieve a significant activation z-score. This illustrates the varied and non-focussed nature of the TB-IRIS MP/MM dataset.

5.2.3 Inter-condition Canonical Pathways Analysis: TBART vs TB-IRIS

The Ingenuity Pathway suite of software was used to visualise, by way of a stacked bar chart, the over-representation values of various canonical pathways, including the number of up- and down-regulated proteins within that particular pathway. The TB-IRIS MP/MM, TBART PP/MM and TB-IRIS MP/MM datasets (Figure 5.7) show a number of interesting trends in the changes of protein expression profiles within individual canonical pathways.

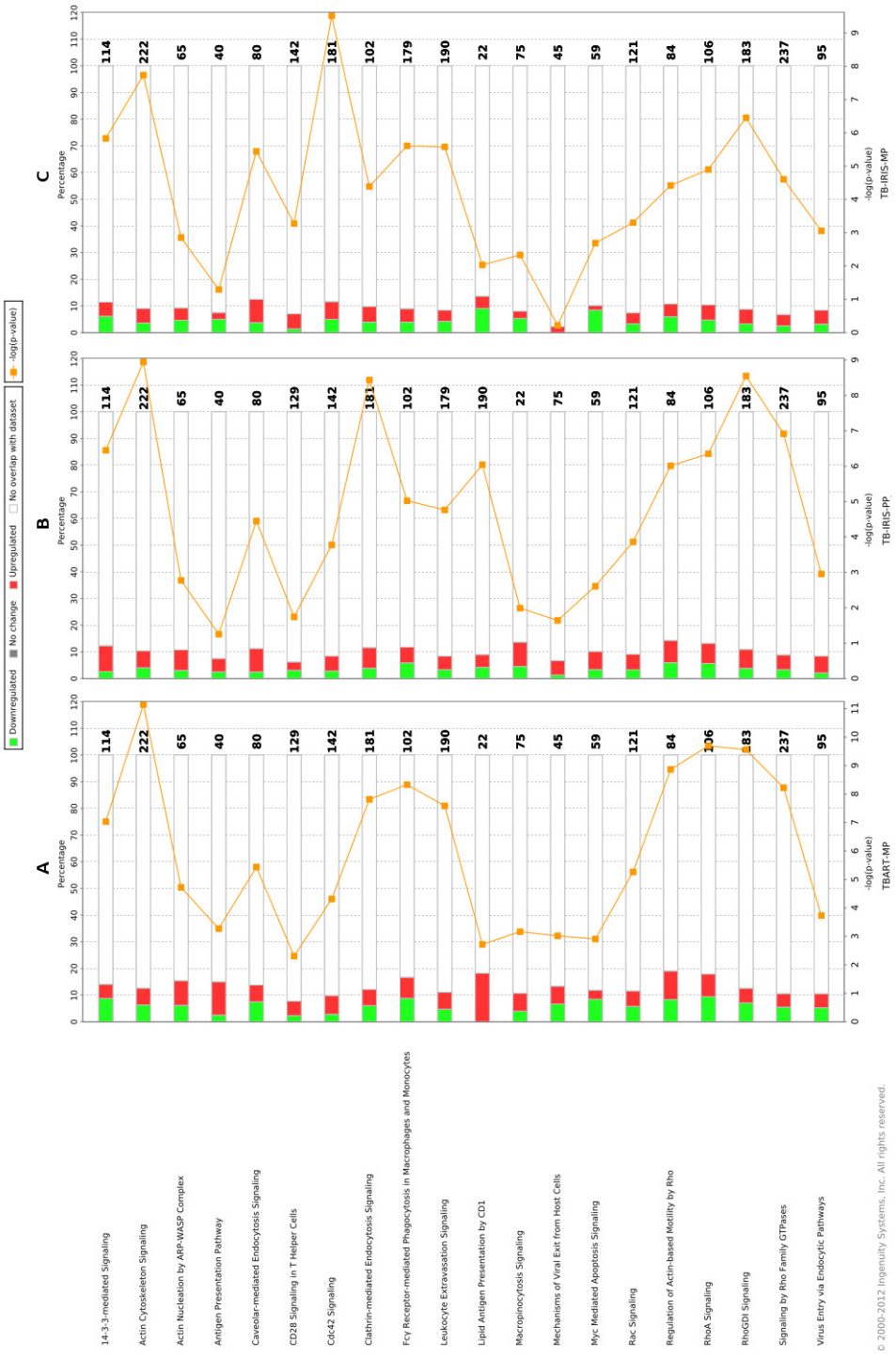

Figure 5.7: IPA generated stacked bar chart of TB-IRIS MP/MM dataset

Listed are 20 of the most relevant canonical pathways across the three datasets. The -$\log_{10}$ of the p-value of over-representation is represented on the right axis scale for each diagram and the percentage coverage of experimentally observed proteins relative to the total number of proteins in that pathway is on the left axis. The bold numbers at the end of each bar represents the total number of proteins involved in the pathway in the reference database. A = TBART MP/MM dataset, B = TB-IRIS PP/MM dataset, C = TB-IRIS MP/MP dataset. The bar chart represents percentage coverage of each pathway, separated into up- (red) or down- (green) regulated protein sets. The line plot represents the p-values for each pathway.

Changes in canonical pathway over-representation profiles across the TB-IRIS and TBART samples were also analysed, using only proteins common to both paired datasets and then adjusting these values using the log[ratio of changes between paired datasets].

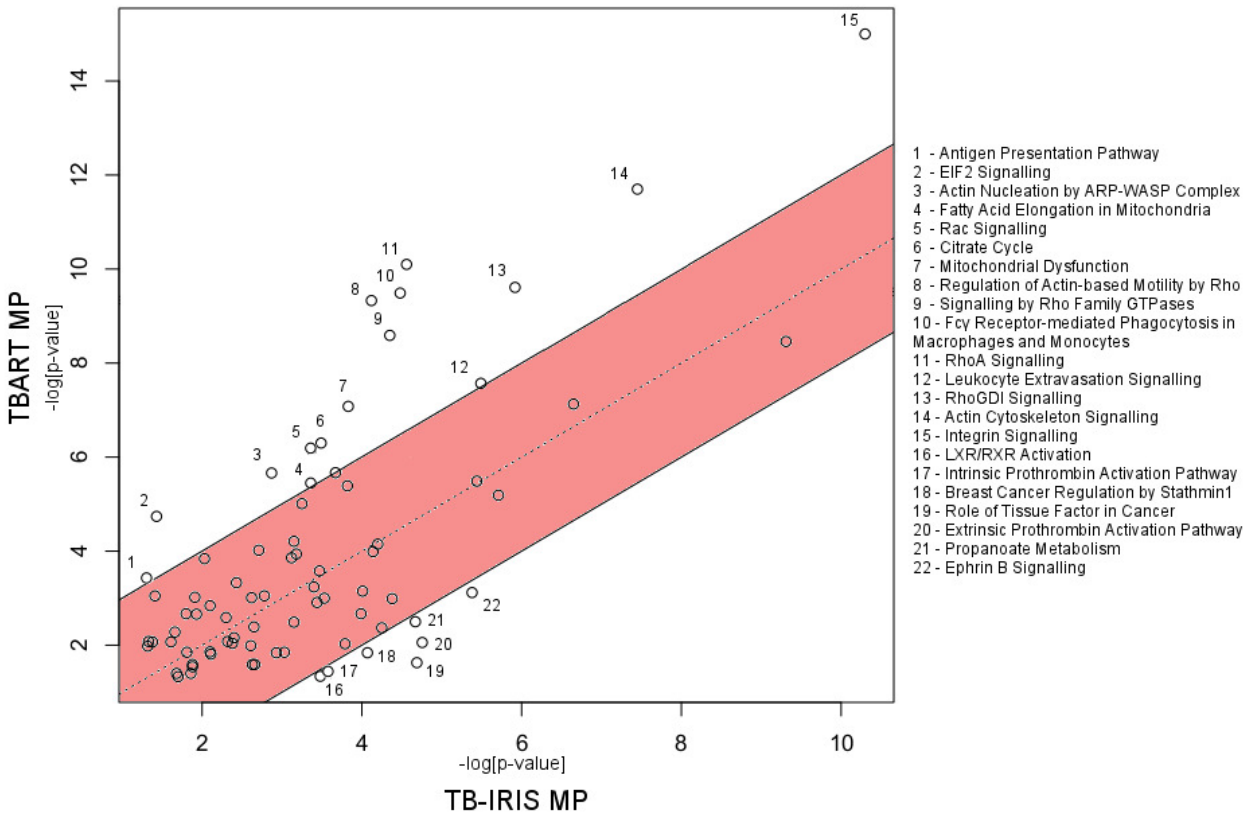

Figure 5.8: Over-representation analysis of canonical pathways

The -log[*p*-value] for common and significantly over-represented canonical pathways was plotted on a Cartesian plane, with the x-axis representing TB-IRIS values and the y-axis TBART values. The dotted line represents the null hypothesis that the over-representation for a given pathway is equal for both TB-IRIS and TBART samples. The pink band sets a threshold of change in the *p*-value of 0.01 from this null hypothesis line for both sets of data, thus highlighting those canonical pathways that exceed this level of significance.

Figure 5.8 clearly indicates that a number of canonical pathways have been significantly over-represented for both patient datasets when analysed using Ingenuity Pathway Analysis software. Significant differences found in these pathway associated *p*-values (represented as -log[*p*-value]) between the datasets can be used to determine which of the pathways are more highly represented - and therefore likely to be more functionally important - in the TB-IRIS or TBART samples.

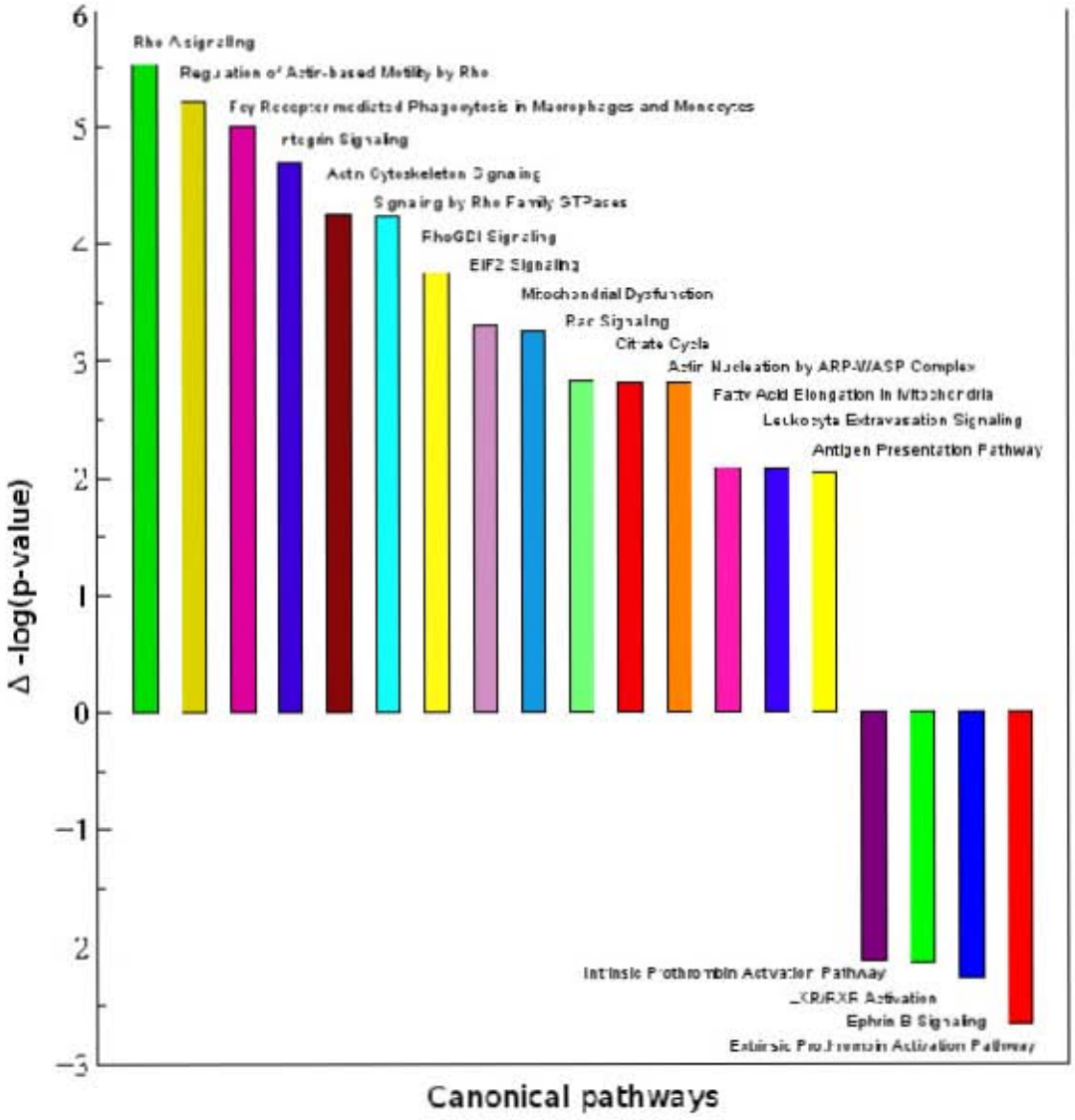

Figure 5.9: Differential analysis of significantly over-represented canonical pathways
The Δ -log[*p*-value] was determined by subtracting the -log[*p*-value] for TB-IRIS from the -log[*p*-value] for TBART associated canonical pathways for the pathways highlighted in Figure 5.8. A positive Δ -log[*p*-value] indicate a greater over-representation of the associated pathway in TBART patient derived data, whereas a negative Δ -log[*p*-value] indicate a greater over-representation of the associated pathway in TB-IRIS patient derived data.

Based upon this analysis, it is clear that there are a number of canonical pathways that are significantly over-represented for the TBART derived PBMCs when compared against the TB-IRIS derived PBMCs. Interestingly many of these canonical pathways are connected in the context of the role they play at level of the cellular cytoskeleton with regards to cellular

organisation, motility, function, recruitment, signalling and maintenance.

5.2.4 Pathway analyses of the effect of dexamethasone

To determine the effect of dexamethasone on the changes in canonical pathway over-representation profiles, common proteins from paired ratio datasets (TBART MP/MM vs TB-IRIS PP/MM; TB-IRIS PP/MM vs TB-IRIS MP/MM) were plotted.

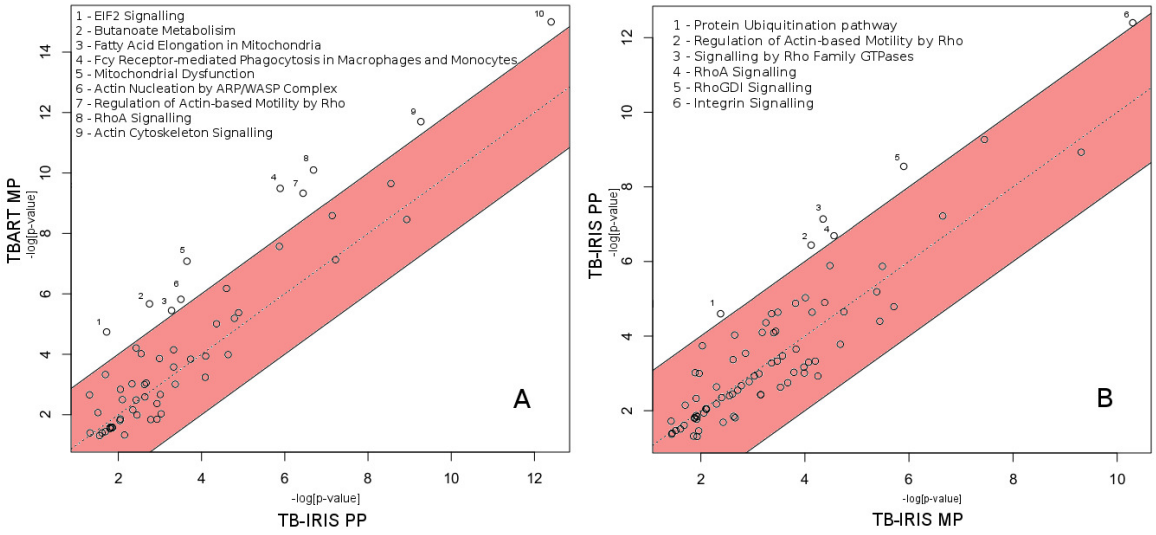

Figure 5.10: Canonical pathway analysis of effect of dexamethasone

The -log[*p*-value] for common and significantly over-represented canonical pathways was plotted on a Cartesian plane. The dotted line represents the null hypothesis that the over-representation for a given pathway is equal for both TB-IRIS and TBART samples. The pink band sets a threshold of change in the *p*-value of 0.01 from this null hypothesis line for both sets of data, thus highlighting those canonical pathways that exceed this level of significance. Graph A (left) represents TBART MP vs TB-IRIS PP and graph B (right) represents TB-IRIS PP vs TB-IRIS MP.

A comparison of the changes in significantly over-represented canonical pathways in the presence or absence of dexamethasone from a TBART and TB-IRIS perspective can be seen in Figure 5.11.

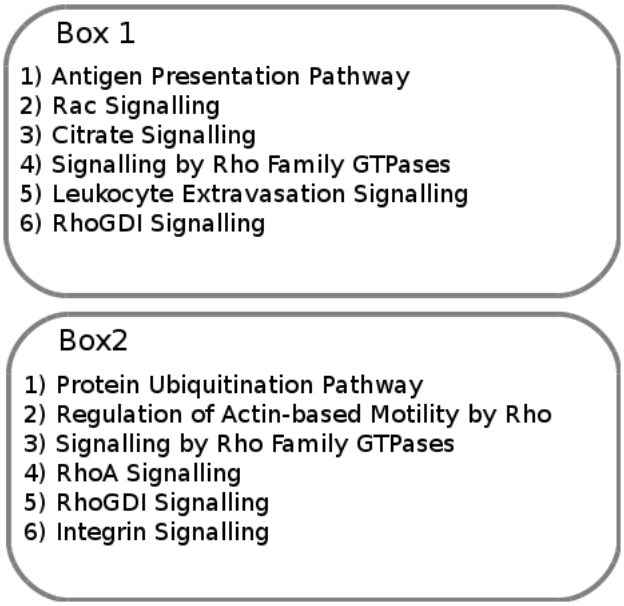

Figure 5.11: Effect of dexamethasone on canonical pathway profiles

Box 1 represents canonical pathways that were significantly over-represented in TBART MP/MM dataset when compared against the TB-IRIS MP/MM but which are absent when the TBART MP/MM dataset was compared against the TB-IRIS PP/MM dataset (Figure 5.8). Box 2 represents canonical pathways that were significantly over-represented in TB-IRIS PP/MM dataset in comparison to the TB-IRIS MP/MM dataset (Figure 5.10).

5.2.5 Analysis of unique pathways

Pathways that were significantly over-represented for three pairwise datasets (TB-IRIS PP-MM, TB-IRIS MP-MM, TBART MP-MM) were also analysed using a Venn diagram (Figure 5.12) to identify pathways that were unique to particular datasets or had other characteristics of interest.

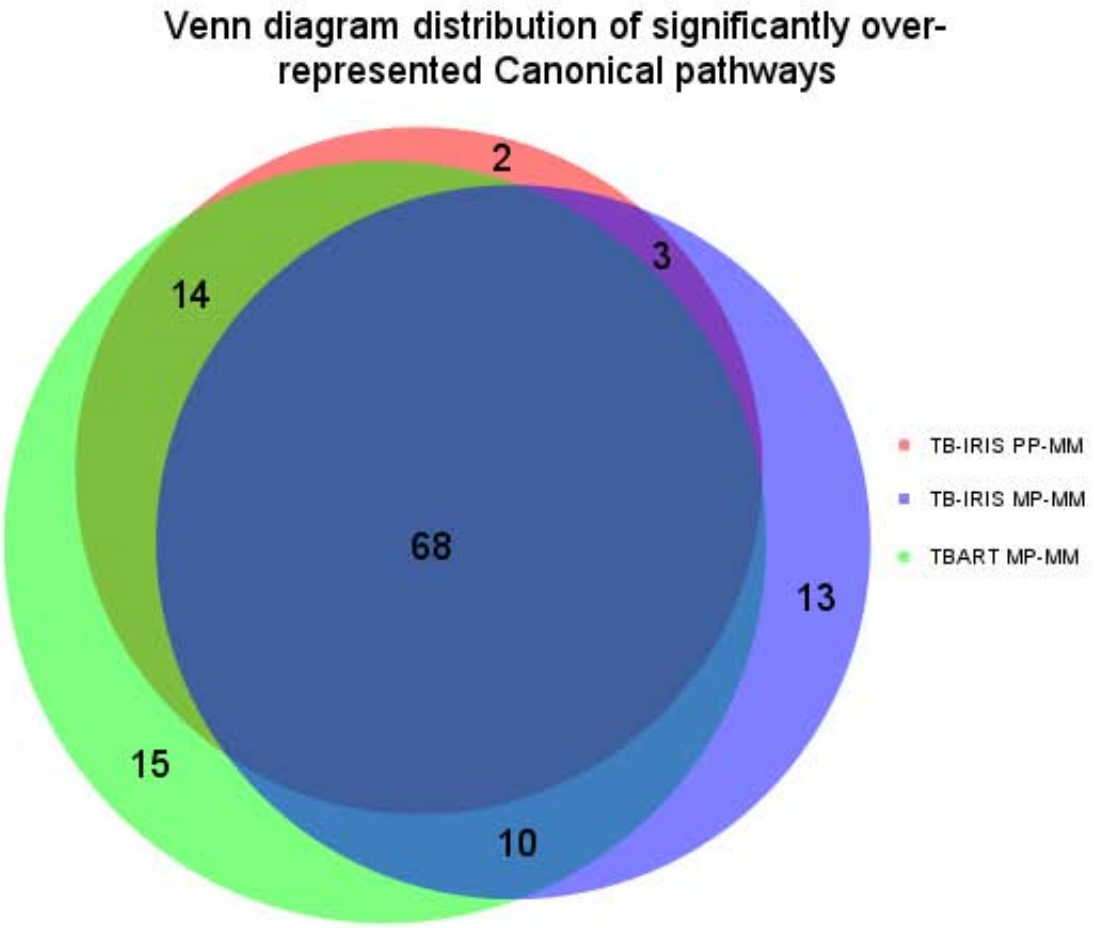

Figure 5.12: Venn diagram of canonical pathway analysis

Venn diagram of significantly over-represented canonical pathways (p-value ≤ 0.05) for the three pairwise datasets. Red circle = TB-IRIS PP-MM, blue circle = TB-IRIS MP-MM, green circle = TBART MP-MM. Numbers represent the number of pathways that are shared by the corresponding datasets or are unique to one dataset.

Table 5.6, lists the individual pathways that are unique across the datasets and as such would have been removed from the previous paired dataset analysis as that was based on significantly over-represented canonical pathways that were common to both sets of data.

Dataset	Pathway	-log[p-value]
TB-IRIS PP-MM	Calcium Signalling	1.35
	Prostate Cancer Signalling	1.45
TB-IRIS MP-MM	Amyloid Processing	1.62
	Antiproliferative Role of Somatostatin Receptor 2	1.33
	Apoptosis Signalling	1.35
	Cardiac β-adrenergic Signalling	1.57
	Colorectal Cancer Metastasis Signalling	1.85
	DNA Double-Strand Break Repair by Non-Homologous End Joining	1.43
	Dopamine Receptor Signalling	1.59
	Endothelin-1 Signalling	1.52
	HIF1α Signalling	1.64
	Hypoxia Signalling in the Cardiovascular System	1.94
	IL-1 Signalling	1.30
	Metabolism of Xenobiotics by Cytochrome P450	1.37
	Sphingosine-1-phosphate Signalling	1.45
	Tumoricidal Function of Hepatic Natural Killer Cells	1.82
TBART MP-MM	Aminosugars Metabolism	1.37
	Amyotrophic Lateral Sclerosis Signalling	1.33
	Bile Acid Biosynthesis	1.37
	Calcium-induced T Lymphocyte Apoptosis	1.70
	Fructose and Mannose Metabolism	1.37
	Galactose Metabolism	1.62
	Glyoxylate and Dicarboxylate Metabolism	2.00
	Mechanisms of Viral Exit from Host Cells	3.19
	nNOS Signalling in Neurons	1.46
	Pentose Phosphate Pathway	1.37
	Primary Immunodeficiency Signalling	1.43
	Tight Junction Signalling	1.66
	Tryptophan Metabolism	1.55

Table 5.6: Unique canonical pathways from IPA analysis
The list of unique canonical pathways identified in Figure 5.12 for the three different datasets used in this analysis.

6 Discussion

It is clear from clinical and immunological data that inflammatory responses to the *M.tb* pathogen differ *in vivo* between TB-IRIS and TBART patients. This study was therefore undertaken to develop a broader understanding of the proteomic phenotypes of TB-IRIS and TBART patient derived PBMCs to better understand at a sub-cellular level the development TB-IRIS. PBMCs were selected to model this difference *in vitro,* using changes in the proteomic expression profiles of these cells in response to *M.tb* to study underlying mechanistic differences as well as to identify potential biomarkers. PBMCs in cell culture represent a well defined model and analysis of their proteome seems likely to reveal a greater degree of complexity than previous immunology studies, built upon the analysis of a limited number of secreted or cell surface marker proteins, have been able to do.

The results of this study provide some fascinating insights regarding the possible mechanisms associated with the development of TB-IRIS, as well as regarding the physiological changes that are induced in TB-IRIS PBMCs by treatment with dexamethasone. Due to the nature of the experimental design, in particular the limiting supply of patient samples and the need to pool samples post-culturing it was not possible to perform biological replicates here; indeed there was not even enough sample for technical replicates. A discussion at the pathway level of analysis therefore appears a more robust approach than that of a protein level analysis in terms of the differences between the expression profiles of TBART and TB-IRIS derived PBMCs. The focus on pathway analysis makes it difficult to identify with great certainty definite biomarkers, but it does provide a platform from which to further study and validate potential biomarkers. The strength of this approach and subsequent data analysis lies in the identification of differences in sub-cellular pathways that have been utilised in response to the dual infections of HIV and TB.

Extraction conundrum: It is important to remember the complexity of the nature of protein extraction. Mass spectrometry based high throughput proteomics inherently requires a protein extraction protocol that is robust, easily repeatable and does not result in a bias towards certain subsets of proteins (unless this is specifically required). This is easier said than done as there is

a trade off that needs to be made during the protein extraction and processing steps. This trade off comes from the need to use relatively harsh lysis buffers to ensure that as complete a protein compliment is extracted in as small a volume as possible. The lysis buffer must also cause the least amount of chemical or other modifications possible (for example the accidental removal of phosphate groups). However these lysis buffers often contain detergents and other reagents that are incompatible with either the enzymatic digestion process or with the LC or mass spectrometer itself. Harsher detergents may yield greater concentrations of proteins but will result in a need for more processing, and subsequent sample loss, before they can be analysed by LC-MS. Not using detergents may result in a poor protein yield that requires little processing before digestion or LC-MS. There is no simple one method for all occasions in proteomics and researchers should always ensure that they understand the research question that the experiment is attempting to answer. Thus it is important to note that an analysis of the proteome at the pathway level should be especially informative on the nature of the sample preparation and the quality of the extraction protocols that have been used.

6.1 Pathway level analysis

The differences at the macro-level of biological functions that were detailed in Figure 5.4 provides a clear indication that there are quantitative differences in the activation and expression profiles of the TB-IRIS and TBART PBMCs. However it is from Figure 5.6 that the qualitative differences can be most easily assessed.

Of particular interest is that there appears to be a decrease in the communication of blood cells in the TB-IRIS MP/MM condition. Despite registering signs of an immune response, deduced from the increased activity in the formation of cellular protrusions and movement of PBMCs and the overall strong overrepresentation of inflammatory response pathways (Figure 5.4), it appears these TB-IRIS PBMCs do not exhibit signs of having a co-ordinated immune response to any measurable degree since they are lacking activation of a number of any distinct innate or adaptive responses. There were a number of immune responses that were identified with a z-score below two (i.e. not activated) and it is plausible that these cells lack a co-ordinated response to the high antigen load that would be present in typical TB-IRIS patients.

By contrast it appears that treatment of TB-IRIS PBMCs with dexamethasone (the TB-IRIS PP/MM dataset) results in a greater number of biological pathways related to an innate immune response being activated, pathways relating to neutrophils, phagocytes, antigen presenting cells and myeloid cells. Whether this is a function of the dexamethasone upregulating these specific

responses or suppressing other immune responses to the extent that a focussed immune response is apparently produced is as yet unclear.

The correlation between the ability of TBART patients to effectively cope with the dual infections of HIV and TB in combination with appropriate treatment could be based on an effective adaptive immune response. The evidence for this can be observed in the fact that PBMCs for the TBART MP/MM dataset exhibit signs of an activated pathway for the adhesion of monocytes and a proliferative T-cell response. This suggests that these cells are capable of recruiting monocytes and activating these an adaptive immune response. These TBART PBMCs also exhibit evidence of having better cellular organisation and it may be that with this improved cellular organisation there is an improved capacity for these cells to form functional granulomas and effectively contain the often excessive *M.tb* antigen load at dispersed sites of disease.

6.1.1 The differing patient responses: TBART vs TB-IRIS

Over representation analysis of identified proteins common to both TBART and TB-IRIS patient derived PBMCs within the context of specific canonical pathways is perhaps a more robust means of analysing differences between these two patient groups who have been shown to display distinctly different patterns of disease progression and responses to treatment *in vivo*.

A closer inspection of the results of the expression profiles in Figure 5.9 reveals that the TBART patient derived PBMCs had consistently higher levels of expression in certain canonical pathways when compared to the TB-IRIS derived patient PBMCs when re-stimulated with H37Rv. Most notable of these pathways were the RhoA signalling pathway, regulation of actin-based motility by Rho pathway, Fcγ receptor-mediated phagocytosis in macrophages and monocytes pathway, integrin signalling pathway, actin cytoskeleton signalling pathway, signalling by Rho Family GTPases pathway, RhoGDI signalling pathway, EIF2 signalling pathway, Rac signalling pathway, actin nucleation by ARP/WASP complex pathway, leukocyte extravasation signalling pathway & the antigen presentation pathway.

Many of these pathways are very closely related and often overlap in terms of pathway regulation or directly flow from one into the other; Figure 6.1 illustrates this for the proteins identified in the TBART MP/MM dataset.

The common factor linking all of these is the role of the actin cytoskeleton in the maintenance and functioning of these cells, notably with respects to: extra-cellular mediated signalling and recruitment of other lymphocytes and leukocytes, cellular motility, engulfing foreign particles, presentation of internally digested antigens, cellular apoptosis and the subsequent clearance of

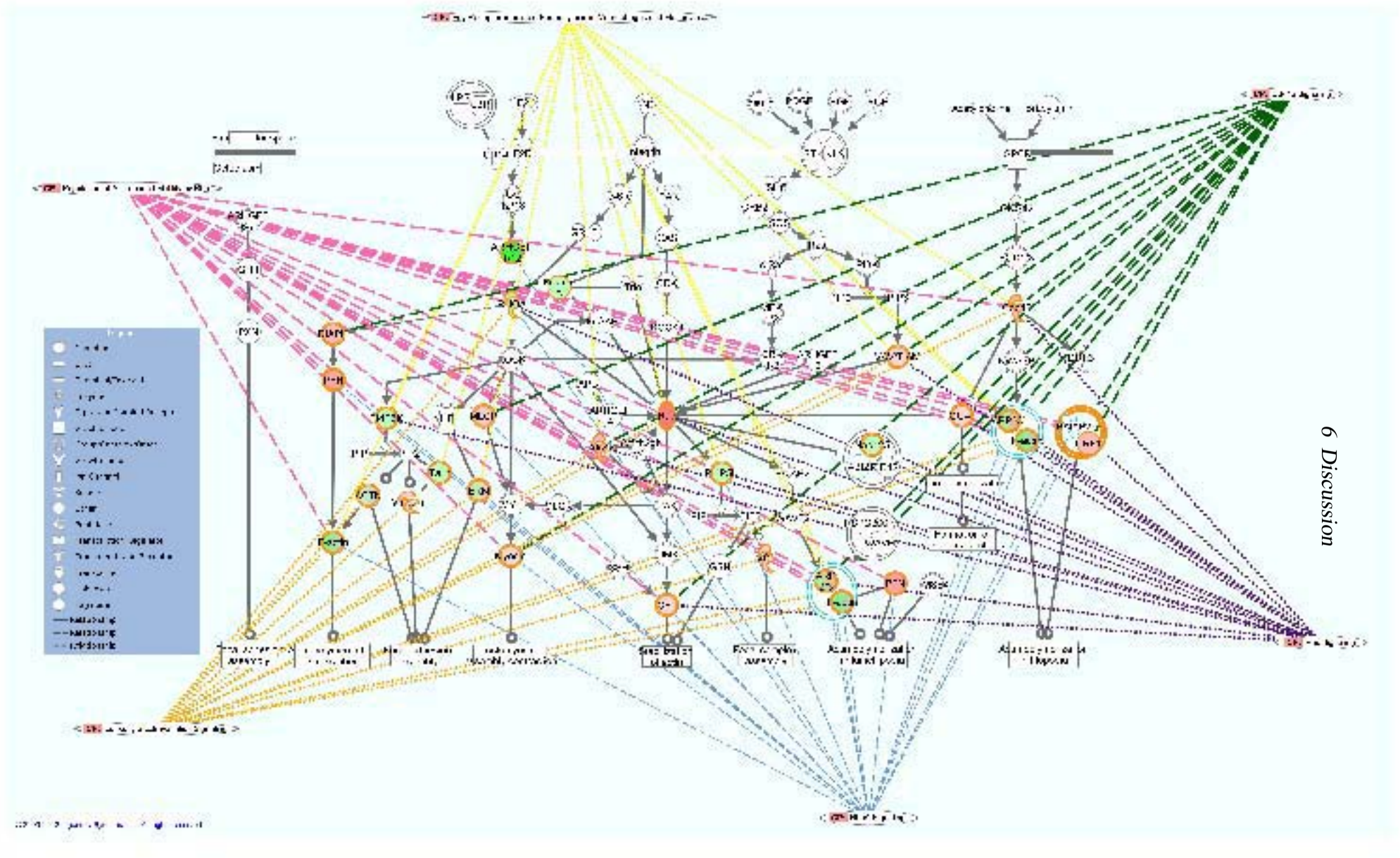

Figure 6.1: Integration of multiple canonical pathways

The base Canonical Pathway represented is Actin Cytoskeleton Signalling and it has been overlaid with other pathways to illustrate how these pathways are integrated specifically at those proteins that have been identified in the TBART MP/MM dataset.

remaining antigens. All of these functions are crucial when combating infections, particularly TB where the capacity to engulf foreign particles or form functional granulomas is of great importance and diminished by dual infection with HIV.

6.1.1.1 Actin cytoskeleton organisation

This key cellular structure (specifically the actin cytoskeleton) can be thought of as a dynamic filament network and is a key structural component of the cell, mediating many biological functions that are dependant on cellular structure such as: cell motility, phagocytosis, antigen presentation, signalling and apoptosis. There are three distinct branches in the actin cytoskeleton organisation pathway and they are activated by various classes of transmembrane receptors, such as integrin receptors, receptor tyrosine kinase or G protein-coupled receptors.

6.1.1.2 Cellular motility

Cellular movement is a result of adhesion, loss of attachment and subsequent re-adhesion of filopodia and lamellipodia structural elements of the cell in a cyclical manner and is perhaps the most relevant of the actin cytoskeleton related cellular functions. It is primarily regulated through the Rho family of small GTPases - notably RhoA, Rac and cell division cycle 42 protein (Cdc42). RhoA is implicated in the formation of actin stress fibres, focal adhesion and actinomyosin assembly. RhoA binds and activates Rho kinase (ROCK), which has several downstream cytoskeletal targets including; increasing myosin light chain (MYL) phosphorylation by directly phosphorylating MYL and inhibiting the myosin light chain phosphatase (MLCP) leading to actinomyosin assembly. ROCK also phosphorylates LIM-kinase (LIMK), which subsequently phosphorylates the actin depolymerising protein, cofilin (CFL), inhibiting its function and resulting in stabilisation of actin. While RhoA causes the formation of stress fibres, stimulation of Rac, through the activation of WAVE and the actin-related protein (ARP) 2/3-actin complex, induces the formation of lamellipodia and activation of Cdc42 leads to the formation of filopodia, through the binding of N-WASP.

These cellular activities need to be tightly controlled and this is achieved, both spatially and temporally, through the nucleation of new actin filaments and the elongation of existing filaments using key regulators of the Wiskott-Aldrich Syndrome Protein (WASP) family, such as N-WASP and up to three variants of SCAR/WAVE (WAVE 1, 2, 3). Nucleation of new actin filaments is spatially controlled by the ARP2/3 complex which is an important regulator of actin nucleation in many cellular processes and is responsible for nucleation of a branched network of

actin filaments at the leading edge of cells - pushing the plasma membrane forward and causing protrusions.

The regulation of cellular motility is integrated and regulated through a number of key canonical pathways, namely: Actin Nucleation by ARP/WASP Complex, Rac signalling, Regulation of Actin-based Motility by Rho, RhoA signalling, RhoGDI signalling and Signalling by Rho Family GTPases. All of these canonical pathways are significantly more over-represented in the TBART MP/MM dataset than in the TB-IRIS MP/MM dataset, suggesting that the TBART derived PBMCs have a better capacity to co-ordinate and execute the required regulation of this important biological function. It conceivable that PBMCs belonging to the TBART patients are more capable of being mobilised to sites of infection and once there are able to elicit a proliferative T-cell response, unlike what has been observed for the TB-IRIS derived PBMCs.

6.1.1.3 Phagocytosis

The capacity to engulf extra-cellular compounds for consumption (in the case of nutrients), destruction (in the case of pathogens) or clearance from the extra-cellular space (in the case of antigens) is an important function of lymphocytes and monocytes. The process of phagocytosis is complicated and normally refers to a number of events that have been grouped together, for example: particle binding, receptor clustering, actin nucleation, pseudopod extension, membrane recycling and phagosome closure. The Fcγ receptors (FcγR) of the immunoglobulin superfamily are well characterized phagocytic receptors in macrophages and monocytes. The receptors signal via immunoreceptor based tyrosine activation motifs (ITAM) when they are activated. When IgG opsonised particles bind to the FcγR and activate it there is resultant tyrosine
phosphorylation of the associated ITAM, creating a binding site for the SRC kinase members like LYN and HCK and the spleen tyrosine kinase (SYK). As previously mentioned, actin assembly and organisation is a crucial step in phagocytosis (especially early in the process) and is triggered by G proteins like Rac and Cdc42 through the activation of the ARP 2/3 complex amongst others. Local polymerization of actin filaments is crucial for the formation and protrusion of pseudopodia that eventually internalize the opsinised particle and this is controlled be a large molecular complex containing WASP that is recruited to the newly formed phagosome and plays a crucial role in actin polymerization and pseudopod extension.

From Figures 6.2 - 6.4 it is clear that the TBART-MP/MM dataset has a greater degree of activation of this pathway compared to the TB-IRIS MP/MM and PP/MM datasets. This ability to clear antigen effectively therefore appears to be one of the key differences between the TBART and TB-IRIS patient derived PBMCs observed here. When looking at the integration of

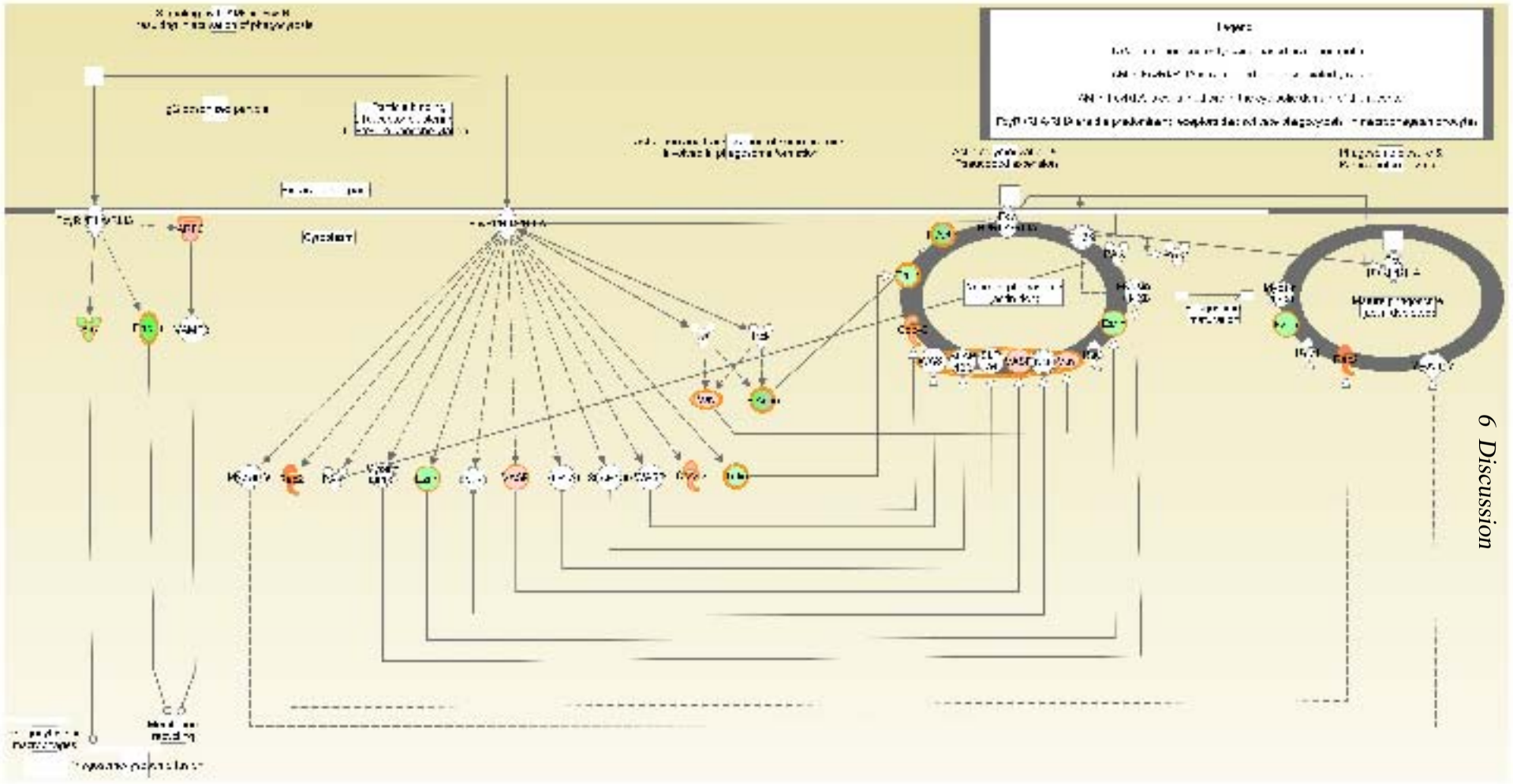

Figure 6.2: Fcγ Receptor-mediated phagocytosis: TBART MP/MM

The three pairwise datasets have each had their identified proteins overlaid on the "Fcγ receptor-mediated phagocytosis in Macrophages and Monocytes" canonical pathway - this Figure represents the TBART MP/MM pairwise dataset. The coloured sections (red - green) represent proteins in the pathway that have been identified and quantified (red is upregulated, green is down regulated) in the respective data sets.

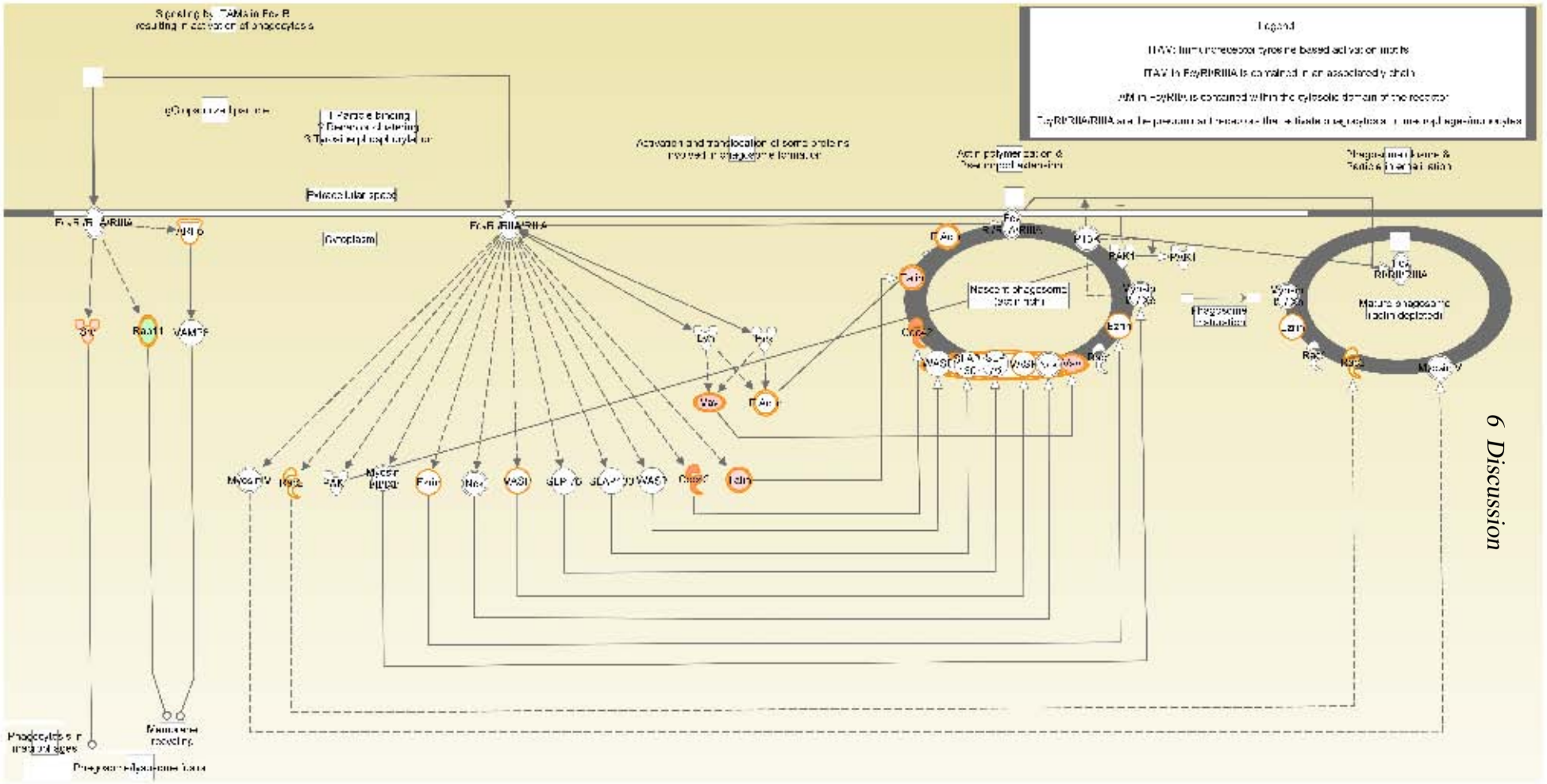

Figure 6.3: Fcγ Receptor-mediated phagocytosis: TB-IRIS MP/MM

The three pairwise datasets have each had their identified proteins overlaid on the "Fcγ receptor-mediated phagocytosis in Macrophages and Monocytes" canonical pathway - this Figure represents the TB-IRIS MP/MM pairwise dataset. The coloured sections (red - green) represent proteins in the pathway that have been identified and quantified (red is upregulated, green is down regulated) in the respective data sets.

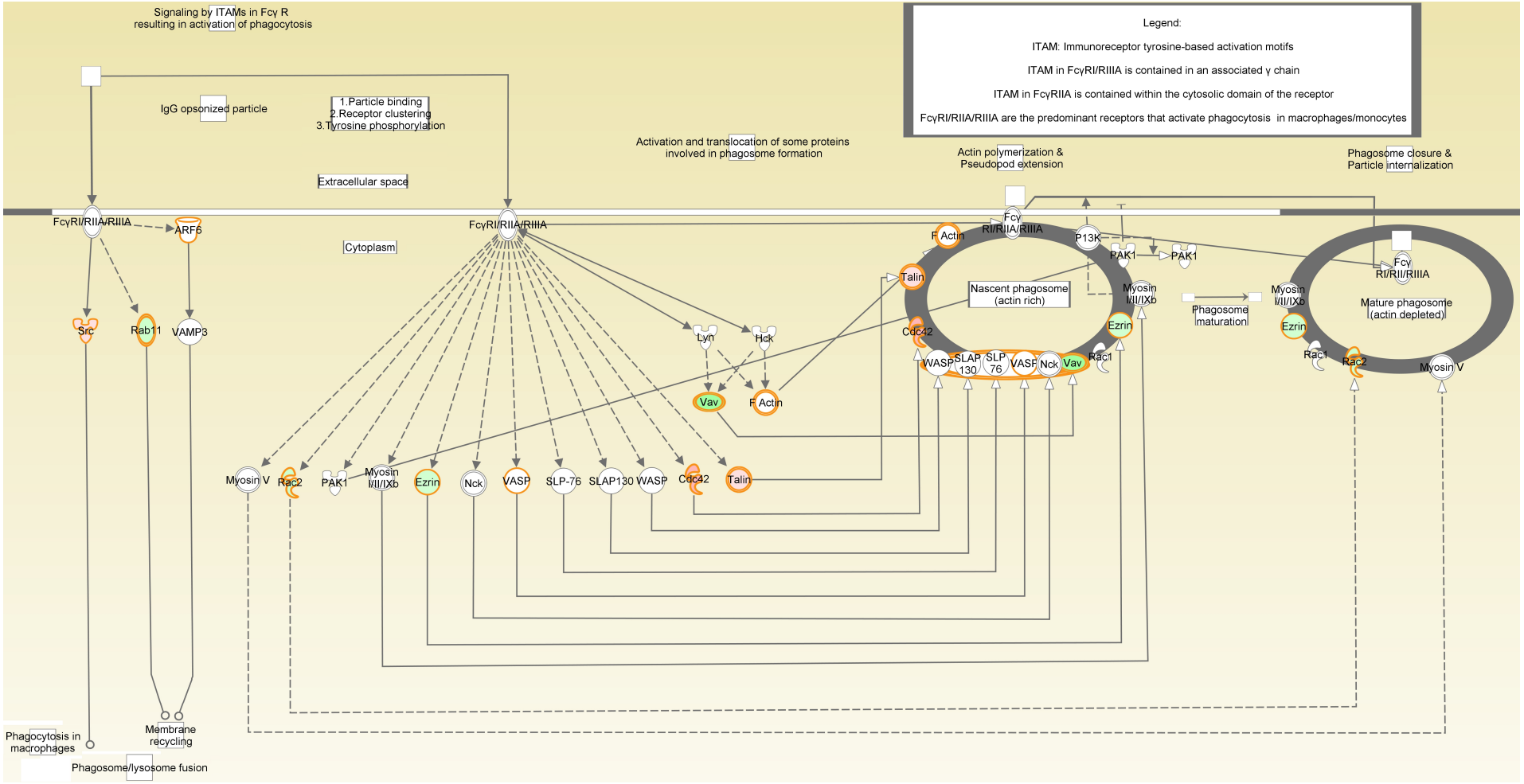

Figure 6.4: Fcγ Receptor-mediated phagocytosis: TB-IRIS PP/MM

The three pairwise datasets have each had their identified proteins overlaid on the "Fcγ receptor-mediated phagocytosis in Macrophages and Monocytes" canonical pathway - this Figure represents the TB-IRIS PP/MM pairwise dataset. The coloured sections (red - green) represent proteins in the pathway that have been identified and quantified (red is upregulated, green is down regulated) in the respective data sets.

identified proteins from the TBART MP/MM dataset in the Fcγ receptor-mediated phagocytic pathway with other canonical pathways that are important in actin cytoskeleton organisation, it becomes obvious that there are a number of key proteins (Table 6.1) that act as regulators for several different pathways and are of importance for the effective functioning of this phagocytic pathway (Figure 6.5).

Protein	Connections
Rac	3
Cdc42	9
N-WASP	6
ARP2/3	8
VASP	3
ROCK	7

Table 6.1: Key proteins integrated in the multiple canonical pathways
The proteins in the above table are key regulators of the "Fcγ Receptor-mediated phagocytosis in Macrophages and Monocytes" canonical as well as key regulators in key canonical pathways that have been identified as significant in Figure 5.8. The connections column denotes within how many of these key pathways these pathways play a regulatory role.

It is also interesting to note that a recent gene expression study on correlates of pathogenesis-driven gene expression signatures in TB observed an up-regulation of the FcγR1 gene as a hallmark of active TB [255]. This perhaps, suggests that TBART derived PBMCs are responding to TB antigen in a similar manner to an HIV negative patient, whilst TB-IRIS derived PBMCs are somehow responding aberrantly.

6.1.1.4 Antigen presentation

The actin cytoskeleton has a key role to play in the presentation of internally produced antigens and is thus a critical component of the host cell's defence against phagocytosed pathogens. The canonical pathway associated with this mechanism is known as the antigen presentation pathway and is intricately linked to the presentation of both internal foreign particles (e.g. proteins or lipids) or endogenously derived antigens. In the case of intra-cellular antigens, such as those derived from tumour cell proteins, this is achieved using the major histocompatibility complex (MHC) Class I system. The MHC Class II system is associated with the presentation of extra-cellular pathogen derived antigens that have been generated through phagocytosis of the pathogen and degradation of the organism in the lysozome before transporting antigenic molecules loaded onto MHC II complexes to the host cell surface. This antigen presentation

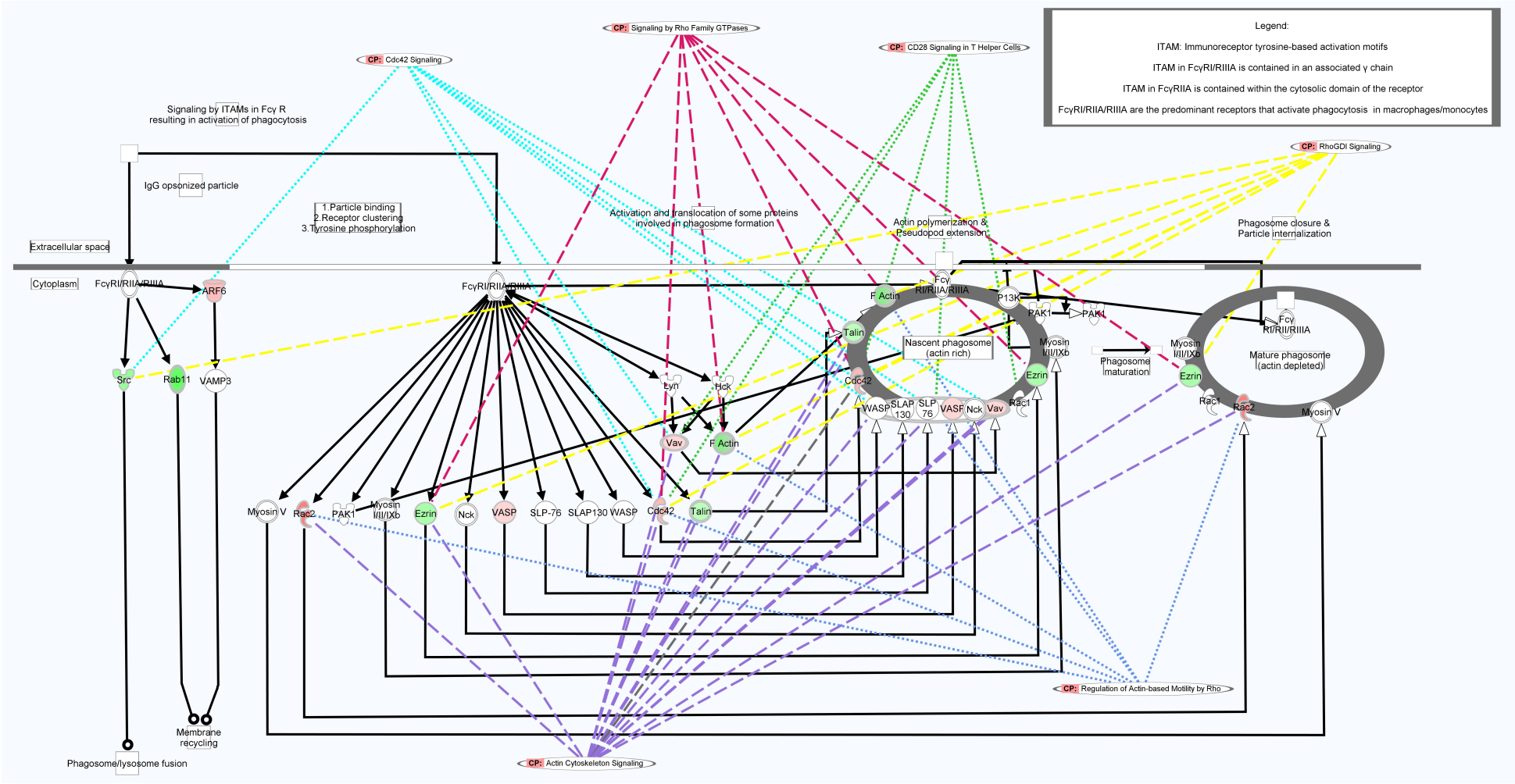

Figure 6.5: Integration of Fcγ receptor-mediated phagocytosis

The base Canonical Pathway represented is Fcγ receptor-mediated phagocytosis in monocytes and macrophages and it has been overlaid with other related pathways to illustrate how these pathways are integrated with other key canonical pathways via specific proteins that have been identified in the TBART MP/MM dataset.

canonical pathway is significantly over-represented in the TBART MP/MM dataset compared to the TB-IRIS MP/MM dataset. A functional antigen presentation process will often result in the activation of an adaptive immune response against the responsible antigen and its source; interestingly, only the TBART PBMCs showed any form of co-ordinated adaptive immune response, as seen in Figure 5.6.

6.1.1.5 Extra-cellular signalling and leukocyte recruitment

The capacity of leukocytes to communicate with the extra-cellular matrix (ECM) that surrounds them is critical for the functioning of these cells as it informs them of what is happening outside of their immediate environment as well as provides an opportunity to communicate any important information about their own internal workings, or failings in the case of intra-cellular infections, to the cells in their immediate environment. Integrin signalling is central to this function and provides the mechanism for these cells to communicate with the ECM. A direct consequence of effective integrin signalling would be the recruitment of leukocytes to sites of inflammation as well as the activation of an adaptive immune response. The TBART PBMCs showed significant over-representation in integrin signalling and the leukocyte extravasation canonical pathways (which is the process whereby leukocytes migrate from blood to tissue during inflammation) compared to the TB-IRIS PBMC datasets, suggesting that these cells were able to effectively communicate with the ECM and recruit more leukocytes to the site of disease.

6.1.1.6 Apoptosis

Apoptosis is a process that most cells undergo at some point in time. There exist a number of mechanisms that can induce apoptosis and many of these are dependent on the health of the cell concerned. Properly functioning cells are capable of inducing apoptosis when required, for instance if infected with a pathogen or if there is dysregulation in the mitochondrial functioning of the cell such as occurs in many cancers. The eukaryotic initiation factor-2 (eIF2) canonical pathway is involved in the synthesis of proteins within the cell and is intricately linked to cell growth and proliferation, intracellular and second messenger signalling, as well as cellular stress and injury responses. Phosphorylation of the eIF2-α subunit ceases protein production and leads to cell apoptosis. This particular canonical pathway was significantly upregulated in the TB-IRIS PBMCs compared to the TBART PBMCs, suggesting these cells are more prone to undergo cellular apoptosis. The root cause of this apoptosis is not clear but it may simply be that the TB-IRIS PBMCs were more fatigued (it is important to remember that these

cells are derived from severely immunocompromised patients at a critical point during their infection, three weeks after HAART initiation, and are likely to be very fragile), or that these cells are unable to effectively deal with the dual infection and are being overrun, resulting in their apoptosis. Regardless of molecular origin though, it is interesting that the TBART derived PBMCs did not have as significant an over-representation of apoptotic pathways as the TB-IRIS patient derived PBMCs.

6.1.2 The effect of dexamethasone

The effect of the dexamethasone treatment would be expected *a priori* to resemble what has already been published with regards to corticosteroids (essentially a broad spectrum suppression of the host immune response)[246, 256–259]. When analysing the differences in canonical pathway over-representation of the TB-IRIS PP and TB-IRIS MP datasets, the assumption is that the only difference in these datasets should be induced by the addition of dexamethasone. A comparative analysis of the TBART MP dataset with respect to the TB-IRIS PP and TB-IRIS MP datasets then represents a further effort to understand whether dexamethasone resolves a TB-IRIS phenotype to a TBART phenotype, or whether it has some other effect.

It is interesting to note the significantly over-represented canonical pathways that are identified in the TBART MP/MM vs TB-IRIS MP/MM comparison (Figure 5.8) but which are absent in the TBART MP/MM vs TB-IRIS PP/MM comparison (Figure 5.10); these patterns are listed in Box 1, Figure 5.11. A more detailed analysis behind the disappearance of these pathways is needed: if these pathways are still present but have a smaller difference between the -log[*p*-values] for pathway over-representation, it would suggest that the effect of the dexamethasone is to induce a more significant response in the associated pathway; however if the pathway becomes absent (has no significant over-representation because not enough proteins belonging to the pathway have been identified) then it is possible that the effect of the dexamethasone is to suppress the associated pathway. Of the six canonical pathways listed in Box 1 of Figure 5.11, four are seen to have an increased degree of over-representation - the two exceptions being the citrate cycle and the antigen presentation pathway.

Similarly, an analysis of the changes in significance of over-representation for the TB-IRIS PP/MM and TB-IRIS MP/MM datasets provides some insight into the differences induced by treatment with dexamethasone. From Box 2, Figure 5.11, it is clear that many of the pathways that are more highly over-represented in the TBART MP/MM dataset comparable to TB-IRIS MP/MM dataset are also more highly over-represented for the TB-IRIS PP/MM dataset compared to the TB-IRIS MP/MM dataset. This suggests that treatment with

dexamethasone results in induction of a number of pathways that are responsible for the correct functioning of TB-IRIS patient derived PBMCs in response to TB antigen - although it appears that it is not to the same extent as in the TBART MP/MM dataset. A notable exception is the protein ubiquitination canonical pathway which shows a greater degree of over-representation in the TB-IRIS PP/MM dataset when compared to the TB-IRIS MP/MM dataset and is not represented at any level of significance for the TBART MP/MM dataset.

6.1.3 Unique canonical pathways

There were a number of canonical pathways that were identified above the threshold level of significance ($p \leq 0.05$) in only one of the datasets and consequently was excluded from the more detailed analyses and comparisons. The lack of replicate data means that inferring too much from these pathways is hazardous. In the field of proteomics, the failure to identify all proteins present in any one experiment might be due to a number of variables (sample complexity, equipment sensitivity and equipment accuracy being some of the many variables) that make it difficult to state with absolute certainty that if a protein has not been identified in a complex sample then it does not exist in that sample. A pathway level analysis alleviates this risk to an extend in that if a few proteins from a pathway are not identified but a number of others are, the pathway will still have a high degree of over-representation.

With this in mind, Table 5.6 represents those canonical pathways that were uniquely identified to any one dataset and which had a level of significance of over-representation. This Table was derived from a Venn diagram analysis of significantly over-represented canonical pathways in all three datasets (Figure 5.12). Encouragingly, more than half of the identified pathways (68 / 125) were common to all 3 datasets and less than 12 % (maximum of 15 / 125) were unique to any one dataset. Of the unique canonical pathways, the majority have a level of significance that is marginal, except for three in particular, namely: the “Glyoxylate and Dicarboxylate Metabolism” and “Mechanisms of Viral Exit from Host Cells” in the TBART MP/MM dataset as well as the “Hypoxia Signalling in the Cardiovascular System” within the TB-IRIS MP/MM dataset. The mechanism of viral exit may seem counter-intuitive initially as the majority of the data suggests that the TBART patient derived PBMCs have lymphocytes that are more capable of cellular maintenance and structure and as such have improved cellular functioning. Furthermore, given that the PBMCs were cultured in the presence of ARVs, viral replication - and hence viral exit from host cells - should have been blocked in all samples. Further investigation of this non-intuitive observation may therefore be warranted in the future.

6.2 Protein level analysis

A brief discussion pertaining to individual strongly differentially expressed identified proteins is merited. However, this discussion must be viewed in the context of the caveats that have been previously mentioned, chief among them being the absence of experimental repeats thus meaning that absolute fold changes observed should be treated with a little caution.

The methodology used in generating these results mean these comparisons are strictly within each patient group (TBART or TB-IRIS) when compared against their baseline expression profiles (i.e. test conditions compared to baseline PBMCs that have been cultured in the absence of dexamethasone and absence of re-stimulation by heat killed H37Rv).

6.2.1 Protein profiles of TBART and TB-IRIS cultured PBMCs

When looking at the proteins for the TBART MP/MM and TB-IRIS MP/MM datasets there are a few interesting trends that appear. For both the fold change data (Tables 5.2 & 5.3) and the log[ratio] data (Figures 5.1 & 5.2) the protein Thioredoxin domain-containing protein 5 (TXNDC5) appears to be up-regulated in the TBART MP/MM dataset whilst being down-regulated for the TB-IRIS MP/MM dataset. TXNDC5 is thought to be located in the lumen of the endoplasmic reticulum and has been shown to be associated with the obstruction of apoptotic pathways in human umbilical vein endothelial cells [260]. The opposing expression profile for the TBART MP/PP and TB-IRIS MP/MM datasets adds to the evidence suggesting that TB-IRIS PBMCs are more likely to undergo apoptosis and consequently exacerbate the dysfunctional immune response seen in TB-IRIS patients. Other proteins identified in these lists have been shown to have prominent roles in some important canonical pathways such as integrin signalling, RhoGDI signalling, Fcγ Receptor-mediated phagocytosis and Rac signalling; these pathways have been considered previously (Subsection 6.1.1) so these individual pathways will not be discussed further here.

6.2.2 Changes in protein expression in response to dexamethasone

The list of proteins with the greatest changes in expression levels for the TB-IRIS MP/MM and TB-IRIS PP/MM datasets have a two proteins that are shared (PDIA4 and INF2). Protein disulfide-isomerase A4 catalyses the arrangement of disulphide bonds in proteins and inverted formin-2 (INF2) is thought to have a role in the severing of actin filaments and accelerates their polymerisation and depolymerisation. Cell division control protein 42 (Cdc42) is a plasma

membrane-associated small GTPase and has been shown to be an important regulatory protein for a number of cellular processes. There also appear to be a greater number of proteins from the TB-IRIS PP/MM dataset that are associated with similar canonical pathways as those found in the TBART MP/MM dataset, although this is not exclusively so.

6.3 Conclusion

6.3.1 The molecular origin of TB-IRIS

Previous work in mouse fibroblasts has shown the importance of the actin cytoskeleton in the functioning, maintenance and motility of these cells. The dynamic nature of the actin cytoskeleton in response to external stimuli can be seen in Figure 6.6.

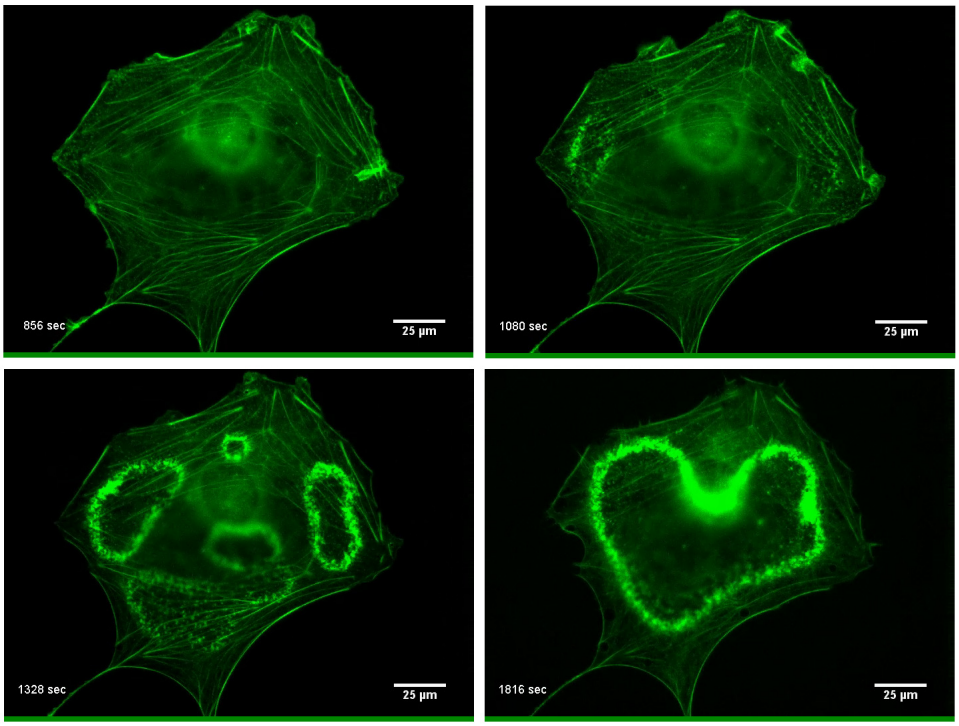

Figure 6.6: Time lapse sequence of GFP-actin stained ruffles in mouse fibroblast
The sequence of pictures are a set of still shots that have been acquired from a time-lapse video and shows live-cell imaging of an actin-GFP expressing mouse fibroblast responding to platelet-derived growth factor (PDGF) with circular dorsal ruffles. Circular dorsal ruffles are dynamic, F-actin-enriched plasma membrane structures that transiently occur on the dorsal surface of fibroblasts in response to mitogenic stimuli such as PDGF. These dynamic structures form within minutes of stimulation and generally disappear within 30 minutes. The proposed functions of these dorsal ruffles include the internalization of growth factor receptors, macropinocytosis/fluid phase uptake, and cytoskeletal rearrangements required for cell movement. Note that ruffles expand into circles that eventually coalesce, in this unusual case to generate the image of a heart [261].

It is clear from Figure 5.8 that there are differences in the *in vitro* canonical pathway expression profiles of TB-IRIS and TBART patient derived PBMCs when re-stimulated with heat killed H37Rv. Many of the pathways that are positively associated to the TBART PBMCs are involved in the organisational maintenance of the actin cytoskeleton and consequently the cellular structure of these cells. Correct cellular organisation of the actin cytoskeleton is critical for motility, maintenance, signalling and proper biological functioning, thus it is plausible that the lack of this cellular organisation within TB-IRIS patient derived PBMCs *in vitro* could be associated with the dysfunctional immune response that is the primary characteristic of TB-IRIS patients *in vivo*.

The differences in the activation scores of specific biological functions (Figure 5.6), are also indicative of fundamental differences in the type of immune response that these patient derived PBMCs are undergoing. TB-IRIS MP PBMCs appear to have a number of pathways activated, but few reach the statistically significant threshold scores of $-2 \geq x \geq 2$, suggesting that there is a lack of co-ordination in how these cells are responding to re-stimulation with TB antigen. Thus, despite the overall immune response being vigourous, it appears to be ineffective in dealing with the root cause of the problem. Perhaps the most illuminating activation score is the interaction of blood cells, which decreases significantly, strongly supporting the hypothesis that these cells lack a co-ordinated immune response of any sorts. By treating these cells with dexamethasone (the TB-IRIS PP/MM dataset) it appears that the response tends towards becoming a co-ordinated innate response - however the exact molecular mechanism by which this is achieved is not immediately clear. It may be that the dexamethasone dampens some of the numerous inflammatory responses that the untreated cells activate in the presence of TB antigen, leading to the innate responses becoming seemingly more up-regulated; or it may be that the dexamethasone stimulates the innate pathways directly and thus achieving the same apparent result. For the TBART patient derived PBMCs there is a clear activation of T-cell response functions which suggests that these patients have a innate capacity to contain and clear the TB antigen using an adaptive immune response, which is in contrast to the TB-IRIS patients.

Most of the canonical pathways that were positively associated with the TB-IRIS patient derived PBMCs have been shown to have a strong link to cellular apoptosis. Whether this is due to cellular fatigue or immunologically functional fatigue (which is a hallmark of HIV, especially if a patient has been has been infected for a long time) or is as a consequence of a dysregulated immune response is as yet unclear.

The difference in incubation times prior to the development of clinical symptoms for "paradoxical" TB-IRIS patients post HAART initiation may be rooted in the failure of TB-IRIS patient derived PBMCs to organise their cytoskeletal structure. Thus, resulting in the decline in the capacity of the host immune response to contain the TB infection within functional

granulomas and leading to an aberrant inflammatory response to potentially higher loads of systemic antigenic compounds.

6.3.2 The mechanism of action of dexamethasone

The initial hypotheses on the mechanism of action for dexamethasone as a treatment for TB-IRIS patient derived PBMCs was that the dexamethasone somehow affected the cell morphology and phenotype of the PBMCs and caused these cells to behave more like TBART patient derived PBMCs.

The over-representation of canonical pathway expression profiles of these three datasets suggests that treatment TB-IRIS derived PBMCs with dexamethasone *in vitro* does induce a change in the canonical pathway expression profile that has a number of similarities with the proteins identified in the TBART MP/MM dataset. The degree of this overlap is difficult to quantify however since there are a greater number of pathways that overlap between the TB-IRIS MP/MM and TB-IRIS PP/MM datasets whilst only a few key pathways change. It may be that the suppression of the inflammatory response that is a consequence of treatment with a corticosteroid may result in the PBMCs being provided an environment in which they are able to partly better maintain their cellular cytoskeletal structure, with this resulting in a slightly improved response to the infections with TB and HIV. It is plausible that despite an opportunity to improve cellular structure in these patients through concurrent dexamethasone treatment, the fundamental immune dysregulation would result in these patients suffering an inflammatory relapse if they were to stop corticosteroid treatment before sufficient antigen clearance had occurred. This theory could explain the approximately 20 % of TB-IRIS patients on prednisone who in fact have halted their corticosteroid treatment and promptly suffered from severe
inflammatory relapse.

6.3.3 Identification of possible biomarkers

As previously stated, the nature of the experimental design has made it difficult to identify biomarkers with any statistical confidence, yet there were a number of proteins whose expression profiles proved to be interesting. Not surprisingly the majority of these appeared within the regulatory pathways related to the functioning of the actin cytoskeleton or related to Fcγ receptor-mediated phagocytosis. Identifying a biomarker suffers from a number of constraints as the target molecule behaviour may be varied. A biomarker could be said to

be completely absent in the test or control group, only present in the test or control group or have a change in expression levels (either up or down) in the test versus control group. Thus it is important to establish the nature of the biomarker before being able to speculate with confidence about potential biomarkers. Some of the biomarkers identified in Table 5.4 are associated with antigen presentation and receptor signalling and may provide an interesting starting point for future research into the identification of viable biomarkers of TB-IRIS risk.

7 Future work

Previous and current literature suggests that TB-IRIS is somehow connected to the dysregulation of the Th1/Th2 (Figure 7.1) response system as well as to differences in the ability to elicit a primed innate response resulting in a co-ordinated adaptive immune response[262, 263].

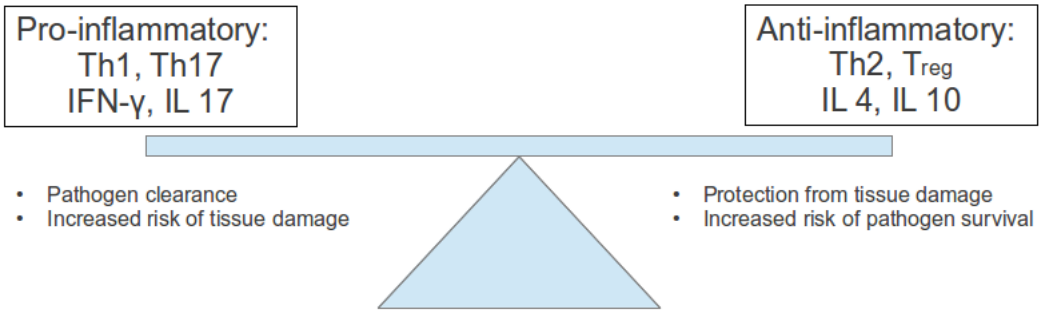

Figure 7.1: Th1/Th2 response mechanism

A simplistic overview of the components of the Th1/Th2 response mechanism that is prevalent in the host defense against pathogenic infections such as *M.tb*. A balanced response would see an increase in the Th1 activators to control an infection and then followed by the restriction of this response through an increase in the Th2 activators once the infection is under control.

These hypotheses have been founded mainly on cytokine data, which has previously been the dominant source of evidence in this field of study. The new data generated the present study using high throughput proteomics has shown that PBMCs derived from TB-IRIS and TBART patients behave differently and often in a manner that is consistent with current hypotheses - yet the large amount of new data has led to new hypotheses centering on the differing nature of the inflammatory response and antigen processing that TBART and TB-IRIS patients appear to experience, as described in Figure 7.2.

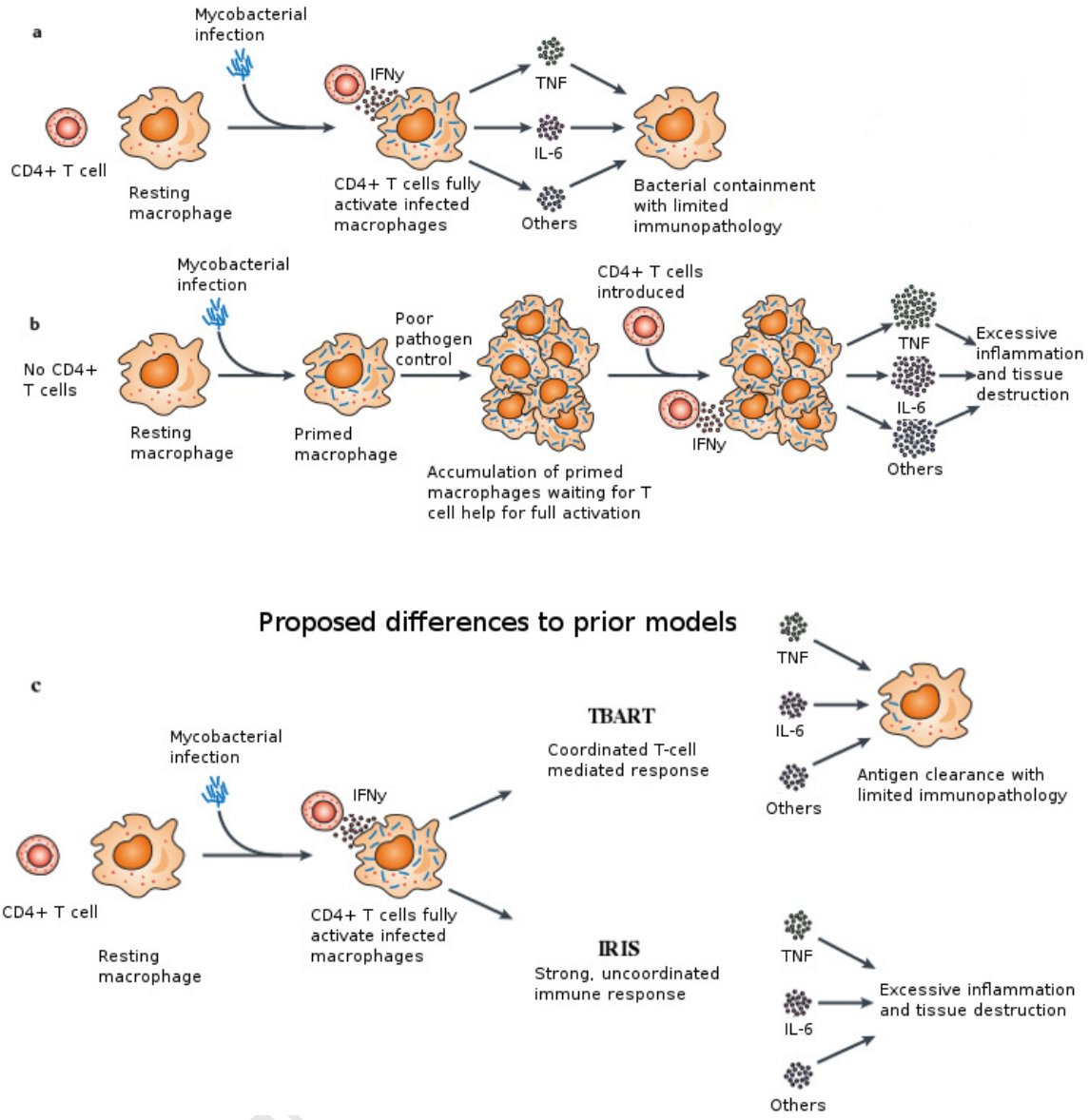

Figure 7.2: A model of TB-IRIS

The TB-IRIS model depicted here is adapted from Barber *et al* [263], who proposes that there is an uncoupling of the innate and adaptive immune responses during *M.tb* infection, resulting in excessive inflammation. (A) A normal response = Macrophages require two signals to become fully activated. Firstly, the innate host response recognises microbial products by pattern recognition receptors, which prime the cells for further activation leading to the second response involving interaction with IFNγ-producing CD4+ T cells, thus leading to fully activated macrophages and the production of high levels of pro-inflammatory mediators such as TNF and IL-6. (B) T-cell deficient response = the host infected macrophage cells become primed by microbial products but never become fully activated and execute their pro-inflammatory effector functions. This leads to an increase in pathogen load and results in an exaggerated T cell response after the immune system reconstitutes. (C) Our adapted model showing the differences between the TBART and TB-IRIS patients whereby it appears the TBART patients are able to elicit a priming innate response leading to an adaptive immune response in a well co-ordinated manner, however the TB-IRIS patients elicit strong but uncoordinated innate immune responses that do not result in an effective adaptive immune response, resulting in a severe inflammatory response after the immune system reconstitutes.

Critically these differences appear to be CD4 T-cell independent, unlike the Barer model. Instead, the data generated here suggests that either there is some intrinsic defect in monocytes/ NK cells in TB-IRIS patients or, perhaps more likely, that there is a difference in the activation of these cells in TB-IRIS patients. The present data also suggests a possible role for B-cell deficiencies in TB-IRIS patients since the Fcγ receptor pathways appear to be down regulated compared to TBART patients.

Fresh perspectives using high throughput proteomics have led to new questions and it would be of significant interest to isolate and identify the differing proteomic profiles of specific sub-populations of PBMCs (e.g. B cells, T cells etc.) so as to ascertain which of these cell populations are the key role players in the differing immune responses for both the TBART and TB-IRIS patients as well as to provide a more fine tuned analysis of the qualitative nature of this response at a mechanistic level. Thus future work should focus on initially repeating this work using a more reliable method of quantitation as well a greater number of replicates before delving deeper into the differing nature of the immune response and antigen processing that exists between these two disease states using high throughput proteomic techniques. This would no doubt be made easier if the efficiency of the protein extraction protocol could be improved upon. Transcriptomic analysis would also be a possible avenue for future research depending on what resources were available to the researcher in question.

Another avenue of research that would be of immense value would be to analyse the progression of the immune responses for both disease states using high throughput techniques so as to be able to track the aetiology and progression of pathology from prior to initiation of ARVs through to the development (or not, in the case of TBART patients) of IRIS.

Bibliography

[1] C. Dye, S. Scheele, P. Dolin, V. Pathania, and M. C. Raviglione, "Global Burden of Tuberculosis Estimated Incidence , Prevalence , and Mortality by Country," *Journal of the American Medical Association*, vol. 282, no. 7, pp. 677 – 686, 1999.

[2] T. M. Daniel, J. H. Bates, and K. A. Downes, "History of tuberculosis," in *Tuberculosis: pathogenesis, protection, and control*, B. R. Bloom, Ed. Washington D.C.: ASM Press, 1994, pp. 13–24. [Online]. Available: http://estore.asm.org/viewItemDetails.asp?ItemID=213

[3] A. M. Abdallah, N. C. Gey van Pittius, P. A. D. Champion, J. Cox, J. Luirink, C. M. J. E. Vandenbroucke-Grauls, B. J. Appelmelk, and W. Bitter, "Type VII secretion–mycobacteria show the way." *Nature Reviews Microbiology*, vol. 5, no. 11, pp. 883–91, Nov. 2007. [Online]. Available: http://www.ncbi.nlm.nih.gov/pubmed/17922044

[4] World Health Organization, "Global Tuberculosis Control: WHO report 2011," *Tuberculosis*, p. 246, 2011. [Online]. Available: http://whqlibdoc.who.int/publications/2011/9789241564380_eng.pdf

[5] Government of South Africa, "HIV and AIDS and STI Strategic Plan for South Africa, 2007-2011," Tech. Rep., 2007. [Online]. Available: http://www.info.gov.za/otherdocs/2007/aidsplan2007/index.html

[6] South African National AIDS Council, "National Strategic Plan 2012-2016," Tech. Rep., 2011. [Online]. Available: http://www.sanac.org.za/index.php/component/content/article/80-nsp-2012-2016/national-strategic-plan/103-nsp

[7] S. Gagneux and P. M. Small, "Global phylogeography of Mycobacterium tuberculosis and implications for tuberculosis product development." *The Lancet Infectious Diseases*, vol. 7, no. 5, pp. 328–37, May 2007. [Online]. Available: http://www.ncbi.nlm.nih.gov/pubmed/17448936

[8] S. Gagneux, K. DeRiemer, T. Van, M. Kato-Maeda, B. C. de Jong, S. Narayanan, M. Nicol, S. Niemann, K. Kremer, M. C. Gutierrez, M. Hilty, P. C. Hopewell, and P. M. Small, "Variable host-pathogen compatibility in Mycobacterium tuberculosis." *Proceedings of the National Academy of Sciences of the United States of America*, vol. 103, no. 8, pp. 2869–73, Feb. 2006. [Online]. Available: http://www.pubmedcentral.nih.gov/articlerender.fcgi?artid=1413851&tool=pmcentrez&rendertype=abstract

[9] S. H. E. Kaufmann, "Deadly combination," *Nature*, vol. 453, no. May, 2008.

[10] A. M. Dannenberg, "Immune mechanisms in the pathogenesis of pulmonary tuberculosis." *Reviews of Infectious Diseases*, vol. 11 Suppl 2, pp. S369–78. [Online]. Available: http://www.ncbi.nlm.nih.gov/pubmed/2496453

[11] S. M. Opal, "Anti-Inflammatory Cytokines," *Chest*, vol. 117, no. 4, pp. 1162–1172, Apr. 2000. [Online]. Available: http://www.chestjournal.org/cgi/doi/10.1378/chest.117.4.1162

[12] B. M. Saunders and A. M. Cooper, "Restraining mycobacteria: role of granulomas in mycobacterial infections." *Immunology and Cell Biology*, vol. 78, no. 4, pp. 334–41, 2000. [Online]. Available: http://www.ncbi.nlm.nih.gov/pubmed/10947857

[13] D. O. Adams, "The granulomatous inflammatory response. A review." *American Journal Pathology*, vol. 84, no. 1, pp. 164 – 192, 1976.

[14] J. Daniel, H. Maamar, C. Deb, T. D. Sirakova, and P. E. Kolattukudy, "Mycobacterium tuberculosis uses host triacylglycerol to accumulate lipid droplets and acquires a dormancy-like phenotype in lipid-loaded macrophages." *PLoS Pathogens*, vol. 7, no. 6, p. e1002093, Jun. 2011. [Online]. Available: http://www.pubmedcentral.nih.gov/articlerender.fcgi?artid=3121879&tool=pmcentrez&rendertype=abstract

[15] J. Gomez, "M. tuberculosis persistence, latency, and drug tolerance," *Tuberculosis*, vol. 84, no. 1-2, pp. 29–44, 2004. [Online]. Available: http://linkinghub.elsevier.com/retrieve/pii/S1472979203000866

[16] C. Watt, M. Hosseini, K. Lönnroth, B. Williams, and C. Dye, "The global epidemiology of tuberculosis," in *Tuberculosis: a comprehensive clinical reference*, S. S and Z. A, Eds. Philadelphia, PA: Saunders, 2009, pp. 17 – 27.

[17] S. Cole, R. Brosch, J. Parkhill, and T. Garnier, "Deciphering the biology of Mycobacterium tuberculosis from the complete genome sequence," *Nature*, vol. 396, no. NOVEMBER, 1998. [Online]. Available: http://www.nature.com/nature/journal/v393/n6685/abs/393537a0.html

[18] J. Camus, M. Pryor, C. Médigue, and S. Cole, "Re-annotation of the genome sequence of Mycobacterium tuberculosis H37Rv," *Microbiology*, vol. 148, no. 10, p. 2967, 2002. [Online]. Available: http://mic.sgmjournals.org/content/148/10/2967.short

[19] D. B. Meya and K. P. W. J. McAdam, "The TB pandemic: an old problem seeking new solutions." *Journal of Internal Medicine*, vol. 261, no. 4, pp. 309–29, 2007. [Online]. Available: http://www.ncbi.nlm.nih.gov/pubmed/17391107

[20] C. Boehme, E. Molokova, F. Minja, S. Geis, T. Loscher, L. Maboko, V. Koulchin, and M. Hoelscher, "Detection of mycobacterial lipoarabinomannan with an antigen-capture ELISA in unprocessed urine of Tanzanian patients with suspected tuberculosis." *Transactions of the Royal Society of Tropical Medicine and Hygiene*, vol. 99, no. 12, pp. 893–900, Dec. 2005. [Online]. Available: http://www.ncbi.nlm.nih.gov/pubmed/16139316

[21] S. D. Lawn and M. P. Nicol, "Xpert MTB/RIF assay: development, evaluation and implementation of a new rapid molecular diagnostic for tuberculosis and rifampicin resistance." *Future Microbiology*, vol. 6, pp. 1067–82, Sep. 2011. [Online]. Available: http://www.ncbi.nlm.nih.gov/pubmed/21958145

[22] M. Harboe, "Antigens of PPD, old tuberculin, and autoclaved Mycobacterium bovis BCG studied by crossed immunoelectrophoresis." *The American Review of Respiratory Disease*, vol. 124, no. 1, pp. 80–7, Jul. 1981. [Online]. Available: http://www.ncbi.nlm.nih.gov/pubmed/7020505

[23] H. Sarrazin, K. A. Wilkinson, J. Andersson, M. X. Rangaka, L. Radler, K. van Veen, C. Lange, and R. J. Wilkinson, "Association between tuberculin skin test reactivity, the memory CD4 cell subset, and circulating FoxP3-expressing cells in HIV-infected persons." *The Journal of Infectious Diseases*, vol. 199, no. 5, pp. 702–10, Mar. 2009. [Online]. Available: http://www.ncbi.nlm.nih.gov/pubmed/19199536

[24] C. S. Hirsch, J. L. Johnson, and J. J. Ellner, "Pulmonary tuberculosis." *Current Opinion in Pulmonary Medicine*, vol. 5, no. 3, pp. 143–50, May 1999. [Online]. Available: http://www.ncbi.nlm.nih.gov/pubmed/10228738

[25] R. E. Huebner, M. F. Schein, and J. B. Bass, "The tuberculin skin test." *Clinical Infectious Diseases*, vol. 17, no. 6, pp. 968–75, Dec. 1993. [Online]. Available: http://www.ncbi.nlm.nih.gov/pubmed/8110954

[26] T. Oni, J. Patel, H. P. Gideon, R. Seldon, K. Wood, Y. Hlombe, K. A. Wilkinson, M. X. Rangaka, M. Mendelson, and R. J. Wilkinson, "Enhanced diagnosis

of HIV-1-associated tuberculosis by relating T-SPOT.TB and CD4 counts." *The European Respiratory Journal*, vol. 36, no. 3, pp. 594–600, Sep. 2010. [Online]. Available: http://www.pubmedcentral.nih.gov/articlerender.fcgi?artid=3025278&tool=pmcentrez&rendertype=abstract

[27] American Thoracic Society, "Diagnostic Standards and Classification of Tuberculosis in Adults and Children. This official statement of the American Thoracic Society and the Centers for Disease Control and Prevention was adopted by the ATS Board of Directors, July 1999. This statemen," *American Journal of Respiratory and Critical Care Medicine*, vol. 161, no. 4 Pt 1, pp. 1376–95, Apr. 2000. [Online]. Available: http://www.ncbi.nlm.nih.gov/pubmed/10764337

[28] G. Kubica, "Photomicrograph of Mycobacterium tuberculosis bacteria using acid-fast Ziehl-Neelsen stain," 1979. [Online]. Available: http://phil.cdc.gov/PHIL_Images/20040615/d094324845a24eb3a7bfe0d1f8e4a637/5789_lores.jpg

[29] D. A. J. Moore, C. A. W. Evans, R. H. Gilman, L. Caviedes, J. Coronel, A. Vivar, E. Sanchez, Y. Piñedo, J. C. Saravia, C. Salazar, R. Oberhelman, M.-G. Hollm-Delgado, D. LaChira, A. R. Escombe, and J. S. Friedland, "Microscopic-observation drug-susceptibility assay for the diagnosis of TB." *The New England Journal of Medicine*, vol. 355, no. 15, pp. 1539–50, Oct. 2006. [Online]. Available: http://www.pubmedcentral.nih.gov/articlerender.fcgi?artid=1780278&tool=pmcentrez&rendertype=abstract

[30] World Health Organization, "WHO endorses new rapid tuberculosis test," p. 1, 2010. [Online]. Available: http://www.who.int/mediacentre/news/releases/2010/tb_test_20101208/en/index.html

[31] G. Pantaleo, C. Graziosi, and A. S. Fauci, "New concepts in the immunopathogenesis of human immunodeficiency virus infection." *The New England Journal of Medicine*, vol. 328, no. 5, pp. 327–35, Feb. 1993. [Online]. Available: http://www.ncbi.nlm.nih.gov/pubmed/8093551

[32] F. X. Berthet, P. B. Rasmussen, I. Rosenkrands, P. Andersen, and B. Gicquel, "A Mycobacterium tuberculosis operon encoding ESAT-6 and a novel low-molecular-mass culture filtrate protein (CFP-10)." *Microbiology*, vol. 144 (Pt 1, pp. 3195–203, Nov. 1998. [Online]. Available: http://www.ncbi.nlm.nih.gov/pubmed/9846755

[33] A. L. Sorensen, S. Nagai, G. Houen, P. Andersen, and A. B. Andersen, "Purification and characterization of a low-molecular-mass T-cell antigen secreted by

Mycobacterium tuberculosis." *Infection and Immunity*, vol. 63, no. 5, pp. 1710–7, May 1995. [Online]. Available: http://www.pubmedcentral.nih.gov/articlerender.fcgi?artid=173214&tool=pmcentrez&rendertype=abstract

[34] A. S. Mustafa, "Recombinant and synthetic peptides to identify Mycobacterium tuberculosis antigens and epitopes of diagnostic and vaccine relevance." *Tuberculosis*, vol. 85, no. 5-6, pp. 367–76, 2005. [Online]. Available: http://www.ncbi.nlm.nih.gov/pubmed/16253561

[35] L. Leidl, H. Mayanja-Kizza, G. Sotgiu, J. Baseke, M. Ernst, C. Hirsch, D. Goletti, Z. Toossi, and C. Lange, "Relationship of immunodiagnostic assays for tuberculosis and numbers of circulating CD4+ T-cells in HIV infection." *The European Respiratory Journal*, vol. 35, no. 3, pp. 619–26, Mar. 2010. [Online]. Available: http://www.ncbi.nlm.nih.gov/pubmed/19608590

[36] M. Sester, C. Giehl, U. Sester, and a. Meyerhans, "Management of tuberculosis in HIV infection: where T-cells matter." *The European Respiratory Journal*, vol. 35, no. 3, pp. 475–6, Mar. 2010. [Online]. Available: http://www.ncbi.nlm.nih.gov/pubmed/20190327

[37] a. Jindani, a. J. Nunn, and D. a. Enarson, "Two 8-month regimens of chemotherapy for treatment of newly diagnosed pulmonary tuberculosis: international multicentre randomised trial." *The Lancet*, vol. 364, no. 9441, pp. 1244–51, 2004. [Online]. Available: http://www.ncbi.nlm.nih.gov/pubmed/15464185

[38] A. Pablos-Méndez, M. C. Raviglione, A. Laszlo, N. Binkin, H. L. Rieder, F. Bustreo, D. L. Cohn, C. S. Lambregts-van Weezenbeek, S. J. Kim, P. Chaulet, and P. Nunn, "Global surveillance for antituberculosis-drug resistance, 1994-1997. World Health Organization-International Union against Tuberculosis and Lung Disease Working Group on Anti-Tuberculosis Drug Resistance Surveillance." *The New England Journal of Medicine*, vol. 338, no. 23, pp. 1641–9, Jun. 1998. [Online]. Available: http://www.ncbi.nlm.nih.gov/pubmed/9614254

[39] M. A. Espinal, A. Laszlo, L. Simonsen, F. Boulahbal, S. J. Kim, A. Reniero, S. Hoffner, H. L. Rieder, N. Binkin, C. Dye, R. Williams, and M. C. Raviglione, "Global trends in resistance to antituberculosis drugs. World Health Organization-International Union against Tuberculosis and Lung Disease Working Group on Anti-Tuberculosis Drug Resistance Surveillance." *The New England Journal of Medicine*, vol. 344, no. 17, pp. 1294–303, Apr. 2001. [Online]. Available: http://www.ncbi.nlm.nih.gov/pubmed/11320389

[40] M. Zignol, M. S. Hosseini, A. Wright, C. L.-v. Weezenbeek, P. Nunn, C. J. Watt, B. G. Williams, and C. Dye, "Global incidence of multidrug-resistant tuberculosis." *The Journal of Infectious Diseases*, vol. 194, no. 4, pp. 479–85, Aug. 2006. [Online]. Available: http://www.ncbi.nlm.nih.gov/pubmed/16845631

[41] N. R. Gandhi, A. Moll, a. W. Sturm, R. Pawinski, T. Govender, U. Lalloo, K. Zeller, J. Andrews, and G. Friedland, "Extensively drug-resistant tuberculosis as a cause of death in patients co-infected with tuberculosis and HIV in a rural area of South Africa." *The Lancet*, vol. 368, no. 9547, pp. 1575–80, Nov. 2006. [Online]. Available: http://www.ncbi.nlm.nih.gov/pubmed/17084757

[42] H. S. Schaaf, A. P. Moll, and K. Dheda, "Multidrug- and extensively drug-resistant tuberculosis in Africa and South America: epidemiology, diagnosis and management in adults and children." *Clinics in Chest Medicine*, vol. 30, no. 4, pp. 667–83, vii–viii, 2009. [Online]. Available: http://www.ncbi.nlm.nih.gov/pubmed/19925960

[43] G. B. Migliori, M. D'Arcy Richardson, G. Sotgiu, and C. Lange, "Multidrug-resistant and extensively drug-resistant tuberculosis in the West. Europe and United States: epidemiology, surveillance, and control." *Clinics in Chest Medicine*, vol. 30, no. 4, pp. 637–65, vii, 2009. [Online]. Available: http://www.ncbi.nlm.nih.gov/pubmed/19925959

[44] V. N. Chihota, B. Müller, C. K. Mlambo, M. Pillay, M. Tait, E. M. Streicher, E. Marais, G. D. van der Spuy, M. Hanekom, G. Coetzee, A. Trollip, C. Hayes, M. E. Bosman, N. C. Gey van Pittius, T. C. Victor, P. D. van Helden, and R. M. Warren, "Population structure of multi- and extensively drug-resistant Mycobacterium tuberculosis strains in South Africa." *Journal of Clinical Microbiology*, vol. 50, no. 3, pp. 995–1002, Mar. 2012. [Online]. Available: http://www.pubmedcentral.nih.gov/articlerender.fcgi?artid=3295122&tool=pmcentrez&rendertype=abstract

[45] T. H. Holtz, "XDR-TB in South Africa: revised definition." *PLoS Medicine*, vol. 4, no. 4, p. e161, Apr. 2007. [Online]. Available: http://www.pubmedcentral.nih.gov/articlerender.fcgi?artid=1779818&tool=pmcentrez&rendertype=abstracthttp://www.pubmedcentral.nih.gov/articlerender.fcgi?artid=1876419&tool=pmcentrez&rendertype=abstract

[46] World Health Organization, "Multidrug and extensively drug-resistant TB (M/XDR-TB): 2010 global report on surveillance and response," World Health Organisation, Geneva, Switzerland, Tech. Rep., 2010. [Online]. Available: http://whqlibdoc.who.int/publications/2010/9789241599191_eng.pdfhttp://scholar.google.com/scholar?hl=en&btnG=Search&q=intitle:Multidrug+and+

extensively+drug-resistant+TB+(M/XDR-TB):+2010+global+report+on+surveillance+and+response.#0

[47] A. A. Velayati, M. R. Masjedi, P. Farnia, P. Tabarsi, J. Ghanavi, A. H. Ziazarifi, and S. E. Hoffner, "Emergence of new forms of totally drug-resistant tuberculosis bacilli: super extensively drug-resistant tuberculosis or totally drug-resistant strains in iran." *Chest*, vol. 136, no. 2, pp. 420–5, Aug. 2009. [Online]. Available: http://www.ncbi.nlm.nih.gov/pubmed/19349380

[48] Z. F. Udwadia, R. A. Amale, K. K. Ajbani, and C. Rodrigues, "Totally Drug-Resistant Tuberculosis in India." *Clinical Infectious Diseases*, Dec. 2011. [Online]. Available: http://www.ncbi.nlm.nih.gov/pubmed/22190562

[49] H. C. Bucher, L. E. Griffith, G. H. Guyatt, P. Sudre, M. Naef, P. Sendi, and M. Battegay, "Isoniazid prophylaxis for tuberculosis in HIV infection: a meta-analysis of randomized controlled trials." *AIDS*, vol. 13, no. 4, pp. 501–7, Mar. 1999. [Online]. Available: http://www.ncbi.nlm.nih.gov/pubmed/10197379

[50] D. Wilkinson, S. B. Squire, and P. Garner, "Effect of preventive treatment for tuberculosis in adults infected with HIV: systematic review of randomised placebo controlled trials." *BMJ*, vol. 317, no. 7159, pp. 625–9, Oct. 1998. [Online]. Available: http://www.pubmedcentral.nih.gov/articlerender.fcgi?artid=28654&tool=pmcentrez&rendertype=abstract

[51] C. Akolo, I. Adetifa, S. Shepperd, and J. Volmink, "Treatment of latent tuberculosis infection in HIV infected persons." *Cochrane Database of Systematic Reviews*, no. 1, p. 83, Jan. 2010. [Online]. Available: http://www.ncbi.nlm.nih.gov/pubmed/20091503

[52] L. Elzi, M. Schlegel, R. Weber, B. Hirschel, M. Cavassini, P. Schmid, E. Bernasconi, M. Rickenbach, and H. Furrer, "Reducing tuberculosis incidence by tuberculin skin testing, preventive treatment, and antiretroviral therapy in an area of low tuberculosis transmission." *Clinical Infectious Diseases*, vol. 44, no. 1, pp. 94–102, Jan. 2007. [Online]. Available: http://www.ncbi.nlm.nih.gov/pubmed/17143823

[53] T. Cohen, M. Lipsitch, R. P. Walensky, and M. Murray, "Beneficial and perverse effects of isoniazid preventive therapy for latent tuberculosis infection in HIV-tuberculosis coinfected populations." *Proceedings of the National Academy of Sciences of the United States of America*, vol. 103, no. 18, pp. 7042–7, May 2006. [Online]. Available: http://www.ncbi.nlm.nih.gov/pubmed/16632605

[54] National Institutes of Health, "International Committee on Taxonomy of Viruses," 2009. [Online]. Available: http://ictvonline.org/virusTaxonomy.asp?version=2009

[55] J. D. Reeves and R. W. Doms, "Human immunodeficiency virus type 2." *The Journal of General Virology*, vol. 83, no. Pt 6, pp. 1253–65, Jul. 2002. [Online]. Available: http://www.pubmedcentral.nih.gov/articlerender.fcgi?artid=400359&tool=pmcentrez&rendertype=abstracthttp://www.ncbi.nlm.nih.gov/pubmed/12029140

[56] C. Kuiken, T. Leitner, B. Foley, B. Hahn, P. Marx, F. McCutchan, S. Wolinsky, and B. Korber, "HIV Sequence Compendium 2009," *Theoretical Biology and Biophysics*, pp. 1–436, 2009.

[57] National Institute of Allergy and Infectious Diseases, "How HIV Causes AIDS," National Institutes of Health (NIH), Tech. Rep., 2004. [Online]. Available: http://www.niaid.nih.gov/factsheets/howhiv.htm

[58] R. A. Weiss, "How does HIV cause AIDS?" *Science*, vol. 260, no. 5112, pp. 1273–9, May 1993. [Online]. Available: http://www.ncbi.nlm.nih.gov/pubmed/8493571

[59] A. E. Friedman-Kien, "Disseminated Kaposi's sarcoma syndrome in young homosexual men." *Journal of the American Academy of Dermatology*, vol. 5, no. 4, pp. 468–71, Oct. 1981. [Online]. Available: http://www.ncbi.nlm.nih.gov/pubmed/7287964

[60] M. S. Gottlieb, R. Schroff, H. M. Schanker, J. D. Weisman, P. T. Fan, R. A. Wolf, and A. Saxon, "Pneumocystis carinii pneumonia and mucosal candidiasis in previously healthy homosexual men: evidence of a new acquired cellular immunodeficiency." *The New England Journal of Medicine*, vol. 305, no. 24, pp. 1425–31, Dec. 1981. [Online]. Available: http://www.ncbi.nlm.nih.gov/pubmed/6272109

[61] H. Masur, M. A. Michelis, J. B. Greene, I. Onorato, R. A. Stouwe, R. S. Holzman, G. Wormser, L. Brettman, M. Lange, H. W. Murray, and S. Cunningham-Rundles, "An outbreak of community-acquired Pneumocystis carinii pneumonia: initial manifestation of cellular immune dysfunction." *The New England Journal of Medicine*, vol. 305, no. 24, pp. 1431–8, Dec. 1981. [Online]. Available: http://www.ncbi.nlm.nih.gov/pubmed/6975437

[62] F. P. Siegal, C. Lopez, G. S. Hammer, A. E. Brown, S. J. Kornfeld, J. Gold, J. Hassett, S. Z. Hirschman, C. Cunningham-Rundles, and B. R. Adelsberg, "Severe acquired immunodeficiency in male homosexuals, manifested by chronic perianal ulcerative herpes simplex lesions." *The New England Journal of Medicine*, vol. 305, no. 24,

pp. 1439–44, Dec. 1981. [Online]. Available: http://www.ncbi.nlm.nih.gov/pubmed/6272110

[63] M. Marmor, A. E. Friedman-Kien, L. Laubenstein, R. D. Byrum, D. C. William, S. D'onofrio, and N. Dubin, "Risk factors for Kaposi's sarcoma in homosexual men." *The Lancet*, vol. 1, no. 8281, pp. 1083–7, May 1982. [Online]. Available: http://www.ncbi.nlm.nih.gov/pubmed/6122889

[64] F. Barré-Sinoussi, J. C. Chermann, F. Rey, M. T. Nugeyre, S. Chamaret, J. Gruest, C. Dauguet, C. Axler-Blin, F. Vézinet-Brun, C. Rouzioux, W. Rozenbaum, and L. Montagnier, "Isolation of a T-lymphotropic retrovirus from a patient at risk for acquired immune deficiency syndrome (AIDS)." *Science*, vol. 220, no. 4599, pp. 868–71, May 1983. [Online]. Available: http://www.ncbi.nlm.nih.gov/pubmed/6189183

[65] R. C. Gallo, P. S. Sarin, E. P. Gelmann, M. Robert-Guroff, E. Richardson, V. S. Kalyanaraman, D. Mann, G. D. Sidhu, R. E. Stahl, S. Zolla-Pazner, J. Leibowitch, and M. Popovic, "Isolation of human T-cell leukemia virus in acquired immune deficiency syndrome (AIDS)." *Science*, vol. 220, no. 4599, pp. 865–7, May 1983. [Online]. Available: http://www.ncbi.nlm.nih.gov/pubmed/6601823

[66] UNAIDS, "Global Report: UNAIDS Report on the Global AIDS Epidemic," UNAIDS, Tech. Rep., 2010. [Online]. Available: http://www.unaids.org/globalreport/Global_report.htm

[67] R. Wyatt and J. Sodroski, "The HIV-1 Envelope Glycoproteins: Fusogens, Antigens, and Immunogens," *Science*, vol. 280, no. 5371, pp. 1884–1888, Jun. 1998. [Online]. Available: http://www.sciencemag.org/cgi/doi/10.1126/science.280.5371.1884

[68] D. C. Chan and P. S. Kim, "HIV Entry and Its Inhibition," *Cell*, vol. 93, no. 5, pp. 681–684, 1998. [Online]. Available: http://linkinghub.elsevier.com/retrieve/pii/S0092867400814300

[69] Disparity, "HIV gross cycle," 2008. [Online]. Available: http://en.wikipedia.org/wiki/File:HIV_gross_cycle_only.png

[70] J. Tang and R. A. Kaslow, "The impact of host genetics on HIV infection and disease progression in the era of highly active antiretroviral therapy." *AIDS*, vol. 17 Suppl 4, pp. S51–60, Jan. 2003. [Online]. Available: http://www.ncbi.nlm.nih.gov/pubmed/15080180

[71] Y.-H. Zheng, N. Lovsin, and B. M. Peterlin, "Newly identified host factors modulate HIV replication." *Immunology Letters*, vol. 97, no. 2, pp. 225–34, Mar. 2005. [Online]. Available: http://www.ncbi.nlm.nih.gov/pubmed/15752562

[72] J. Hiscott, H. Kwon, and P. Genin, "Hostile takeovers: viral appropriation of the NF-κB pathway," *Journal of Clinical Investigation*, vol. 107, no. 2, pp. 143–151, 2001.

[73] V. W. Pollard and M. H. Malim, "The HIV-1 Rev protein." *Annual Review of Microbiology*, vol. 52, no. 52, pp. 491–532, Jan. 1998. [Online]. Available: http://www.ncbi.nlm.nih.gov/pubmed/9891806

[74] C. Goldsmith, P. Feorino, E. L. Palmer, and W. R. McManus, "Scanning electron micrograph of HIV-1 budding from cultured lymphocyte." [Online]. Available: http://phil.cdc.gov/phil/details.asp?pid=10000

[75] G. Burton, "Follicular dendritic cell contributions to HIV pathogenesis," *Seminars in Immunology*, vol. 14, no. 4, pp. 275–284, Aug. 2002. [Online]. Available: http://linkinghub.elsevier.com/retrieve/pii/S104453230200060X

[76] C. J. Pitcher, C. Quittner, D. M. Peterson, M. Connors, R. A. Koup, V. C. Maino, and L. J. Picker, "HIV-1-specific CD4+ T cells are detectable in most individuals with active HIV-1 infection, but decline with prolonged viral suppression." *Nature Medicine*, vol. 5, no. 5, pp. 518–25, May 1999. [Online]. Available: http://www.ncbi.nlm.nih.gov/pubmed/10229228

[77] G. Hütter, D. Nowak, M. Mossner, S. Ganepola, A. Müß ig, K. Allers, T. Schneider, J. Hofmann, C. Kücherer, O. Blau, and Others, "Long-term control of HIV by CCR5 Delta32/Delta32 stem-cell transplantation," *New England Journal of Medicine*, vol. 360, no. 7, pp. 692–698, 2009. [Online]. Available: http://www.nejm.org/doi/full/10.1056/NEJMoa0802905

[78] C. L. Daley, "Tropical respiratory medicine. 1. Pulmonary infections in the tropics: impact of HIV infection." *Thorax*, vol. 49, no. 4, pp. 370–8, May 1994. [Online]. Available: http://www.pubmedcentral.nih.gov/articlerender.fcgi?artid=475375&tool=pmcentrez&rendertype=abstract

[79] G. J. Churchyard and A. D. Grant, "HIV infection, tuberculosis and non-tuberculous mycobacteria." *South African Medical Journal*, vol. 90, no. 5, pp. 472–6, May 2000. [Online]. Available: http://www.ncbi.nlm.nih.gov/pubmed/10901814

[80] M. Badri, D. Wilson, and R. Wood, "Effect of highly active antiretroviral therapy on incidence of tuberculosis in South Africa: a cohort study." *The Lancet*, vol. 359, no. 9323, pp. 2059–64, Jun. 2002. [Online]. Available: http://www.ncbi.nlm.nih.gov/pubmed/12086758

[81] P. a. Selwyn, D. Hartel, V. a. Lewis, E. E. Schoenbaum, S. H. Vermund, R. S. Klein, a. T. Walker, and G. H. Friedland, "A prospective study of the risk of tuberculosis among intravenous drug users with human immunodeficiency virus infection." *The New England journal of medicine*, vol. 320, no. 9, pp. 545–50, Mar. 1989. [Online]. Available: http://www.ncbi.nlm.nih.gov/pubmed/2915665

[82] G. Antonucci, E. Girardi, M. C. Raviglione, and G. Ippolito, "Risk factors for tuberculosis in HIV-infected persons. A prospective cohort study. The Gruppo Italiano di Studio Tubercolosi e AIDS (GISTA)." *Journal of the American Medical Association*, vol. 274, no. 2, pp. 143–8, Jul. 1995. [Online]. Available: http://www.ncbi.nlm.nih.gov/pubmed/7596002

[83] N. Markowitz, N. I. Hansen, P. C. Hopewell, J. Glassroth, P. A. Kvale, B. T. Mangura, T. C. Wilcosky, J. M. Wallace, M. J. Rosen, and L. B. Reichman, "Incidence of tuberculosis in the United States among HIV-infected persons. The Pulmonary Complications of HIV Infection Study Group." *Annals of internal medicine*, vol. 126, no. 2, pp. 123–32, Jan. 1997. [Online]. Available: http://www.ncbi.nlm.nih.gov/pubmed/9005746

[84] S. Moreno, J. Baraia-Etxaburu, E. Bouza, F. Parras, M. Pérez-Tascón, P. Miralles, T. Vicente, J. C. Alberdi, J. Cosín, and D. López-Gay, "Risk for developing tuberculosis among anergic patients infected with HIV." *Annals of Internal Medicine*, vol. 119, no. 3, pp. 194–8, Aug. 1993. [Online]. Available: http://www.ncbi.nlm.nih.gov/pubmed/8100693

[85] World Health Organization, "Towards Universal access: Scaling up priority HIV/AIDS interventions in the health sector," 2008.

[86] G. Santoro-Lopes, A. M. F. de Pinho, L. H. Harrison, and M. Schechter, "Reduced risk of tuberculosis among Brazilian patients with advanced human immunodeficiency virus infection treated with highly active antiretroviral therapy." *Clinical Infectious Diseases*, vol. 34, no. 4, pp. 543–6, Mar. 2002. [Online]. Available: http://www.ncbi.nlm.nih.gov/pubmed/11797184

[87] E. Girardi, C. a. Sabin, A. d'Arminio Monforte, B. Hogg, A. N. Phillips, M. J. Gill, F. Dabis, P. Reiss, O. Kirk, E. Bernasconi, S. Grabar, A. Justice, S. Staszewski, G. Fätkenheuer, and J. a. C. Sterne, "Incidence of Tuberculosis among HIV-infected patients receiving highly active antiretroviral therapy in Europe and North America." *Clinical Infectious Diseases*, vol. 41, no. 12, pp. 1772–82, Dec. 2005. [Online]. Available: http://www.ncbi.nlm.nih.gov/pubmed/16288403

[88] S. D. Lawn, L. Myer, L.-G. Bekker, and R. Wood, "Burden of tuberculosis in an antiretroviral treatment programme in sub-Saharan Africa: impact on treatment outcomes and implications for tuberculosis control." *AIDS*, vol. 20, no. 12, pp. 1605–12, Aug. 2006. [Online]. Available: http://www.ncbi.nlm.nih.gov/pubmed/16868441

[89] M. A. French, N. Lenzo, M. John, S. A. Mallal, E. J. McKinnon, I. R. James, P. Price, J. P. Flexman, and M. L. Tay-Kearney, "Immune restoration disease after the treatment of immunodeficient HIV-infected patients with highly active antiretroviral therapy." *HIV Medicine*, vol. 1, no. 2, pp. 107–15, Mar. 2000. [Online]. Available: http://www.ncbi.nlm.nih.gov/pubmed/11737333

[90] M. A. French, P. Price, and S. F. Stone, "Immune restoration disease after antiretroviral therapy." *AIDS*, vol. 18, no. 12, pp. 1615–27, Aug. 2004. [Online]. Available: http://www.ncbi.nlm.nih.gov/pubmed/15280772

[91] N. Singh and J. R. Perfect, "Immune reconstitution syndrome associated with opportunistic mycoses." *The Lancet Infectious Diseases*, vol. 7, no. 6, pp. 395–401, Jun. 2007. [Online]. Available: http://www.ncbi.nlm.nih.gov/pubmed/17521592

[92] S. D. Lawn, L.-G. Bekker, and R. F. Miller, "Immune reconstitution disease associated with mycobacterial infections in HIV-infected individuals receiving antiretrovirals." *The Lancet Infectious Diseases*, vol. 5, no. 6, pp. 361–73, Jun. 2005. [Online]. Available: http://www.ncbi.nlm.nih.gov/pubmed/15919622

[93] S. A. Shelburne, R. J. Hamill, M. C. Rodriguez-Barradas, S. B. Greenberg, R. L. Atmar, D. W. Musher, J. C. Gathe, F. Visnegarwala, and B. W. Trautner, "Immune reconstitution inflammatory syndrome: emergence of a unique syndrome during highly active antiretroviral therapy." *Medicine*, vol. 81, no. 3, pp. 213–27, May 2002. [Online]. Available: http://www.ncbi.nlm.nih.gov/pubmed/11997718

[94] R. Colebunders, L. John, V. Huyst, A. Kambugu, F. Scano, and L. Lynen, "Tuberculosis immune reconstitution inflammatory syndrome in countries with limited resources." *The International Journal of Tuberculosis and Lung Disease*, vol. 10, no. 9, pp. 946–53, Sep. 2006. [Online]. Available: http://www.ncbi.nlm.nih.gov/pubmed/16964782

[95] M. A. French, P. Price, N. Mathiot, R. Krueger, S. Stone, and N. M. Keane, "Immune dysfunction and immune restoration disease in HIV patients given highly active antiretroviral therapy." *Journal of Clinical Virology*, vol. 22, no. 3, pp. 279–87, Oct. 2001. [Online]. Available: http://www.ncbi.nlm.nih.gov/pubmed/11564593

[96] G. Meintjes, S. D. Lawn, F. Scano, G. Maartens, M. A. French, W. Worodria, J. H. Elliott, D. Murdoch, R. J. Wilkinson, C. Seyler, L. John, M. S. van Der Loeff, P. Reiss, L. Lynen, E. N. Janoff, C. Gilks, and R. Colebunders, "Tuberculosis-associated immune reconstitution inflammatory syndrome: case definitions for use in resource-limited settings." *The Lancet Infectious Diseases*, vol. 8, no. 8, pp. 516–23, Aug. 2008. [Online]. Available: http://www.ncbi.nlm.nih.gov/pubmed/18652998

[97] N. Kumarasamy, S. Chaguturu, K. H. Mayer, S. Solomon, H. T. Yepthomi, P. Balakrishnan, and T. P. Flanigan, "Incidence of immune reconstitution syndrome in HIV/tuberculosis-coinfected patients after initiation of generic antiretroviral therapy in India." *Journal of Acquired Immune Deficiency Syndromes*, vol. 37, no. 5, pp. 1574–6, Dec. 2004. [Online]. Available: http://www.ncbi.nlm.nih.gov/pubmed/15577411

[98] M. Narita, A. E. Pitchenik, D. Ashkin, and E. S. Hollender, "Paradoxical worsening of tuberculosis following antiretroviral therapy in patients with AIDS." *American Journal of Respiratory and Critical Care Medicine*, vol. 158, no. 1, pp. 157–61, Jul. 1998. [Online]. Available: http://www.ncbi.nlm.nih.gov/pubmed/9655723

[99] M. A. French, "Disorders of immune reconstitution in patients with HIV infection responding to antiretroviral therapy." *Current HIV/AIDS Reports*, vol. 4, no. 1, pp. 16–21, Feb. 2007. [Online]. Available: http://www.ncbi.nlm.nih.gov/pubmed/17338856

[100] G. Meintjes and L. Lynen, "Prevention and treatment of the immune reconstitution inflammatory syndrome." *Current Opinion in HIV and AIDS*, vol. 3, no. 4, pp. 468–76, Jul. 2008. [Online]. Available: http://www.ncbi.nlm.nih.gov/pubmed/19373007

[101] G. Breton, X. Duval, C. Estellat, X. Poaletti, D. Bonnet, D. Mvondo Mvondo, P. Longuet, C. Leport, and J.-L. Vildé, "Determinants of immune reconstitution inflammatory syndrome in HIV type 1-infected patients with tuberculosis after initiation of antiretroviral therapy." *Clinical Infectious Diseases*, vol. 39, no. 11, pp. 1709–12, Dec. 2004. [Online]. Available: http://www.ncbi.nlm.nih.gov/pubmed/15578375

[102] S. A. Shelburne, F. Visnegarwala, J. Darcourt, E. A. Graviss, T. P. Giordano, A. C. White, and R. J. Hamill, "Incidence and risk factors for immune reconstitution inflammatory syndrome during highly active antiretroviral therapy." *AIDS*, vol. 19, no. 4, pp. 399–406, Mar. 2005. [Online]. Available: http://www.ncbi.nlm.nih.gov/pubmed/15750393

[103] C. Michailidis, A. L. Pozniak, S. Mandalia, S. Basnayake, M. R. Nelson, and B. G. Gazzard, "Clinical characteristics of IRIS syndrome in patients with HIV and tuberculosis." *Antiviral Therapy*, vol. 10, no. 3, pp. 417–22, 2005. [Online]. Available: http://www.ncbi.nlm.nih.gov/pubmed/15918332

[104] W. Manosuthi, S. Kiertiburanakul, T. Phoorisri, and S. Sungkanuparph, "Immune reconstitution inflammatory syndrome of tuberculosis among HIV-infected patients receiving antituberculous and antiretroviral therapy." *The Journal of Infection*, vol. 53, no. 6, pp. 357–63, Dec. 2006. [Online]. Available: http://www.ncbi.nlm.nih.gov/pubmed/16487593

[105] S. D. Lawn, L. Myer, L.-G. Bekker, and R. Wood, "Tuberculosis-associated immune reconstitution disease: incidence, risk factors and impact in an antiretroviral treatment service in South Africa." *AIDS*, vol. 21, no. 3, pp. 335–41, Jan. 2007. [Online]. Available: http://www.ncbi.nlm.nih.gov/pubmed/17255740

[106] W. Burman, A. Vernon, A. Khan, S. Weis, D. Benator, B. Jones, C. Silva, B. King, C. LaHart, B. Mangura, M. Weiner, and W. El-Sadr, "Frequency, severity and duration of immune reconstitution events in HIV-related tuberculosis." *The International Journal of Tuberculosis and Lung Disease*, vol. 11, no. 12, pp. 1282–9, Dec. 2007. [Online]. Available: http://www.ncbi.nlm.nih.gov/pubmed/18229435

[107] R. a. M. Breen, C. J. Smith, H. Bettinson, S. Dart, B. Bannister, M. a. Johnson, and M. C. I. Lipman, "Paradoxical reactions during tuberculosis treatment in patients with and without HIV co-infection." *Thorax*, vol. 59, no. 8, pp. 704–7, Aug. 2004. [Online]. Available: http://www.pubmedcentral.nih.gov/articlerender.fcgi?artid=1747098&tool=pmcentrez&rendertype=abstract

[108] M. Müller, S. Wandel, R. Colebunders, S. Attia, H. Furrer, and M. Egger, "Immune reconstitution inflammatory syndrome in patients starting antiretroviral therapy for HIV infection: a systematic review and meta-analysis." *The Lancet Infectious Diseases*, vol. 10, no. 4, pp. 251–61, Apr. 2010. [Online]. Available: http://www.ncbi.nlm.nih.gov/pubmed/20334848

[109] S. S. A. Karim, G. J. Churchyard, Q. A. Karim, and S. D. Lawn, "HIV infection and tuberculosis in South Africa: an urgent need to escalate the public health response," *The Lancet*, vol. 374, no. 9693, pp. 921–933, Sep. 2009. [Online]. Available: http://linkinghub.elsevier.com/retrieve/pii/S0140673609609168

[110] P. M. Grant, L. Komarow, J. Andersen, I. Sereti, S. Pahwa, M. M. Lederman, J. Eron, I. Sanne, W. Powderly, E. Hogg, C. Suckow, and A. Zolopa, "Risk factor analyses for immune reconstitution inflammatory syndrome in a randomized study of early vs. deferred ART during an opportunistic infection." *PLoS One*, vol. 5, no. 7, p. e11416, Jan. 2010. [Online]. Available: http://www.pubmedcentral.nih.gov/articlerender.fcgi?artid=2895658&tool=pmcentrez&rendertype=abstract

[111] D. M. Murdoch, W. D. F. Venter, C. Feldman, and A. Van Rie, "Incidence and risk factors for the immune reconstitution inflammatory syndrome in HIV patients in South Africa: a prospective study." *AIDS*, vol. 22, no. 5, pp. 601–10, Mar. 2008. [Online]. Available: http://www.ncbi.nlm.nih.gov/pubmed/18317001

[112] Y. C. Manabe, J. D. Campbell, E. Sydnor, and R. D. Moore, "Immune reconstitution inflammatory syndrome: risk factors and treatment implications." *Journal of Acquired Immune Deficiency Syndromes*, vol. 46, no. 4, pp. 456–62, Dec. 2007. [Online]. Available: http://www.ncbi.nlm.nih.gov/pubmed/18077835

[113] A. Zolopa, J. Andersen, W. Powderly, A. Sanchez, I. Sanne, C. Suckow, E. Hogg, and L. Komarow, "Early antiretroviral therapy reduces AIDS progression/death in individuals with acute opportunistic infections: a multicenter randomized strategy trial." *PLoS One*, vol. 4, no. 5, p. e5575, Jan. 2009. [Online]. Available: http://www.pubmedcentral.nih.gov/articlerender.fcgi?artid=2680972&tool=pmcentrez&rendertype=abstract

[114] S. D. Lawn, A. D. Harries, X. Anglaret, L. Myer, and R. Wood, "Early mortality among adults accessing antiretroviral treatment programmes in sub-Saharan Africa." *AIDS*, vol. 22, no. 15, pp. 1897–908, 2008. [Online]. Available: http://www.ncbi.nlm.nih.gov/pubmed/18784453

[115] S. S. Abdool Karim, K. Naidoo, A. Grobler, N. Padayatchi, C. Baxter, A. Gray, T. Gengiah, G. Nair, S. Bamber, A. Singh, M. Khan, J. Pienaar, W. El-Sadr, G. Friedland, and Q. Abdool Karim, "Timing of initiation of antiretroviral drugs during tuberculosis therapy." *The New England Journal of Medicine*, vol. 362, no. 8, pp. 697–706, Mar. 2010. [Online]. Available: http://www.pubmedcentral.nih.gov/articlerender.fcgi?artid=3076221&tool=pmcentrez&rendertype=abstract

[116] F.-x. Blanc, T. Sok, D. Laureillard, L. Borand, C. Rekacewicz, E. Nerrienet, Y. Madec, O. Marcy, S. Chan, N. Prak, C. Kim, K. Kim Lak, C. Hak, B. Dim, C. Im Sin, S. Sun, B. Guillard, B. Sar, S. Vong, M. Fernandez, L. Fox, J.-F. Delfraissy, and A. E. Goldfeld, "Early (2 weeks) vs. late (8 weeks) initiation of highly active antiretroviral treatment (HAART) significantly enhance survival of severely immunosuppressed HIV-infected adults with newly diagnosed tuberculosis: results of the CAMELIA clinical trial," *BMC Proceedings*, vol. 5, no. Suppl 1, p. O11, 2011. [Online]. Available: http://www.biomedcentral.com/1753-6561/5/S1/O11

[117] F.-X. Blanc, T. Sok, D. Laureillard, L. Borand, C. Rekacewicz, E. Nerrienet, Y. Madec, O. Marcy, S. Chan, N. Prak, C. Kim, K. K. Lak, C. Hak, B. Dim, C. I. Sin, S. Sun, B. Guillard, B. Sar, S. Vong, M. Fernandez, L. Fox, J.-F. Delfraissy, and A. E.

Goldfeld, "Earlier versus later start of antiretroviral therapy in HIV-infected adults with tuberculosis." *The New England Journal of Medicine*, vol. 365, no. 16, pp. 1471–81, Oct. 2011. [Online]. Available: http://www.ncbi.nlm.nih.gov/pubmed/22010913

[118] World Health Organization, "Antiretroviral Therapy for HIV Infection in Adults and Adolescents: Recommendations for a Public Health Approach - 2010 Revision," World Health Organisation, Geneva, Tech. Rep., 2010.

[119] G. Meintjes, R. J. Wilkinson, C. Morroni, D. J. Pepper, K. Rebe, M. X. Rangaka, T. Oni, and G. Maartens, "Randomized placebo-controlled trial of prednisone for paradoxical tuberculosis-associated immune reconstitution inflammatory syndrome." *AIDS*, vol. 24, no. 15, pp. 2381–90, Sep. 2010. [Online]. Available: http://www.pubmedcentral.nih.gov/articlerender.fcgi?artid=2940061&tool=pmcentrez&rendertype=abstract

[120] ——, "Randomized placebo-controlled trial of prednisone for paradoxical tuberculosis-associated immune reconstitution inflammatory syndrome." *AIDS*, vol. 24, no. 15, pp. 2381–90, Sep. 2010. [Online]. Available: http://www.pubmedcentral.nih.gov/articlerender.fcgi?artid=2940061&tool=pmcentrez&rendertype=abstract

[121] R. Van den Bergh, G. Vanham, G. Raes, P. De Baetselier, and R. Colebunders, "Mycobacterium-associated immune reconstitution disease: macrophages running wild?" *The Lancet Infectious Diseases*, vol. 6, no. 1, pp. 2–3; author reply 4–5, Jan. 2006. [Online]. Available: http://www.ncbi.nlm.nih.gov/pubmed/16377524

[122] A. Bourgarit, G. Carcelain, V. Martinez, C. Lascoux, V. Delcey, B. Gicquel, E. Vicaut, P. H. Lagrange, D. Sereni, and B. Autran, "Explosion of tuberculin-specific Th1-responses induces immune restoration syndrome in tuberculosis and HIV co-infected patients." *AIDS*, vol. 20, no. 2, pp. F1–7, Jan. 2006. [Online]. Available: http://www.ncbi.nlm.nih.gov/pubmed/16511406

[123] A. Bourgarit, G. Carcelain, A. Samri, C. Parizot, M. Lafaurie, S. Abgrall, V. Delcey, E. Vicaut, D. Sereni, and B. Autran, "Tuberculosis-associated immune restoration syndrome in HIV-1-infected patients involves tuberculin-specific CD4 Th1 cells and KIR-negative gammadelta T cells." *Journal of Immunology*, vol. 183, no. 6, pp. 3915–23, Sep. 2009. [Online]. Available: http://www.ncbi.nlm.nih.gov/pubmed/19726768

[124] N. W. Schluger, "Reconstitution of Immune Responses to Tuberculosis in Patients With HIV Infection Who Receive Antiretroviral Therapy*," *Chest*, vol. 122, no. 2, pp. 597–602, Aug. 2002. [Online]. Available: http://www.chestjournal.org/cgi/doi/10.1378/chest.122.2.597

[125] M. A. French, S. A. Mallal, and R. L. Dawkins, "Zidovudine-induced restoration of cell-mediated immunity to mycobacteria in immunodeficient HIV-infected patients." *AIDS*, vol. 6, no. 11, pp. 1293–7, Dec. 1992. [Online]. Available: http://www.ncbi.nlm.nih.gov/pubmed/1472334

[126] P. del Giudice, J. Durant, E. Counillon, V. Mondain, E. Bernard, P. M. Roger, and P. Dellamonica, "Mycobacterial cutaneous manifestations: a new sign of immune restoration syndrome in patients with acquired immunodeficiency syndrome." *Archives of Dermatology*, vol. 135, no. 9, pp. 1129–30, Oct. 1999. [Online]. Available: http://www.ncbi.nlm.nih.gov/pubmed/10490130

[127] S. D. Lawn, T. A. Bicanic, and D. C. Macallan, "Pyomyositis and cutaneous abscesses due to Mycobacterium avium: an immune reconstitution manifestation in a patient with AIDS." *Clinical Infectious Diseases*, vol. 38, no. 3, pp. 461–3, Mar. 2004. [Online]. Available: http://www.ncbi.nlm.nih.gov/pubmed/12414430http://www.ncbi.nlm.nih.gov/pubmed/14727228

[128] E. Zamir, H. Hudson, R. R. Ober, S. K. Kumar, R. C. Wang, R. W. Read, and N. A. Rao, "Massive mycobacterial choroiditis during highly active antiretroviral therapy: another immune-recovery uveitis?" *Ophthalmology*, vol. 109, no. 11, pp. 2144–8, Dec. 2002. [Online]. Available: http://www.ncbi.nlm.nih.gov/pubmed/12414430

[129] P. B. Bartley, a. M. Allworth, and D. P. Eisen, "Mycobacterium avium complex causing endobronchial disease in AIDS patients after partial immune restoration." *The International Journal of Tuberculosis and Lung Disease*, vol. 3, no. 12, pp. 1132–6, Dec. 1999. [Online]. Available: http://www.ncbi.nlm.nih.gov/pubmed/10599019

[130] G. Matsuzaki and M. Umemura, "Interleukin-17 as an effector molecule of innate and acquired immunity against infections." *Microbiology and Immunology*, vol. 51, no. 12, pp. 1139–47, Jan. 2007. [Online]. Available: http://www.ncbi.nlm.nih.gov/pubmed/18094532

[131] T. J. Scriba, B. Kalsdorf, D.-a. Abrahams, F. Isaacs, J. Hofmeister, G. Black, H. Y. Hassan, R. J. Wilkinson, G. Walzl, S. J. Gelderbloem, H. Mahomed, G. D. Hussey, and W. A. Hanekom, "Distinct, specific IL-17- and IL-22-producing CD4+ T cell subsets contribute to the human anti-mycobacterial immune response." *Journal of Immunology*, vol. 180, no. 3, pp. 1962–70, Mar. 2008. [Online]. Available: http://www.pubmedcentral.nih.gov/articlerender.fcgi?artid=2219462&tool=pmcentrez&rendertype=abstract

[132] P. Price, G. Morahan, D. Huang, E. Stone, K. Y. M. Cheong, A. Castley, M. Rodgers, M. Q. McIntyre, L. J. Abraham, and M. a. French, "Polymorphisms in cytokine

genes define subpopulations of HIV-1 patients who experienced immune restoration diseases." *AIDS*, vol. 16, no. 15, pp. 2043–7, Oct. 2002. [Online]. Available: http://www.ncbi.nlm.nih.gov/pubmed/12370503

[133] I. Sereti, A. J. Rodger, and M. a. French, "Biomarkers in immune reconstitution inflammatory syndrome: signals from pathogenesis." *Current Opinion in HIV and AIDS*, vol. 5, no. 6, pp. 504–10, Nov. 2010. [Online]. Available: http://www.ncbi.nlm.nih.gov/pubmed/20966640

[134] P. Mallick and B. Kuster, "Proteomics: a pragmatic perspective." *Nature Biotechnology*, vol. 28, no. 7, pp. 695–709, Jul. 2010. [Online]. Available: http://www.ncbi.nlm.nih.gov/pubmed/20622844

[135] "Biomarkers on a roll." *Nature Biotechnology*, vol. 28, no. 5, p. 431, May 2010. [Online]. Available: http://www.ncbi.nlm.nih.gov/pubmed/20458308

[136] S. P. Gygi, G. L. Corthals, Y. Zhang, Y. Rochon, and R. Aebersold, "Evaluation of two-dimensional gel electrophoresis-based proteome analysis technology." *Proceedings of the National Academy of Sciences of the United States of America*, vol. 97, no. 17, pp. 9390–5, Aug. 2000. [Online]. Available: http://www.pubmedcentral.nih.gov/articlerender.fcgi?artid=16874&tool=pmcentrez&rendertype=abstract

[137] J. Cox and M. Mann, "Quantitative, high-resolution proteomics for data-driven systems biology." *Annual Review of Biochemistry*, vol. 80, pp. 273–99, Jun. 2011. [Online]. Available: http://www.ncbi.nlm.nih.gov/pubmed/21548781

[138] M. M. Savitski, M. L. Nielsen, and R. a. Zubarev, "ModifiComb, a new proteomic tool for mapping substoichiometric post-translational modifications, finding novel types of modifications, and fingerprinting complex protein mixtures." *Molecular & Cellular Proteomics*, vol. 5, no. 5, pp. 935–48, May 2006. [Online]. Available: http://www.ncbi.nlm.nih.gov/pubmed/16439352

[139] N. L. Anderson, "The Human Plasma Proteome: History, Character, and Diagnostic Prospects," *Molecular & Cellular Proteomics*, vol. 1, no. 11, pp. 845–867, Oct. 2002. [Online]. Available: http://www.mcponline.org/cgi/doi/10.1074/mcp.R200007-MCP200

[140] M. Karas, D. Bachmann, and F. Hillenkamp, "Influence of the wavelength in high-irradiance ultraviolet laser desorption mass spectrometry of organic molecules," *Analytical Chemistry*, vol. 57, no. 14, pp. 2935–2939, Dec. 1985. [Online]. Available: http://pubs.acs.org/doi/abs/10.1021/ac00291a042

[141] M. Karas and F. Hillenkamp, "Laser desorption ionization of proteins with molecular masses exceeding 10,000 daltons." *Analytical Chemistry*, vol. 60, no. 20, pp. 2299–301, Oct. 1988. [Online]. Available: http://www.ncbi.nlm.nih.gov/pubmed/3239801

[142] F. Hillenkamp and M. Karas, "Mass spectrometry of peptides and proteins by matrix-assisted ultraviolet laser desorption/ionization." *Methods in Enzymology*, vol. 193, pp. 280–95, Jan. 1990. [Online]. Available: http://www.ncbi.nlm.nih.gov/pubmed/1963669

[143] F. Hillenkamp, M. Karas, R. C. Beavis, and B. T. Chait, "Matrix-assisted laser desorption/ionization mass spectrometry of biopolymers." *Analytical Chemistry*, vol. 63, no. 24, pp. 1193A–1203A, Dec. 1991. [Online]. Available: http://www.ncbi.nlm.nih.gov/pubmed/1789447

[144] K. Tanaka, "The origin of macromolecule ionization by laser irradiation (Nobel lecture)." *Angewandte Chemie*, vol. 42, no. 33, pp. 3860–70, Aug. 2003. [Online]. Available: http://www.ncbi.nlm.nih.gov/pubmed/12949860

[145] J. B. Fenn, M. Mann, C. K. Meng, S. F. Wong, and C. M. Whitehouse, "Electrospray ionization for mass spectrometry of large biomolecules." *Science*, vol. 246, no. 4926, pp. 64–71, Oct. 1989. [Online]. Available: http://www.ncbi.nlm.nih.gov/pubmed/2675315

[146] G. Taylor, "Disintegration of water drops in an electric field," *Proceedings of the Royal Society of London*, vol. 280, pp. 383–97, 1964.

[147] C. Schaeffer-Reiss, "A brief summary of the different types of mass spectrometers used in proteomics." in *Functional Proteomics: Methods in Molecular Biology*, ser. Methods in Molecular Biology, J. D. Thompson, M. Ueffing, and C. Schaeffer-Reiss, Eds. Totowa, NJ: Humana Press, Jan. 2008, vol. 484, no. 2, ch. 1, pp. 3–16. [Online]. Available: http://www.springerlink.com/index/10.1007/978-1-59745-398-1http://www.ncbi.nlm.nih.gov/pubmed/18592169

[148] R. Aebersold and M. Mann, "Mass spectrometry-based proteomics." *Nature*, vol. 422, no. 6928, pp. 198–207, Mar. 2003. [Online]. Available: http://www.ncbi.nlm.nih.gov/pubmed/12634793

[149] Q. Hu, R. J. Noll, H. Li, A. Makarov, M. Hardman, and R. Graham Cooks, "The Orbitrap: a new mass spectrometer." *Journal of Mass Spectrometry*, vol. 40, no. 4, pp. 430–43, Apr. 2005. [Online]. Available: http://www.ncbi.nlm.nih.gov/pubmed/15838939

[150] J. R. Yates, C. I. Ruse, and A. Nakorchevsky, "Proteomics by mass spectrometry: approaches, advances, and applications." *Annual Review of Biomedical Engineering*, vol. 11, no. c, pp. 49–79, Jan. 2009. [Online]. Available: http://www.ncbi.nlm.nih.gov/pubmed/19400705

[151] A. Keller, A. I. Nesvizhskii, E. Kolker, and R. Aebersold, "Empirical statistical model to estimate the accuracy of peptide identifications made by MS/MS and database search." *Analytical chemistry*, vol. 74, no. 20, pp. 5383–92, Oct. 2002. [Online]. Available: http://www.ncbi.nlm.nih.gov/pubmed/12403597

[152] L. Y. Geer, S. P. Markey, J. A. Kowalak, L. Wagner, M. Xu, D. M. Maynard, X. Yang, W. Shi, and S. H. Bryant, "Open mass spectrometry search algorithm." *Journal of Proteome Research*, vol. 3, no. 5, pp. 958–964, 2004. [Online]. Available: http://arxiv.org/abs/q-bio/0406002

[153] J. E. Elias and S. P. Gygi, "Target-decoy search strategy for increased confidence in large-scale protein identifications by mass spectrometry." *Nature Methods*, vol. 4, no. 3, pp. 207–14, Mar. 2007. [Online]. Available: http://www.ncbi.nlm.nih.gov/pubmed/17327847

[154] H. Choi, D. Ghosh, and A. I. Nesvizhskii, "Statistical validation of peptide identifications in large-scale proteomics using the target-decoy database search strategy and flexible mixture modeling." *Journal of Proteome Research*, vol. 7, no. 1, pp. 286–92, Jan. 2008. [Online]. Available: http://www.ncbi.nlm.nih.gov/pubmed/18078310

[155] L. Käll, J. D. Storey, M. J. MacCoss, and W. S. Noble, "Assigning significance to peptides identified by tandem mass spectrometry using decoy databases." *Journal of Proteome Research*, vol. 7, no. 1, pp. 29–34, Jan. 2008. [Online]. Available: http://www.ncbi.nlm.nih.gov/pubmed/18067246

[156] H. Choi and A. I. Nesvizhskii, "False discovery rates and related statistical concepts in mass spectrometry-based proteomics." *Journal of Proteome Research*, vol. 7, no. 1, pp. 47–50, Jan. 2008. [Online]. Available: http://www.ncbi.nlm.nih.gov/pubmed/18067251

[157] M. Fitzgibbon, Q. Li, and M. McIntosh, "Modes of inference for evaluating the confidence of peptide identifications." *Journal of Proteome Research*, vol. 7, no. 1, pp. 35–9, Jan. 2008. [Online]. Available: http://www.ncbi.nlm.nih.gov/pubmed/18067248

[158] E. A. Kapp, F. Schütz, L. M. Connolly, J. A. Chakel, J. E. Meza, C. A. Miller, D. Fenyo, J. K. Eng, J. N. Adkins, G. S. Omenn, and R. J. Simpson, "An evaluation, comparison,

and accurate benchmarking of several publicly available MS/MS search algorithms: sensitivity and specificity analysis." *Proteomics*, vol. 5, no. 13, pp. 3475–90, Aug. 2005. [Online]. Available: http://www.ncbi.nlm.nih.gov/pubmed/16047398

[159] C. Y. Park, A. A. Klammer, L. Käll, M. J. MacCoss, and W. S. Noble, "Rapid and accurate peptide identification from tandem mass spectra." *Journal of Proteome Research*, vol. 7, no. 7, pp. 3022–7, Jul. 2008. [Online]. Available: http://www.pubmedcentral.nih.gov/articlerender.fcgi?artid=2667385&tool=pmcentrez&rendertype=abstract

[160] S. Tanner, H. Shu, A. Frank, L.-c. Wang, E. Zandi, M. Mumby, P. A. Pevzner, and V. Bafna, "InsPecT : Identification of Posttranslationally Modified Peptides from Tandem Mass Spectra is key to understanding various cellular regulatory pro- proved to be very successful in genomics searches . Given selects a small fraction of database D that is gu," *Analytical Chemistry*, vol. 77, no. 14, pp. 4626–4639, 2005.

[161] P. J. Kersey, J. Duarte, A. Williams, Y. Karavidopoulou, E. Birney, and R. Apweiler, "The International Protein Index: an integrated database for proteomics experiments." *Proteomics*, vol. 4, no. 7, pp. 1985–8, Jul. 2004. [Online]. Available: http://www.ncbi.nlm.nih.gov/pubmed/15221759

[162] W. J. Henzel, J. T. Stults, and C. Watanabe, "Proceedings of the Third Symposium of the Protein Society;," in *Proceedings of the Third Symposium of the Protein Society*, Seattle, WA, 1989.

[163] W. Henzel, T. Billeci, J. T. Stults, S. C. Wong, C. Grimley, and C. Watanabe, "Identifying proteins from two-dimensional gels by molecular mass searching of peptide fragments in protein sequence databases," *Proceedings of the National Academy of Sciences of the United States of America*, vol. 90, no. 11, pp. 5011–15, 1993. [Online]. Available: http://www.pnas.org/content/90/11/5011.short

[164] D. J. Pappin, P. Hojrup, and A. J. Bleasby, "Rapid identification of proteins by peptide-mass fingerprinting." *Current Biology*, vol. 3, no. 6, pp. 327–32, Jun. 1993. [Online]. Available: http://www.ncbi.nlm.nih.gov/pubmed/15335725

[165] L. McHugh and J. W. Arthur, "Computational methods for protein identification from mass spectrometry data." *PLoS Computational Biology*, vol. 4, no. 2, p. e12, 2008. [Online]. Available: http://www.ncbi.nlm.nih.gov/pubmed/18463710

[166] L. Martens and R. Apweiler, "Algorithms and databases." in *Proteomics Methods and Protocols Methods in Molecular Biology*, Jan. 2009, vol. 564, ch. 14, pp. 245–59. [Online]. Available: http://www.ncbi.nlm.nih.gov/pubmed/19544027

[167] M. P. Washburn, D. Wolters, and J. R. Yates, "Large-scale analysis of the yeast proteome by multidimensional protein identification technology." *Nature Biotechnology*, vol. 19, no. 3, pp. 242–7, Mar. 2001. [Online]. Available: http://www.ncbi.nlm.nih.gov/pubmed/11231557

[168] L. M. Mikesh, B. Ueberheide, A. Chi, J. J. Coon, J. E. P. Syka, J. Shabanowitz, and D. F. Hunt, "The utility of ETD mass spectrometry in proteomic analysis." *Biochimica et Biophysica Acta*, vol. 1764, no. 12, pp. 1811–22, Dec. 2006. [Online]. Available: http://www.pubmedcentral.nih.gov/articlerender.fcgi?artid=1853258&tool=pmcentrez&rendertype=abstract

[169] J. J. Coon, J. Shabanowitz, D. F. Hunt, and J. E. P. Syka, "Electron transfer dissociation of peptide anions." *Journal of the American Society for Mass Spectrometry*, vol. 16, no. 6, pp. 880–2, Jun. 2005. [Online]. Available: http://www.ncbi.nlm.nih.gov/pubmed/15907703

[170] R. H. Bateman, R. Carruthers, J. B. Hoyes, C. Jones, J. I. Langridge, A. Millar, and J. P. C. Vissers, "A novel precursor ion discovery method on a hybrid quadrupole orthogonal acceleration time-of-flight (Q-TOF) mass spectrometer for studying protein phosphorylation." *Journal of the American Society for Mass Spectrometry*, vol. 13, no. 7, pp. 792–803, Jul. 2002. [Online]. Available: http://www.ncbi.nlm.nih.gov/pubmed/12148804

[171] A. Chi, C. Huttenhower, L. Y. Geer, J. J. Coon, J. E. P. Syka, D. L. Bai, J. Shabanowitz, D. J. Burke, O. G. Troyanskaya, and D. F. Hunt, "Analysis of phosphorylation sites on proteins from Saccharomyces cerevisiae by electron transfer dissociation (ETD) mass spectrometry." *Proceedings of the National Academy of Sciences of the United States of America*, vol. 104, no. 7, pp. 2193–8, Mar. 2007. [Online]. Available: http://www.pubmedcentral.nih.gov/articlerender.fcgi?artid=1892997&tool=pmcentrez&rendertype=abstract

[172] A. Shevchenko, I. Chernushevich, M. Wilm, and M. Mann, "De Novo peptide sequencing by nanoelectrospray tandem mass spectrometry using triple quadrupole and quadrupole/time-of-flight instruments." in *Mass Spectrometry of Proteins and Peptides Methods in Molecular Biology*, Jan. 2000, vol. 146, ch. 1, pp. 1–16. [Online]. Available: http://www.ncbi.nlm.nih.gov/pubmed/10948493

[173] A. Shevchenko, I. Chernushevic, A. Shevchenko, M. Wilm, and M. Mann, ""De novo" sequencing of peptides recovered from in-gel digested proteins by nanoelectrospray tandem mass spectrometry." *Molecular Biotechnology*, vol. 20, no. 1, pp. 107–18,

Jan. 2002. [Online]. Available: http://www.ncbi.nlm.nih.gov/pubmed/1876295http://www.ncbi.nlm.nih.gov/pubmed/11876295

[174] K. R. Clauser, P. Baker, and A. L. Burlingame, "Role of accurate mass measurement (+/- 10 ppm) in protein identification strategies employing MS or MS/MS and database searching." *Analytical Chemistry*, vol. 71, no. 14, pp. 2871–82, Jul. 1999. [Online]. Available: http://www.ncbi.nlm.nih.gov/pubmed/10424174

[175] U. K. Laemmli, "Cleavage of Structural Proteins during the Assembly of the Head of Bacteriophage T4," *Nature*, vol. 227, no. 5259, pp. 680–685, Aug. 1970. [Online]. Available: http://www.nature.com/doifinder/10.1038/227680a0

[176] M. Unlue, M. Morgan, and J. Minden, "Difference gel electrophoresis: A single gel method for detecting changes in protein extracts," *Electrophoresis*, vol. 18, pp. 2071–77, 1997.

[177] O. Greengauz-Roberts, H. Stöppler, S. Nomura, H. Yamaguchi, J. R. Goldenring, R. H. Podolsky, J. R. Lee, and W. S. Dynan, "Saturation labeling with cysteine-reactive cyanine fluorescent dyes provides increased sensitivity for protein expression profiling of laser-microdissected clinical specimens." *Proteomics*, vol. 5, no. 7, pp. 1746–57, May 2005. [Online]. Available: http://www.ncbi.nlm.nih.gov/pubmed/15761955

[178] T. Kondo and S. Hirohashi, "Application of highly sensitive fluorescent dyes (CyDye DIGE Fluor saturation dyes) to laser microdissection and two-dimensional difference gel electrophoresis (2D-DIGE) for cancer proteomics." *Nature Protocols*, vol. 1, no. 6, pp. 2940–56, Jan. 2006. [Online]. Available: http://www.ncbi.nlm.nih.gov/pubmed/17406554

[179] A. J. Alpert, "Hydrophilic-interaction chromatography for the separation of peptides, nucleic acids and other polar compounds." *Journal of Chromatography*, vol. 499, pp. 177–96, Jan. 1990. [Online]. Available: http://www.ncbi.nlm.nih.gov/pubmed/2324207

[180] P. Hemström and K. Irgum, *Hydrophilic interaction chromatography*, Aug. 2006, vol. 29, no. 12. [Online]. Available: http://doi.wiley.com/10.1002/jssc.200600199

[181] R. Kay, C. Barton, L. Ratcliffe, B. Matharoo-Ball, P. Brown, J. Roberts, P. Teale, and C. Creaser, "Enrichment of low molecular weight serum proteins using acetonitrile precipitation for mass spectrometry based proteomic analysis." *Rapid Communications in Mass Spectrometry*, vol. 22, no. 20, pp. 3255–60, Oct. 2008. [Online]. Available: http://www.ncbi.nlm.nih.gov/pubmed/18803344

[182] G. Biosa, M. F. Addis, A. Tanca, S. Pisanu, T. Roggio, S. Uzzau, and D. Pagnozzi, "Comparison of blood serum peptide enrichment methods by Tricine SDS-PAGE and mass spectrometry." *Journal of Proteomics*, vol. 75, no. 1, pp. 93–9, Dec. 2011. [Online]. Available: http://www.ncbi.nlm.nih.gov/pubmed/21757041

[183] H. B. Krishnan and S. S. Natarajan, "A rapid method for depletion of Rubisco from soybean (Glycine max) leaf for proteomic analysis of lower abundance proteins." *Phytochemistry*, vol. 70, no. 17-18, pp. 1958–64, Dec. 2009. [Online]. Available: http://www.ncbi.nlm.nih.gov/pubmed/19766275

[184] B. de Roos, S. J. Duthie, A. C. J. Polley, F. Mulholland, F. G. Bouwman, C. Heim, G. J. Rucklidge, I. T. Johnson, E. C. Mariman, H. Daniel, and R. M. Elliott, "Proteomic methodological recommendations for studies involving human plasma, platelets, and peripheral blood mononuclear cells." *Journal of Proteome Research*, vol. 7, no. 6, pp. 2280–90, Jun. 2008. [Online]. Available: http://www.ncbi.nlm.nih.gov/pubmed/18489134

[185] A. R. Vaezzadeh, A. C. Briscoe, H. Steen, and R. S. Lee, "One-step sample concentration, purification, and albumin depletion method for urinary proteomics." *Journal of Proteome Research*, vol. 9, no. 11, pp. 6082–9, Nov. 2010. [Online]. Available: http://www.pubmedcentral.nih.gov/articlerender.fcgi?artid=2974758&tool=pmcentrez&rendertype=abstract

[186] S. B. Ficarro, M. L. McCleland, P. T. Stukenberg, D. J. Burke, M. M. Ross, J. Shabanowitz, D. F. Hunt, and F. M. White, "Phosphoproteome analysis by mass spectrometry and its application to Saccharomyces cerevisiae." *Nature Biotechnology*, vol. 20, no. 3, pp. 301–5, Mar. 2002. [Online]. Available: http://www.ncbi.nlm.nih.gov/pubmed/11875433

[187] M. Larsen, M. Trelle, T. Thingholm, and O. Jensen, "Analysis of posttranslational modifications of proteins by tandem mass spectrometry," *BioTechniques*, vol. 40, no. 6, pp. 790–798, Jun. 2006. [Online]. Available: http://www.biotechniques.com/article/000112201

[188] H. Zhou, R. Tian, M. Ye, S. Xu, S. Feng, C. Pan, X. Jiang, X. Li, and H. Zou, "Highly specific enrichment of phosphopeptides by zirconium dioxide nanoparticles for phosphoproteome analysis." *Electrophoresis*, vol. 28, no. 13, pp. 2201–15, Jul. 2007. [Online]. Available: http://www.ncbi.nlm.nih.gov/pubmed/17539039

[189] C. Sykora, R. Hoffmann, and P. Hoffmann, "Enrichment of multiphosphorylated peptides by immobilized metal affinity chromatography using Ga(III)- and Fe(III)-complexes."

Protein and Peptide Letters, vol. 14, no. 5, pp. 489–96, Jan. 2007. [Online]. Available: http://www.ncbi.nlm.nih.gov/pubmed/17584176

[190] Y. Li, X. Xu, D. Qi, C. Deng, P. Yang, and X. Zhang, "Novel Fe3O4@TiO2 core-shell microspheres for selective enrichment of phosphopeptides in phosphoproteome analysis." *Journal of Proteome Research*, vol. 7, no. 6, pp. 2526–38, Jun. 2008. [Online]. Available: http://www.ncbi.nlm.nih.gov/pubmed/18473453

[191] M. Mann and O. N. Jensen, "Proteomic analysis of post-translational modifications." *Nature Biotechnology*, vol. 21, no. 3, pp. 255–61, Mar. 2003. [Online]. Available: http://www.ncbi.nlm.nih.gov/pubmed/12610572

[192] B. Bodenmiller, J. Malmstrom, B. Gerrits, D. Campbell, H. Lam, A. Schmidt, O. Rinner, L. N. Mueller, P. T. Shannon, P. G. Pedrioli, C. Panse, H.-K. Lee, R. Schlapbach, and R. Aebersold, "PhosphoPep–a phosphoproteome resource for systems biology research in Drosophila Kc167 cells." *Molecular Systems Biology*, vol. 3, no. 139, p. 139, Jan. 2007. [Online]. Available: http://www.pubmedcentral.nih.gov/articlerender.fcgi?artid=2063582&tool=pmcentrez&rendertype=abstract

[193] J. C. Trinidad, C. G. Specht, A. Thalhammer, R. Schoepfer, and A. L. Burlingame, "Comprehensive identification of phosphorylation sites in postsynaptic density preparations." *Molecular & Cellular Proteomics*, vol. 5, no. 5, pp. 914–22, May 2006. [Online]. Available: http://www.ncbi.nlm.nih.gov/pubmed/16452087

[194] J. Villén, S. a. Beausoleil, S. a. Gerber, and S. P. Gygi, "Large-scale phosphorylation analysis of mouse liver." *Proceedings of the National Academy of Sciences of the United States of America*, vol. 104, no. 5, pp. 1488–93, Jan. 2007. [Online]. Available: http://www.pubmedcentral.nih.gov/articlerender.fcgi?artid=1785252&tool=pmcentrez&rendertype=abstract

[195] M. O. Collins, L. Yu, M. P. Coba, H. Husi, I. Campuzano, W. P. Blackstock, J. S. Choudhary, and S. G. N. Grant, "Proteomic analysis of in vivo phosphorylated synaptic proteins." *The Journal of Biological Chemistry*, vol. 280, no. 7, pp. 5972–82, Feb. 2005. [Online]. Available: http://www.ncbi.nlm.nih.gov/pubmed/15572359

[196] G. T. Cantin, W. Yi, B. Lu, S. K. Park, T. Xu, J.-D. Lee, and J. R. Yates, "Combining protein-based IMAC, peptide-based IMAC, and MudPIT for efficient phosphoproteomic analysis." *Journal of Proteome Research*, vol. 7, no. 3, pp. 1346–51, Mar. 2008. [Online]. Available: http://www.ncbi.nlm.nih.gov/pubmed/18220336

[197] M. W. H. Pinkse, P. M. Uitto, M. J. Hilhorst, B. Ooms, and A. J. R. Heck, "Selective isolation at the femtomole level of phosphopeptides from proteolytic digests using 2D-NanoLC-ESI-MS/MS and titanium oxide precolumns." *Analytical Chemistry*, vol. 76, no. 14, pp. 3935–43, Jul. 2004. [Online]. Available: http://www.ncbi.nlm.nih.gov/pubmed/15253627

[198] T. E. Thingholm, T. J. D. Jø rgensen, O. N. Jensen, and M. R. Larsen, "Highly selective enrichment of phosphorylated peptides using titanium dioxide." *Nature Protocols*, vol. 1, no. 4, pp. 1929–35, Jan. 2006. [Online]. Available: http://www.ncbi.nlm.nih.gov/pubmed/17487178

[199] M. R. Larsen, T. E. Thingholm, O. N. Jensen, P. Roepstorff, and T. J. D. Jø rgensen, "Highly selective enrichment of phosphorylated peptides from peptide mixtures using titanium dioxide microcolumns." *Molecular & Cellular Proteomics*, vol. 4, no. 7, pp. 873–86, Jul. 2005. [Online]. Available: http://www.ncbi.nlm.nih.gov/pubmed/15858219

[200] N. Sugiyama, T. Masuda, K. Shinoda, A. Nakamura, M. Tomita, and Y. Ishihama, "Phosphopeptide enrichment by aliphatic hydroxy acid-modified metal oxide chromatography for nano-LC-MS/MS in proteomics applications." *Molecular & Cellular Proteomics*, vol. 6, no. 6, pp. 1103–9, Jun. 2007. [Online]. Available: http://www.ncbi.nlm.nih.gov/pubmed/17322306

[201] J. Rush, A. Moritz, K. A. Lee, A. Guo, V. L. Goss, E. J. Spek, H. Zhang, X.-M. Zha, R. D. Polakiewicz, and M. J. Comb, "Immunoaffinity profiling of tyrosine phosphorylation in cancer cells." *Nature Biotechnology*, vol. 23, no. 1, pp. 94–101, Jan. 2005. [Online]. Available: http://www.ncbi.nlm.nih.gov/pubmed/15592455

[202] M. P. Stokes, C. L. Farnsworth, A. Moritz, J. C. Silva, X. Jia, K. a. Lee, A. Guo, R. D. Polakiewicz, and M. J. Comb, "PTMScan direct: identification and quantification of peptides from critical signaling proteins by immunoaffinity enrichment coupled with LC-MS/MS." *Molecular & Cellular Proteomics*, vol. 11, no. 5, pp. 187–201, May 2012. [Online]. Available: http://www.pubmedcentral.nih.gov/articlerender.fcgi?artid=3418847&tool=pmcentrez&rendertype=abstract

[203] P. J. Boersema, L. Y. Foong, V. M. Y. Ding, S. Lemeer, B. van Breukelen, R. Philp, J. Boekhorst, B. Snel, J. den Hertog, A. B. H. Choo, and A. J. R. Heck, "In-depth qualitative and quantitative profiling of tyrosine phosphorylation using a combination of phosphopeptide immunoaffinity purification and stable isotope dimethyl labeling." *Molecular & Cellular Proteomics*, vol. 9, no. 1, pp. 84–99, Jan. 2010. [Online]. Available: http://www.pubmedcentral.nih.gov/articlerender.fcgi?artid=2808269&tool=pmcentrez&rendertype=abstract

[204] L. Guerrier, P. G. Righetti, and E. Boschetti, "Reduction of dynamic protein concentration range of biological extracts for the discovery of low-abundance proteins by means of hexapeptide ligand library." *Nature Protocols*, vol. 3, no. 5, pp. 883–90, Jan. 2008. [Online]. Available: http://dx.doi.org/10.1038/nprot.2008.59

[205] P. Holden and W. A. Horton, "Crude subcellular fractionation of cultured mammalian cell lines." *BMC Research Notes*, vol. 2, p. 243, Jan. 2009. [Online]. Available: http://www.ncbi.nlm.nih.gov/pubmed/20003239

[206] P. G. Sadowski, T. P. J. Dunkley, I. P. Shadforth, P. Dupree, C. Bessant, J. L. Griffin, and K. S. Lilley, "Quantitative proteomic approach to study subcellular localization of membrane proteins." *Nature Protocols*, vol. 1, no. 4, pp. 1778–89, Jan. 2006. [Online]. Available: http://www.ncbi.nlm.nih.gov/pubmed/17487160

[207] M. W. B. Trotter, P. G. Sadowski, T. P. J. Dunkley, A. J. Groen, and K. S. Lilley, "Improved sub-cellular resolution via simultaneous analysis of organelle proteomics data across varied experimental conditions." *Proteomics*, vol. 10, no. 23, pp. 4213–9, Dec. 2010. [Online]. Available: http://www.ncbi.nlm.nih.gov/pubmed/21058340

[208] D. J. L. Tan, H. Dvinge, A. Christoforou, P. Bertone, A. Martinez Arias, and K. S. Lilley, "Mapping organelle proteins and protein complexes in Drosophila melanogaster." *Journal of Proteome Research*, vol. 8, no. 6, pp. 2667–78, Jun. 2009. [Online]. Available: http://www.ncbi.nlm.nih.gov/pubmed/19317464

[209] S.-E. Ong and M. Mann, "Mass spectrometry-based proteomics turns quantitative." *Nature Chemical Biology*, vol. 1, no. 5, pp. 252–262, 2005. [Online]. Available: http://www.ncbi.nlm.nih.gov/pubmed/16408053

[210] S. P. Gygi, B. Rist, S. A. Gerber, F. Turecek, M. H. Gelb, and R. Aebersold, "Quantitative analysis of complex protein mixtures using isotope-coded affinity tags." *Nature Biotechnology*, vol. 17, no. 10, pp. 994–9, Oct. 1999. [Online]. Available: http://dx.doi.org/10.1038/13690http://www.ncbi.nlm.nih.gov/pubmed/10504701

[211] Y. Oda, T. Owa, T. Sato, B. Boucher, S. Daniels, H. Yamanaka, Y. Shinohara, A. Yokoi, J. Kuromitsu, and T. Nagasu, "Quantitative chemical proteomics for identifying candidate drug targets." *Analytical Chemistry*, vol. 75, no. 9, pp. 2159–65, May 2003. [Online]. Available: http://www.ncbi.nlm.nih.gov/pubmed/12720356

[212] K. C. Hansen, G. Schmitt-Ulms, R. J. Chalkley, J. Hirsch, M. A. Baldwin, and A. L. Burlingame, "Mass spectrometric analysis of protein mixtures at low levels

using cleavable 13C-isotope-coded affinity tag and multidimensional chromatography." *Molecular & Cellular Proteomics*, vol. 2, no. 5, pp. 299–314, May 2003. [Online]. Available: http://www.ncbi.nlm.nih.gov/pubmed/12766231

[213] J. Li, H. Steen, and S. P. Gygi, "Protein profiling with cleavable isotope-coded affinity tag (cICAT) reagents: the yeast salinity stress response." *Molecular & Cellular Proteomics*, vol. 2, no. 11, pp. 1198–204, Nov. 2003. [Online]. Available: http://www.ncbi.nlm.nih.gov/pubmed/14506205

[214] E. C. Yi, X.-J. Li, K. Cooke, H. Lee, B. Raught, A. Page, V. Aneliunas, P. Hieter, D. R. Goodlett, and R. Aebersold, "Increased quantitative proteome coverage with (13)C/(12)C-based, acid-cleavable isotope-coded affinity tag reagent and modified data acquisition scheme." *Proteomics*, vol. 5, no. 2, pp. 380–7, Feb. 2005. [Online]. Available: http://www.ncbi.nlm.nih.gov/pubmed/15648049

[215] P. J. Boersema, R. Raijmakers, S. Lemeer, S. Mohammed, and A. J. R. Heck, "Multiplex peptide stable isotope dimethyl labeling for quantitative proteomics." *Nature Protocols*, vol. 4, no. 4, pp. 484–94, Jan. 2009. [Online]. Available: http://www.ncbi.nlm.nih.gov/pubmed/19300442

[216] K. Rose, M. G. Simona, R. E. Offord, C. P. Prior, B. Otto, and D. R. Thatcher, "A new mass-spectrometric C-terminal sequencing technique finds a similarity between gamma-interferon and alpha 2-interferon and identifies a proteolytically clipped gamma-interferon that retains full antiviral activity." *The Biochemical Journal*, vol. 215, no. 2, pp. 273–7, Nov. 1983. [Online]. Available: http://www.pubmedcentral.nih.gov/articlerender.fcgi?artid=1152394&tool=pmcentrez&rendertype=abstract

[217] M. Schnölzer, P. Jedrzejewski, and W. D. Lehmann, "Protease-catalyzed incorporation of 18O into peptide fragments and its application for protein sequencing by electrospray and matrix-assisted laser desorption/ionization mass spectrometry." *Electrophoresis*, vol. 17, no. 5, pp. 945–53, May 1996. [Online]. Available: http://www.ncbi.nlm.nih.gov/pubmed/8783021

[218] C. Fenselau and X. Yao, "Proteolytic labeling with 18O for comparative proteomics studies: preparation of 18O-labeled peptides and the 18O/16O peptide mixture." in *Quantitative Proteomics by Mass Spectrometry Methods in molecular biology (Clifton, N.J.)*, Jan. 2007, vol. 359, ch. 9, pp. 135–42. [Online]. Available: http://www.ncbi.nlm.nih.gov/pubmed/17484115

[219] X. Yan and C. S. Maier, "Hydrogen/deuterium exchange mass spectrometry." in *Mass Spectrometry of Proteins and Peptides Methods in molecular biology*

(Clifton, N.J.), Jan. 2009, vol. 492, ch. 15, pp. 255–71. [Online]. Available: http://www.ncbi.nlm.nih.gov/pubmed/19241038

[220] P. L. Ross, Y. N. Huang, J. N. Marchese, B. Williamson, K. Parker, S. Hattan, N. Khainovski, S. Pillai, S. Dey, S. Daniels, S. Purkayastha, P. Juhasz, S. Martin, M. Bartlet-Jones, F. He, A. Jacobson, and D. J. Pappin, "Multiplexed protein quantitation in Saccharomyces cerevisiae using amine-reactive isobaric tagging reagents." *Molecular & Cellular Proteomics*, vol. 3, no. 12, pp. 1154–69, Dec. 2004. [Online]. Available: http://www.ncbi.nlm.nih.gov/pubmed/15385600

[221] A. Thompson, J. Schäfer, K. Kuhn, S. Kienle, J. Schwarz, G. Schmidt, T. Neumann, and C. Hamon, "Tandem Mass Tags: A Novel Quantification Strategy for Comparative Analysis of Complex Protein Mixtures by MS/MS," *Analytical Chemistry*, vol. 75, no. 8, pp. 1895–1904, Apr. 2003. [Online]. Available: http://www.ncbi.nlm.nih.gov/pubmed/12713048http://pubs.acs.org/doi/abs/10.1021/ac0262560

[222] Y. Levin and S. Bahn, "Quantification of proteins by label-free LC-MS/MS." in *LC-MS/MS in Proteomics Methods and Applications Methods in molecular biology (Clifton, N.J.)*. Humana Press, Jan. 2010, vol. 658, ch. 13, pp. 217–31. [Online]. Available: http://www.ncbi.nlm.nih.gov/pubmed/20839107

[223] W. X. Schulze and B. Usadel, "Quantitation in mass-spectrometry-based proteomics." *Annual Review of Plant Biology*, vol. 61, no. January, pp. 491–516, 2010. [Online]. Available: http://www.ncbi.nlm.nih.gov/pubmed/20192741

[224] B. L. Zybailov, L. Florens, and M. P. Washburn, "Quantitative shotgun proteomics using a protease with broad specificity and normalized spectral abundance factors." *Molecular BioSystems*, vol. 3, no. 5, pp. 354–60, May 2007. [Online]. Available: http://www.ncbi.nlm.nih.gov/pubmed/17460794

[225] J. C. Braisted, S. Kuntumalla, C. Vogel, E. M. Marcotte, A. R. Rodrigues, R. Wang, S.-T. Huang, E. S. Ferlanti, A. I. Saeed, R. D. Fleischmann, S. N. Peterson, and R. Pieper, "The APEX Quantitative Proteomics Tool: generating protein quantitation estimates from LC-MS/MS proteomics results." *BMC Bioinformatics*, vol. 9, p. 529, 2008. [Online]. Available: http://www.ncbi.nlm.nih.gov/pubmed/19068132

[226] Y. Ishihama, Y. Oda, T. Tabata, T. Sato, T. Nagasu, J. Rappsilber, and M. Mann, "Exponentially modified protein abundance index (emPAI) for estimation of absolute protein amount in proteomics by the number of sequenced peptides per protein." *Molecular cellular proteomics MCP*, vol. 4, no. 9, pp. 1265–1272, 2005. [Online]. Available: http://www.ncbi.nlm.nih.gov/pubmed/15958392

[227] D. C. Trudgian, G. Ridlova, R. Fischer, M. M. Mackeen, N. Ternette, O. Acuto, B. M. Kessler, and B. Thomas, "Comparative evaluation of label-free SINQ normalized spectral index quantitation in the central proteomics facilities pipeline." *Proteomics*, vol. 11, no. 14, pp. 2790–7, Jul. 2011. [Online]. Available: http://www.ncbi.nlm.nih.gov/pubmed/21656681

[228] N. M. Griffin, J. Yu, F. Long, P. Oh, S. Shore, Y. Li, J. a. Koziol, and J. E. Schnitzer, "Label-free, normalized quantification of complex mass spectrometry data for proteomic analysis." *Nature Biotechnology*, vol. 28, no. 1, pp. 83–9, Jan. 2010. [Online]. Available: http://www.pubmedcentral.nih.gov/articlerender.fcgi?artid=2805705&tool=pmcentrez&rendertype=abstract

[229] R. E. Kaiser, R. E. Higgs, and R. K. Julian, "System and Methods for Quantitatively Comparing Complex Mixtures Using Single Ion Chromatograms Derived From Spectroscopic Analysis of Such Admixtures," 1999.

[230] R. E. Higgs, M. D. Knierman, V. Gelfanova, J. P. Butler, and J. E. Hale, "Comprehensive label-free method for the relative quantification of proteins from biological samples." *Journal of Proteome Research*, vol. 4, no. 4, pp. 1442–50, 2005. [Online]. Available: http://www.ncbi.nlm.nih.gov/pubmed/16083298

[231] L. N. Mueller, O. Rinner, A. Schmidt, S. Letarte, B. Bodenmiller, M.-Y. Brusniak, O. Vitek, R. Aebersold, and M. Müller, "SuperHirn - a novel tool for high resolution LC-MS-based peptide/protein profiling." *Proteomics*, vol. 7, no. 19, pp. 3470–80, Oct. 2007. [Online]. Available: http://www.ncbi.nlm.nih.gov/pubmed/17726677

[232] J. Cox and M. Mann, "MaxQuant enables high peptide identification rates, individualized p.p.b.-range mass accuracies and proteome-wide protein quantification." *Nature Biotechnology*, vol. 26, no. 12, pp. 1367–72, Dec. 2008. [Online]. Available: http://www.ncbi.nlm.nih.gov/pubmed/19029910

[233] B. Schwanhäusser, D. Busse, N. Li, G. Dittmar, J. Schuchhardt, J. Wolf, W. Chen, and M. Selbach, "Global quantification of mammalian gene expression control." *Nature*, vol. 473, no. 7347, pp. 337–42, May 2011. [Online]. Available: http://www.ncbi.nlm.nih.gov/pubmed/21593866

[234] J. C. Silva, M. V. Gorenstein, G.-Z. Li, J. P. C. Vissers, and S. J. Geromanos, "Absolute quantification of proteins by LCMSE: a virtue of parallel MS acquisition." *Molecular & Cellular Proteomics*, vol. 5, no. 1, pp. 144–56, Jan. 2006. [Online]. Available: http://www.ncbi.nlm.nih.gov/pubmed/16219938

[235] E. Ahrné, L. Molzahn, T. Glatter, and A. Schmidt, "Critical assessment of proteome-wide label-free absolute abundance estimation strategies." *Proteomics*, pp. 1–29, Jun. 2013. [Online]. Available: http://onlinelibrary.wiley.com/doi/10.1002/pmic.201300135/abstracthttp://www.ncbi.nlm.nih.gov/pubmed/23794183

[236] A. Schmidt, M. Beck, J. Malmström, H. Lam, M. Claassen, D. Campbell, and R. Aebersold, "Absolute quantification of microbial proteomes at different states by directed mass spectrometry," *Molecular Systems Biology*, vol. 7, no. 510, pp. 1–16, Jul. 2011. [Online]. Available: http://www.nature.com/doifinder/10.1038/msb.2011.37

[237] J. Malmström, M. Beck, A. Schmidt, V. Lange, E. W. Deutsch, and R. Aebersold, "Proteome-wide cellular protein concentrations of the human pathogen Leptospira interrogans." *Nature*, vol. 460, no. 7256, pp. 762–5, Aug. 2009. [Online]. Available: http://www.pubmedcentral.nih.gov/articlerender.fcgi?artid=2723184&tool=pmcentrez&rendertype=abstract

[238] T.-C. Chao, N. Hansmeier, and R. U. Halden, "Towards proteome standards: the use of absolute quantitation in high-throughput biomarker discovery." *Journal of Proteomics*, vol. 73, no. 8, pp. 1641–6, Jun. 2010. [Online]. Available: http://www.pubmedcentral.nih.gov/articlerender.fcgi?artid=2885480&tool=pmcentrez&rendertype=abstract

[239] M. H. St Clair, K. N. Pennington, J. Rooney, and D. W. Barry, "In vitro comparison of selected triple-drug combinations for suppression of HIV-1 replication: The Inter-Company Collaboration Protocol," *Journal of Acquired Immune Deficiency Syndromes*, vol. 10 Suppl 2, pp. S83–91, Jan. 1995. [Online]. Available: http://www.ncbi.nlm.nih.gov/pubmed/7552518

[240] A. I. Veldkamp, M. Harris, J. S. Montaner, G. Moyle, B. Gazzard, M. Youle, M. Johnson, M. O. Kwakkelstein, H. Carlier, R. van Leeuwen, J. H. Beijnen, J. M. Lange, P. Reiss, and R. M. Hoetelmans, "The steady-state pharmacokinetics of efavirenz and nevirapine when used in combination in human immunodeficiency virus type 1-infected persons." *The Journal of Infectious Diseases*, vol. 184, no. 1, pp. 37–42, 2001. [Online]. Available: http://www.ncbi.nlm.nih.gov/pubmed/11398107

[241] W. A. McAllister, P. J. Thompson, S. M. Al-Habet, and H. J. Rogers, "Rifampicin reduces effectiveness and bioavailability of prednisolone." *British Medical Journal*, vol. 286, no. 6369, pp. 923–5, Mar. 1983. [Online]. Available: http://www.ncbi.nlm.nih.gov/pubmed/6403136

[242] J. Chen and K. Raymond, "Roles of rifampicin in drug-drug interactions: underlying molecular mechanisms involving the nuclear pregnane X receptor." *Annals of*

Clinical Microbiology and Antimicrobials, vol. 5, p. 3, Jan. 2006. [Online]. Available: http://www.pubmedcentral.nih.gov/articlerender.fcgi?artid=1395332&tool=pmcentrez&rendertype=abstract

[243] C. Schutz, G. Meintjes, F. Almajid, R. J. Wilkinson, and A. Pozniak, "Clinical Management of Tuberculosis and HIV-1 co-infection." *The European Respiratory Journal*, vol. 36, no. 6, pp. 1460–1481, Oct. 2010. [Online]. Available: http://www.ncbi.nlm.nih.gov/pubmed/20947678

[244] Department of Health and Human Services, "Guidelines for the use of antiretroviral agents in HIV-infected adults and adolescents." Office of AIDS Research Advisory Council (OARAC), Tech. Rep. 2, Jan. 2011. [Online]. Available: http://www.aidsinfo.nih.gov/Con-tentFiles/AdultandAdolescentGL.pdf

[245] Division of Clinical Pharmacology, *The South African Medicines Formulary*, 9th ed., D. Rossiter, Ed. Cape Town, South Africa: Health and Medical Publishing Group, 2012. [Online]. Available: http://web.uct.ac.za/depts/pha/samf.php

[246] L. M. Enomoto, K. J. Kloberdanz, D. G. Mack, D. Elizabeth, and A. Weinberg, "Ex vivo effect of estrogen and progesterone compared with dexamethasone on cell-mediated immunity of HIV-infected and uninfected subjects." *Journal of Acquired Immune Deficiency Syndromes*, vol. 45, no. 2, pp. 137–43, Jun. 2007. [Online]. Available: http://www.ncbi.nlm.nih.gov/pubmed/17356463

[247] R. Chacón-Salinas, J. Serafín-López, R. Ramos-Payán, P. Méndez-Aragón, R. Hernández-Pando, D. Van Soolingen, L. Flores-Romo, S. Estrada-Parra, and I. Estrada-García, "Differential pattern of cytokine expression by macrophages infected in vitro with different Mycobacterium tuberculosis genotypes." *Clinical & Developmental Immunology*, vol. 140, no. 3, pp. 443–9, Jun. 2005. [Online]. Available: http://www.ncbi.nlm.nih.gov/pubmed/15932505

[248] M. Skopeliti, U. Kratzer, F. Altenberend, G. Panayotou, H. Kalbacher, S. Stevanovic, W. Voelter, and O. E. Tsitsilonis, "Proteomic exploitation on prothymosin alpha-induced mononuclear cell activation." *Proteomics*, vol. 7, no. 11, pp. 1814–24, 2007. [Online]. Available: http://www.ncbi.nlm.nih.gov/pubmed/17474146

[249] J. R. Wiśniewski, D. F. Zielinska, and M. Mann, "Comparison of ultrafiltration units for proteomic and N-glycoproteomic analysis by the filter-aided sample preparation method." *Analytical Biochemistry*, vol. 410, no. 2, pp. 307–9, Mar. 2011. [Online]. Available: http://www.ncbi.nlm.nih.gov/pubmed/21144814

[250] M. J. Hubbard and P. Cohen, "On target with a new mechanism for the regulation of protein phosphorylation." *Trends in Biochemical Sciences*, vol. 18, no. 5, pp. 172–7, May 1993. [Online]. Available: http://www.ncbi.nlm.nih.gov/pubmed/8392229

[251] J. R. Wiśniewski, A. Zougman, N. Nagaraj, and M. Mann, "Universal sample preparation method for proteome analysis. - Supplimentary Data," *Nature Methods*, vol. 6, no. 5, pp. 359–62, May 2009. [Online]. Available: http://www.ncbi.nlm.nih.gov/pubmed/19377485

[252] A. Conesa-Botella, G. Meintjes, A. K. Coussens, H. van der Plas, R. Goliath, C. Schutz, R. Moreno-Reyes, M. Mehta, A. R. Martineau, R. J. Wilkinson, R. Colebunders, and K. A. Wilkinson, "Corticosteroid therapy, vitamin D status, and inflammatory cytokine profile in the HIV-TB immune reconstitution inflammatory syndrome (TB-IRIS)." *Clinical Infectious Diseases*, pp. 1–26, Jun. 2012. [Online]. Available: http://cid.oxfordjournals.org/content/early/2012/06/19/cid.cis577.shorthttp://www.ncbi.nlm.nih.gov/pubmed/22715179

[253] M. Spivak, D. Tomazela, J. Weston, M. J. Maccoss, and W. S. Noble, "Direct maximization of protein identifications from tandem mass spectra." *Molecular & Cellular Proteomics*, pp. 1–20, Nov. 2011. [Online]. Available: http://www.ncbi.nlm.nih.gov/pubmed/22052992

[254] J. Liu, A. W. Bell, J. J. M. Bergeron, C. M. Yanofsky, B. Carrillo, C. E. H. Beaudrie, and R. E. Kearney, "Methods for peptide identification by spectral comparison." *Proteome Science*, vol. 5, p. 3, Jan. 2007. [Online]. Available: http://www.pubmedcentral.nih.gov/articlerender.fcgi?artid=1783643&tool=pmcentrez&rendertype=abstract

[255] J. Maertzdorf, M. Ota, D. Repsilber, H. J. Mollenkopf, J. Weiner, P. C. Hill, and S. H. E. Kaufmann, "Functional correlations of pathogenesis-driven gene expression signatures in tuberculosis." *PloS One*, vol. 6, no. 10, p. e26938, Jan. 2011. [Online]. Available: http://www.pubmedcentral.nih.gov/articlerender.fcgi?artid=3203931&tool=pmcentrez&rendertype=abstract

[256] J. D. Ashwell, F. W. Lu, and M. S. Vacchio, "Glucocorticoids in T cell development and function," *Annual Review of Immunology*, vol. 18, no. 18, pp. 309–45, Jan. 2000. [Online]. Available: http://www.ncbi.nlm.nih.gov/pubmed/10837061

[257] T. Rhen and J. A. Cidlowski, "Antiinflammatory Action of Glucocorticoids - New Mechanisms for Old Drugs," *The New England Journal of Medicine*, no. 353, pp. 1711–1723, 2005.

[258] A. Winiski, S. Wang, B. Schwendinger, and A. Stuetz, "Inhibition of T-cell activation in vitro in human peripheral blood mononuclear cells by pimecrolimus and glucocorticosteroids and combinations thereof." *Experimental Dermatology*, vol. 16, no. 8, pp. 699–704, 2007. [Online]. Available: http://www.ncbi.nlm.nih.gov/pubmed/17620098

[259] T. Kadhiravan and S. Deepanjali, "Role of corticosteroids in the treatment of tuberculosis: an evidence-based update." *The Indian Journal of Chest Diseases & Allied Sciences*, vol. 52, no. 3, pp. 153–8, 2010. [Online]. Available: http://www.ncbi.nlm.nih.gov/pubmed/20949734

[260] A. Bruneel, V. Labas, A. Mailloux, S. Sharma, N. Royer, J. Vinh, P. Pernet, M. Vaubourdolle, and B. Baudin, "Proteomics of human umbilical vein endothelial cells applied to etoposide-induced apoptosis." *Proteomics*, vol. 5, no. 15, pp. 3876–84, Oct. 2005. [Online]. Available: http://www.ncbi.nlm.nih.gov/pubmed/16130169

[261] H. Shen, "CIL:7762," 2012. [Online]. Available: http://www.cellimagelibrary.org/images/7762

[262] R. Tadokera, G. Meintjes, K. H. Skolimowska, K. a. Wilkinson, K. Matthews, R. Seldon, N. N. Chegou, G. Maartens, M. X. Rangaka, K. Rebe, G. Walzl, and R. J. Wilkinson, "Hypercytokinaemia accompanies HIV-tuberculosis immune reconstitution inflammatory syndrome." *The European Respiratory Journal*, Sep. 2010. [Online]. Available: http://www.ncbi.nlm.nih.gov/pubmed/20817712

[263] D. L. Barber, B. B. Andrade, I. Sereti, and A. Sher, "Immune reconstitution inflammatory syndrome: the trouble with immunity when you had none." *Nature Reviews Microbiology*, vol. 10, no. 2, pp. 150–6, Feb. 2012. [Online]. Available: http://www.ncbi.nlm.nih.gov/pubmed/22230950

Appendix

Crux parameter file

```
# Which isotopes to use in calculating fragment ion mass.
# <string>=average|mono. Default=mono.
# Parameter file only. Used by crux-search-for-matches and crux-predict-peptide-ions.
fragment-mass=mono

# Print to stdout additional information about the spectrum.
# Avaliable only for crux-get-ms2-spectrum. Does not affect contents of the output file.
stats=false

# Specifies the operator that is used to compare an entry in the specified column to the value
# given on the command line.
# (eq|gt|gte|lt|lte|neq). Default: eq.
# Available for crux extract-rows
comparison=eq

# Minimum number of points for estimating the Weibull parameters.
# Default=4000.
# Available for crux search-for-xlinks
min-weibull-points=4000

# Number of consecutive MS1 scans over which a peptide must be observed to be considered
# real. Gaps in persistence are allowed when setting –gap-tolerance. Default = 3.
# Available for crux bullseye
scan-tolerance=3

# Predict the given number of isotope peaks (0|1|2). Default=0.
# Only available for crux-predict-peptide-ion. Automatically set to 0 for Sp scoring and 1 for
# xcorr scoring.
isotope=0
```

```
# Window type to use for selecting decoy peptides from precursor mz.
# <string>=mass|mz|ppm. Default=mass.
# Available for crux search-for-matches
precursor-window-type-decoy=mass

# The ion series to predict (b,y,by,bya). Default='by' (both b and y ions).
# Only available for crux-predict-peptide-ions. Set automatically to 'by' for searching.
primary-ions=by

# Perform parsimony analysis on the proteins and report a parsimony rank column in
# output file. Default=none. Can be
# <string>=none|simple|greedy
# Available for spectral-counts.
parsimony=none

# Which isotopes to use in calculating peptide mass.
# <string>=average|mono. Default=average.
# Used from command line or parameter file by crux-create-index and
# crux-generate-peptides. Parameter file only for crux-search-for-matches.
isotopic-mass=mono

# Include self-loop peptides in the database. Default=T.
# Available for crux search-for-xlinks program.
xlink-include-selfloops=true

# Quantification at protein or peptide level (PROTEIN,PEPTIDE).
# Default=PROTEIN.
# Available for spectral-counts and either NSAF and SIN.
quant-level=protein

# Window type to use for selecting candidate peptides.
# <string>=mass|mz|ppm. Default=mass.
# Available for search-for-matches, search-for-xlinks.
precursor-window-type=mass

# Search peptides within +/- 'precursor-window' of the spectrum mass.
# Definition of precursor window depends upon precursor-window-type.
# Default=3.0.
# Available from the parameter file only for crux-search-for-matches, crux-create-index, and
# crux-generate-peptides.
precursor-window=3.000000
```

```
# Set the precision for masses and m/z written to sqt and .txt files.
# Default=4
# Available from parameter file for all commands.
mass-precision=4

# Specify rules for in silico digestion of proteins. See HTML documentation for syntax.
# Default is trypsin.
# Overrides the enzyme option. Two lists of residues are given enclosed in square brackets or
# curly braces and separated by a |. The first list contains residues required/prohibited before
# the cleavage site and the second list is residues after the cleavage site. If the residues are
# required for digestion, they are in square brackets, '[' and ']'. If the residues prevent digestion,
# then they are enclosed in curly braces, '{' and '}'. Use X to indicate all residues. For example,
# trypsin cuts after R or K but not before P which is represented as [RK]|{P}. AspN cuts
# after any residue but only before D which is represented as [X]|[D].
custom-enzyme=__NULL_STR

# Predict flanking peaks for b and y ions (T,F). Default=F.
# Only available for crux-predict-peptide-ion.
flanking=false

# Include peaks +/- 1da around b/y ions in theoretical spectrum.
# sequest-search and search-for-xlinks default=T. search-for-matches default=F.
# Available in the paramter file for all search commands.
use-flanking-peaks=true

# Change the mass of all amino acids 'A' by the given amount.
# For parameter file only. Default=no mass change.
A=0.000000

# Change the mass of all amino acids 'C' by the given amount.
# For parameter file only. Default=+57.0214637206.
C=57.021464

# Change the mass of all amino acids 'D' by the given amount.
# For parameter file only. Default=no mass change.
D=0.000000

# Change the mass of all amino acids 'E' by the given amount.
# For parameter file only. Default=no mass change.
E=0.000000
```

```
# Specify the width of the bins used to discretize the m/z axis. Also used as tolerance for
# assigning ions. Default=1.0005079 for monoisotopic mass or 1.0011413 for average mass.
# Available for crux-search-for-matches and xlink-assign-ions.
mz-bin-width=1.000508

# Change the mass of all amino acids 'F' by the given amount.
# For parameter file only. Default=no mass change.
F=0.000000

# Change the mass of all amino acids 'G' by the given amount.
# For parameter file only. Default=no mass change.
G=0.000000

# Change the mass of all amino acids 'H' by the given amount.
# For parameter file only. Default=no mass change.
H=0.000000

# Change the mass of all amino acids 'I' by the given amount.
# For parameter file only. Default=no mass change.
I=0.000000

# Change the mass of all amino acids 'K' by the given amount.
# For parameter file only. Default=no mass change.
K=0.000000

# Change the mass of all amino acids 'L' by the given amount.
# For parameter file only. Default=no mass change.
L=0.000000

# Change the mass of all amino acids 'M' by the given amount.
# For parameter file only. Default=no mass change.
M=0.000000

# Change the mass of all amino acids 'N' by the given amount.
# For parameter file only. Default=no mass change.
N=0.000000

# Change the mass of all amino acids 'P' by the given amount.
# For parameter file only. Default=no mass change.
P=0.000000
```

# Change the mass of all amino acids 'Q' by the given amount.
# For parameter file only. Default=no mass change.
Q=0.000000

# Change the mass of all amino acids 'R' by the given amount.
# For parameter file only. Default=no mass change.
R=0.000000

# Change the mass of all amino acids 'S' by the given amount.
# For parameter file only. Default=no mass change.
S=0.000000

# Change the mass of all amino acids 'T' by the given amount.
# For parameter file only. Default=no mass change.
T=0.000000

# Change the mass of all amino acids 'V' by the given amount.
# For parameter file only. Default=no mass change.
V=0.000000

# Change the mass of all amino acids 'W' by the given amount.
# For parameter file only. Default=no mass change.
W=0.000000

# Change the mass of all amino acids 'Y' by the given amount.
# For parameter file only. Default=no mass change.
Y=0.000000

# Print version number and quit.
# Available for all crux programs. On command line use '–version T'.
version=false

# Set the resolution of the observed spectra at m/z 400. Used in conjunction with –instrument
# The default is 100000.
# Available for crux hardklor
resolution=100000.000000

The format to write the output spectra to. By default, the spectra will be output in the same
format as the MS/MS input.
Available for crux bullseye
spectrum-format=__NULL_STR

The minimum length of peptides to consider. Default=6.
Used from the command line or parameter file by crux-create-index and crux-generate-peptides.
Parameter file only for crux-search-for-matches.
min-length=6

Predict the precursor ions, and all associated ions (neutral-losses, multiple charge states)
consistent with the other specified options. (T,F) Default=F.
Only available for crux-predict-peptide-ions.
precursor-ions=false

# Degree of digestion used to generate peptides.
# <string>=full-digest|partial-digest. Either both ends or one end of a peptide must conform to
# enzyme specificity rules. Default=full-digest.
# Used in conjunction with enzyme option when enzyme is not set to 'no-enzyme'. Available
# from command line or parameter file for crux-generate-peptides and crux create-index.
# Available from parameter file for crux search-for-matches. Digestion rules are as follows:
# enzyme name [cuts after one of these residues][but not before one of these residues].
# trypsin [RK][P], elastase [ALIV][P], chymotrypsin [FWY][P].
digestion=full-digest

# Replace existing files (T) or exit if attempting to overwrite (F).
# Default=F.
# Available for all crux programs. Applies to parameter file as well as index, search, and analysis
# output files.
overwrite=T

Choose the algorithm for analyzing combinations of multiple peptide or protein isotope
distributions. (basic | fewest-peptides | fast-fewest-peptides | fewest-peptides-choice |
fast-fewest-peptides-choice) Default=fast-fewest-peptides.
Available for crux hardklor
hardklor-algorithm=fast-fewest-peptides

Set additional options with values in the given file.
Available for all crux programs. Any options specified on the command line will override
values in the parameter file.
parameter-file=/opt/exp_soft/medbio/program_options/crux_1_37/parameters/mono_target_peptide-shuffle.txt

The minimum number of peaks a spectrum must have for it to be searched. Default=20.
Parameter file only for search-for-matches and sequest-search.
min-peaks=20

```
# Predict peaks with the given maximum number of nh3 neutral loss modifications. Default=0.
# Only available for crux-predict-peptide-ions.
nh3=0

# Type of analysis to make on the match results: (RAW|NSAF|dNSAF|SIN|EMPAI). Default=NSAF.
# Available for spectral-counts. RAW is raw counts, NSAF is Normalized Spectral Abundance
# Factor, dNSAF is Distributed Spectral Abundance Factor, SIN is Spectral Index Normalized
# and EMPAI is Exponentially Modified Protein Abundance
Index measure=NSAF

# Number of psms per spectrum to score with xcorr after preliminary scoring with Sp.
# Set to 0 to score all psms with xcorr. Default=500.
# Used by crux-search-for-matches. For positive values, the Sp (preliminary) score acts as a
# filter; only high scoring psms go on to be scored with xcorr. This saves some time. If set to 0,
# all psms are scored with both scores.
max-rank-preliminary=2000

# The maximum number of modifications that can be applied to a single peptide.
# Default=no limit.
# Available from parameter file for crux-search-for-matches.
max-mods=255

# Set the tolerance (+/-ppm) for finding persistent peptides. Default = 10.0.
# Available for crux bullseye
persist-tolerance=10.000000

# Spectrum charge states to search. <string>=1|2|3|all. Default=all.
# Used by crux-search-for-matches to limit the charge states considered in the search. With 'all'
# every spectrum will be searched and spectra with multiple charge states will be searched
# once at each charge state. With 1, 2 ,or 3 only spectra with that that charge will be searched.
spectrum-charge=all

# MS2 file corresponding to the psm file. Required for SIN.
# Available for spectral-counts with measure=SIN.
input-ms2=__NULL_STR

# Show search progress by printing every n spectra searched.
# Default=10.
# Set to 0 to show no search progress. Available for crux search-for-matches from parameter
# file.
print-search-progress=10
```

```
# Restrict analysis to only a small window in each segment ( (min-max) in m/z).
# The user must specify the starting and ending m/z values between which the analysis will be
# performed. By default the whole spectrum is analyzed.
# Available for crux hardklor
mz-window=__NULL_STR

# Use MSToolkit to parse spectra. Default=F.
# Available for crux-search-for-matches
use-mstoolkit=false

# Set the signal-to-noise threshold. Any integer or decimal value greater than or equal to 0.0
# is valid. The default value is 1.0.
# Available for crux hardklor
signal-to-noise=1.000000

# The estimated percent of target scores that are drawn from the null distribution.
# Used by compute-q-values, percolator and q-ranker
pi-zero=1.000000

# Reports peptide intensities as the distribution area. Default false.
# Available for crux hardklor
distribution-area=false

# Prefix added to output file names. Default=none.
# Used by crux search-for-matches, crux sequest-search, crux percolator
# crux compute-q-values, and crux q-ranker.
fileroot=__NULL_STR

# If true, Hardklor will calculate the local noise levels across the spectrum using –sn-window,
# then select a floor of this set of noise levels to apply to the whole spectrum.
# Available for crux hardklor
static-sn=true

# Sort in ascending order. Otherwise, descending. Default: True.
# Available for sort-by-column
ascending=true

# Compute the Sp score for all candidate peptides. Default=F
# Available for search-for-matches. Sp scoring is always done for sequest-search.
compute-sp=false
```

```
# Set the correlation threshold [0,1.0] to accept a predicted isotope distribution. Default=0.85
# Available for crux hardklor
corr=0.850000

# The maximum mass of peptides to consider. Default=8000.
# Available from command line or parameter file for crux bullseye
bullseye-max-mass=8000.000000

# If the target and decoy searches were run separately, rather than using a concatenated database,
# then Q-ranker will assume that the database search results provided as a required argument
# are from the target database search. This option then allows the user to specify the location of
# the decoy search results. Like the required arguments, these search results can be provided as
# a single file, a list of files or a directory. However, the choice (file, list or directory) must be
# consistent for the MS2 files and the target and decoy SQT files. Also, if the MS2 and SQT
# files are provided in directories, then Q-ranker will use the MS2 filename (foo.ms2) to identify
# corresponding target and decoy SQT files with names like foo*.target.sqt and foo*.decoy.sqt.
# This naming convention allows the target and decoy SQT files to reside in the same directory.
# Available for q-ranker and barista.
separate-searches=__NULL_STR

# Set level of output to stderr (0-100). Default=30.
# Available for all crux programs. Each level prints the following messages, including all those
# at lower verbosity levels: 0-fatal errors, 10-non-fatal errors, 20-warnings, 30-information on
# the progress of execution, 40-more progress information, 50-debug info, 60-detailed
# debug info.
verbosity=30

# Specify the location of the left edge of the first bin used to discretize the m/z axis. Default=0.68
# Available for crux-search-for-matches.
mz-bin-offset=0.680000

# Create an ASCII version of the peptide list. Default=F.
# Creates an ASCII file in the output directory containing one peptide per line.
peptide-list=false

# Choose the charge state determination method. (B|F|P|Q|S). Default=Q.
# Available for crux hardklor
cdm=Q

# The minimum mass of peptides to consider. Default=600.
```

```
# Available from command line or parameter file for crux bullseye
bullseye-min-mass=600.000000

# Print the theoretical spectrum
# Available for xlink-predict-peptide-ions (Default=F).
print-theoretical-spectrum=false

# Use MGF file format for parsing files
# Available for search-for-xlinks program (Default=F).
use-mgf=false

# Set the tolerance (+/-units) around the retention time over which a peptide can be matched to
# the MS/MS spectrum. The unit of time is whatever unit is used in your data file (usually
# minutes). Default = 0.5.
# Available for crux bullseye
retention-tolerance=0.500000

# Set the maximum charge state to look for when analyzing a spectrum.
# Default=5.
# Available for crux hardklor
max-charge=5

# Number of decoy peptides to search for every target peptide searched.Only valid for fasta
# searches when –decoys is not none. Default=0.
# Use –decoy-location to control where they are returned (which file(s)) and –decoys to
# control how targets are randomized.
# Available for search-for-matches and sequest-search when searching a fasta file.
num-decoys-per-target=1

# Search only select spectra specified as a single scan number or as a range as in x-y.
# Default=search all.
# The search range x-y is inclusive of x and y.
scan-number=__NULL_STR

# The maximum number of modified amino acids that can appear in one peptide.
# Each aa can be modified multiple times. Default=no limit.
# Available from parameter file for search-for-matches.
max-aas-modified=255

# Include peptides with up to n missed cleavage sites. Default=0.
# Available from command line or parameter file for crux-create-index and crux-generate-peptides.
```

Parameter file only for crux-search-for-matches. When used with
enzyme=<trypsin|elastase|chymotrpysin> includes peptides containing one or more potential
cleavage sites.
missed-cleavages=0

Output filename for complete list of decoy p-values.
Default='search.decoy.p.txt'
Only available for crux search-for-matches. The location of this file is controlled by –output-dir.
search-decoy-pvalue-file=search.decoy.p.txt

Search decoy-peptides within +/- 'mass-window-decoy' of the spectrum mass.
Default=20.0.
Available for crux search-for-xlinks.
precursor-window-decoy=20.000000

# Set the depth of combinatorial analysis. Default 3.
# Available for crux hardklor
depth=3

Re-run a previous Q-ranker analysis using a previously computed set of lookup tables.
Available for q-ranker and barista.
re-run=__NULL_STR

Specify "no base" averagine. Only modified averagine models will be used in the analysis.
Default = F
Available for crux hardklor
no-base=false

# Print the header line of the tsv file. Default=T.
# Available for crux extract-columns and extract-rows
header=true

Minimum mass of spectra to be searched. Default=0.
Available for crux-search-for-matches.
spectrum-min-mass=0.000000

Folder to which results will be written. Default='crux-output'.
Used by crux create-index, crux search-for-matches, crux compute-q-values, and crux percolator.
output-dir=/scratch01/liam/TB_IRIS_discovery_2/crux_1_37/output/sequest-search_file_mono_target_peptide-shuffle/IRIS_Dec2011_PE_conc/Reference_Proteome_uniprot-organism_9606_1185_22Jan2012_mono_peptide-shuffle/IRIS_MM_PE/

```
# Include dead-end peptides in the database. Default=T.
# Available for crux search-for-xlinks program.
xlink-include-deadends=true

# Gap size tolerance when checking for peptides across consecutive MS1 scans.
# Used in conjunction with –scan-tolerance. Default = 1.
# Available for crux bullseye
gap-tolerance=1

# Type of instrument (fticr|orbiltof|qit) on which the data was collected.
# Used in conjuction with –resolution. The default is fticr.
# Available for crux hardklor
instrument=fticr

# The maximum length of peptides to consider. Default=50.
# Available from command line or parameter file for crux-create-index and
# crux-generate-peptides. Parameter file only for crux-search-for-matches.
max-length=50

# Set a filter for mzXML files. Default=none
# Available for crux hardklor
mzxml-filter=none

# Generate peptides only once, even if they appear in more than one protein (T,F). Default=F.
# Available from command line or parameter file for crux-genereate-peptides.
# Returns one line per peptide when true or one line per peptide per protein occurence when
# false.
unique-peptides=true

# Q-ranker analysis begins with a pre-processsing step that creates a set of lookup tables
# which are then used during training. Normally, these lookup tables are deleted at the
# end of the Q-ranker analysis, but setting this option to T prevents the deletion of these tables.
# Subsequently, the Q-ranker analysis can be repeated more efficiently by specifying the
# –re-run option. Default = F.
# Available for q-ranker and barista.
skip-cleanup=false

# Predict ions up to max charge state (1,2,...,6) or up to the charge state of the peptide (peptide).
# If the max-ion-charge is greater than the charge state of the peptide, then the max is the
# peptide charge. Default='peptide'.
```

```
# Available for predict-peptide-ions and search-for-xlinks. Set to 'peptide' for search.
max-ion-charge=peptide

# The maximum mass of peptides to consider. Default=7200.
# Available from command line or parameter file for crux-create-index and
# crux-generate-peptides.Parameter file only for crux-search-for-matches.
max-mass=7200.000000

# Ignore peptides that persist for this length. The unit of time is whatever unit is used in
# your data file (usually minutes). These peptides are considered contaminants. Default = 2.0.
# Available for crux bullseye
max-persist=2.000000

# The minimum mass of peptides to consider. Default=200.
# Available from command line or parameter file for crux-create-index and
# crux-generate-peptides. Parameter file only for crux-search-for-matches.
min-mass=200.000000

# Set the maximum number of peptides or proteins that are estimated from the peaks found in a
# spectrum segment. The default value is 10.
# Available for crux hardklor
max-p=10

# Set the precision for scores written to sqt and text files. Default=8.
# Available from parameter file for crux search-for-matches, percolator, and compute-q-values.
precision=8

# Specify location of decoy search results.
# <string>=target-file|one-decoy-file|separate-decoy-files.
# Default=separate-decoy-files.
# Applies when decoys is not none. Use 'target-file' to mix target and decoy search results in
# one file. 'one-decoy-file' will return target results in one file and all decoys in another.
# 'separate-decoy-files' will create as many decoy files as num-decoys-per-target.
decoy-location=target-file

# The p-value or q-value threshold. Default=0.01.
# Available for spectral-counts. All PSMs with q-value higher than this will be ignored.
threshold=0.010000

# Set the tolerance (+/-ppm) for exact match searches. Default = 10.0.
# Available for crux bullseye
exact-tolerance=10.000000
```

```
# Specify a fixed modification to apply to the N-terminus of peptides.
# Available from parameter file for crux sequest-search and search-for-matches.
nmod-fixed=NO

# Q-ranker uses enriched feature set derived from the spectra in ms2 files.
# It can be forced to use minimal feature set by setting the –use-spec-features option to F.
# Default T.
# Available for q-ranker and barista.
use-spec-features=true

# Set the maximum width of any set of peaks in a spectrum when computing the results (in
# m/z).Thus, if the value was 5.0, then sets of peaks greater than 5 m/z are divided into smaller
# sets prior to analysis. The default value is 4.0.
# Available for crux hardklor
max-width=4.000000

# Specify a fixed modification to apply to the C-terminus of peptides.
# Available from parameter file for crux sequest-search and search-for-matches.
cmod-fixed=NO

# Optional file into which psm features are printed. Default=F.
# Available for percolator and q-ranker. File will be named <fileroot>.percolator.features.txt
# or <fileroot>.qranker.features.txt.
feature-file=false

# Set the signal-to-noise window length (in m/z). Because noise may be non-uniform across a
# spectra, this value adjusts the segment size considered when calculating a signal-over-noise
# ratio. The default value is 250.0.
# Available for crux hardklor
sn-window=250.000000

# Enzyme to use for in silico digestion of proteins.
# <string>=trypsin|chymotrypsin|elastase|clostripain|
# cyanogen-bromide|iodosobenzoate|proline-endopeptidase|
# staph-protease|aspn|modified-chymotrypsin|no-enzyme. Default=trypsin.
# Used in conjunction with the options digestion and missed-cleavages.
# Use 'no-enzyme' for non-specific digestion. Available from command line or parameter file
# for crux-generate-peptides and crux create-index. Available from parameter file for crux
# search-for-matches. Digestion rules: enzyme name [cuts after one of these
# residues]|{but not before one of these residues}. trypsin [RK]|{P}, elastase [ALIV]|{P},
```

```
# chymotrypsin [FWY]|{P}, clostripain [R]|[], cyanogen-bromide [M]|[], iodosobenzoate [W]|[],
# proline-endopeptidase [P]|[], staph-protease [E]|[], modified-chymotrypsin [FWYL]|{P},
# elastase-trypsin-chymotrypsin [ALIVKRWFY]|{P},aspn []|[D] (cuts before D).
enzyme=trypsin

# Specifies the data type the column contains (int|real|string) Default: string
# Available for crux extract-rows
column-type=string

# Predict peaks with the given maximum number of h2o neutral loss modifications. Default=0.
# Only available for crux-predict-peptide-ions.
h2o=0

# Ignore peptides with multiple mappings to proteins (T,F). Default=F.
# Available for spectral-counts.
unique-mapping=false

# Set the sensitivity level. There are four levels, 0 (low), 1 (moderate), 2 (high), and 3 (max).
# The default value is 2.
# Available for crux hardklor
sensitivity=2

# Compute p-values for the main score type. Default=F.
# Currently only implemented for XCORR.
compute-p-values=false

# Require an exact match to the precursor ion. Rather than use wide precursor boundaries,
# this flag forces Bullseye to match precursors to the base isotope peak identified in Hardklor.
# The tolerance is set with the –persist-tolerance flag. Default = F.
# Available for crux bullseye
exact-match=false

# Include alternative averagine models in the analysis that incorporate additional atoms or
# isotopic enrichments.
# Available for crux hardklor
averagine-mod=__NULL_STR

# The number of PSMs per spectrum written to the output file(s). Default=5.
# Available from parameter file for crux-search-for-matches.
top-match=5
```

```
# Maximum mass of spectra to search. Default no maximum.
# Available for crux-search-for-matches.
spectrum-max-mass=1000000000.000000

# Include linear peptides in the database. Default=T.
# Available for crux search-for-xlinks program (Default=T).
xlink-include-linears=true

# Specifies the prefix of the protein names that indicates a decoy. Default = rand_.
# Available for q-ranker and barista.
decoy-prefix=rand_

# Include a decoy version of every peptide by shuffling or reversing the target sequence.
# <string>=none|reverse|protein-shuffle|peptide-shuffle. Use 'none' for no decoys.
# Default=protein-shuffle. For create-index, store the decoys in the index. For search, either
# use decoys in the index or generate them from the fasta file.
decoys=peptide-shuffle

# Set the minimum charge state to look for when analyzing a spectrum. Default=1.
# Available for crux hardklor
min-charge=1

# Print peptide sequence (T,F). Default=F.
# Available only for crux-generate-peptides.
output-sequence=false

# Print the masses of modified sequences in one of three ways 'mod-only', 'total' (residue mass
# plus modification), or 'separate' (for multiple mods to one residue): Default 'mod-only'.
# Available in the parameter file for search-for-matches, sequest-search and generate-peptides.
mod-mass-format=mod-only

# Specify a variable modification to apply to peptides. <mass change>:<aa list>:
# <max per peptide>:<prevents cleavage>:<prevents cross-link>. Sub-parameters prevents
# cleavage and prevents cross-link are optional (T|F). Default=no mods.
# Available from parameter file for crux-generate-peptides and crux-search-for-matches and
# the the same must be used for crux compute-q-value.
mod=NO MODS

# Specify a variable modification to apply to N-terminus of peptides.
# <mass change>:<max distance from protein n-term (-1 for no max)>
```

# Available from parameter file for crux-generate-peptides and crux-search-for-matches and
# the same must be used for crux compute-q-value.
nmod=NO MODS

# Specify a variable modification to apply to C-terminus of peptides.
# <mass change>:<max distance from protein c-term (-1 for no max)>. Default=no mods.
# Available from parameter file for crux-generate-peptides and crux-search-for-matches and
# the same must be used for crux compute-q-value.
cmod=NO MODS

IPA parameters

The following sets of figures are screenshots that were taken of the parameters used during the data analysis using IPA. The pictures include how the data was uploaded, what filters were set for the dataset processing and how the data was processed for the Core analysis.

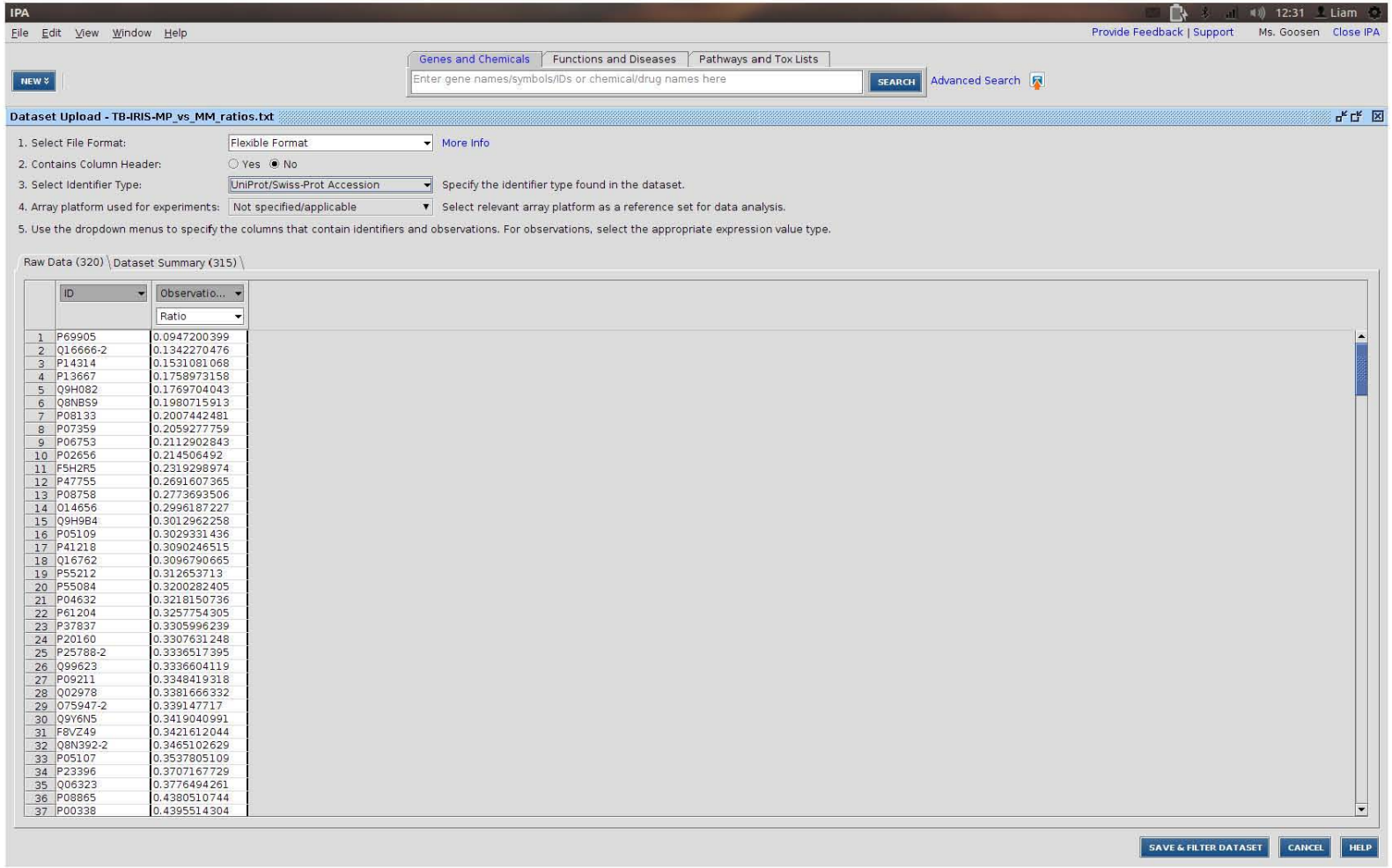
IPA
12:31 Liam
File Edit View Window Help
Provide Feedback | Support Ms. Goosen Close IPA
Genes and Chemicals
Functions and Diseases
Pathways and Tox Lists
NEW
Enter gene names/symbols/IDs or chemical/drug names here
SEARCH
Advanced Search
Dataset Upload - TB-IRIS-MP_vs_MM_ratios.txt
1. Select File Format: Flexible Format More Info
2. Contains Column Header: Yes No
3. Select Identifier Type: UniProt/Swiss-Prot Accession Specify the identifier type found in the dataset.
4. Array platform used for experiments: Not specified/applicable Select relevant array platform as a reference set for data analysis.
5. Use the dropdown menus to specify the columns that contain identifiers and observations. For observations, select the appropriate expression value type.
Raw Data (320) Dataset Summary (315)
ID
Observatio...
Ratio
1 P69905 0.0947200399
2 Q16666-2 0.1342270476
3 P14314 0.1531081068
4 P13667 0.1758973158
5 Q9H082 0.1769704043
6 Q8NBS9 0.1980715913
7 P08133 0.2007442481
8 P07359 0.2059277759
9 P06753 0.2112902843
10 P02656 0.214506492
11 F5H2R5 0.2319298974
12 P47755 0.2691607365
13 P08758 0.2773693506
14 O14656 0.2996187227
15 Q9H9B4 0.3012962258
16 P05109 0.3029331436
17 P41218 0.3090246515
18 Q16762 0.3096790665
19 P55212 0.312653713
20 P55084 0.3200282405
21 P04632 0.3218150736
22 P61204 0.3257754305
23 P37837 0.3305996239
24 P20160 0.3307631248
25 P25788-2 0.3336517395
26 Q99623 0.3336604119
27 P09211 0.3348419318
28 Q02978 0.3381666332
29 O75947-2 0.339147717
30 Q9Y6N5 0.3419040991
31 F8VZ49 0.3421612044
32 Q8N392-2 0.3465102629
33 P05107 0.3537805109
34 P23396 0.3707167729
35 Q06323 0.3776494261
36 P08865 0.4380510744
37 P00338 0.4395514304
SAVE & FILTER DATASET
CANCEL
HELP

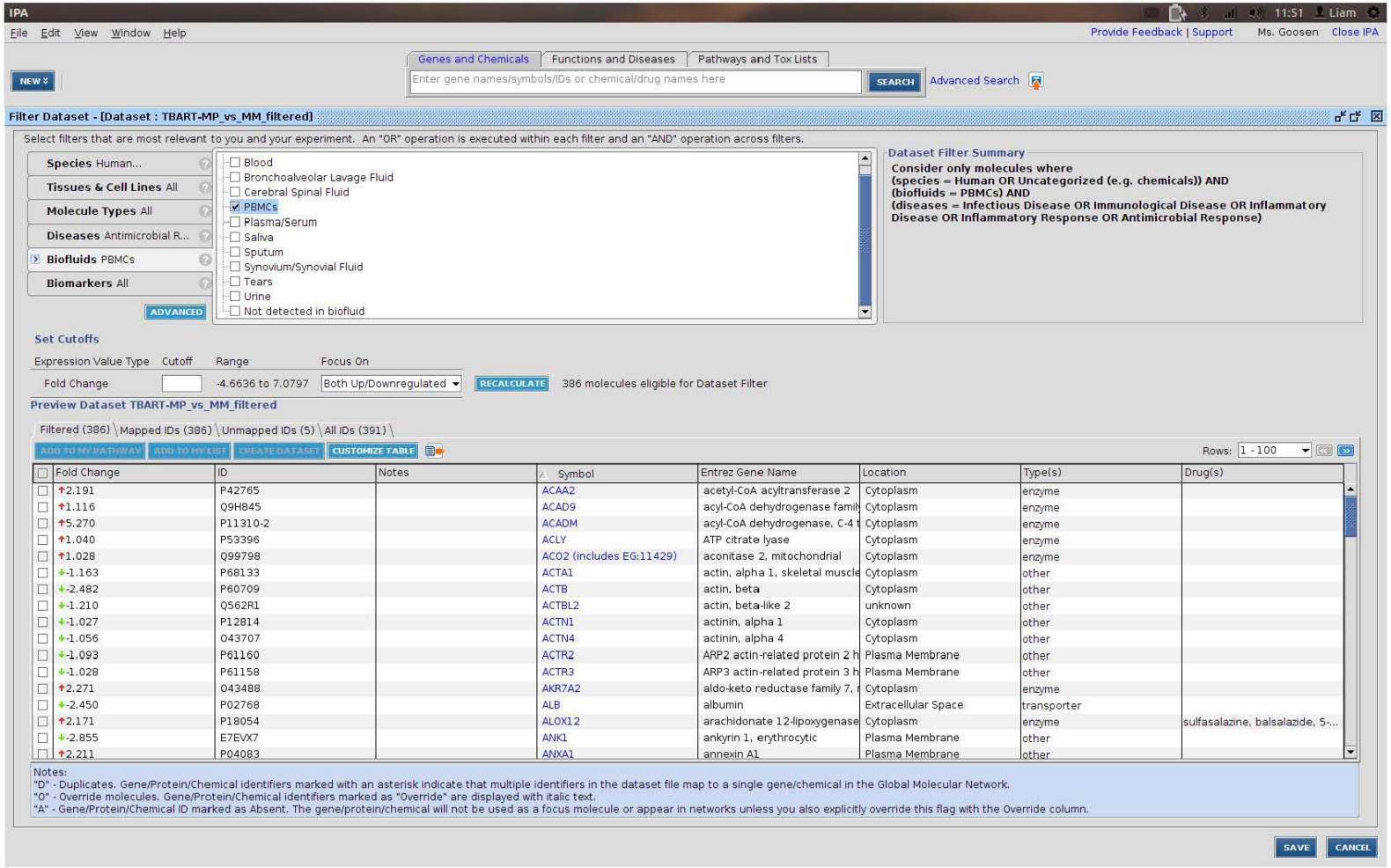
IPA
File Edit View Window Help
Provide Feedback | Support
Ms. Goosen
Close IPA
Genes and Chemicals
Functions and Diseases
Pathways and Tox Lists
NEW
Enter gene names/symbols/IDs or chemical/drug names here
SEARCH
Advanced Search
Filter Dataset - [Dataset : TBART-MP_vs_MM_filtered]
Select filters that are most relevant to you and your experiment. An "OR" operation is executed within each filter and an "AND" operation across filters.
Species Human...
Tissues & Cell Lines All
Molecule Types All
Diseases Antimicrobial R...
Biofluids PBMCs
Biomarkers All
ADVANCED
Blood
Bronchoalveolar Lavage Fluid
Cerebral Spinal Fluid
PBMCs
Plasma/Serum
Saliva
Sputum
Synovium/Synovial Fluid
Tears
Urine
Not detected in biofluid
Dataset Filter Summary
Consider only molecules where
(species = Human OR Uncategorized (e.g. chemicals)) AND
(biofluids = PBMCs) AND
(diseases = Infectious Disease OR Immunological Disease OR Inflammatory Disease OR Inflammatory Response OR Antimicrobial Response)
Set Cutoffs
Expression Value Type
Cutoff
Range
Focus On
Fold Change
-4.6636 to 7.0797
Both Up/Downregulated
RECALCULATE
386 molecules eligible for Dataset Filter
Preview Dataset TBART-MP_vs_MM_filtered
Filtered (386)
Mapped IDs (386)
Unmapped IDs (5)
All IDs (391)
ADD TO MY PATHWAY
ADD TO MY LIST
CREATE DATASET
CUSTOMIZE TABLE
Rows: 1 - 100
Fold Change
ID
Notes
Symbol
Entrez Gene Name
Location
Type(s)
Drug(s)
2.191 P42765 ACAA2 acetyl-CoA acyltransferase 2 Cytoplasm enzyme
1.116 Q9H845 ACAD9 acyl-CoA dehydrogenase family Cytoplasm enzyme
5.270 P11310-2 ACADM acyl-CoA dehydrogenase, C-4 t Cytoplasm enzyme
1.040 P53396 ACLY ATP citrate lyase Cytoplasm enzyme
1.028 Q99798 ACO2 (includes EG:11429) aconitase 2, mitochondrial Cytoplasm enzyme
-1.163 P68133 ACTA1 actin, alpha 1, skeletal muscle Cytoplasm other
-2.482 P60709 ACTB actin, beta Cytoplasm other
-1.210 Q562R1 ACTBL2 actin, beta-like 2 unknown other
-1.027 P12814 ACTN1 actinin, alpha 1 Cytoplasm other
-1.056 O43707 ACTN4 actinin, alpha 4 Cytoplasm other
-1.093 P61160 ACTR2 ARP2 actin-related protein 2 h Plasma Membrane other
-1.028 P61158 ACTR3 ARP3 actin-related protein 3 h Plasma Membrane other
2.271 O43488 AKR7A2 aldo-keto reductase family 7, r Cytoplasm enzyme
-2.450 P02768 ALB albumin Extracellular Space transporter
2.171 P18054 ALOX12 arachidonate 12-lipoxygenase Cytoplasm enzyme sulfasalazine, balsalazide, 5-...
-2.855 E7EVX7 ANK1 ankyrin 1, erythrocytic Plasma Membrane other
2.211 P04083 ANXA1 annexin A1 Plasma Membrane other
Notes:
"D" - Duplicates. Gene/Protein/Chemical identifiers marked with an asterisk indicate that multiple identifiers in the dataset file map to a single gene/chemical in the Global Molecular Network.
"O" - Override molecules. Gene/Protein/Chemical identifiers marked as "Override" are displayed with italic text.
"A" - Gene/Protein/Chemical ID marked as Absent. The gene/protein/chemical will not be used as a focus molecule or appear in networks unless you also explicitly override this flag with the Override column.
SAVE
CANCEL

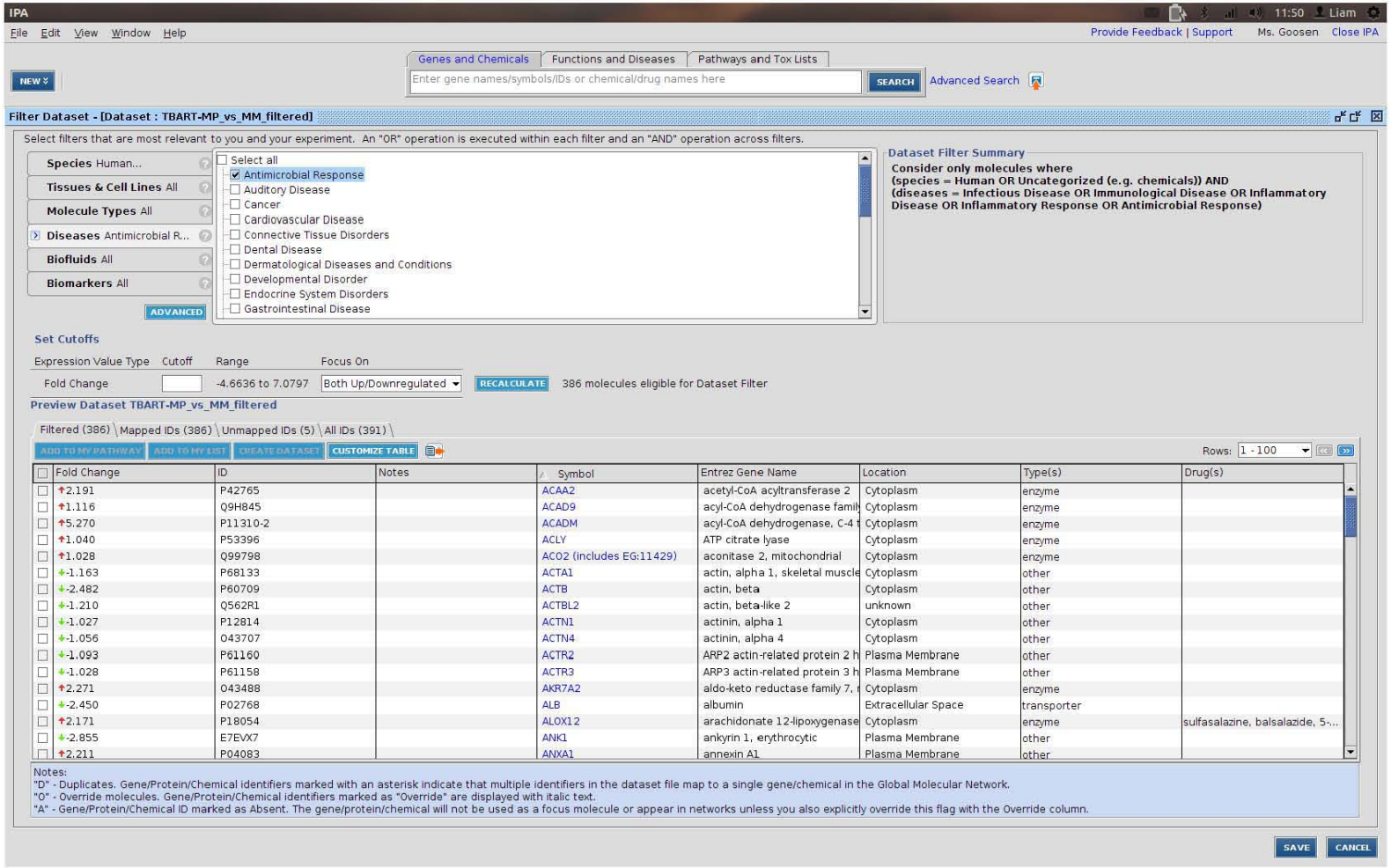
IPA
File Edit View Window Help
Provide Feedback | Support
Ms. Goosen
Close IPA
Genes and Chemicals
Functions and Diseases
Pathways and Tox Lists
NEW
Enter gene names/symbols/IDs or chemical/drug names here
SEARCH
Advanced Search
Filter Dataset - [Dataset : TBART-MP_vs_MM_filtered]
Select filters that are most relevant to you and your experiment. An "OR" operation is executed within each filter and an "AND" operation across filters.
Species Human...
Tissues & Cell Lines All
Molecule Types All
Diseases Antimicrobial R...
Biofluids All
Biomarkers All
ADVANCED
Select all
Antimicrobial Response
Auditory Disease
Cancer
Cardiovascular Disease
Connective Tissue Disorders
Dental Disease
Dermatological Diseases and Conditions
Developmental Disorder
Endocrine System Disorders
Gastrointestinal Disease
Dataset Filter Summary
Consider only molecules where
(species = Human OR Uncategorized (e.g. chemicals)) AND
(diseases = Infectious Disease OR Immunological Disease OR Inflammatory Disease OR Inflammatory Response OR Antimicrobial Response)
Set Cutoffs
Expression Value Type
Cutoff
Range
Focus On
Fold Change
-4.6636 to 7.0797
Both Up/Downregulated
RECALCULATE
386 molecules eligible for Dataset Filter
Preview Dataset TBART-MP_vs_MM_filtered
Filtered (386)
Mapped IDs (386)
Unmapped IDs (5)
All IDs (391)
ADD TO MY PATHWAY
ADD TO MY LIST
CREATE DATASET
CUSTOMIZE TABLE
Rows: 1 - 100
Fold Change
ID
Notes
Symbol
Entrez Gene Name
Location
Type(s)
Drug(s)
↑2.191 P42765 ACAA2 acetyl-CoA acyltransferase 2 Cytoplasm enzyme
↑1.116 Q9H845 ACAD9 acyl-CoA dehydrogenase family Cytoplasm enzyme
↑5.270 P11310-2 ACADM acyl-CoA dehydrogenase, C-4 t Cytoplasm enzyme
↑1.040 P53396 ACLY ATP citrate lyase Cytoplasm enzyme
↑1.028 Q99798 ACO2 (includes EG:11429) aconitase 2, mitochondrial Cytoplasm enzyme
↓-1.163 P68133 ACTA1 actin, alpha 1, skeletal muscle Cytoplasm other
↓-2.482 P60709 ACTB actin, beta Cytoplasm other
↓-1.210 Q562R1 ACTBL2 actin, beta-like 2 unknown other
↓-1.027 P12814 ACTN1 actinin, alpha 1 Cytoplasm other
↓-1.056 O43707 ACTN4 actinin, alpha 4 Cytoplasm other
↓-1.093 P61160 ACTR2 ARP2 actin-related protein 2 h Plasma Membrane other
↓-1.028 P61158 ACTR3 ARP3 actin-related protein 3 h Plasma Membrane other
↑2.271 O43488 AKR7A2 aldo-keto reductase family 7, Cytoplasm enzyme
↓-2.450 P02768 ALB albumin Extracellular Space transporter
↑2.171 P18054 ALOX12 arachidonate 12-lipoxygenase Cytoplasm enzyme sulfasalazine, balsalazide, 5-...
↓-2.855 E7EVX7 ANK1 ankyrin 1, erythrocytic Plasma Membrane other
↑2.211 P04083 ANXA1 annexin A1 Plasma Membrane other
Notes:
"D" - Duplicates. Gene/Protein/Chemical identifiers marked with an asterisk indicate that multiple identifiers in the dataset file map to a single gene/chemical in the Global Molecular Network.
"O" - Override molecules. Gene/Protein/Chemical identifiers marked as "Override" are displayed with italic text.
"A" - Gene/Protein/Chemical ID marked as Absent. The gene/protein/chemical will not be used as a focus molecule or appear in networks unless you also explicitly override this flag with the Override column.
SAVE
CANCEL

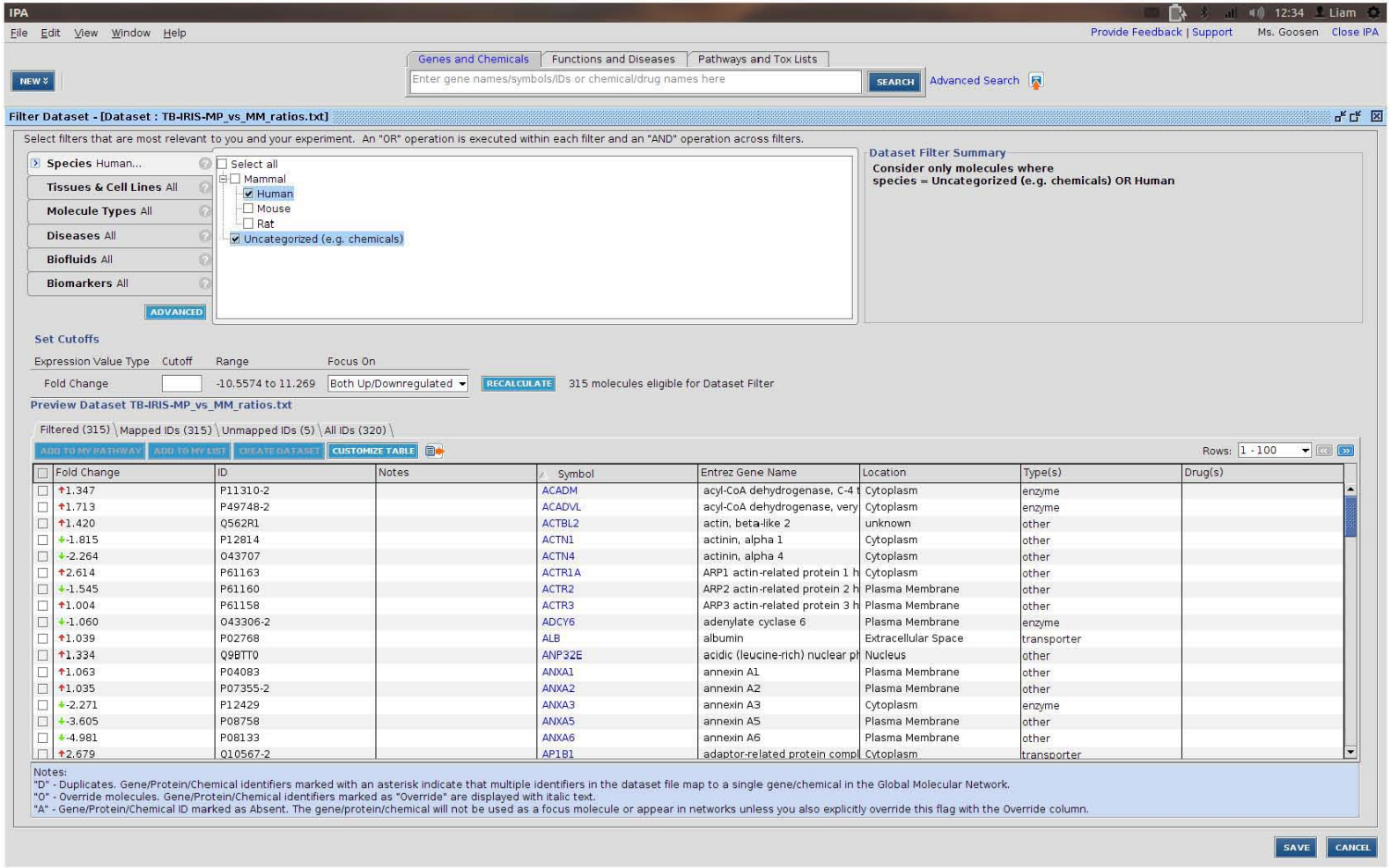
IPA
File Edit View Window Help
Provide Feedback | Support
Ms. Goosen
Close IPA
Genes and Chemicals
Functions and Diseases
Pathways and Tox Lists
NEW
Enter gene names/symbols/IDs or chemical/drug names here
SEARCH
Advanced Search
Filter Dataset - [Dataset : TB-IRIS-MP_vs_MM_ratios.txt]
Select filters that are most relevant to you and your experiment. An "OR" operation is executed within each filter and an "AND" operation across filters.
Species Human...
Tissues & Cell Lines All
Molecule Types All
Diseases All
Biofluids All
Biomarkers All
ADVANCED
Select all
Mammal
Human
Mouse
Rat
Uncategorized (e.g. chemicals)
Dataset Filter Summary
Consider only molecules where
species = Uncategorized (e.g. chemicals) OR Human
Set Cutoffs
Expression Value Type
Cutoff
Range
Focus On
Fold Change
-10.5574 to 11.269
Both Up/Downregulated
RECALCULATE
315 molecules eligible for Dataset Filter
Preview Dataset TB-IRIS-MP_vs_MM_ratios.txt
Filtered (315)
Mapped IDs (315)
Unmapped IDs (5)
All IDs (320)
ADD TO MY PATHWAY
ADD TO MY LIST
CREATE DATASET
CUSTOMIZE TABLE
Rows: 1 - 100
Fold Change
ID
Notes
Symbol
Entrez Gene Name
Location
Type(s)
Drug(s)
↑1.347 P11310-2 ACADM acyl-CoA dehydrogenase, C-4 t Cytoplasm enzyme
↑1.713 P49748-2 ACADVL acyl-CoA dehydrogenase, very Cytoplasm enzyme
↑1.420 Q562R1 ACTBL2 actin, beta-like 2 unknown other
↓-1.815 P12814 ACTN1 actinin, alpha 1 Cytoplasm other
↓-2.264 O43707 ACTN4 actinin, alpha 4 Cytoplasm other
↑2.614 P61163 ACTR1A ARP1 actin-related protein 1 h Cytoplasm other
↓-1.545 P61160 ACTR2 ARP2 actin-related protein 2 h Plasma Membrane other
↑1.004 P61158 ACTR3 ARP3 actin-related protein 3 h Plasma Membrane other
↓-1.060 O43306-2 ADCY6 adenylate cyclase 6 Plasma Membrane enzyme
↑1.039 P02768 ALB albumin Extracellular Space transporter
↑1.334 Q9BTT0 ANP32E acidic (leucine-rich) nuclear ph Nucleus other
↑1.063 P04083 ANXA1 annexin A1 Plasma Membrane other
↑1.035 P07355-2 ANXA2 annexin A2 Plasma Membrane other
↓-2.271 P12429 ANXA3 annexin A3 Cytoplasm enzyme
↓-3.605 P08758 ANXA5 annexin A5 Plasma Membrane other
↓-4.981 P08133 ANXA6 annexin A6 Plasma Membrane other
↑2.679 Q10567-2 AP1B1 adaptor-related protein compl Cytoplasm transporter
Notes:
"D" - Duplicates. Gene/Protein/Chemical identifiers marked with an asterisk indicate that multiple identifiers in the dataset file map to a single gene/chemical in the Global Molecular Network.
"O" - Override molecules. Gene/Protein/Chemical identifiers marked as "Override" are displayed with italic text.
"A" - Gene/Protein/Chemical ID marked as Absent. The gene/protein/chemical will not be used as a focus molecule or appear in networks unless you also explicitly override this flag with the Override column.
SAVE
CANCEL

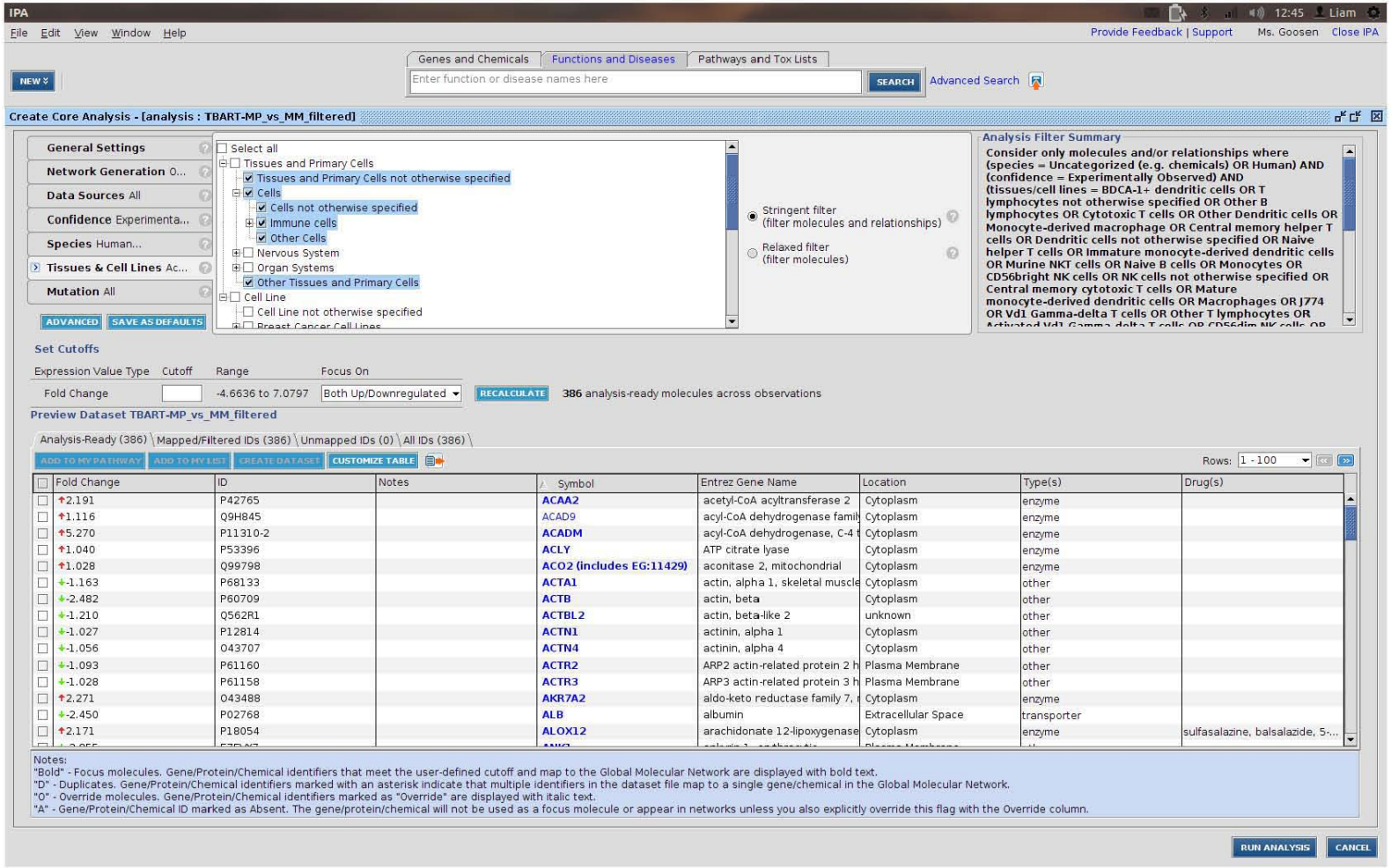
IPA
File Edit View Window Help
Provide Feedback | Support
Ms. Goosen
Close IPA
Genes and Chemicals
Functions and Diseases
Pathways and Tox Lists
NEW
Enter function or disease names here
SEARCH
Advanced Search
Create Core Analysis - [analysis : TBART-MP_vs_MM_filtered]
General Settings
Network Generation O...
Data Sources All
Confidence Experimenta...
Species Human...
Tissues & Cell Lines Ac...
Mutation All
ADVANCED
SAVE AS DEFAULTS
Select all
Tissues and Primary Cells
Tissues and Primary Cells not otherwise specified
Cells
Cells not otherwise specified
Immune cells
Other Cells
Nervous System
Organ Systems
Other Tissues and Primary Cells
Cell Line
Cell Line not otherwise specified
Stringent filter
(filter molecules and relationships)
Relaxed filter
(filter molecules)
Analysis Filter Summary
Consider only molecules and/or relationships where
(species = Uncategorized (e.g. chemicals) OR Human) AND
(confidence = Experimentally Observed) AND
(tissues/cell lines = BDCA-1+ dendritic cells OR T
lymphocytes not otherwise specified OR Other B
lymphocytes OR Cytotoxic T cells OR Other Dendritic cells OR
Monocyte-derived macrophage OR Central memory helper T
cells OR Dendritic cells not otherwise specified OR Naive
helper T cells OR Immature monocyte-derived dendritic cells
OR Murine NKT cells OR Naive B cells OR Monocytes OR
CD56bright NK cells OR NK cells not otherwise specified OR
Central memory cytotoxic T cells OR Mature
monocyte-derived dendritic cells OR Macrophages OR J774
OR Vd1 Gamma-delta T cells OR Other T lymphocytes OR
Set Cutoffs
Expression Value Type
Cutoff
Range
Focus On
Fold Change
-4.6636 to 7.0797
Both Up/Downregulated
RECALCULATE
386 analysis-ready molecules across observations
Preview Dataset TBART-MP_vs_MM_filtered
Analysis-Ready (386)
Mapped/Filtered IDs (386)
Unmapped IDs (0)
All IDs (386)
ADD TO MY PATHWAY
ADD TO MY LIST
CREATE DATASET
CUSTOMIZE TABLE
Rows: 1 - 100
Fold Change
ID
Notes
Symbol
Entrez Gene Name
Location
Type(s)
Drug(s)
↑2.191 P42765 ACAA2 acetyl-CoA acyltransferase 2 Cytoplasm enzyme
↑1.116 Q9H845 ACAD9 acyl-CoA dehydrogenase family Cytoplasm enzyme
↑5.270 P11310-2 ACADM acyl-CoA dehydrogenase, C-4 t Cytoplasm enzyme
↑1.040 P53396 ACLY ATP citrate lyase Cytoplasm enzyme
↑1.028 Q99798 ACO2 (includes EG:11429) aconitase 2, mitochondrial Cytoplasm enzyme
↓-1.163 P68133 ACTA1 actin, alpha 1, skeletal muscle Cytoplasm other
↓-2.482 P60709 ACTB actin, beta Cytoplasm other
↓-1.210 Q562R1 ACTBL2 actin, beta-like 2 unknown other
↓-1.027 P12814 ACTN1 actinin, alpha 1 Cytoplasm other
↓-1.056 O43707 ACTN4 actinin, alpha 4 Cytoplasm other
↓-1.093 P61160 ACTR2 ARP2 actin-related protein 2 h Plasma Membrane other
↓-1.028 P61158 ACTR3 ARP3 actin-related protein 3 h Plasma Membrane other
↑2.271 O43488 AKR7A2 aldo-keto reductase family 7, r Cytoplasm enzyme
↓-2.450 P02768 ALB albumin Extracellular Space transporter
↑2.171 P18054 ALOX12 arachidonate 12-lipoxygenase Cytoplasm enzyme sulfasalazine, balsalazide, 5-...
Notes:
"Bold" - Focus molecules. Gene/Protein/Chemical identifiers that meet the user-defined cutoff and map to the Global Molecular Network are displayed with bold text.
"D" - Duplicates. Gene/Protein/Chemical identifiers marked with an asterisk indicate that multiple identifiers in the dataset file map to a single gene/chemical in the Global Molecular Network.
"O" - Override molecules. Gene/Protein/Chemical identifiers marked as "Override" are displayed with italic text.
"A" - Gene/Protein/Chemical ID marked as Absent. The gene/protein/chemical will not be used as a focus molecule or appear in networks unless you also explicitly override this flag with the Override column.
RUN ANALYSIS
CANCEL

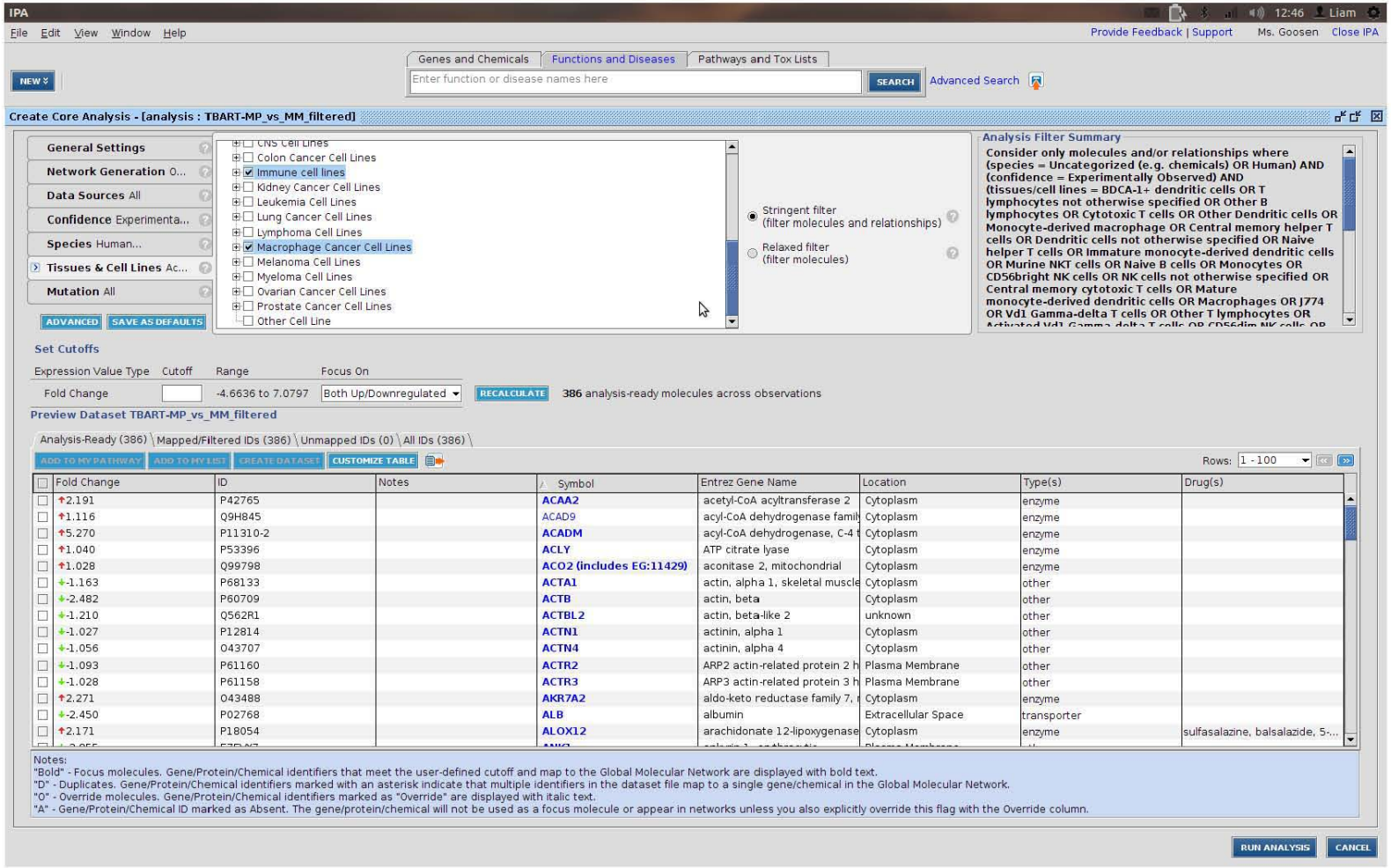
IPA
File Edit View Window Help
Provide Feedback | Support
Ms. Goosen
Close IPA
Genes and Chemicals
Functions and Diseases
Pathways and Tox Lists
NEW
Enter function or disease names here
SEARCH
Advanced Search
Create Core Analysis - [analysis : TBART-MP_vs_MM_filtered]
General Settings
Network Generation O...
Data Sources All
Confidence Experimenta...
Species Human...
Tissues & Cell Lines Ac...
Mutation All
ADVANCED
SAVE AS DEFAULTS
Colon Cancer Cell Lines
Immune cell lines
Kidney Cancer Cell Lines
Leukemia Cell Lines
Lung Cancer Cell Lines
Lymphoma Cell Lines
Macrophage Cancer Cell Lines
Melanoma Cell Lines
Myeloma Cell Lines
Ovarian Cancer Cell Lines
Prostate Cancer Cell Lines
Other Cell Line
Stringent filter
(filter molecules and relationships)
Relaxed filter
(filter molecules)
Analysis Filter Summary
Consider only molecules and/or relationships where (species = Uncategorized (e.g. chemicals) OR Human) AND (confidence = Experimentally Observed) AND (tissues/cell lines = BDCA-1+ dendritic cells OR T lymphocytes not otherwise specified OR Other B lymphocytes OR Cytotoxic T cells OR Other Dendritic cells OR Monocyte-derived macrophage OR Central memory helper T cells OR Dendritic cells not otherwise specified OR Naive helper T cells OR Immature monocyte-derived dendritic cells OR Murine NKT cells OR Naive B cells OR Monocytes OR CD56bright NK cells OR NK cells not otherwise specified OR Central memory cytotoxic T cells OR Mature monocyte-derived dendritic cells OR Macrophages OR J774 OR Vd1 Gamma-delta T cells OR Other T lymphocytes OR
Set Cutoffs
Expression Value Type
Cutoff
Range
Focus On
Fold Change
-4.6636 to 7.0797
Both Up/Downregulated
RECALCULATE
386 analysis-ready molecules across observations
Preview Dataset TBART-MP_vs_MM_filtered
Analysis-Ready (386)
Mapped/Filtered IDs (386)
Unmapped IDs (0)
All IDs (386)
ADD TO MY PATHWAY
ADD TO MY LIST
CREATE DATASET
CUSTOMIZE TABLE
Rows: 1 - 100
Fold Change
ID
Notes
Symbol
Entrez Gene Name
Location
Type(s)
Drug(s)
↑2.191 P42765 ACAA2 acetyl-CoA acyltransferase 2 Cytoplasm enzyme
↑1.116 Q9H845 ACAD9 acyl-CoA dehydrogenase family Cytoplasm enzyme
↑5.270 P11310-2 ACADM acyl-CoA dehydrogenase, C-4 t Cytoplasm enzyme
↑1.040 P53396 ACLY ATP citrate lyase Cytoplasm enzyme
↑1.028 Q99798 ACO2 (includes EG:11429) aconitase 2, mitochondrial Cytoplasm enzyme
↓-1.163 P68133 ACTA1 actin, alpha 1, skeletal muscle Cytoplasm other
↓-2.482 P60709 ACTB actin, beta Cytoplasm other
↓-1.210 Q562R1 ACTBL2 actin, beta-like 2 unknown other
↓-1.027 P12814 ACTN1 actinin, alpha 1 Cytoplasm other
↓-1.056 O43707 ACTN4 actinin, alpha 4 Cytoplasm other
↓-1.093 P61160 ACTR2 ARP2 actin-related protein 2 h Plasma Membrane other
↓-1.028 P61158 ACTR3 ARP3 actin-related protein 3 h Plasma Membrane other
↑2.271 O43488 AKR7A2 aldo-keto reductase family 7, Cytoplasm enzyme
↓-2.450 P02768 ALB albumin Extracellular Space transporter
↑2.171 P18054 ALOX12 arachidonate 12-lipoxygenase Cytoplasm enzyme sulfasalazine, balsalazide, 5-...
Notes:
"Bold" - Focus molecules. Gene/Protein/Chemical identifiers that meet the user-defined cutoff and map to the Global Molecular Network are displayed with bold text.
"D" - Duplicates. Gene/Protein/Chemical identifiers marked with an asterisk indicate that multiple identifiers in the dataset file map to a single gene/chemical in the Global Molecular Network.
"O" - Override molecules. Gene/Protein/Chemical identifiers marked as "Override" are displayed with italic text.
"A" - Gene/Protein/Chemical ID marked as Absent. The gene/protein/chemical will not be used as a focus molecule or appear in networks unless you also explicitly override this flag with the Override column.
RUN ANALYSIS
CANCEL

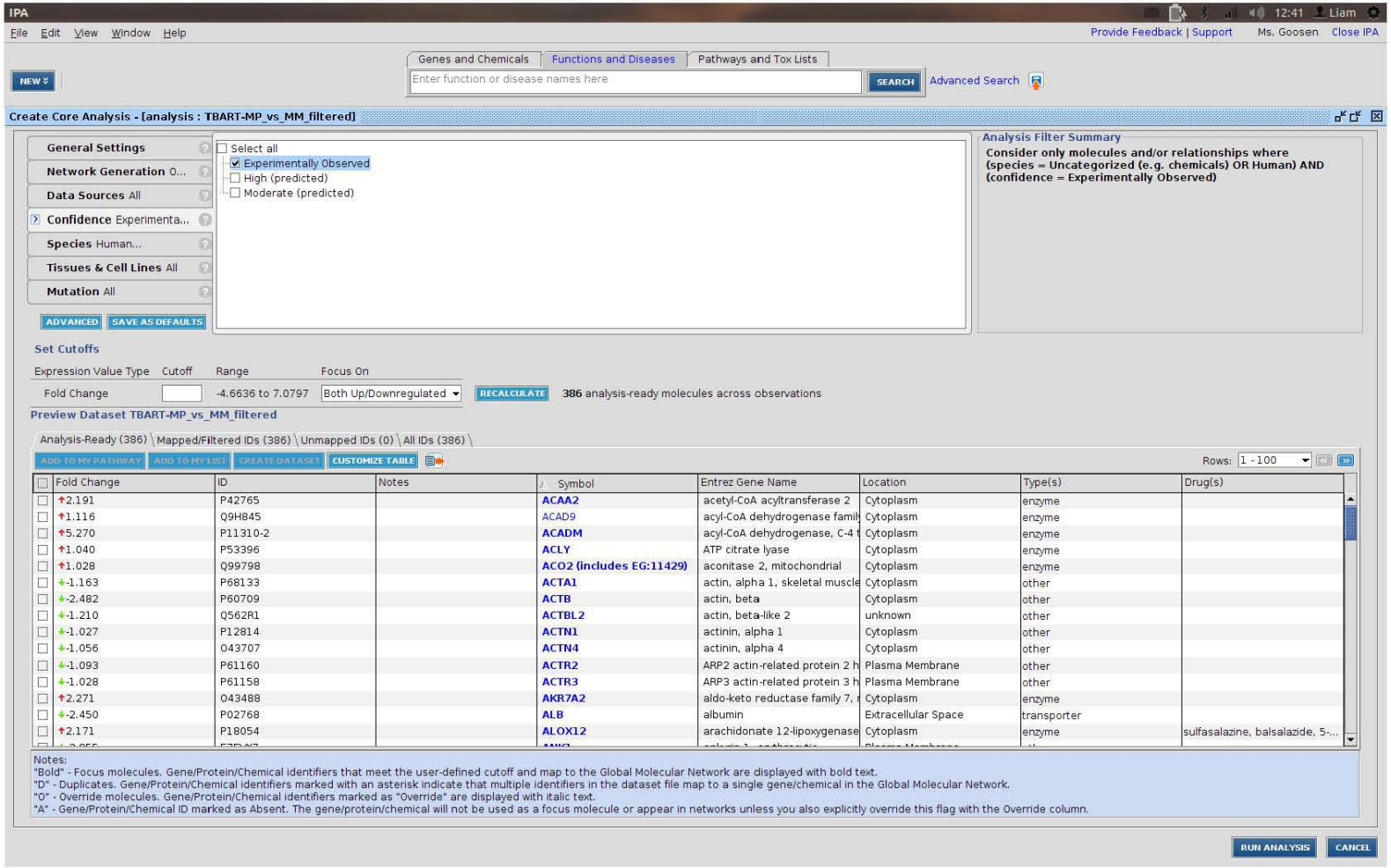
IPA
File Edit View Window Help
Provide Feedback | Support
Ms. Goosen
Close IPA
Genes and Chemicals
Functions and Diseases
Pathways and Tox Lists
NEW
Enter function or disease names here
SEARCH
Advanced Search
Create Core Analysis - [analysis : TBART-MP_vs_MM_filtered]
General Settings
Network Generation O...
Data Sources All
Confidence Experimenta...
Species Human...
Tissues & Cell Lines All
Mutation All
ADVANCED
SAVE AS DEFAULTS
Select all
Experimentally Observed
High (predicted)
Moderate (predicted)
Analysis Filter Summary
Consider only molecules and/or relationships where (species = Uncategorized (e.g. chemicals) OR Human) AND (confidence = Experimentally Observed)
Set Cutoffs
Expression Value Type
Cutoff
Range
Focus On
Fold Change
-4.6636 to 7.0797
Both Up/Downregulated
RECALCULATE
386 analysis-ready molecules across observations
Preview Dataset TBART-MP_vs_MM_filtered
Analysis-Ready (386)
Mapped/Filtered IDs (386)
Unmapped IDs (0)
All IDs (386)
ADD TO MY PATHWAY
ADD TO MY LIST
CREATE DATASET
CUSTOMIZE TABLE
Rows: 1 - 100
Fold Change
ID
Notes
Symbol
Entrez Gene Name
Location
Type(s)
Drug(s)
2.191 P42765 ACAA2 acetyl-CoA acyltransferase 2 Cytoplasm enzyme
1.116 Q9H845 ACAD9 acyl-CoA dehydrogenase family Cytoplasm enzyme
5.270 P11310-2 ACADM acyl-CoA dehydrogenase, C-4 t Cytoplasm enzyme
1.040 P53396 ACLY ATP citrate lyase Cytoplasm enzyme
1.028 Q99798 ACO2 (includes EG:11429) aconitase 2, mitochondrial Cytoplasm enzyme
-1.163 P68133 ACTA1 actin, alpha 1, skeletal muscle Cytoplasm other
-2.482 P60709 ACTB actin, beta Cytoplasm other
-1.210 Q562R1 ACTBL2 actin, beta-like 2 unknown other
-1.027 P12814 ACTN1 actinin, alpha 1 Cytoplasm other
-1.056 O43707 ACTN4 actinin, alpha 4 Cytoplasm other
-1.093 P61160 ACTR2 ARP2 actin-related protein 2 h Plasma Membrane other
-1.028 P61158 ACTR3 ARP3 actin-related protein 3 h Plasma Membrane other
2.271 O43488 AKR7A2 aldo-keto reductase family 7, r Cytoplasm enzyme
-2.450 P02768 ALB albumin Extracellular Space transporter
2.171 P18054 ALOX12 arachidonate 12-lipoxygenase Cytoplasm enzyme sulfasalazine, balsalazide, 5-...
Notes:
"Bold" - Focus molecules. Gene/Protein/Chemical identifiers that meet the user-defined cutoff and map to the Global Molecular Network are displayed with bold text.
"D" - Duplicates. Gene/Protein/Chemical identifiers marked with an asterisk indicate that multiple identifiers in the dataset file map to a single gene/chemical in the Global Molecular Network.
"O" - Override molecules. Gene/Protein/Chemical identifiers marked as "Override" are displayed with italic text.
"A" - Gene/Protein/Chemical ID marked as Absent. The gene/protein/chemical will not be used as a focus molecule or appear in networks unless you also explicitly override this flag with the Override column.
RUN ANALYSIS
CANCEL

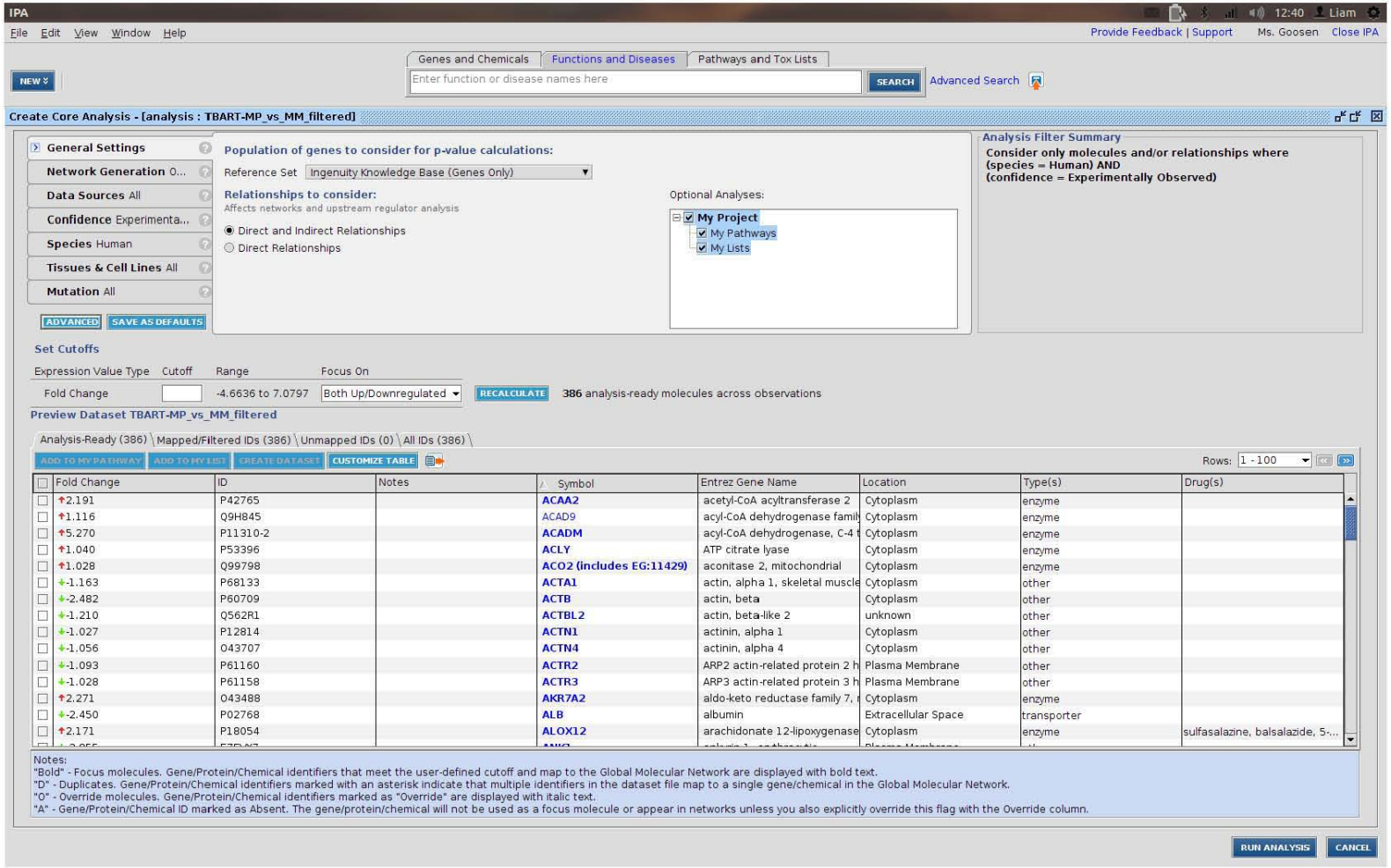
IPA
File Edit View Window Help
Provide Feedback | Support
Ms. Goosen
Close IPA
Genes and Chemicals
Functions and Diseases
Pathways and Tox Lists
NEW
Enter function or disease names here
SEARCH
Advanced Search
Create Core Analysis - [analysis : TBART-MP_vs_MM_filtered]
General Settings
Network Generation O...
Data Sources All
Confidence Experimenta...
Species Human
Tissues & Cell Lines All
Mutation All
ADVANCED
SAVE AS DEFAULTS
Population of genes to consider for p-value calculations:
Reference Set
Ingenuity Knowledge Base (Genes Only)
Relationships to consider:
Affects networks and upstream regulator analysis
Direct and Indirect Relationships
Direct Relationships
Optional Analyses:
My Project
My Pathways
My Lists
Analysis Filter Summary
Consider only molecules and/or relationships where
(species = Human) AND
(confidence = Experimentally Observed)
Set Cutoffs
Expression Value Type
Cutoff
Range
Focus On
Fold Change
-4.6636 to 7.0797
Both Up/Downregulated
RECALCULATE
386 analysis-ready molecules across observations
Preview Dataset TBART-MP_vs_MM_filtered
Analysis-Ready (386)
Mapped/Filtered IDs (386)
Unmapped IDs (0)
All IDs (386)
ADD TO MY PATHWAY
ADD TO MY LIST
CREATE DATASET
CUSTOMIZE TABLE
Rows: 1 - 100
Fold Change
ID
Notes
Symbol
Entrez Gene Name
Location
Type(s)
Drug(s)
2.191 P42765 ACAA2 acetyl-CoA acyltransferase 2 Cytoplasm enzyme
1.116 Q9H845 ACAD9 acyl-CoA dehydrogenase family Cytoplasm enzyme
5.270 P11310-2 ACADM acyl-CoA dehydrogenase, C-4 t Cytoplasm enzyme
1.040 P53396 ACLY ATP citrate lyase Cytoplasm enzyme
1.028 Q99798 ACO2 (includes EG:11429) aconitase 2, mitochondrial Cytoplasm enzyme
-1.163 P68133 ACTA1 actin, alpha 1, skeletal muscle Cytoplasm other
-2.482 P60709 ACTB actin, beta Cytoplasm other
-1.210 Q562R1 ACTBL2 actin, beta-like 2 unknown other
-1.027 P12814 ACTN1 actinin, alpha 1 Cytoplasm other
-1.056 O43707 ACTN4 actinin, alpha 4 Cytoplasm other
-1.093 P61160 ACTR2 ARP2 actin-related protein 2 h Plasma Membrane other
-1.028 P61158 ACTR3 ARP3 actin-related protein 3 h Plasma Membrane other
2.271 O43488 AKR7A2 aldo-keto reductase family 7, r Cytoplasm enzyme
-2.450 P02768 ALB albumin Extracellular Space transporter
2.171 P18054 ALOX12 arachidonate 12-lipoxygenase Cytoplasm enzyme sulfasalazine, balsalazide, 5-...
Notes:
"Bold" - Focus molecules. Gene/Protein/Chemical identifiers that meet the user-defined cutoff and map to the Global Molecular Network are displayed with bold text.
"D" - Duplicates. Gene/Protein/Chemical identifiers marked with an asterisk indicate that multiple identifiers in the dataset file map to a single gene/chemical in the Global Molecular Network.
"O" - Override molecules. Gene/Protein/Chemical identifiers marked as "Override" are displayed with italic text.
"A" - Gene/Protein/Chemical ID marked as Absent. The gene/protein/chemical will not be used as a focus molecule or appear in networks unless you also explicitly override this flag with the Override column.
RUN ANALYSIS
CANCEL

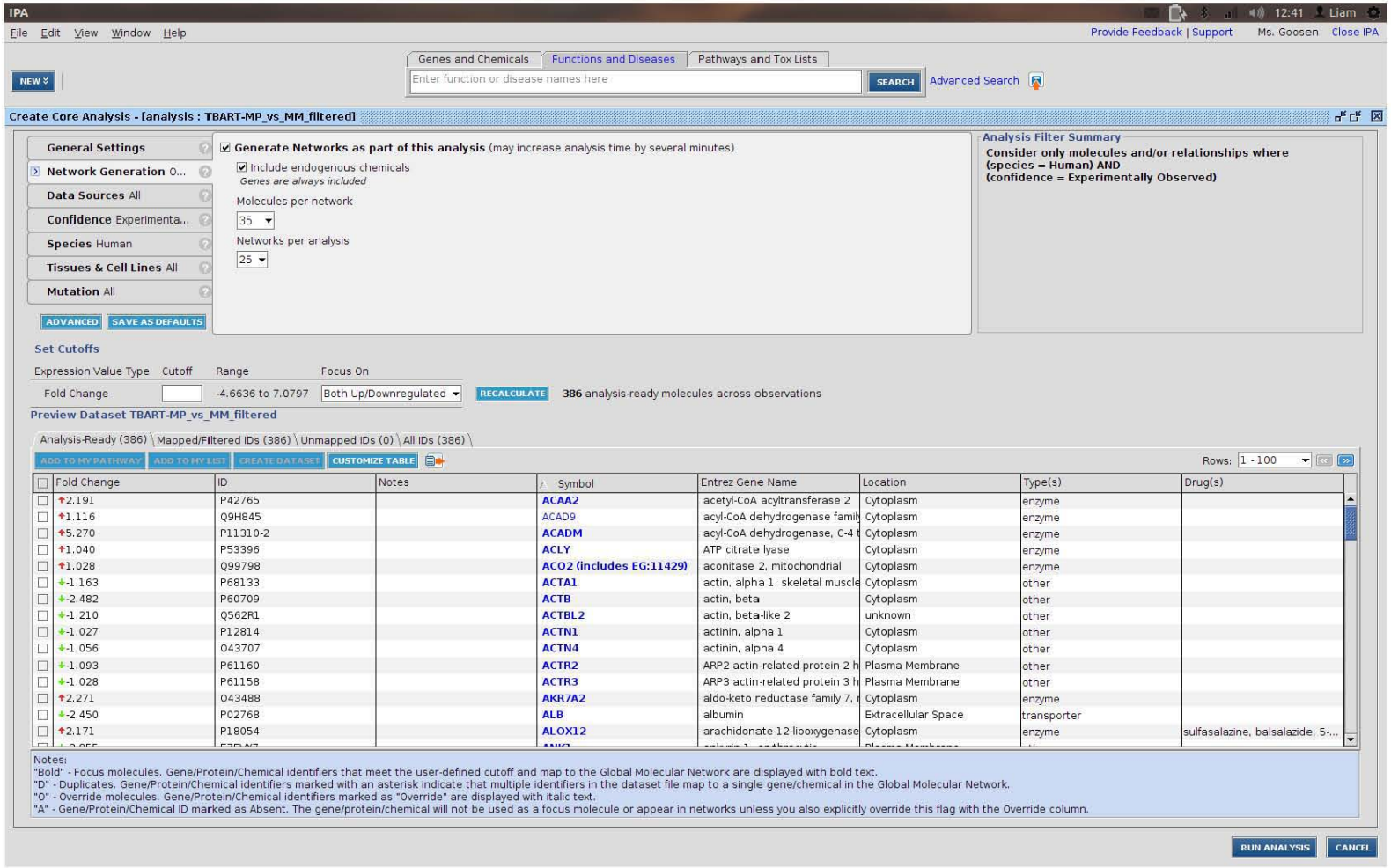
IPA
File Edit View Window Help
Provide Feedback | Support
Ms. Goosen
Close IPA
Genes and Chemicals
Functions and Diseases
Pathways and Tox Lists
NEW
Enter function or disease names here
SEARCH
Advanced Search
Create Core Analysis - [analysis : TBART-MP_vs_MM_filtered]
General Settings
Network Generation O...
Data Sources All
Confidence Experimenta...
Species Human
Tissues & Cell Lines All
Mutation All
ADVANCED
SAVE AS DEFAULTS
Generate Networks as part of this analysis (may increase analysis time by several minutes)
Include endogenous chemicals
Genes are always included
Molecules per network
35
Networks per analysis
25
Analysis Filter Summary
Consider only molecules and/or relationships where
(species = Human) AND
(confidence = Experimentally Observed)
Set Cutoffs
Expression Value Type
Cutoff
Range
Focus On
Fold Change
-4.6636 to 7.0797
Both Up/Downregulated
RECALCULATE
386 analysis-ready molecules across observations
Preview Dataset TBART-MP_vs_MM_filtered
Analysis-Ready (386)
Mapped/Filtered IDs (386)
Unmapped IDs (0)
All IDs (386)
ADD TO MY PATHWAY
ADD TO MY LIST
CREATE DATASET
CUSTOMIZE TABLE
Rows: 1 - 100
Fold Change
ID
Notes
Symbol
Entrez Gene Name
Location
Type(s)
Drug(s)
2.191 P42765 ACAA2 acetyl-CoA acyltransferase 2 Cytoplasm enzyme
1.116 Q9H845 ACAD9 acyl-CoA dehydrogenase family Cytoplasm enzyme
5.270 P11310-2 ACADM acyl-CoA dehydrogenase, C-4 t Cytoplasm enzyme
1.040 P53396 ACLY ATP citrate lyase Cytoplasm enzyme
1.028 Q99798 ACO2 (includes EG:11429) aconitase 2, mitochondrial Cytoplasm enzyme
-1.163 P68133 ACTA1 actin, alpha 1, skeletal muscle Cytoplasm other
-2.482 P60709 ACTB actin, beta Cytoplasm other
-1.210 Q562R1 ACTBL2 actin, beta-like 2 unknown other
-1.027 P12814 ACTN1 actinin, alpha 1 Cytoplasm other
-1.056 O43707 ACTN4 actinin, alpha 4 Cytoplasm other
-1.093 P61160 ACTR2 ARP2 actin-related protein 2 h Plasma Membrane other
-1.028 P61158 ACTR3 ARP3 actin-related protein 3 h Plasma Membrane other
2.271 O43488 AKR7A2 aldo-keto reductase family 7, r Cytoplasm enzyme
-2.450 P02768 ALB albumin Extracellular Space transporter
2.171 P18054 ALOX12 arachidonate 12-lipoxygenase Cytoplasm enzyme sulfasalazine, balsalazide, 5-...
Notes:
"Bold" - Focus molecules. Gene/Protein/Chemical identifiers that meet the user-defined cutoff and map to the Global Molecular Network are displayed with bold text.
"D" - Duplicates. Gene/Protein/Chemical identifiers marked with an asterisk indicate that multiple identifiers in the dataset file map to a single gene/chemical in the Global Molecular Network.
"O" - Override molecules. Gene/Protein/Chemical identifiers marked as "Override" are displayed with italic text.
"A" - Gene/Protein/Chemical ID marked as Absent. The gene/protein/chemical will not be used as a focus molecule or appear in networks unless you also explicitly override this flag with the Override column.
RUN ANALYSIS
CANCEL

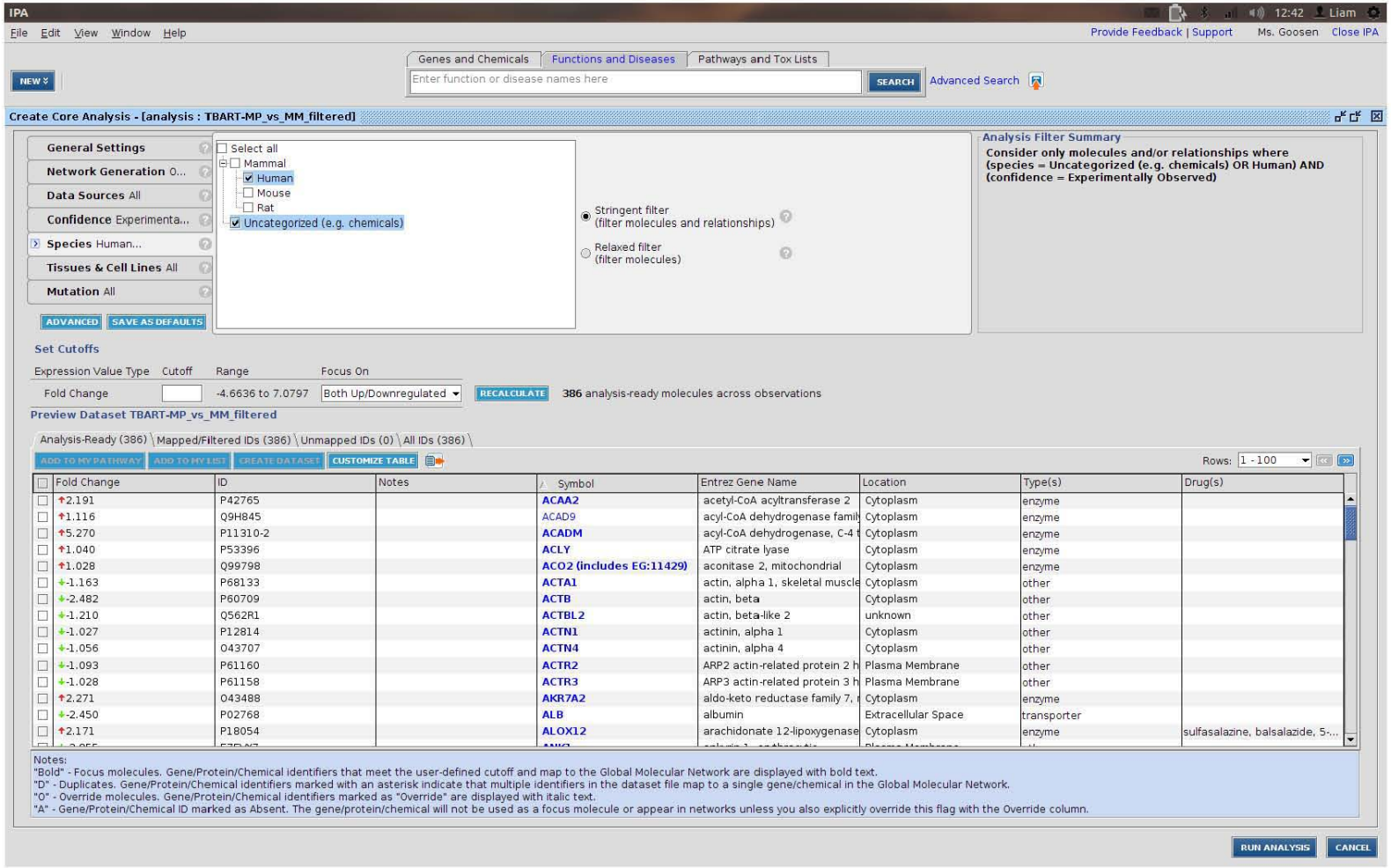
IPA
File Edit View Window Help
Provide Feedback | Support
Ms. Goosen
Close IPA
Genes and Chemicals
Functions and Diseases
Pathways and Tox Lists
NEW
Enter function or disease names here
SEARCH
Advanced Search
Create Core Analysis - [analysis : TBART-MP_vs_MM_filtered]
General Settings
Network Generation O...
Data Sources All
Confidence Experimenta...
Species Human...
Tissues & Cell Lines All
Mutation All
ADVANCED
SAVE AS DEFAULTS
Select all
Mammal
Human
Mouse
Rat
Uncategorized (e.g. chemicals)
Stringent filter
(filter molecules and relationships)
Relaxed filter
(filter molecules)
Analysis Filter Summary
Consider only molecules and/or relationships where
(species = Uncategorized (e.g. chemicals) OR Human) AND
(confidence = Experimentally Observed)
Set Cutoffs
Expression Value Type
Cutoff
Range
Focus On
Fold Change
-4.6636 to 7.0797
Both Up/Downregulated
RECALCULATE
386 analysis-ready molecules across observations
Preview Dataset TBART-MP_vs_MM_filtered
Analysis-Ready (386)
Mapped/Filtered IDs (386)
Unmapped IDs (0)
All IDs (386)
ADD TO MY PATHWAY
ADD TO MY LIST
CREATE DATASET
CUSTOMIZE TABLE
Rows: 1 - 100
Fold Change
ID
Notes
Symbol
Entrez Gene Name
Location
Type(s)
Drug(s)
2.191 P42765 ACAA2 acetyl-CoA acyltransferase 2 Cytoplasm enzyme
1.116 Q9H845 ACAD9 acyl-CoA dehydrogenase family Cytoplasm enzyme
5.270 P11310-2 ACADM acyl-CoA dehydrogenase, C-4 t Cytoplasm enzyme
1.040 P53396 ACLY ATP citrate lyase Cytoplasm enzyme
1.028 Q99798 ACO2 (includes EG:11429) aconitase 2, mitochondrial Cytoplasm enzyme
-1.163 P68133 ACTA1 actin, alpha 1, skeletal muscle Cytoplasm other
-2.482 P60709 ACTB actin, beta Cytoplasm other
-1.210 Q562R1 ACTBL2 actin, beta-like 2 unknown other
-1.027 P12814 ACTN1 actinin, alpha 1 Cytoplasm other
-1.056 O43707 ACTN4 actinin, alpha 4 Cytoplasm other
-1.093 P61160 ACTR2 ARP2 actin-related protein 2 h Plasma Membrane other
-1.028 P61158 ACTR3 ARP3 actin-related protein 3 h Plasma Membrane other
2.271 O43488 AKR7A2 aldo-keto reductase family 7, Cytoplasm enzyme
-2.450 P02768 ALB albumin Extracellular Space transporter
2.171 P18054 ALOX12 arachidonate 12-lipoxygenase Cytoplasm enzyme sulfasalazine, balsalazide, 5-...
Notes:
"Bold" - Focus molecules. Gene/Protein/Chemical identifiers that meet the user-defined cutoff and map to the Global Molecular Network are displayed with bold text.
"D" - Duplicates. Gene/Protein/Chemical identifiers marked with an asterisk indicate that multiple identifiers in the dataset file map to a single gene/chemical in the Global Molecular Network.
"O" - Override molecules. Gene/Protein/Chemical identifiers marked as "Override" are displayed with italic text.
"A" - Gene/Protein/Chemical ID marked as Absent. The gene/protein/chemical will not be used as a focus molecule or appear in networks unless you also explicitly override this flag with the Override column.
RUN ANALYSIS
CANCEL

Protein lists

Below are the protein lists of the shared proteins across the three paired datasets that were studied, namely: TBART MP/MM, TB-IRIS MP/MM and TB-IRIS PP/MM. The lists include fold change, UniProt ID, Entrez gene name, cellular location and protein type.

The TB-IRIS PP/MM paired dataset (Table 5.1) was generated using proteins commonly identified in the TB-IRIS PDE PP and the TB-IRIS PDE MM datasets (Table 4.2).

Fold Change	UniProt ID	Symbol	TB-IRIS MM			TB-IRIS PP			Entrez Gene Name	Location	Type(s)
			q-value	Barista score	# of peptides	q-value	Barista score	# of peptides			
-1.049	A8KA46	RSU1	0.000000	19.36	7	0.000000	29.21	8	Ras suppressor protein 1	Cytoplasm	other
-1.778	B4DR52	HIST2H2BF	0.002447	3.90	5	0.000000	7.07	4	histone cluster 2, H2bf	Nucleus	other
-5.082	D6RF44	HNRNPD	0.000000	8.86	3	0.001741	5.32	3	heterogeneous nuclear ribonucleoprotein D (AU-rich element RNA binding protein 1, 37kDa)	Nucleus	transcription regulator
-1.721	F5GWR5	FHL1	0.000000	11.87	3	0.000000	11.67	4	four and a half LIM domains 1	Cytoplasm	other
3.982	O00160	MYO1F	0.000000	5.68	7	0.000000	11.23	10	myosin IF	Cytoplasm	other
-1.658	O00194	RAB27B	0.000000	23.40	5	0.000000	29.44	9	RAB27B, member RAS oncogene family	Cytoplasm	enzyme
12.200	O00231	PSMD11	0.049129	2.35	4	0.013478	3.27	3	proteasome (prosome, macropain) 26S subunit, non-ATPase, 11	Cytoplasm	other
-1.471	O00264	PGRMC1	0.000000	5.53	2	0.001741	6.19	2	progesterone receptor membrane component 1	Plasma Membrane	transmembrane receptor
-1.054	O00299	CLIC1	0.000000	35.82	9	0.000000	49.83	11	chloride intracellular channel 1	Nucleus	ion channel
-1.104	O00303	EIF3F	0.000000	10.98	2	0.000000	39.82	3	eukaryotic translation initiation factor 3, subunit F	Cytoplasm	translation regulator
-4.839	O14818	PSMA7	0.000000	7.77	3	0.000000	7.89	3	proteasome (prosome, macropain) subunit, alpha type, 7	Cytoplasm	peptidase
-1.205	O14880	MGST3	0.000000	8.26	1	0.000000	13.43	2	microsomal glutathione S-transferase 3	Cytoplasm	enzyme
1.186	O14950	MYL12B	0.002447	4.24	2	0.001741	4.32	4	myosin, light chain 12B, regulatory	Cytoplasm	other
-1.714	O15143	ARPC1B	0.000000	14.17	4	0.000000	16.55	6	actin related protein 2/3 complex, subunit 1B, 41kDa	Cytoplasm	other
1.198	O15144	ARPC2	0.000000	12.17	7	0.000000	37.01	12	actin related protein 2/3 complex, subunit 2, 34kDa	Cytoplasm	other
2.499	O15173	PGRMC2	0.000000	16.28	4	0.000000	22.20	4	progesterone receptor membrane component 2	Nucleus	other
1.130	O43169	CYB5B	0.002447	4.11	1	0.000000	14.11	3	cytochrome b5 type B (outer mitochondrial membrane)	Cytoplasm	enzyme
1.954	O43488	AKR7A2	0.000000	11.46	5	0.000000	15.00	2	aldo-keto reductase family 7, member A2 (aflatoxin aldehyde reductase)	Cytoplasm	enzyme
-1.525	O43684-2	BUB3	0.000000	4.99	3	0.001741	4.50	2	budding uninhibited by benzimidazoles 3 homolog (yeast)	Nucleus	other
-2.046	O43707	ACTN4	0.000000	23.40	25	0.000000	20.98	22	actinin, alpha 4	Cytoplasm	other
1.106	O60610-2	DIAPH1	0.000000	9.05	9	0.000000	29.03	13	diaphanous homolog 1 (Drosophila)	Plasma Membrane	other
-1.293	O75083	WDR1	0.000000	28.48	9	0.000000	48.94	20	WD repeat domain 1	Extracellular Space	other
-3.213	O75367-2	H2AFY	0.000000	10.19	4	0.000000	12.07	3	H2A histone family, member Y	Nucleus	other
2.337	O75390	CS	0.000000	5.52	2	0.000000	12.61	5	citrate synthase	Cytoplasm	enzyme
1.230	O75396	SEC22B	0.000000	8.06	2	0.000000	10.14	3	SEC22 vesicle trafficking protein homolog B (S. cerevisiae) (gene/pseudogene)	Cytoplasm	other

Fold Change	UniProt ID	Symbol	TB-IRIS MM			TB-IRIS PP			Entrez Gene Name	Location	Type(s)
			q-value	Barista score	# of peptides	q-value	Barista score	# of peptides			
-1.127	O75489	NDUFS3	0.000000	14.05	6	0.000000	22.55	8	NADH dehydrogenase (ubiquinone) Fe-S protein 3, 30kDa (NADH-coenzyme Q reductase)	Cytoplasm	enzyme
-1.390	O75558	STX11	0.000000	21.58	5	0.000000	13.45	3	syntaxin 11	Plasma Membrane	transporter
-3.064	O75608-2	LYPLA1	0.000000	6.01	2	0.001741	5.86	2	lysophospholipase I	Cytoplasm	enzyme
-3.077	O75915	ARL6IP5	0.000000	6.56	1	0.000000	8.76	1	ADP-ribosylation-like factor 6 interacting protein 5	Cytoplasm	other
2.621	O76074-2	PDE5A	0.002447	4.45	5	0.000000	9.61	5	phosphodiesterase 5A, cGMP-specific	Cytoplasm	enzyme
1.147	O94804	STK10	0.049129	2.37	2	0.000000	7.16	5	serine/threonine kinase 10	Cytoplasm	kinase
3.036	O94919	ENDOD1	0.037459	2.57	3	0.000000	11.80	5	endonuclease domain containing 1	Extracellular Space	enzyme
-1.164	O95810	SDPR	0.000000	8.86	4	0.000000	17.91	4	serum deprivation response	Plasma Membrane	other
-1.333	P00387-2	CYB5R3	0.000000	15.76	6	0.000000	16.54	7	cytochrome b5 reductase 3	Cytoplasm	enzyme
1.859	P00488	F13A1	0.000000	12.55	13	0.000000	47.45	17	coagulation factor XIII, A1 polypeptide	Extracellular Space	enzyme
1.000	P00558	PGK1	0.000000	11.83	4	0.000000	15.39	6	phosphoglycerate kinase 1	Cytoplasm	kinase
1.516	P01834	IGKC	0.000000	6.80	1	0.000000	9.41	3	immunoglobulin kappa constant	Extracellular Space	other
1.000	P02042	HBD	0.000000	10.44	6	0.000000	15.78	7	hemoglobin, delta	Cytoplasm	transporter
-1.315	P02533	KRT14	0.000000	45.10	12	0.000000	71.41	15	keratin 14	Cytoplasm	other
1.121	P02647	APOA1	0.000000	7.38	1	0.000000	13.55	3	apolipoprotein A-I	Extracellular Space	transporter
-2.665	P02656	APOC3	0.000000	9.81	1	0.000000	6.85	1	apolipoprotein C-III	Extracellular Space	transporter
1.000	P02671	FGA	0.000000	19.28	9	0.000000	25.81	9	fibrinogen alpha chain	Extracellular Space	other
1.083	P02675	FGB	0.000000	27.56	7	0.000000	42.06	10	fibrinogen beta chain	Extracellular Space	other
-1.054	P02679-2	FGG	0.000000	37.52	13	0.000000	43.35	15	fibrinogen gamma chain	Extracellular Space	other
1.409	P02730	SLC4A1	0.000000	17.15	4	0.000000	46.71	8	solute carrier family 4, anion exchanger, member 1 (erythrocyte membrane protein band 3, Diego blood group)	Plasma Membrane	transporter

Fold Change	UniProt ID	Symbol	TB-IRIS MM			TB-IRIS PP			Entrez Gene Name	Location	Type(s)
			q-value	Barista score	# of peptides	q-value	Barista score	# of peptides			
-1.521	P02765	AHSG	0.000000	5.97	2	0.006396	3.72	2	alpha-2-HS-glycoprotein	Extracellular Space	other
-1.075	P02768	ALB	0.000000	11.99	6	0.000000	12.15	9	albumin	Extracellular Space	transporter
1.349	P02788	LTF	0.000000	55.30	17	0.000000	97.57	19	lactotransferrin	Extracellular Space	peptidase
-1.674	P04004	VTN	0.002447	4.77	3	0.000000	7.22	1	vitronectin	Extracellular Space	other
-1.063	P04083	ANXA1	0.000000	23.51	10	0.000000	37.29	11	annexin A1	Plasma Membrane	other
1.045	P04259	KRT6B	0.000000	11.62	12	0.001741	5.57	14	keratin 6B	Cytoplasm	other
1.000	P04264	KRT1	0.000000	162.77	25	0.000000	208.36	24	keratin 1	Cytoplasm	other
-1.173	P04632	CAPNS1	0.000000	8.72	2	0.000000	15.62	4	calpain, small subunit 1	Cytoplasm	peptidase
1.236	P04843	RPN1	0.000000	7.66	4	0.000000	16.23	14	ribophorin I	Cytoplasm	enzyme
1.084	P04844	RPN2	0.000000	15.90	4	0.000000	34.85	8	ribophorin II	Cytoplasm	enzyme
-1.083	P04899	GNAI2	0.000000	24.69	7	0.000000	26.14	8	guanine nucleotide binding protein (G protein), alpha inhibiting activity polypeptide 2	Plasma Membrane	enzyme
1.063	P05106	ITGB3	0.000000	73.84	21	0.000000	93.27	23	integrin, beta 3 (platelet glycoprotein IIIa, antigen CD61)	Plasma Membrane	transmembrane receptor
1.177	P05109	S100A8	0.000000	5.70	1	0.001741	5.92	2	S100 calcium binding protein A8	Cytoplasm	other
1.322	P05164-2	MPO	0.000000	23.29	9	0.000000	37.74	12	myeloperoxidase	Cytoplasm	enzyme
-3.322	P05198	EIF2S1	0.000000	5.80	5	0.001741	5.96	4	eukaryotic translation initiation factor 2, subunit 1 alpha, 35kDa	Cytoplasm	translation regulator
3.194	P05388	RPLP0	0.000000	9.91	4	0.000000	13.60	4	ribosomal protein, large, P0	Cytoplasm	other
1.402	P05455	SSB	0.004792	3.63	2	0.001741	4.36	3	Sjogren syndrome antigen B (autoantigen La)	Nucleus	enzyme
1.057	P06576	ATP5B	0.000000	34.75	8	0.000000	43.60	13	ATP synthase, H+ transporting, mitochondrial F1 complex, beta polypeptide	Cytoplasm	transporter
1.339	P06733	ENO1	0.000000	16.77	7	0.000000	22.88	15	enolase 1, (alpha)	Cytoplasm	transcription regulator
1.649	P06753-2	TPM3	0.000000	19.35	5	0.000000	18.62	5	tropomyosin 3	Cytoplasm	other

Fold Change	UniProt ID	Symbol	TB-IRIS MM			TB-IRIS PP			Entrez Gene Name	Location	Type(s)
			q-value	Barista score	# of peptides	q-value	Barista score	# of peptides			
1.324	P07195	LDHB	0.000000	10.83	5	0.000000	13.42	6	lactate dehydrogenase B	Cytoplasm	enzyme
-1.514	P07237	P4HB	0.000000	19.69	9	0.000000	18.45	9	prolyl 4-hydroxylase, beta polypeptide	Cytoplasm	enzyme
-1.023	P07339	CTSD	0.004792	3.57	3	0.001741	6.58	5	cathepsin D	Cytoplasm	peptidase
-1.688	P07355-2	ANXA2	0.000000	13.49	10	0.000000	18.61	11	annexin A2	Plasma Membrane	other
-1.724	P07359	GP1BA	0.000000	5.11	4	0.000000	6.96	7	glycoprotein Ib (platelet), alpha polypeptide	Plasma Membrane	other
1.144	P07384	CAPN1	0.000000	19.47	12	0.000000	45.97	20	calpain 1, (mu/I) large subunit	Cytoplasm	peptidase
1.048	P07437	TUBB	0.000000	11.41	12	0.000000	53.87	12	tubulin, beta class I	Cytoplasm	other
-1.716	P07900-2	HSP90AA1	0.000000	14.26	14	0.000000	40.40	14	heat shock protein 90kDa alpha (cytosolic), class A member 1	Cytoplasm	enzyme
1.363	P07996	THBS1	0.000000	56.21	27	0.000000	83.11	27	thrombospondin 1	Extracellular Space	other
-1.186	P08133	ANXA6	0.000000	14.48	12	0.000000	13.22	13	annexin A6	Plasma Membrane	other
-1.182	P08238	HSP90AB1	0.000000	31.70	15	0.000000	18.89	12	heat shock protein 90kDa alpha (cytosolic), class B member 1	Cytoplasm	enzyme
1.309	P08514	ITGA2B	0.000000	215.17	19	0.000000	338.33	23	integrin, alpha 2b (platelet glycoprotein IIb of IIb/IIIa complex, antigen CD41)	Plasma Membrane	transmembrane receptor
-1.063	P08559	PDHA1	0.000000	5.58	3	0.001741	5.40	3	pyruvate dehydrogenase (lipoamide) alpha 1	Cytoplasm	enzyme
2.087	P08567	PLEK	0.000000	17.41	6	0.000000	33.84	6	pleckstrin	Cytoplasm	other
-1.182	P08575-2	PTPRC	0.000000	37.56	9	0.000000	36.14	8	protein tyrosine phosphatase, receptor type, C	Plasma Membrane	phosphatase
1.045	P08670	VIM	0.000000	48.91	19	0.000000	68.64	22	vimentin	Cytoplasm	other
-1.414	P08758	ANXA5	0.000000	14.31	6	0.000000	13.23	5	annexin A5	Plasma Membrane	other
-1.356	P08779	KRT16	0.000000	8.85	12	0.000000	19.48	12	keratin 16	Cytoplasm	other
-1.690	P08865	RPSA	0.000000	7.53	4	0.000000	8.21	5	ribosomal protein SA	Cytoplasm	translation regulator
-1.722	P09211	GSTP1	0.000000	15.35	3	0.000000	10.37	3	glutathione S-transferase pi 1	Cytoplasm	enzyme
-1.683	P0CG47	UBB	0.000000	6.18	2	0.000000	6.64	2	ubiquitin B	Cytoplasm	enzyme
-1.468	P10768	ESD	0.000000	5.83	3	0.001741	6.27	1	esterase D	Cytoplasm	enzyme

Fold Change	UniProt ID	Symbol	TB-IRIS MM			TB-IRIS PP			Entrez Gene Name	Location	Type(s)
			q-value	Barista score	# of peptides	q-value	Barista score	# of peptides			
1.837	P10809	HSPD1	0.000000	12.00	5	0.000000	53.17	13	heat shock 60kDa protein 1 (chaperonin)	Cytoplasm	enzyme
1.358	P10909-2	CLU	0.000000	6.18	3	0.000000	9.94	3	clusterin	Extracellular Space	other
-1.024	P11021	HSPA5	0.000000	49.38	16	0.000000	44.84	16	heat shock 70kDa protein 5 (glucose-regulated protein, 78kDa)	Cytoplasm	enzyme
-1.687	P11169	SLC2A3	0.002447	4.25	2	0.022426	2.83	2	solute carrier family 2 (facilitated glucose transporter), member 3	Plasma Membrane	transporter
2.165	P11215	ITGAM	0.000000	9.84	7	0.000000	27.02	14	integrin, alpha M (complement component 3 receptor 3 subunit)	Plasma Membrane	other
4.135	P11216	PYGB	0.000000	9.89	9	0.000000	17.39	12	phosphorylase, glycogen; brain	Cytoplasm	enzyme
2.473	P11310-2	ACADM	0.000000	4.89	3	0.000000	33.38	7	acyl-CoA dehydrogenase, C-4 to C-12 straight chain	Cytoplasm	enzyme
1.131	P11586	MTHFD1	0.035702	2.62	2	0.022426	2.74	8	methylenetetrahydrofolate dehydrogenase (NADP+ dependent) 1, methenyltetrahydrofolate cyclohydrolase, formyltetrahydrofolate synthetase	Cytoplasm	enzyme
1.064	P11678	EPX	0.000000	11.15	8	0.000000	20.84	8	eosinophil peroxidase	Cytoplasm	enzyme
-1.063	P12236	SLC25A6	0.000000	18.14	6	0.000000	27.71	6	solute carrier family 25 (mitochondrial carrier; adenine nucleotide translocator), member 6	Cytoplasm	transporter
-9.885	P12259	F5	0.000000	8.72	6	0.000000	6.74	14	coagulation factor V (proaccelerin, labile factor)	Plasma Membrane	enzyme
-1.348	P12814	ACTN1	0.000000	91.53	33	0.000000	110.30	35	actinin, alpha 1	Cytoplasm	other
1.678	P12931-2	SRC	0.000000	9.68	6	0.000000	21.85	9	v-src sarcoma (Schmidt-Ruppin A-2) viral oncogene homolog (avian)	Cytoplasm	kinase
-1.594	P12956	XRCC6	0.002447	4.27	9	0.030237	2.54	8	X-ray repair complementing defective repair in Chinese hamster cells 6	Nucleus	enzyme
-1.971	P13224-2	GP1BB	0.000000	16.11	6	0.000000	8.71	6	glycoprotein Ib (platelet), beta polypeptide	Plasma Membrane	other
-1.251	P13489	RNH1	0.000000	8.86	6	0.000000	14.22	6	ribonuclease/angiogenin inhibitor 1	Cytoplasm	other
-1.050	P13639	EEF2	0.000000	10.56	8	0.000000	20.64	9	eukaryotic translation elongation factor 2	Cytoplasm	translation regulator
1.000	P13645	KRT10	0.000000	174.18	20	0.000000	209.96	21	keratin 10	Cytoplasm	other
1.022	P13647	KRT5	0.000000	39.43	15	0.000000	59.37	16	keratin 5	Cytoplasm	other
-6.061	P13667	PDIA4	0.000000	13.06	7	0.001741	4.58	9	protein disulfide isomerase family A, member 4	Cytoplasm	enzyme
1.020	P13796	LCP1	0.000000	17.66	18	0.000000	30.53	26	lymphocyte cytosolic protein 1 (L-plastin)	Cytoplasm	other
-5.114	P13804	ETFA	0.000000	23.33	6	0.000000	13.85	4	electron-transfer-flavoprotein, alpha polypeptide	Cytoplasm	transporter

Fold Change	UniProt ID	Symbol	TB-IRIS MM			TB-IRIS PP			Entrez Gene Name	Location	Type(s)
			q-value	Barista score	# of peptides	q-value	Barista score	# of peptides			
-3.068	P14222	PRF1	0.000000	5.42	3	0.000000	9.19	2	perforin 1 (pore forming protein)	Cytoplasm	other
-2.047	P14314	PRKCSH	0.000000	14.21	6	0.000000	17.68	5	protein kinase C substrate 80K-H	Cytoplasm	enzyme
1.358	P14618	PKM	0.000000	37.93	12	0.000000	58.65	18	pyruvate kinase, muscle	unknown	kinase
1.368	P14625	HSP90B1	0.000000	13.73	10	0.000000	39.29	12	heat shock protein 90kDa beta (Grp94), member 1	Cytoplasm	other
1.449	P14770	GP9	0.000000	5.31	4	0.000000	14.36	3	glycoprotein IX (platelet)	Plasma Membrane	other
1.744	P14780	MMP9	0.000000	7.13	5	0.000000	31.37	13	matrix metallopeptidase 9 (gelatinase B, 92kDa gelatinase, 92kDa type IV collagenase)	Extracellular Space	peptidase
-1.339	P15153	RAC2	0.000000	10.24	4	0.000000	13.43	5	ras-related C3 botulinum toxin substrate 2 (rho family, small GTP binding protein Rac2)	Cytoplasm	enzyme
-1.249	P15311	EZR	0.000000	7.93	8	0.003380	4.21	8	ezrin	Plasma Membrane	other
-2.647	P15498	VAV1	0.002447	4.63	3	0.022426	2.79	4	vav 1 guanine nucleotide exchange factor	Nucleus	transcription regulator
1.717	P16109	SELP	0.000000	11.72	2	0.000000	24.98	6	selectin P (granule membrane protein 140kDa, antigen CD62)	Plasma Membrane	other
3.892	P16671	CD36	0.000000	15.25	4	0.000000	62.83	7	CD36 molecule (thrombospondin receptor)	Plasma Membrane	transmembrane receptor
-1.026	P17066	HSPA6	0.002447	3.78	9	0.001741	5.05	8	heat shock 70kDa protein 6 (HSP70B')	unknown	other
1.970	P17612-2	PRKACA	0.000000	5.09	3	0.001741	4.92	5	protein kinase, cAMP-dependent, catalytic, alpha	Cytoplasm	kinase
-1.188	P17987	TCP1	0.002447	4.37	4	0.000000	8.37	5	t-complex 1	Cytoplasm	other
-1.401	P18124	RPL7	0.009294	3.31	2	0.013478	3.24	3	ribosomal protein L7	Nucleus	transcription regulator
1.080	P18206-2	VCL	0.000000	41.05	23	0.000000	65.46	29	vinculin	Plasma Membrane	enzyme
-1.434	P18669	PGAM1	0.004792	3.52	2	0.001741	6.06	1	phosphoglycerate mutase 1 (brain)	Cytoplasm	phosphatase
1.246	P19878	NCF2	0.004792	3.63	5	0.001741	6.20	4	neutrophil cytosolic factor 2	Cytoplasm	enzyme
1.140	P20160	AZU1	0.000000	5.00	2	0.000000	10.00	4	azurocidin 1	Cytoplasm	peptidase
-3.056	P21266	GSTM3	0.000000	9.50	3	0.000000	11.75	2	glutathione S-transferase mu 3 (brain)	Cytoplasm	enzyme
1.097	P21333-2	FLNA	0.000000	192.02	64	0.000000	311.78	85	filamin A, alpha	Cytoplasm	other

Fold Change	UniProt ID	Symbol	TB-IRIS MM			TB-IRIS PP			Entrez Gene Name	Location	Type(s)
			q-value	Barista score	# of peptides	q-value	Barista score	# of peptides			
-1.171	P21796	VDAC1	0.000000	44.22	8	0.000000	63.10	9	voltage-dependent anion channel 1	Cytoplasm	ion channel
1.138	P22314	UBA1	0.000000	12.75	11	0.000000	17.48	12	ubiquitin-like modifier activating enzyme 1	Cytoplasm	enzyme
1.173	P22626-2	HNRNPA2B1	0.000000	18.05	4	0.000000	13.96	6	heterogeneous nuclear ribonucleoprotein A2/B1	Nucleus	other
-2.633	P22894	MMP8	0.000000	15.90	3	0.000000	16.14	4	matrix metallopeptidase 8 (neutrophil collagenase)	Extracellular Space	peptidase
2.585	P23219-2	PTGS1	0.043607	2.44	3	0.000000	22.69	5	prostaglandin-endoperoxide synthase 1 (prostaglandin G/H synthase and cyclooxygenase)	Cytoplasm	enzyme
-1.632	P23381-2	WARS	0.035702	2.62	2	0.035105	2.49	2	tryptophanyl-tRNA synthetase	Cytoplasm	enzyme
-1.124	P23528	CFL1	0.000000	21.31	2	0.000000	21.84	3	cofilin 1 (non-muscle)	Nucleus	other
2.577	P24539	ATP5F1	0.018039	3.11	3	0.000000	22.12	5	ATP synthase, H+ transporting, mitochondrial Fo complex, subunit B1	Cytoplasm	transporter
16.228	P25325	MPST	0.043607	2.42	3	0.010891	3.41	2	mercaptopyruvate sulfurtransferase	Cytoplasm	enzyme
-1.065	P25705	ATP5A1	0.000000	46.86	16	0.000000	53.57	14	ATP synthase, H+ transporting, mitochondrial F1 complex, alpha subunit 1, cardiac muscle	Cytoplasm	transporter
-1.166	P25788-2	PSMA3	0.000000	6.92	3	0.000000	8.44	3	proteasome (prosome, macropain) subunit, alpha type, 3	Cytoplasm	peptidase
1.377	P25789	PSMA4	0.000000	7.07	5	0.001741	5.43	3	proteasome (prosome, macropain) subunit, alpha type, 4	Cytoplasm	peptidase
1.142	P26038	MSN	0.000000	29.04	17	0.000000	38.55	17	moesin	Plasma Membrane	other
-1.181	P26641	EEF1G	0.000000	13.90	6	0.000000	19.68	5	eukaryotic translation elongation factor 1 gamma	Cytoplasm	translation regulator
1.000	P27105	STOM	0.000000	48.32	7	0.000000	51.13	9	stomatin	Plasma Membrane	other
1.107	P27338	MAOB	0.021696	2.86	2	0.000000	6.62	4	monoamine oxidase B	Cytoplasm	enzyme
1.059	P27348	YWHAQ	0.000000	23.88	8	0.000000	41.32	10	tyrosine 3-monooxygenase/tryptophan 5-monooxygenase activation protein, theta polypeptide	Cytoplasm	other
1.828	P27797	CALR	0.002447	4.09	3	0.000000	15.68	4	calreticulin	Cytoplasm	transcription regulator
-1.355	P27824	CANX	0.000000	54.20	7	0.000000	71.82	8	calnexin	Cytoplasm	other
-1.384	P28066	PSMA5	0.015941	3.14	4	0.001741	5.68	3	proteasome (prosome, macropain) subunit, alpha type, 5	Cytoplasm	peptidase
2.691	P28331	NDUFS1	0.000000	5.48	4	0.000000	21.94	10	NADH dehydrogenase (ubiquinone) Fe-S protein 1, 75kDa (NADH-coenzyme Q reductase)	Cytoplasm	enzyme
-1.425	P28676	GCA	0.000000	9.18	1	0.006396	3.73	1	grancalcin, EF-hand calcium binding protein	Cytoplasm	other

Fold Change	UniProt ID	Symbol	TB-IRIS MM			TB-IRIS PP			Entrez Gene Name	Location	Type(s)
			q-value	Barista score	# of peptides	q-value	Barista score	# of peptides			
1.794	P30041	PRDX6	0.000000	13.41	5	0.000000	16.23	5	peroxiredoxin 6	Cytoplasm	enzyme
1.144	P30048	PRDX3	0.000000	17.17	3	0.000000	12.44	3	peroxiredoxin 3	Cytoplasm	enzyme
3.172	P30084	ECHS1	0.000000	4.82	2	0.000000	24.22	5	enoyl CoA hydratase, short chain, 1, mitochondrial	Cytoplasm	enzyme
1.545	P30101	PDIA3	0.000000	9.62	8	0.000000	36.45	15	protein disulfide isomerase family A, member 3	Cytoplasm	peptidase
2.270	P30153	PPP2R1A	0.000000	10.94	6	0.000000	30.77	9	protein phosphatase 2, regulatory subunit A, alpha	Cytoplasm	phosphatase
1.238	P31146	CORO1A	0.000000	29.74	7	0.000000	40.02	12	coronin, actin binding protein, 1A	Cytoplasm	other
2.201	P31150	GDI1	0.000000	7.26	6	0.000000	9.89	9	GDP dissociation inhibitor 1	Cytoplasm	other
-1.536	P31937	HIBADH	0.002447	4.38	2	0.003380	4.11	3	3-hydroxyisobutyrate dehydrogenase	Cytoplasm	enzyme
-1.012	P31946-2	YWHAB	0.000000	22.81	9	0.000000	56.42	10	tyrosine 3-monooxygenase/tryptophan 5-monooxygenase activation protein, beta polypeptide	Cytoplasm	transcription regulator
1.209	P33947-2	KDELR2	0.011501	3.28	2	0.004979	3.97	2	KDEL (Lys-Asp-Glu-Leu) endoplasmic reticulum protein retention receptor 2	Cytoplasm	other
-4.155	P34932	HSPA4	0.009294	3.36	4	0.003380	4.13	3	heat shock 70kDa protein 4	Cytoplasm	other
-1.461	P35232	PHB	0.000000	29.02	7	0.000000	40.29	8	prohibitin	Nucleus	transcription regulator
1.000	P35527	KRT9	0.000000	142.55	15	0.000000	188.39	18	keratin 9	Cytoplasm	other
1.023	P35579	MYH9	0.000000	144.29	50	0.000000	161.26	55	myosin, heavy chain 9, non-muscle	Cytoplasm	transporter
1.442	P35606	COPB2	0.000000	6.84	8	0.000000	20.01	10	coatomer protein complex, subunit beta 2 (beta prime)	Cytoplasm	transporter
1.000	P35908	KRT2	0.000000	65.47	20	0.000000	95.63	22	keratin 2	Cytoplasm	other
-1.228	P37802	TAGLN2	0.000000	14.22	3	0.000000	20.53	3	transgelin 2	Cytoplasm	other
-3.082	P37837	TALDO1	0.000000	26.11	6	0.000000	7.74	2	transaldolase 1	Cytoplasm	enzyme
1.465	P38117-2	ETFB	0.043607	2.39	2	0.000000	8.61	5	electron-transfer-flavoprotein, beta polypeptide	Cytoplasm	transporter
1.867	P38646	HSPA9	0.000000	26.70	9	0.000000	49.07	11	heat shock 70kDa protein 9 (mortalin)	Cytoplasm	other
-1.018	P39656	DDOST	0.000000	8.77	5	0.000000	12.16	6	dolichyl-diphosphooligosaccharide–protein glycosyltransferase	Cytoplasm	enzyme
2.002	P40197	GP5	0.000000	8.53	2	0.000000	9.97	4	glycoprotein V (platelet)	Plasma Membrane	other
1.240	P40227	CCT6A	0.000000	5.07	3	0.000000	8.03	7	chaperonin containing TCP1, subunit 6A (zeta 1)	Cytoplasm	other
1.050	P40939	HADHA	0.000000	8.39	2	0.000000	16.69	8	hydroxyacyl-CoA dehydrogenase/3-ketoacyl-CoA thiolase/enoyl-CoA hydratase (trifunctional protein), alpha subunit	Cytoplasm	enzyme
-1.692	P41091	EIF2S3	0.004792	3.62	3	0.000000	7.18	4	eukaryotic translation initiation factor 2, subunit 3 gamma, 52kDa	Cytoplasm	translation regulator

Fold Change	UniProt ID	Symbol	TB-IRIS MM			TB-IRIS PP			Entrez Gene Name	Location	Type(s)
			q-value	Barista score	# of peptides	q-value	Barista score	# of peptides			
-1.429	P41218	MNDA	0.000000	6.61	4	0.001741	6.20	4	myeloid cell nuclear differentiation antigen	Nucleus	transcription regulator
1.118	P42224-2	STAT1	0.000000	11.87	7	0.000000	22.01	9	signal transducer and activator of transcription 1, 91kDa	Nucleus	transcription regulator
1.030	P45880-1	VDAC2	0.000000	17.56	7	0.000000	37.02	8	voltage-dependent anion channel 2	Cytoplasm	ion channel
2.369	P46940	IQGAP1	0.000000	8.01	15	0.000000	22.14	23	IQ motif containing GTPase activating protein 1	Cytoplasm	other
-2.773	P47755	CAPZA2	0.000000	11.25	3	0.000000	9.03	3	capping protein (actin filament) muscle Z-line, alpha 2	Cytoplasm	other
1.062	P47756-2	CAPZB	0.000000	12.57	3	0.000000	19.34	6	capping protein (actin filament) muscle Z-line, beta	Cytoplasm	other
1.401	P47985	UQCRFS1	0.040879	2.48	1	0.000000	8.02	2	ubiquinol-cytochrome c reductase, Rieske iron-sulfur polypeptide 1	Cytoplasm	enzyme
1.131	P48047	ATP5O	0.000000	7.57	3	0.000000	18.94	5	ATP synthase, H+ transporting, mitochondrial F1 complex, O subunit	Cytoplasm	transporter
-1.041	P48059	LIMS1	0.000000	15.78	8	0.000000	19.87	7	LIM and senescent cell antigen-like domains 1	Plasma Membrane	other
-6.329	P48426	PIP4K2A	0.000000	10.67	5	0.006396	3.90	3	phosphatidylinositol-5-phosphate 4-kinase, type II, alpha	Cytoplasm	kinase
-1.171	P48643	CCT5	0.000000	6.58	7	0.000000	16.24	5	chaperonin containing TCP1, subunit 5 (epsilon)	Cytoplasm	other
1.948	P48735	IDH2	0.000000	18.79	6	0.000000	41.15	12	isocitrate dehydrogenase 2 (NADP+), mitochondrial	Cytoplasm	enzyme
2.040	P49327	FASN	0.007133	3.44	8	0.000000	20.14	12	fatty acid synthase	Cytoplasm	enzyme
-1.420	P49368-2	CCT3	0.002447	4.44	4	0.004979	3.95	4	chaperonin containing TCP1, subunit 3 (gamma)	Cytoplasm	other
4.802	P49407-2	ARRB1	0.002447	4.25	3	0.004979	4.01	4	arrestin, beta 1	Cytoplasm	other
-1.383	P49593	PPM1F	0.023587	2.80	5	0.000000	7.10	4	protein phosphatase, Mg2+/Mn2+ dependent, 1F	Cytoplasm	phosphatase
-1.431	P49748-2	ACADVL	0.000000	7.31	6	0.000000	9.49	7	acyl-CoA dehydrogenase, very long chain	Cytoplasm	enzyme
2.551	P50148	GNAQ	0.000000	9.00	2	0.000000	13.46	6	guanine nucleotide binding protein (G protein), q polypeptide	Plasma Membrane	enzyme
1.130	P50226	SULT1A2	0.000000	7.86	3	0.000000	12.64	6	sulfotransferase family, cytosolic, 1A, phenol-preferring, member 2	Cytoplasm	enzyme
-1.447	P50570-2	DNM2	0.000000	7.03	10	0.000000	9.50	10	dynamin 2	Plasma Membrane	enzyme
-1.095	P50990	CCT8	0.000000	11.91	9	0.000000	17.47	11	chaperonin containing TCP1, subunit 8 (theta)	Cytoplasm	enzyme
-1.452	P50991	CCT4	0.002447	4.20	2	0.001741	5.82	3	chaperonin containing TCP1, subunit 4 (delta)	Cytoplasm	other
1.149	P51148	RAB5C	0.000000	7.26	2	0.000000	24.49	5	RAB5C, member RAS oncogene family	Cytoplasm	enzyme
1.697	P51149	RAB7A	0.000000	19.18	6	0.000000	39.09	8	RAB7A, member RAS oncogene family	Cytoplasm	enzyme
1.773	P51452	DUSP3	0.000000	9.34	1	0.000000	10.20	3	dual specificity phosphatase 3	Cytoplasm	phosphatase
1.250	P52565	ARHGDIA	0.000000	5.93	1	0.001741	5.87	1	Rho GDP dissociation inhibitor (GDI) alpha	Cytoplasm	other

Fold Change	UniProt ID	Symbol	TB-IRIS MM			TB-IRIS PP			Entrez Gene Name	Location	Type(s)
			q-value	Barista score	# of peptides	q-value	Barista score	# of peptides			
-1.125	P52597	HNRNPF	0.000000	13.42	4	0.000000	10.26	5	heterogeneous nuclear ribonucleoprotein F	Nucleus	other
-1.155	P52907	CAPZA1	0.002447	4.34	3	0.000000	22.42	7	capping protein (actin filament) muscle Z-line, alpha 1	Cytoplasm	other
-1.491	P53801	PTTG1IP	0.002447	4.27	1	0.001741	4.68	1	pituitary tumor-transforming 1 interacting protein	Nucleus	other
-1.487	P54136-2	RARS	0.015941	3.22	3	0.006396	3.93	3	arginyl-tRNA synthetase	Cytoplasm	enzyme
-1.765	P54920	NAPA	0.000000	14.46	6	0.000000	18.24	7	N-ethylmaleimide-sensitive factor attachment protein, alpha	Cytoplasm	transporter
-1.047	P55072	VCP	0.000000	12.56	7	0.000000	19.99	16	valosin containing protein	Cytoplasm	enzyme
2.088	P55160	NCKAP1L	0.000000	9.80	7	0.000000	17.16	5	NCK-associated protein 1-like	Plasma Membrane	other
3.017	P59998	ARPC4	0.000000	6.85	3	0.001741	5.55	3	actin related protein 2/3 complex, subunit 4, 20kDa	unknown	other
2.483	P60842	EIF4A1	0.002447	4.57	5	0.000000	18.19	11	eukaryotic translation initiation factor 4A1	Cytoplasm	translation regulator
-3.186	P60900	PSMA6	0.002447	4.65	4	0.001741	6.08	4	proteasome (prosome, macropain) subunit, alpha type, 6	Cytoplasm	peptidase
4.276	P60953	CDC42	0.009294	3.30	3	0.000000	22.69	5	cell division cycle 42 (GTP binding protein, 25kDa)	Cytoplasm	enzyme
1.316	P61006	RAB8A	0.000000	8.72	3	0.000000	25.24	8	RAB8A, member RAS oncogene family	Plasma Membrane	other
1.065	P61026	RAB10	0.000000	12.40	5	0.000000	30.05	8	RAB10, member RAS oncogene family	Cytoplasm	enzyme
1.197	P61106	RAB14	0.002447	4.70	4	0.000000	18.49	7	RAB14, member RAS oncogene family	Cytoplasm	enzyme
-1.184	P61158	ACTR3	0.000000	15.41	4	0.000000	31.30	10	ARP3 actin-related protein 3 homolog (yeast)	Plasma Membrane	other
1.007	P61160	ACTR2	0.000000	25.61	5	0.000000	40.58	8	ARP2 actin-related protein 2 homolog (yeast)	Plasma Membrane	other
-1.196	P61204	ARF3	0.000000	7.81	4	0.000000	13.46	3	ADP-ribosylation factor 3	Cytoplasm	enzyme
-1.233	P61224	RAP1B	0.000000	32.01	9	0.000000	41.07	8	RAP1B, member of RAS oncogene family	Cytoplasm	enzyme
-1.277	P61225	RAP2B	0.000000	7.81	1	0.000000	9.77	2	RAP2B, member of RAS oncogene family	Plasma Membrane	enzyme
-1.446	P61247	RPS3A	0.000000	7.49	2	0.000000	13.24	4	ribosomal protein S3A	Cytoplasm	other
1.246	P61586	RHOA	0.000000	18.93	4	0.000000	25.11	7	ras homolog family member A	Cytoplasm	enzyme
1.358	P61978-2	HNRNPK	0.004792	3.63	5	0.000000	15.01	6	heterogeneous nuclear ribonucleoprotein K	Nucleus	other
1.406	P61981	YWHAG	0.000000	12.72	5	0.000000	35.68	9	tyrosine 3-monooxygenase/tryptophan 5-monooxygenase activation protein, gamma polypeptide	Cytoplasm	other

Fold Change	UniProt ID	Symbol	TB-IRIS MM			TB-IRIS PP			Entrez Gene Name	Location	Type(s)
			q-value	Barista score	# of peptides	q-value	Barista score	# of peptides			
1.000	P62258	YWHAE	0.000000	21.85	6	0.000000	29.31	7	tyrosine 3-monooxygenase/tryptophan 5-monooxygenase activation protein, epsilon polypeptide	Cytoplasm	other
-1.415	P62491	RAB11A	0.000000	20.33	7	0.000000	20.29	7	RAB11A, member RAS oncogene family	Cytoplasm	enzyme
-3.114	P62495	ETF1	0.000000	6.67	8	0.001741	5.15	5	eukaryotic translation termination factor 1	Cytoplasm	translation regulator
-2.324	P62826	RAN	0.000000	16.58	6	0.000000	13.82	6	RAN, member RAS oncogene family	Nucleus	enzyme
1.454	P62873	GNB1	0.000000	18.25	3	0.000000	22.15	5	guanine nucleotide binding protein (G protein), beta polypeptide 1	Plasma Membrane	enzyme
2.413	P62937	PPIA	0.002447	4.20	2	0.001741	4.58	2	peptidylprolyl isomerase A (cyclophilin A)	Cytoplasm	enzyme
-1.492	P63104	YWHAZ	0.000000	58.83	9	0.000000	48.05	11	tyrosine 3-monooxygenase/tryptophan 5-monooxygenase activation protein, zeta polypeptide	Cytoplasm	enzyme
-1.532	P63244	GNB2L1	0.002447	3.81	3	0.001741	5.27	2	guanine nucleotide binding protein (G protein), beta polypeptide 2-like 1	Cytoplasm	enzyme
-1.536	P67809	YBX1	0.000000	17.83	1	0.000000	11.68	1	Y box binding protein 1	Nucleus	transcription regulator
-1.112	P67936	TPM4	0.000000	13.47	6	0.000000	14.04	5	tropomyosin 4	Cytoplasm	other
1.419	P68366	TUBA4A	0.000000	46.10	13	0.000000	24.60	12	tubulin, alpha 4a	Cytoplasm	other
1.135	P68371	TUBB4B	0.000000	37.31	12	0.000000	12.04	11	tubulin, beta 4B class IVb	Cytoplasm	other
1.000	P68871	HBB	0.000000	29.65	8	0.000000	24.34	7	hemoglobin, beta	Cytoplasm	transporter
1.184	P78417	GSTO1	0.000000	8.69	4	0.000000	7.61	3	glutathione S-transferase omega 1	Cytoplasm	enzyme
1.847	P81605	DCD	0.000000	11.00	2	0.000000	8.73	2	dermcidin	Extracellular Space	other
-2.296	Q00325-2	SLC25A3	0.000000	6.68	4	0.001741	4.56	5	solute carrier family 25 (mitochondrial carrier; phosphate carrier), member 3	Cytoplasm	transporter
1.529	Q00610-2	CLTC	0.000000	60.86	18	0.000000	142.49	28	clathrin, heavy chain (Hc)	Plasma Membrane	other
-1.465	Q00839-2	HNRNPU	0.000000	13.59	5	0.000000	25.13	8	heterogeneous nuclear ribonucleoprotein U (scaffold attachment factor A)	Nucleus	transporter
1.051	Q01813	PFKP	0.000000	13.06	8	0.000000	31.54	9	phosphofructokinase, platelet	Cytoplasm	kinase
-1.012	Q02978	SLC25A11	0.000000	11.27	5	0.000000	14.19	6	solute carrier family 25 (mitochondrial carrier; oxoglutarate carrier), member 11	Cytoplasm	transporter

Fold Change	UniProt ID	Symbol	TB-IRIS MM			TB-IRIS PP			Entrez Gene Name	Location	Type(s)
			q-value	Barista score	# of peptides	q-value	Barista score	# of peptides			
1.109	Q04917	YWHAH	0.000000	26.47	11	0.000000	32.03	12	tyrosine 3-monooxygenase/tryptophan 5-monooxygenase activation protein, eta polypeptide	Cytoplasm	transcription regulator
-1.739	Q06323	PSME1	0.000000	19.46	7	0.000000	16.09	7	proteasome (prosome, macropain) activator subunit 1 (PA28 alpha)	Cytoplasm	other
1.782	Q07020	RPL18	0.018039	3.09	1	0.000000	7.12	2	ribosomal protein L18	Cytoplasm	other
-1.040	Q07021	C1QBP	0.000000	13.85	5	0.000000	23.20	6	complement component 1, q subcomponent binding protein	Cytoplasm	other
4.183	Q07960	ARHGAP1	0.002447	4.16	2	0.000000	14.63	7	Rho GTPase activating protein 1	Cytoplasm	other
1.000	Q08211	DHX9	0.002447	4.60	9	0.000000	6.93	8	DEAH (Asp-Glu-Ala-His) box polypeptide 9	Nucleus	enzyme
1.369	Q08AF3	SLFN5	0.021696	2.84	3	0.001741	6.40	2	schlafen family member 5	Nucleus	enzyme
2.591	Q10567-2	AP1B1	0.000000	7.06	4	0.000000	16.91	9	adaptor-related protein complex 1, beta 1 subunit	Cytoplasm	transporter
1.350	Q13201	MMRN1	0.000000	22.53	16	0.000000	46.06	18	multimerin 1	Extracellular Space	other
10.660	Q13418	ILK	0.002447	4.19	7	0.001741	5.80	7	integrin-linked kinase	Plasma Membrane	kinase
2.114	Q13637	RAB32	0.000000	7.98	5	0.000000	25.00	6	RAB32, member RAS oncogene family	Cytoplasm	other
-1.179	Q14165	MLEC	0.000000	19.29	5	0.000000	22.32	5	malectin	Plasma Membrane	other
-1.365	Q14697-2	GANAB	0.000000	9.22	6	0.000000	18.44	9	glucosidase, alpha; neutral AB	Cytoplasm	enzyme
1.674	Q14739	LBR	0.000000	10.64	4	0.000000	13.45	5	lamin B receptor	Nucleus	enzyme
1.567	Q14974	KPNB1	0.000000	11.51	7	0.000000	16.91	11	karyopherin (importin) beta 1	Nucleus	transporter
-1.412	Q15005	SPCS2	0.042544	2.45	1	0.013478	3.36	2	signal peptidase complex subunit 2 homolog (S. cerevisiae)	Cytoplasm	other
2.055	Q15019-2	SEPT2	0.000000	8.41	5	0.000000	12.66	5	septin 2	Cytoplasm	enzyme
3.463	Q15233	NONO	0.002447	4.45	3	0.000000	10.46	2	non-POU domain containing, octamer-binding	Nucleus	other
-1.309	Q15555	MAPRE2	0.000000	7.85	2	0.000000	9.31	2	microtubule-associated protein, RP/EB family, member 2	Cytoplasm	other
-1.353	Q15942	ZYX	0.000000	16.50	4	0.000000	16.60	4	zyxin	Plasma Membrane	other
-1.670	Q16181-2	SEPT7	0.000000	19.92	6	0.000000	15.78	6	septin 7	Cytoplasm	other
1.782	Q07020	RPL18	0.018039	3.09	1	0.000000	7.12	2	ribosomal protein L18	Cytoplasm	other
-1.040	Q07021	C1QBP	0.000000	13.85	5	0.000000	23.20	6	complement component 1, q subcomponent binding protein	Cytoplasm	other
4.183	Q07960	ARHGAP1	0.002447	4.16	2	0.000000	14.63	7	Rho GTPase activating protein 1	Cytoplasm	other
1.000	Q08211	DHX9	0.002447	4.60	9	0.000000	6.93	8	DEAH (Asp-Glu-Ala-His) box polypeptide 9	Nucleus	enzyme

Fold Change	UniProt ID	Symbol	TB-IRIS MM			TB-IRIS PP			Entrez Gene Name	Location	Type(s)
			q-value	Barista score	# of peptides	q-value	Barista score	# of peptides			
1.369	Q08AF3	SLFN5	0.021696	2.84	3	0.001741	6.40	2	schlafen family member 5	Nucleus	enzyme
2.591	Q10567-2	AP1B1	0.000000	7.06	4	0.000000	16.91	9	adaptor-related protein complex 1, beta 1 subunit	Cytoplasm	transporter
1.350	Q13201	MMRN1	0.000000	22.53	16	0.000000	46.06	18	multimerin 1	Extracellular Space	other
10.660	Q13418	ILK	0.002447	4.19	7	0.001741	5.80	7	integrin-linked kinase	Plasma Membrane	kinase
2.114	Q13637	RAB32	0.000000	7.98	5	0.000000	25.00	6	RAB32, member RAS oncogene family	Cytoplasm	other
-1.179	Q14165	MLEC	0.000000	19.29	5	0.000000	22.32	5	malectin	Plasma Membrane	other
-1.365	Q14697-2	GANAB	0.000000	9.22	6	0.000000	18.44	9	glucosidase, alpha; neutral AB	Cytoplasm	enzyme
1.674	Q14739	LBR	0.000000	10.64	4	0.000000	13.45	5	lamin B receptor	Nucleus	enzyme
1.567	Q14974	KPNB1	0.000000	11.51	7	0.000000	16.91	11	karyopherin (importin) beta 1	Nucleus	transporter
-1.412	Q15005	SPCS2	0.042544	2.45	1	0.013478	3.36	2	signal peptidase complex subunit 2 homolog (S. cerevisiae)	Cytoplasm	other
2.055	Q15019-2	SEPT2	0.000000	8.41	5	0.000000	12.66	5	septin 2	Cytoplasm	enzyme
3.463	Q15233	NONO	0.002447	4.45	3	0.000000	10.46	2	non-POU domain containing, octamer-binding	Nucleus	other
-1.309	Q15555	MAPRE2	0.000000	7.85	2	0.000000	9.31	2	microtubule-associated protein, RP/EB family, member 2	Cytoplasm	other
-1.353	Q15942	ZYX	0.000000	16.50	4	0.000000	16.60	4	zyxin	Plasma Membrane	other
-1.670	Q16181-2	SEPT7	0.000000	19.92	6	0.000000	15.78	6	septin 7	Cytoplasm	other
-2.606	Q16666-2	IFI16	0.000000	9.03	5	0.000000	6.97	5	interferon, gamma-inducible protein 16	Nucleus	transcription regulator
-3.365	Q16762	TST	0.000000	8.74	4	0.001741	4.95	3	thiosulfate sulfurtransferase (rhodanese)	Cytoplasm	enzyme
1.464	Q16795	NDUFA9	0.000000	5.12	5	0.000000	8.92	5	NADH dehydrogenase (ubiquinone) 1 alpha subcomplex, 9, 39kDa	Cytoplasm	enzyme
-1.637	Q1KMD3	HNRNPUL2	0.023587	2.79	1	0.006396	3.93	3	heterogeneous nuclear ribonucleoprotein U-like 2	Nucleus	other
4.069	Q27J81-2	INF2	0.000000	6.21	7	0.000000	13.34	5	inverted formin, FH2 and WH2 domain containing	Cytoplasm	other
1.410	Q53GQ0	HSD17B12	0.000000	6.70	4	0.000000	9.80	3	hydroxysteroid (17-beta) dehydrogenase 12	Cytoplasm	enzyme
1.000	Q562R1	ACTBL2	0.011501	3.26	6	0.000000	9.73	6	actin, beta-like 2	unknown	other
-3.907	Q5T4S7-2	UBR4	0.033912	2.67	13	0.001741	4.49	27	ubiquitin protein ligase E3 component n-recognin 4	Nucleus	other
1.538	Q6NUK1-2	SLC25A24	0.000000	7.55	3	0.000000	15.35	4	solute carrier family 25 (mitochondrial carrier; phosphate carrier), member 24	Cytoplasm	other

Fold Change	UniProt ID	Symbol	TB-IRIS MM			TB-IRIS PP			Entrez Gene Name	Location	Type(s)
			q-value	Barista score	# of peptides	q-value	Barista score	# of peptides			
-5.265	Q6UX06	OLFM4	0.000000	18.80	3	0.000000	10.07	4	olfactomedin 4	Extracellular Space	other
1.342	Q70J99-3	UNC13D	0.000000	14.13	5	0.000000	27.14	12	unc-13 homolog D (C. elegans)	Cytoplasm	other
1.233	Q71U36	TUBA1A	0.000000	85.26	13	0.000000	17.77	12	tubulin, alpha 1a	Cytoplasm	other
-1.334	Q7Z3Y8	KRT27	0.043607	2.40	3	0.003380	4.07	6	keratin 27	unknown	other
1.941	Q7Z4W1	DCXR	0.000000	10.94	2	0.001741	5.94	2	dicarbonyl/L-xylulose reductase	Cytoplasm	enzyme
-1.174	Q7Z794	KRT77	0.007133	3.48	7	0.000000	14.58	8	keratin 77	unknown	other
1.006	Q86UX7-2	FERMT3	0.000000	99.21	27	0.000000	126.18	25	fermitin family member 3	Cytoplasm	enzyme
-1.124	Q86VP6-2	CAND1	0.000000	7.03	6	0.001741	6.03	4	cullin-associated and neddylation-dissociated 1	Cytoplasm	transcription regulator
1.214	Q86YW5-2	TREML1	0.040879	2.49	1	0.000000	8.57	3	triggering receptor expressed on myeloid cells-like 1	Plasma Membrane	other
1.796	Q8IXQ6-2	PARP9	0.047469	2.38	4	0.000000	8.76	3	poly (ADP-ribose) polymerase family, member 9	Nucleus	other
-1.619	Q8NBS9	TXNDC5	0.000000	5.15	2	0.001741	5.35	3	thioredoxin domain containing 5 (endoplasmic reticulum)	Cytoplasm	enzyme
-3.075	Q8TF42	UBASH3B	0.000000	6.68	2	0.001741	5.38	6	ubiquitin associated and SH3 domain containing B	unknown	enzyme
-1.401	Q8WY22	BRI3BP	0.011501	3.26	3	0.000000	7.42	2	BRI3 binding protein	Extracellular Space	other
2.431	Q92882	OSTF1	0.000000	5.18	2	0.000000	8.74	1	osteoclast stimulating factor 1	Nucleus	transcription regulator
2.145	Q92900-2	UPF1	0.021696	2.88	4	0.000000	7.32	6	UPF1 regulator of nonsense transcripts homolog (yeast)	Nucleus	enzyme
-1.084	Q93084-6	ATP2A3	0.000000	16.04	9	0.000000	17.97	11	ATPase, Ca++ transporting, ubiquitous	Cytoplasm	transporter
-2.279	Q96HE7	ERO1L	0.000000	9.70	7	0.000000	8.97	5	ERO1-like (S. cerevisiae)	Cytoplasm	enzyme
-3.043	Q96NY7-2	CLIC6	0.000000	9.03	3	0.006396	3.88	2	chloride intracellular channel 6	Plasma Membrane	ion channel
2.652	Q96QK1	VPS35	0.002447	4.42	5	0.000000	10.22	10	vacuolar protein sorting 35 homolog (S. cerevisiae)	Cytoplasm	transporter
-1.384	Q99426	TBCB	0.002447	3.92	2	0.013478	3.35	2	tubulin folding cofactor B	Cytoplasm	other
-1.004	Q99456	KRT12	0.000000	5.82	4	0.000000	6.96	3	keratin 12	Cytoplasm	other
-1.812	Q99623	PHB2	0.000000	33.94	7	0.000000	39.93	9	prohibitin 2	Cytoplasm	transcription regulator
1.733	Q99714-2	HSD17B10	0.000000	8.87	2	0.000000	45.02	5	hydroxysteroid (17-beta) dehydrogenase 10	Cytoplasm	enzyme

Fold Change	UniProt ID	Symbol	TB-IRIS MM			TB-IRIS PP			Entrez Gene Name	Location	Type(s)
			q-value	Barista score	# of peptides	q-value	Barista score	# of peptides			
2.517	Q99829	CPNE1	0.002447	3.70	4	0.001741	4.75	4	copine I	unknown	transporter
-1.699	Q99832	CCT7	0.035702	2.63	2	0.000000	7.70	2	chaperonin containing TCP1, subunit 7 (eta)	Cytoplasm	other
5.037	Q9BSJ8-2	ESYT1	0.000000	5.70	7	0.000000	73.20	15	extended synaptotagmin-like protein 1	unknown	other
-1.371	Q9BUN8-2	DERL1	0.021696	2.84	3	0.000000	12.46	2	derlin 1	Cytoplasm	other
1.343	Q9BVC6	TMEM109	0.000000	7.01	1	0.000000	6.73	1	transmembrane protein 109	Cytoplasm	other
1.099	Q9H082	RAB33B	0.049129	2.37	1	0.022426	2.76	2	RAB33B, member RAS oncogene family	Cytoplasm	enzyme
1.539	Q9H0U4	RAB1B	0.000000	25.18	6	0.000000	42.83	7	RAB1B, member RAS oncogene family	Cytoplasm	other
1.235	Q9H223	EHD4	0.018039	3.09	4	0.041250	2.37	5	EH-domain containing 4	Plasma Membrane	enzyme
-1.100	Q9H2U2-2	PPA2	0.000000	5.38	3	0.000000	8.40	4	pyrophosphatase (inorganic) 2	Cytoplasm	enzyme
-1.718	Q9H3N1	TMX1	0.000000	5.78	4	0.000000	7.72	5	thioredoxin-related transmembrane protein 1	Cytoplasm	enzyme
1.733	Q9H3U1-2	UNC45A	0.009294	3.43	3	0.001741	5.33	2	unc-45 homolog A (C. elegans)	Plasma Membrane	other
-1.167	Q9H4B7	TUBB1	0.000000	22.27	12	0.000000	37.62	13	tubulin, beta 1 class VI	Cytoplasm	other
-1.097	Q9HBI1-2	PARVB	0.000000	24.01	6	0.000000	41.85	7	parvin, beta	Cytoplasm	other
6.640	Q9NQC3-2	RTN4	0.000000	5.25	3	0.000000	34.34	5	reticulon 4	Cytoplasm	other
1.367	Q9NR12-2	PDLIM7	0.019999	3.06	1	0.003380	4.09	2	PDZ and LIM domain 7 (enigma)	Cytoplasm	other
-1.482	Q9NR28-2	DIABLO	0.002447	4.41	1	0.001741	4.45	1	diablo, IAP-binding mitochondrial protein	Cytoplasm	other
1.211	Q9NR31	SAR1A	0.000000	5.22	2	0.001741	5.24	4	SAR1 homolog A (S. cerevisiae)	Cytoplasm	enzyme
1.263	Q9NZN3	EHD3	0.000000	13.77	5	0.000000	21.37	11	EH-domain containing 3	Cytoplasm	other
-1.502	Q9UBV8	PEF1	0.000000	8.54	2	0.022426	2.69	1	penta-EF-hand domain containing 1	Cytoplasm	other
-1.672	Q9UBW8	COPS7A	0.000000	9.05	2	0.001741	4.55	1	COP9 constitutive photomorphogenic homolog subunit 7A (Arabidopsis)	Cytoplasm	other
1.952	Q9UH99	SUN2	0.000000	7.81	4	0.000000	8.84	6	Sad1 and UNC84 domain containing 2	Nucleus	other
1.465	Q9UJZ1	STOML2	0.000000	6.31	2	0.000000	10.29	4	stomatin (EPB72)-like 2	Plasma Membrane	other
1.412	Q9UL46	PSME2	0.000000	11.62	4	0.000000	14.92	4	proteasome (prosome, macropain) activator subunit 2 (PA28 beta)	Cytoplasm	peptidase
1.978	Q9ULV4	CORO1C	0.000000	4.90	2	0.000000	23.16	9	coronin, actin binding protein, 1C	Cytoplasm	other
-2.321	Q9UQ80	PA2G4	0.000000	11.93	6	0.001741	4.72	4	proliferation-associated 2G4, 38kDa	Nucleus	transcription regulator

Fold Change	UniProt ID	Symbol	TB-IRIS MM			TB-IRIS PP			Entrez Gene Name	Location	Type(s)
			q-value	Barista score	# of peptides	q-value	Barista score	# of peptides			
-4.957	Q9Y230	RUVBL2	0.000000	4.84	4	0.040035	2.46	2	RuvB-like 2 (E. coli)	Nucleus	transcription regulator
1.119	Q9Y251	HPSE	0.000000	32.00	3	0.000000	37.03	3	heparanase	Plasma Membrane	enzyme
1.000	Q9Y277	VDAC3	0.000000	56.45	9	0.000000	76.54	9	voltage-dependent anion channel 3	Cytoplasm	ion channel
-1.357	Q9Y3A6	TMED5	0.002447	4.39	1	0.000000	7.78	2	transmembrane emp24 protein transport domain containing 5	Cytoplasm	other
1.094	Q9Y3Z3	SAMHD1	0.000000	16.44	13	0.000000	29.00	15	SAM domain and HD domain 1	Nucleus	enzyme
1.235	Q9Y490	TLN1	0.000000	196.63	66	0.000000	269.70	73	talin 1	Plasma Membrane	other
2.408	Q9Y4D1-2	DAAM1	0.000000	6.04	7	0.000000	6.78	4	dishevelled associated activator of morphogenesis 1	Cytoplasm	other
1.126	Q9Y6C9	MTCH2	0.000000	7.70	3	0.000000	7.23	5	mitochondrial carrier 2	Cytoplasm	other
-3.056	Q9Y6N5	SQRDL	0.000000	9.41	6	0.000000	8.17	8	sulfide quinone reductase-like (yeast)	Cytoplasm	enzyme

The TB-IRIS MP/MM paired dataset (Table 5.1) was generated using proteins commonly identified in the TB-IRIS PDE MP and the TB-IRIS PDE MM datasets (Table 4.2).

Fold Change	UniProt ID	Symbol	TB-IRIS MM			TB-IRIS MP			Entrez Gene Name	Location	Type(s)
			q-value	Barista score	# of peptides	q-value	Barista score	# of peptides			
1.105	A8KA46	RSU1	0	19.36	7	0	66.26	8	Ras suppressor protein 1	Cytoplasm	other
-4.312	F5H2R5	ARHGDIB	0	16.56	3	0	17.86	3	Rho GDP dissociation inhibitor (GDI) beta	Cytoplasm	other
-2.923	F8VZ49	HNRNPA1	0	10.28	3	0.003576	9.46	3	heterogeneous nuclear ribonucleoprotein A1	Nucleus	other
6.053	O00160	MYO1F	0	5.68	7	0	35.56	10	myosin IF	Cytoplasm	other
-1.269	O00194	RAB27B	0	23.4	5	0	67.87	6	RAB27B, member RAS oncogene family	Cytoplasm	enzyme
-1.506	O00264	PGRMC1	0	5.53	2	0	16.02	2	progesterone receptor membrane component 1	Plasma Membrane	transmembrane receptor
-1.045	O00299	CLIC1	0	35.82	9	0	75.8	10	chloride intracellular channel 1	Nucleus	ion channel
-1.553	O00303	EIF3F	0	10.98	2	0	55.53	2	eukaryotic translation initiation factor 3, subunit F	Cytoplasm	translation regulator
-1.485	O14579	COPE	0	4.97	1	0	17.16	2	coatomer protein complex, subunit epsilon	Cytoplasm	transporter
-3.338	O14656	TOR1A	0	8.2	2	0.00508	8.84	1	torsin family 1, member A (torsin A)	Cytoplasm	peptidase
-1.072	O14880	MGST3	0	8.26	1	0	46.59	2	microsomal glutathione S-transferase 3	Cytoplasm	enzyme
3.125	O14980	XPO1	0.002447	4.04	4	0	13.85	7	exportin 1 (CRM1 homolog, yeast)	Nucleus	transporter
-1.022	O15143	ARPC1B	0	14.17	4	0	41.84	4	actin related protein 2/3 complex, subunit 1B, 41kDa	Cytoplasm	other
1.508	O15144	ARPC2	0	12.17	7	0	58.86	7	actin related protein 2/3 complex, subunit 2, 34kDa	Cytoplasm	other
-1.451	O15173	PGRMC2	0	16.28	4	0	21.88	2	progesterone receptor membrane component 2	Nucleus	other
1.263	O43169	CYB5B	0.002447	4.11	1	0	30.95	3	cytochrome b5 type B (outer mitochondrial membrane)	Cytoplasm	enzyme
-1.060	O43306-2	ADCY6	0	10.01	2	0.001809	10.75	3	adenylate cyclase 6	Plasma Membrane	enzyme
-2.264	O43707	ACTN4	0	23.4	25	0	34.33	23	actinin, alpha 4	Cytoplasm	other
1.851	O60610-2	DIAPH1	0	9.05	9	0	49.19	9	diaphanous homolog 1 (Drosophila)	Plasma Membrane	other
1.600	O75083	WDR1	0	28.48	9	0	129.46	16	WD repeat domain 1	Extracellular Space	other
2.391	O75390	CS	0	5.52	2	0	46.71	8	citrate synthase	Cytoplasm	enzyme
1.296	O75396	SEC22B	0	8.06	2	0	23.3	1	SEC22 vesicle trafficking protein homolog B (S. cerevisiae) (gene/pseudogene)	Cytoplasm	other
1.228	O75489	NDUFS3	0	14.05	6	0	62.84	7	NADH dehydrogenase (ubiquinone) Fe-S protein 3, 30kDa (NADH-coenzyme Q reductase)	Cytoplasm	enzyme

Fold Change	UniProt ID	Symbol	TB-IRIS MM			TB-IRIS MP			Entrez Gene Name	Location	Type(s)
			q-value	Barista score	# of peptides	q-value	Barista score	# of peptides			
-1.494	O75558	STX11	0	21.58	5	0	37.86	2	syntaxin 11	Plasma Membrane	transporter
1.954	O75915	ARL6IP5	0	6.56	1	0	34.8	2	ADP-ribosylation-like factor 6 interacting protein 5	Cytoplasm	other
-2.949	O75947-2	ATP5H	0.002447	4.54	2	0.00508	8.82	2	ATP synthase, H+ transporting, mitochondrial Fo complex, subunit d	unknown	enzyme
4.694	O76074-2	PDE5A	0.002447	4.45	5	0	48.39	6	phosphodiesterase 5A, cGMP-specific	Cytoplasm	enzyme
-1.237	O94804	STK10	0.049129	2.37	2	0.015061	6.54	2	serine/threonine kinase 10	Cytoplasm	kinase
-1.694	O94826	TOMM70A	0.009294	3.29	2	0	14.98	3	translocase of outer mitochondrial membrane 70 homolog A (S. cerevisiae)	Cytoplasm	transporter
2.507	O94919	ENDOD1	0.037459	2.57	3	0	21.7	5	endonuclease domain containing 1	Extracellular Space	enzyme
-1.137	O95810	SDPR	0	8.86	4	0	41.71	4	serum deprivation response	Plasma Membrane	other
-1.589	O96008	TOMM40	0	5.51	2	0	22.27	3	translocase of outer mitochondrial membrane 40 homolog (yeast)	Cytoplasm	ion channel
-2.275	P00338	LDHA	0.002447	4.06	4	0	14.28	7	lactate dehydrogenase A	Cytoplasm	enzyme
-1.176	P00387-2	CYB5R3	0	15.76	6	0	36.3	5	cytochrome b5 reductase 3	Cytoplasm	enzyme
2.142	P00488	F13A1	0	12.55	13	0	83.55	17	coagulation factor XIII, A1 polypeptide	Extracellular Space	enzyme
2.055	P00558	PGK1	0	11.83	4	0	76.26	9	phosphoglycerate kinase 1	Cytoplasm	kinase
2.169	P01834	IGKC	0	6.8	1	0	56.8	3	immunoglobulin kappa constant	Extracellular Space	other
-1.718	P02042	HBD	0	10.44	6	0	19.39	4	hemoglobin, delta	Cytoplasm	transporter
-1.248	P02533	KRT14	0	45.1	12	0	124.83	12	keratin 14	Cytoplasm	other
1.236	P02647	APOA1	0	7.38	1	0	21.38	1	apolipoprotein A-I	Extracellular Space	transporter
-4.662	P02656	APOC3	0	9.81	1	0	25.7	1	apolipoprotein C-III	Extracellular Space	transporter
-1.028	P02671	FGA	0	19.28	9	0	53.16	10	fibrinogen alpha chain	Extracellular Space	other
-1.263	P02675	FGB	0	27.56	7	0	83.56	10	fibrinogen beta chain	Extracellular Space	other

Fold Change	UniProt ID	Symbol	TB-IRIS MM			TB-IRIS MP			Entrez Gene Name	Location	Type(s)
			q-value	Barista score	# of peptides	q-value	Barista score	# of peptides			
1.885	P02679-2	FGG	0	37.52	13	0	127.89	14	fibrinogen gamma chain	Extracellular Space	other
3.629	P02730	SLC4A1	0	17.15	4	0	175.39	12	solute carrier family 4, anion exchanger, member 1 (erythrocyte membrane protein band 3, Diego blood group)	Plasma Membrane	transporter
1.039	P02768	ALB	0	11.99	6	0	39.23	8	albumin	Extracellular Space	transporter
1.871	P02788	LTF	0	55.3	17	0	227.12	24	lactotransferrin	Extracellular Space	peptidase
1.955	P04004	VTN	0.002447	4.77	3	0	19.25	2	vitronectin	Extracellular Space	other
1.063	P04083	ANXA1	0	23.51	10	0	95.93	10	annexin A1	Plasma Membrane	other
1.234	P04259	KRT6B	0	11.62	12	0	43.81	13	keratin 6B	Cytoplasm	other
2.843	P04264	KRT1	0	162.77	25	0	493.16	23	keratin 1	Cytoplasm	other
-3.107	P04632	CAPNS1	0	8.72	2	0.024798	6.1	2	calpain, small subunit 1	Cytoplasm	peptidase
1.945	P04792	HSPB1	0.002447	4.22	2	0	13.92	2	heat shock 27kDa protein 1	Cytoplasm	other
1.949	P04843	RPN1	0	7.66	4	0	36.57	13	ribophorin I	Cytoplasm	enzyme
1.343	P04844	RPN2	0	15.9	4	0	62.68	6	ribophorin II	Cytoplasm	enzyme
-1.788	P05106	ITGB3	0	73.84	21	0	153.76	14	integrin, beta 3 (platelet glycoprotein IIIa, antigen CD61)	Plasma Membrane	transmembrane receptor
-2.827	P05107	ITGB2	0.021696	2.85	4	0	12.14	8	integrin, beta 2 (complement component 3 receptor 3 and 4 subunit)	Plasma Membrane	other
-3.301	P05109	S100A8	0	5.7	1	0.00664	8.21	1	S100 calcium binding protein A8	Cytoplasm	other
1.515	P05164-2	MPO	0	23.29	9	0	89.4	13	myeloperoxidase	Cytoplasm	enzyme
3.459	P05388	RPLP0	0	9.91	4	0	51.25	3	ribosomal protein, large, P0	Cytoplasm	other
1.316	P06576	ATP5B	0	34.75	8	0	82.71	13	ATP synthase, H+ transporting, mitochondrial F1 complex, beta polypeptide	Cytoplasm	transporter
1.015	P06733	ENO1	0	16.77	7	0	29.53	6	enolase 1, (alpha)	Cytoplasm	transcription regulator

Fold Change	UniProt ID	Symbol	TB-IRIS MM			TB-IRIS MP			Entrez Gene Name	Location	Type(s)
			q-value	Barista score	# of peptides	q-value	Barista score	# of peptides			
-4.733	P06753	TPM3	0	19.35	5	0.011276	7.82	4	tropomyosin 3	Cytoplasm	other
1.066	P07195	LDHB	0	10.83	5	0	29.21	4	lactate dehydrogenase B	Cytoplasm	enzyme
-1.144	P07237	P4HB	0	19.69	9	0	34.44	7	prolyl 4-hydroxylase, beta polypeptide	Cytoplasm	enzyme
-1.464	P07339	CTSD	0.004792	3.57	3	0.022195	6.3	3	cathepsin D	Cytoplasm	peptidase
1.035	P07355-2	ANXA2	0	13.49	10	0	69.25	9	annexin A2	Plasma Membrane	other
-4.856	P07359	GP1BA	0	5.11	4	0	17.75	6	glycoprotein Ib (platelet), alpha polypeptide	Plasma Membrane	other
1.034	P07384	CAPN1	0	19.47	12	0	70.98	15	calpain 1, (mu/I) large subunit	Cytoplasm	peptidase
1.000	P07437	TUBB	0	11.41	12	0	28.34	16	tubulin, beta class I	Cytoplasm	other
-1.295	P07900-2	HSP90AA1	0	14.26	14	0	44.45	18	heat shock protein 90kDa alpha (cytosolic), class A member 1	Cytoplasm	enzyme
1.879	P07996	THBS1	0	56.21	27	0	216.76	33	thrombospondin 1	Extracellular Space	other
-4.981	P08133	ANXA6	0	14.48	12	0.00508	8.77	8	annexin A6	Plasma Membrane	other
1.043	P08238	HSP90AB1	0	31.7	15	0	112.46	21	heat shock protein 90kDa alpha (cytosolic), class B member 1	Cytoplasm	enzyme
1.008	P08514	ITGA2B	0	215.17	19	0	610.57	27	integrin, alpha 2b (platelet glycoprotein IIb of IIb/IIIa complex, antigen CD41)	Plasma Membrane	transmembrane receptor
3.138	P08567	PLEK	0	17.41	6	0	72.12	7	pleckstrin	Cytoplasm	other
1.817	P08575-2	PTPRC	0	37.56	9	0	168.89	11	protein tyrosine phosphatase, receptor type, C	Plasma Membrane	phosphatase
-1.076	P08670	VIM	0	48.91	19	0	135.26	18	vimentin	Cytoplasm	other
-3.605	P08758	ANXA5	0	14.31	6	0	19.01	4	annexin A5	Plasma Membrane	other
-1.267	P08779	KRT16	0	8.85	12	0	52.93	13	keratin 16	Cytoplasm	other
-2.283	P08865	RPSA	0	7.53	4	0	20.14	2	ribosomal protein SA	Cytoplasm	translation regulator
-2.986	P09211	GSTP1	0	15.35	3	0	30.16	3	glutathione S-transferase pi 1	Cytoplasm	enzyme
-1.496	P0CG47	UBB	0	6.18	2	0	15.51	2	ubiquitin B	Cytoplasm	enzyme

Fold Change	UniProt ID	Symbol	TB-IRIS MM			TB-IRIS MP			Entrez Gene Name	Location	Type(s)
			q-value	Barista score	# of peptides	q-value	Barista score	# of peptides			
-1.528	P10768	ESD	0	5.83	3	0.02569	5.83	1	esterase D	Cytoplasm	enzyme
2.595	P10809	HSPD1	0	12	5	0	112.42	14	heat shock 60kDa protein 1 (chaperonin)	Cytoplasm	enzyme
2.149	P10909-2	CLU	0	6.18	3	0	40.38	7	clusterin	Extracellular Space	other
-1.710	P11021	HSPA5	0	49.38	16	0	96.12	16	heat shock 70kDa protein 5 (glucose-regulated protein, 78kDa)	Cytoplasm	enzyme
1.090	P11142	HSPA8	0	13.56	16	0	163.94	19	heat shock 70kDa protein 8	Cytoplasm	enzyme
1.313	P11169	SLC2A3	0.002447	4.25	2	0	11.48	3	solute carrier family 2 (facilitated glucose transporter), member 3	Plasma Membrane	transporter
2.209	P11215	ITGAM	0	9.84	7	0	84.3	14	integrin, alpha M (complement component 3 receptor 3 subunit)	Plasma Membrane	other
6.235	P11216	PYGB	0	9.89	9	0	65.23	15	phosphorylase, glycogen; brain	Cytoplasm	enzyme
1.347	P11310-2	ACADM	0	4.89	3	0	34.51	3	acyl-CoA dehydrogenase, C-4 to C-12 straight chain	Cytoplasm	enzyme
-1.081	P11678	EPX	0	11.15	8	0	38.46	10	eosinophil peroxidase	Cytoplasm	enzyme
1.538	P12236	SLC25A6	0	18.14	6	0	62.25	5	solute carrier family 25 (mitochondrial carrier; adenine nucleotide translocator), member 6	Cytoplasm	transporter
-2.012	P12259	F5	0	8.72	6	0	26.86	11	coagulation factor V (proaccelerin, labile factor)	Plasma Membrane	enzyme
-2.271	P12429	ANXA3	0	11.53	5	0	20.76	4	annexin A3	Cytoplasm	enzyme
-1.815	P12814	ACTN1	0	91.53	33	0	212.92	31	actinin, alpha 1	Cytoplasm	other
1.410	P12931-2	SRC	0	9.68	6	0	44.71	7	v-src sarcoma (Schmidt-Ruppin A-2) viral oncogene homolog (avian)	Cytoplasm	kinase
1.840	P12956	XRCC6	0.002447	4.27	9	0	17.24	3	X-ray repair complementing defective repair in Chinese hamster cells 6	Nucleus	enzyme
1.079	P13010	XRCC5	0.002447	4.76	4	0	28.27	5	X-ray repair complementing defective repair in Chinese hamster cells 5 (double-strand-break rejoining)	Nucleus	enzyme
-2.266	P13224-2	GP1BB	0	16.11	6	0	35.54	5	glycoprotein Ib (platelet), beta polypeptide	Plasma Membrane	other
-1.208	P13489	RNH1	0	8.86	6	0	29.52	7	ribonuclease/angiogenin inhibitor 1	Cytoplasm	other
1.659	P13639	EEF2	0	10.56	8	0	83.23	10	eukaryotic translation elongation factor 2	Cytoplasm	translation regulator
1.233	P13645	KRT10	0	174.18	20	0	561.8	22	keratin 10	Cytoplasm	other
-1.023	P13647	KRT5	0	39.43	15	0	111.18	17	keratin 5	Cytoplasm	other

Fold Change	UniProt ID	Symbol	TB-IRIS MM			TB-IRIS MP			Entrez Gene Name	Location	Type(s)
			q-value	Barista score	# of peptides	q-value	Barista score	# of peptides			
-5.685	P13667	PDIA4	0	13.06	7	0	19.55	6	protein disulfide isomerase family A, member 4	Cytoplasm	enzyme
-1.372	P13796	LCP1	0	17.66	18	0	50.17	10	lymphocyte cytosolic protein 1 (L-plastin)	Cytoplasm	other
1.071	P13804	ETFA	0	23.33	6	0	67.42	7	electron-transfer-flavoprotein, alpha polypeptide	Cytoplasm	transporter
-1.478	P14222	PRF1	0	5.42	3	0	32.31	3	perforin 1 (pore forming protein)	Cytoplasm	other
-6.531	P14314	PRKCSH	0	14.21	6	0.00664	8.24	1	protein kinase C substrate 80K-H	Cytoplasm	enzyme
1.679	P14618	PKM	0	37.93	12	0	156.46	19	pyruvate kinase, muscle	unknown	kinase
1.335	P14625	HSP90B1	0	13.73	10	0	84.32	15	heat shock protein 90kDa beta (Grp94), member 1	Cytoplasm	other
-1.584	P14770	GP9	0	5.31	4	0	18.73	3	glycoprotein IX (platelet)	Plasma Membrane	other
1.735	P14780	MMP9	0	7.13	5	0	77.28	8	matrix metallopeptidase 9 (gelatinase B, 92kDa gelatinase, 92kDa type IV collagenase)	Extracellular Space	peptidase
-1.078	P15153	RAC2	0	10.24	4	0	24.56	3	ras-related C3 botulinum toxin substrate 2 (rho family, small GTP binding protein Rac2)	Cytoplasm	enzyme
1.902	P15498	VAV1	0.002447	4.63	3	0	47.11	3	vav 1 guanine nucleotide exchange factor	Nucleus	transcription regulator
1.984	P16109	SELP	0	11.72	2	0	67.4	7	selectin P (granule membrane protein 140kDa, antigen CD62)	Plasma Membrane	other
2.874	P16284-2	PECAM1	0.007133	3.51	3	0	22.36	7	platelet/endothelial cell adhesion molecule 1	Plasma Membrane	other
1.063	P17066	HSPA6	0.002447	3.78	9	0.001809	10.29	6	heat shock 70kDa protein 6 (HSP70B')	unknown	other
3.359	P17612-2	PRKACA	0	5.09	3	0	18.43	3	protein kinase, cAMP-dependent, catalytic, alpha	Cytoplasm	kinase
1.070	P17655	CAPN2	0.002447	3.73	3	0	19.06	6	calpain 2, (m/II) large subunit	Cytoplasm	peptidase
-1.192	P17987	TCP1	0.002447	4.37	4	0	18.12	7	t-complex 1	Cytoplasm	other
-1.444	P18124	RPL7	0.009294	3.31	2	0.02569	6	4	ribosomal protein L7	Nucleus	transcription regulator
1.435	P18206-2	VCL	0	41.05	23	0	211.57	34	vinculin	Plasma Membrane	enzyme
1.347	P18669	PGAM1	0.004792	3.52	2	0	19.85	3	phosphoglycerate mutase 1 (brain)	Cytoplasm	phosphatase
-3.023	P20160	AZU1	0	5	2	0.012475	7.18	3	azurocidin 1	Cytoplasm	peptidase
-1.027	P21266	GSTM3	0	9.5	3	0	25.69	3	glutathione S-transferase mu 3 (brain)	Cytoplasm	enzyme

Fold Change	UniProt ID	Symbol	TB-IRIS MM			TB-IRIS MP			Entrez Gene Name	Location	Type(s)
			q-value	Barista score	# of peptides	q-value	Barista score	# of peptides			
1.263	P21333-2	FLNA	0	192.02	64	0	685.25	92	filamin A, alpha	Cytoplasm	other
-1.153	P21796	VDAC1	0	44.22	8	0	108.74	9	voltage-dependent anion channel 1	Cytoplasm	ion channel
1.418	P22314	UBA1	0	12.75	11	0	56.51	10	ubiquitin-like modifier activating enzyme 1	Cytoplasm	enzyme
1.224	P22626-2	HNRNPA2B1	0	18.05	4	0	18.52	5	heterogeneous nuclear ribonucleoprotein A2/B1	Nucleus	other
-1.301	P22894	MMP8	0	15.9	3	0	69.94	6	matrix metallopeptidase 8 (neutrophil collagenase)	Extracellular Space	peptidase
3.052	P23219-2	PTGS1	0.043607	2.44	3	0	62.95	9	prostaglandin-endoperoxide synthase 1 (prostaglandin G/H synthase and cyclooxygenase)	Cytoplasm	enzyme
-2.697	P23396	RPS3	0	13.41	4	0	31.44	5	ribosomal protein S3	Cytoplasm	enzyme
1.124	P23528	CFL1	0	21.31	2	0	54.88	2	cofilin 1 (non-muscle)	Nucleus	other
-1.452	P24539	ATP5F1	0.018039	3.11	3	0.040507	5	2	ATP synthase, H+ transporting, mitochondrial Fo complex, subunit B1	Cytoplasm	transporter
1.013	P25705	ATP5A1	0	46.86	16	0	117.29	16	ATP synthase, H+ transporting, mitochondrial F1 complex, alpha subunit 1, cardiac muscle	Cytoplasm	transporter
-2.997	P25788-2	PSMA3	0	6.92	3	0	16.9	2	proteasome (prosome, macropain) subunit, alpha type, 3	Cytoplasm	peptidase
-1.143	P26038	MSN	0	29.04	17	0	66.6	12	moesin	Plasma Membrane	other
-1.614	P26641	EEF1G	0	13.9	6	0	28.03	6	eukaryotic translation elongation factor 1 gamma	Cytoplasm	translation regulator
-1.195	P27105	STOM	0	48.32	7	0	133.76	11	stomatin	Plasma Membrane	other
1.346	P27338	MAOB	0.021696	2.86	2	0	32.11	5	monoamine oxidase B	Cytoplasm	enzyme
-1.083	P27348	YWHAQ	0	23.88	8	0	49.76	7	tyrosine 3-monooxygenase/tryptophan 5-monooxygenase activation protein, theta polypeptide	Cytoplasm	other
-1.016	P27797	CALR	0.002447	4.09	3	0	11.66	3	calreticulin	Cytoplasm	transcription regulator
1.162	P27824	CANX	0	54.2	7	0	154.81	7	calnexin	Cytoplasm	other
2.998	P28331	NDUFS1	0	5.48	4	0	61.8	11	NADH dehydrogenase (ubiquinone) Fe-S protein 1, 75kDa (NADH-coenzyme Q reductase)	Cytoplasm	enzyme
1.283	P28676	GCA	0	9.18	1	0	28.25	1	grancalcin, EF-hand calcium binding protein	Cytoplasm	other
-1.025	P30041	PRDX6	0	13.41	5	0	14.75	3	peroxiredoxin 6	Cytoplasm	enzyme
1.098	P30048	PRDX3	0	17.17	3	0	47.1	3	peroxiredoxin 3	Cytoplasm	enzyme

Fold Change	UniProt ID	Symbol	TB-IRIS MM			TB-IRIS MP			Entrez Gene Name	Location	Type(s)
			q-value	Barista score	# of peptides	q-value	Barista score	# of peptides			
1.985	P30084	ECHS1	0	4.82	2	0	41.88	4	enoyl CoA hydratase, short chain, 1, mitochondrial	Cytoplasm	enzyme
-1.102	P30101	PDIA3	0	9.62	8	0	31.92	10	protein disulfide isomerase family A, member 3	Cytoplasm	peptidase
3.081	P30153	PPP2R1A	0	10.94	6	0	72.99	8	protein phosphatase 2, regulatory subunit A, alpha	Cytoplasm	phosphatase
1.118	P31040	SDHA	0	5.75	2	0	14.91	5	succinate dehydrogenase complex, subunit A, flavoprotein (Fp)	Cytoplasm	enzyme
1.933	P31146	CORO1A	0	29.74	7	0	127.93	12	coronin, actin binding protein, 1A	Cytoplasm	other
1.000	P31150	GDI1	0	7.26	6	0.001809	10.88	5	GDP dissociation inhibitor 1	Cytoplasm	other
1.390	P31937	HIBADH	0.002447	4.38	2	0	16.81	2	3-hydroxyisobutyrate dehydrogenase	Cytoplasm	enzyme
-1.465	P31946-2	YWHAB	0	22.81	9	0	53.25	9	tyrosine 3-monooxygenase/tryptophan 5-monooxygenase activation protein, beta polypeptide	Cytoplasm	transcription regulator
1.239	P33947-2	KDELR2	0.011501	3.28	2	0	13.98	2	KDEL (Lys-Asp-Glu-Leu) endoplasmic reticulum protein retention receptor 2	Cytoplasm	other
-1.021	P35232	PHB	0	29.02	7	0	86.65	10	prohibitin	Nucleus	transcription regulator
1.192	P35527	KRT9	0	142.55	15	0	464.54	20	keratin 9	Cytoplasm	other
1.270	P35579	MYH9	0	144.29	50	0	437.72	65	myosin, heavy chain 9, non-muscle	Cytoplasm	transporter
1.322	P35606	COPB2	0	6.84	8	0	20.13	11	coatomer protein complex, subunit beta 2 (beta prime)	Cytoplasm	transporter
-1.070	P35908	KRT2	0	65.47	20	0	196.98	24	keratin 2	Cytoplasm	other
-1.927	P37802	TAGLN2	0	14.22	3	0	17.08	3	transgelin 2	Cytoplasm	other
-3.025	P37837	TALDO1	0	26.11	6	0	13.56	2	transaldolase 1	Cytoplasm	enzyme
1.986	P38117-2	ETFB	0.043607	2.39	2	0	38.47	4	electron-transfer-flavoprotein, beta polypeptide	Cytoplasm	transporter
1.729	P38646	HSPA9	0	26.7	9	0	91.05	11	heat shock 70kDa protein 9 (mortalin)	Cytoplasm	other
1.502	P39656	DDOST	0	8.77	5	0	55.46	6	dolichyl-diphosphooligosaccharide–protein glycosyltransferase	Cytoplasm	enzyme
-1.698	P40197	GP5	0	8.53	2	0.012475	7.48	3	glycoprotein V (platelet)	Plasma Membrane	other
4.246	P40227	CCT6A	0	5.07	3	0	25.7	6	chaperonin containing TCP1, subunit 6A (zeta 1)	Cytoplasm	other
-1.556	P40926	MDH2	0	6.91	4	0.02569	5.96	5	malate dehydrogenase 2, NAD (mitochondrial)	Cytoplasm	enzyme
2.179	P40939	HADHA	0	8.39	2	0	70.74	9	hydroxyacyl-CoA dehydrogenase/3-ketoacyl-CoA thiolase/enoyl-CoA hydratase (trifunctional protein), alpha subunit	Cytoplasm	enzyme
-1.692	P41091	EIF2S3	0.004792	3.62	3	0.00508	9.32	1	eukaryotic translation initiation factor 2, subunit 3 gamma, 52kDa	Cytoplasm	translation regulator

Fold Change	UniProt ID	Symbol	TB-IRIS MM			TB-IRIS MP			Entrez Gene Name	Location	Type(s)
			q-value	Barista score	# of peptides	q-value	Barista score	# of peptides			
-3.236	P41218	MNDA	0	6.61	4	0.029517	5.6	2	myeloid cell nuclear differentiation antigen	Nucleus	transcription regulator
-1.035	P42224-2	STAT1	0	11.87	7	0	44.77	8	signal transducer and activator of transcription 1, 91kDa	Nucleus	transcription regulator
-1.482	P42574	CASP3	0	4.9	3	0.00664	8.24	1	caspase 3, apoptosis-related cysteine peptidase	Cytoplasm	peptidase
-1.070	P45880-1	VDAC2	0	17.56	7	0	107.9	9	voltage-dependent anion channel 2	Cytoplasm	ion channel
2.794	P46940	IQGAP1	0	8.01	15	0	51.27	17	IQ motif containing GTPase activating protein 1	Cytoplasm	other
-3.715	P47755	CAPZA2	0	11.25	3	0	12.25	1	capping protein (actin filament) muscle Z-line, alpha 2	Cytoplasm	other
1.185	P47756-2	CAPZB	0	12.57	3	0	33.62	5	capping protein (actin filament) muscle Z-line, beta	Cytoplasm	other
1.988	P48047	ATP5O	0	7.57	3	0	44.48	5	ATP synthase, H+ transporting, mitochondrial F1 complex, O subunit	Cytoplasm	transporter
1.274	P48059	LIMS1	0	15.78	8	0	63.09	9	LIM and senescent cell antigen-like domains 1	Plasma Membrane	other
-1.572	P48426	PIP4K2A	0	10.67	5	0.001809	10.23	3	phosphatidylinositol-5-phosphate 4-kinase, type II, alpha	Cytoplasm	kinase
-1.488	P48507	GCLM	0.009294	3.43	3	0	11.47	1	glutamate-cysteine ligase, modifier subunit	Cytoplasm	enzyme
-1.581	P48643	CCT5	0	6.58	7	0	19.65	6	chaperonin containing TCP1, subunit 5 (epsilon)	Cytoplasm	other
2.803	P48735	IDH2	0	18.79	6	0	95.32	15	isocitrate dehydrogenase 2 (NADP+), mitochondrial	Cytoplasm	enzyme
11.269	P49327	FASN	0.007133	3.44	8	0	60.56	14	fatty acid synthase	Cytoplasm	enzyme
-1.428	P49368-2	CCT3	0.002447	4.44	4	0	16.31	5	chaperonin containing TCP1, subunit 3 (gamma)	Cytoplasm	other
2.003	P49407-2	ARRB1	0.002447	4.25	3	0.026828	5.65	4	arrestin, beta 1	Cytoplasm	other
1.713	P49748-2	ACADVL	0	7.31	6	0	50.93	11	acyl-CoA dehydrogenase, very long chain	Cytoplasm	enzyme
3.360	P50148	GNAQ	0	9	2	0	26.64	5	guanine nucleotide binding protein (G protein), q polypeptide	Plasma Membrane	enzyme
1.589	P50226	SULT1A2	0	7.86	3	0	15.98	6	sulfotransferase family, cytosolic, 1A, phenol-preferring, member 2	Cytoplasm	enzyme
-1.617	P50990	CCT8	0	11.91	9	0	39.54	10	chaperonin containing TCP1, subunit 8 (theta)	Cytoplasm	enzyme
1.619	P50991	CCT4	0.002447	4.2	2	0	45.74	7	chaperonin containing TCP1, subunit 4 (delta)	Cytoplasm	other
1.274	P51148	RAB5C	0	7.26	2	0	30.89	6	RAB5C, member RAS oncogene family	Cytoplasm	enzyme
-1.136	P51149	RAB7A	0	19.18	6	0	53.02	6	RAB7A, member RAS oncogene family	Cytoplasm	enzyme
-1.594	P51452	DUSP3	0	9.34	1	0	22.93	4	dual specificity phosphatase 3	Cytoplasm	phosphatase
1.046	P52597	HNRNPF	0	13.42	4	0	36.3	3	heterogeneous nuclear ribonucleoprotein F	Nucleus	other
-1.192	P52907	CAPZA1	0.002447	4.34	3	0	44.75	5	capping protein (actin filament) muscle Z-line, alpha 1	Cytoplasm	other

Fold Change	UniProt ID	Symbol	TB-IRIS MM			TB-IRIS MP			Entrez Gene Name	Location	Type(s)
			q-value	Barista score	# of peptides	q-value	Barista score	# of peptides			
-1.576	P53597	SUCLG1	0	4.89	1	0	11	5	succinate-CoA ligase, alpha subunit	Cytoplasm	enzyme
-1.575	P53801	PTTG1IP	0.002447	4.27	1	0.00508	8.65	1	pituitary tumor-transforming 1 interacting protein	Nucleus	other
-1.203	P54920	NAPA	0	14.46	6	0	52.84	9	N-ethylmaleimide-sensitive factor attachment protein, alpha	Cytoplasm	transporter
1.953	P55072	VCP	0	12.56	7	0	59.25	11	valosin containing protein	Cytoplasm	enzyme
-3.125	P55084	HADHB	0	5.48	5	0.00664	8.29	9	hydroxyacyl-CoA dehydrogenase/3-ketoacyl-CoA thiolase/enoyl-CoA hydratase (trifunctional protein), beta subunit	Cytoplasm	enzyme
1.214	P55160	NCKAP1L	0	9.8	7	0	41.08	9	NCK-associated protein 1-like	Plasma Membrane	other
-3.198	P55212	CASP6	0	4.81	3	0.024798	6.12	1	caspase 6, apoptosis-related cysteine peptidase	Cytoplasm	peptidase
2.001	P60842	EIF4A1	0.002447	4.57	5	0	26.46	9	eukaryotic translation initiation factor 4A1	Cytoplasm	translation regulator
4.239	P60953	CDC42	0.009294	3.3	3	0	34.52	4	cell division cycle 42 (GTP binding protein, 25kDa)	Cytoplasm	enzyme
-2.262	P61006	RAB8A	0	8.72	3	0	36.92	4	RAB8A, member RAS oncogene family	Plasma Membrane	other
-1.632	P61026	RAB10	0	12.4	5	0	41.77	7	RAB10, member RAS oncogene family	Cytoplasm	enzyme
-1.936	P61106	RAB14	0.002447	4.7	4	0	18.84	5	RAB14, member RAS oncogene family	Cytoplasm	enzyme
1.004	P61158	ACTR3	0	15.41	4	0	73.7	8	ARP3 actin-related protein 3 homolog (yeast)	Plasma Membrane	other
-1.545	P61160	ACTR2	0	25.61	5	0	60.72	7	ARP2 actin-related protein 2 homolog (yeast)	Plasma Membrane	other
2.614	P61163	ACTR1A	0.009294	3.34	3	0	25.62	5	ARP1 actin-related protein 1 homolog A, centractin alpha (yeast)	Cytoplasm	other
-3.070	P61204	ARF3	0	7.81	4	0.001809	10.77	2	ADP-ribosylation factor 3	Cytoplasm	enzyme
-1.269	P61224	RAP1B	0	32.01	9	0	77.3	6	RAP1B, member of RAS oncogene family	Cytoplasm	enzyme
-1.070	P61225	RAP2B	0	7.81	1	0	21.45	1	RAP2B, member of RAS oncogene family	Plasma Membrane	enzyme
-1.460	P61247	RPS3A	0	7.49	2	0	15.93	3	ribosomal protein S3A	Cytoplasm	other
-2.258	P61586	RHOA	0	18.93	4	0	38.14	5	ras homolog family member A	Cytoplasm	enzyme
3.083	P61978-2	HNRNPK	0.004792	3.63	5	0	35.63	7	heterogeneous nuclear ribonucleoprotein K	Nucleus	other
1.634	P61981	YWHAG	0	12.72	5	0	60.11	7	tyrosine 3-monooxygenase/tryptophan 5-monooxygenase activation protein, gamma polypeptide	Cytoplasm	other

Fold Change	UniProt ID	Symbol	TB-IRIS MM			TB-IRIS MP			Entrez Gene Name	Location	Type(s)
			q-value	Barista score	# of peptides	q-value	Barista score	# of peptides			
-1.763	P62491	RAB11A	0	20.33	7	0	52.5	5	RAB11A, member RAS oncogene family	Cytoplasm	enzyme
2.010	P62714	PPP2CB	0	6.24	2	0	24.78	2	protein phosphatase 2, catalytic subunit, beta isozyme	Cytoplasm	phosphatase
-1.642	P62826	RAN	0	16.58	6	0	38.05	4	RAN, member RAS oncogene family	Nucleus	enzyme
1.226	P62873	GNB1	0	18.25	3	0	39.58	4	guanine nucleotide binding protein (G protein), beta polypeptide 1	Plasma Membrane	enzyme
2.567	P62937	PPIA	0.002447	4.2	2	0.003576	9.52	2	peptidylprolyl isomerase A (cyclophilin A)	Cytoplasm	enzyme
-1.504	P63104	YWHAZ	0	58.83	9	0	142.3	9	tyrosine 3-monooxygenase/tryptophan 5-monooxygenase activation protein, zeta polypeptide	Cytoplasm	enzyme
1.428	P63244	GNB2L1	0.002447	3.81	3	0.003576	9.48	6	guanine nucleotide binding protein (G protein), beta polypeptide 2-like 1	Cytoplasm	enzyme
1.509	P68366	TUBA4A	0	46.1	13	0	56.49	11	tubulin, alpha 4a	Cytoplasm	other
1.160	P68371	TUBB4B	0	37.31	12	0	117.64	14	tubulin, beta 4B class IVb	Cytoplasm	other
1.000	P68871	HBB	0	29.65	8	0	54.66	5	hemoglobin, beta	Cytoplasm	transporter
-1.565	P78417	GSTO1	0	8.69	4	0	16.75	3	glutathione S-transferase omega 1	Cytoplasm	enzyme
1.346	P80188-2	LCN2	0	22.44	2	0	41	3	lipocalin 2	Extracellular Space	transporter
1.715	P81605	DCD	0	11	2	0	16.9	2	dermcidin	Extracellular Space	other
-1.200	Q00325-2	SLC25A3	0	6.68	4	0	13.59	6	solute carrier family 25 (mitochondrial carrier; phosphate carrier), member 3	Cytoplasm	transporter
2.868	Q00610-2	CLTC	0	60.86	18	0	457.06	43	clathrin, heavy chain (Hc)	Plasma Membrane	other
1.720	Q00839-2	HNRNPU	0	13.59	5	0	53.5	6	heterogeneous nuclear ribonucleoprotein U (scaffold attachment factor A)	Nucleus	transporter
1.000	Q01518-2	CAP1	0	18.88	9	0	49.81	8	CAP, adenylate cyclase-associated protein 1 (yeast)	Plasma Membrane	other
1.635	Q01813	PFKP	0	13.06	8	0	65.77	9	phosphofructokinase, platelet	Cytoplasm	kinase
-2.957	Q02978	SLC25A11	0	11.27	5	0	27.72	6	solute carrier family 25 (mitochondrial carrier; oxoglutarate carrier), member 11	Cytoplasm	transporter

Fold Change	UniProt ID	Symbol	TB-IRIS MM			TB-IRIS MP			Entrez Gene Name	Location	Type(s)
			q-value	Barista score	# of peptides	q-value	Barista score	# of peptides			
-1.167	Q04917	YWHAH	0	26.47	11	0	60.35	9	tyrosine 3-monooxygenase/tryptophan 5-monooxygenase activation protein, eta polypeptide	Cytoplasm	transcription regulator
-2.648	Q06323	PSME1	0	19.46	7	0	28.13	7	proteasome (prosome, macropain) activator subunit 1 (PA28 alpha)	Cytoplasm	other
-1.154	Q07021	C1QBP	0	13.85	5	0	33.31	8	complement component 1, q subcomponent binding protein	Cytoplasm	other
2.482	Q07960	ARHGAP1	0.002447	4.16	2	0	19.41	4	Rho GTPase activating protein 1	Cytoplasm	other
-1.201	Q08211	DHX9	0.002447	4.6	9	0	15.82	9	DEAH (Asp-Glu-Ala-His) box polypeptide 9	Nucleus	enzyme
-1.664	Q08AF3	SLFN5	0.021696	2.84	3	0	14.69	4	schlafen family member 5	Nucleus	enzyme
2.679	Q10567-2	AP1B1	0	7.06	4	0	23.21	9	adaptor-related protein complex 1, beta 1 subunit	Cytoplasm	transporter
2.579	Q13201	MMRN1	0	22.53	16	0	166.03	26	multimerin 1	Extracellular Space	other
1.660	Q13637	RAB32	0	7.98	5	0	45.45	7	RAB32, member RAS oncogene family	Cytoplasm	other
1.568	Q14141-2	SEPT6	0	5.89	5	0.001809	10.45	2	septin 6	Cytoplasm	other
-2.052	Q14165	MLEC	0	19.29	5	0	25.74	2	malectin	Plasma Membrane	other
-1.856	Q14697-2	GANAB	0	9.22	6	0	20.5	8	glucosidase, alpha; neutral AB	Cytoplasm	enzyme
1.972	Q14739	LBR	0	10.64	4	0	31.57	4	lamin B receptor	Nucleus	enzyme
5.798	Q14766	LTBP1	0	4.8	6	0	52.86	9	latent transforming growth factor beta binding protein 1	Extracellular Space	other
1.170	Q14974	KPNB1	0	11.51	7	0	52.04	8	karyopherin (importin) beta 1	Nucleus	transporter
-1.405	Q15005	SPCS2	0.042544	2.45	1	0.012475	7.13	1	signal peptidase complex subunit 2 homolog (S. cerevisiae)	Cytoplasm	other
1.600	Q15019-2	SEPT2	0	8.41	5	0	36.13	4	septin 2	Cytoplasm	enzyme
1.222	Q15084-2	PDIA6	0	9.49	6	0	44.06	6	protein disulfide isomerase family A, member 6	Cytoplasm	enzyme
4.288	Q15233	NONO	0.002447	4.45	3	0	16.79	4	non-POU domain containing, octamer-binding	Nucleus	other
-7.450	Q16666-2	IFI16	0	9.03	5	0.034306	5.39	4	interferon, gamma-inducible protein 16	Nucleus	transcription regulator
-1.551	Q16698	DECR1	0	8.73	2	0	12.37	5	2,4-dienoyl CoA reductase 1, mitochondrial	Cytoplasm	enzyme
-3.229	Q16762	TST	0	8.74	4	0.033329	5.45	4	thiosulfate sulfurtransferase (rhodanese)	Cytoplasm	enzyme
-1.560	Q16795	NDUFA9	0	5.12	5	0.00508	9.1	4	NADH dehydrogenase (ubiquinone) 1 alpha subcomplex, 9, 39kDa	Cytoplasm	enzyme
1.108	Q1KMD3	HNRNPUL2	0.023587	2.79	1	0	17.95	3	heterogeneous nuclear ribonucleoprotein U-like 2	Nucleus	other
5.562	Q27J81-2	INF2	0	6.21	7	0	37.14	8	inverted formin, FH2 and WH2 domain containing	Cytoplasm	other

Fold Change	UniProt ID	Symbol	TB-IRIS MM			TB-IRIS MP			Entrez Gene Name	Location	Type(s)
			q-value	Barista score	# of peptides	q-value	Barista score	# of peptides			
3.492	Q53GQ0	HSD17B12	0	6.7	4	0	25.07	5	hydroxysteroid (17-beta) dehydrogenase 12	Cytoplasm	enzyme
1.420	Q562R1	ACTBL2	0.011501	3.26	6	0	12.21	7	actin, beta-like 2	unknown	other
1.016	Q6UX06	OLFM4	0	18.8	3	0	44.88	4	olfactomedin 4	Extracellular Space	other
2.567	Q70J99-3	UNC13D	0	14.13	5	0	126.7	19	unc-13 homolog D (C. elegans)	Cytoplasm	other
1.269	Q71U36	TUBA1A	0	85.26	13	0	38.31	12	tubulin, alpha 1a	Cytoplasm	other
-1.478	Q7Z3Y8	KRT27	0.043607	2.4	3	0.026828	5.66	3	keratin 27	unknown	other
-1.431	Q7Z4W1	DCXR	0	10.94	2	0.035468	5.22	2	dicarbonyl/L-xylulose reductase	Cytoplasm	enzyme
1.393	Q86UX7-2	FERMT3	0	99.21	27	0	272.37	28	fermitin family member 3	Cytoplasm	enzyme
-2.247	Q86VP6-2	CAND1	0	7.03	6	0	20.32	10	cullin-associated and neddylation-dissociated 1	Cytoplasm	transcription regulator
1.139	Q8IXQ6-2	PARP9	0.047469	2.38	4	0	14.21	4	poly (ADP-ribose) polymerase family, member 9	Nucleus	other
-2.886	Q8N392-2	ARHGAP18	0.002447	3.77	2	0	11.09	5	Rho GTPase activating protein 18	Cytoplasm	other
-5.049	Q8NBS9	TXNDC5	0	5.15	2	0.00508	9.42	4	thioredoxin domain containing 5 (endoplasmic reticulum)	Cytoplasm	enzyme
-1.210	Q8TC12	RDH11	0	12.05	4	0	42.74	5	retinol dehydrogenase 11 (all-trans/9-cis/11-cis)	Cytoplasm	enzyme
-1.341	Q8TEM1	NUP210	0.002447	4.59	5	0	22.72	10	nucleoporin 210kDa	Nucleus	transporter
-1.529	Q8TF42	UBASH3B	0	6.68	2	0	17.5	8	ubiquitin associated and SH3 domain containing B	unknown	enzyme
-1.429	Q8WY22	BRI3BP	0.011501	3.26	3	0.001809	9.83	2	BRI3 binding protein	Extracellular Space	other
-1.470	Q92882	OSTF1	0	5.18	2	0.012475	7.22	1	osteoclast stimulating factor 1	Nucleus	transcription regulator
2.467	Q96QK1	VPS35	0.002447	4.42	5	0	24.97	5	vacuolar protein sorting 35 homolog (S. cerevisiae)	Cytoplasm	transporter
-2.002	Q99456	KRT12	0	5.82	4	0	12.11	4	keratin 12	Cytoplasm	other
-2.997	-2.997	Q99623	PHB2	0	33.94	7	0	49.81	5	prohibitin 2	Cytoplasm
1.631	Q99714-2	HSD17B10	0	8.87	2	0	59.93	5	hydroxysteroid (17-beta) dehydrogenase 10	Cytoplasm	enzyme
1.870	Q99829	CPNE1	0.002447	3.7	4	0.008111	8.09	4	copine I	unknown	transporter
1.875	Q99832	CCT7	0.035702	2.63	2	0	30.79	6	chaperonin containing TCP1, subunit 7 (eta)	Cytoplasm	other
1.299	Q9BR76	CORO1B	0	5.24	2	0	16.09	3	coronin, actin binding protein, 1B	Cytoplasm	other
8.118	Q9BSJ8-2	ESYT1	0	5.7	7	0	152.72	13	extended synaptotagmin-like protein 1	unknown	other
1.334	Q9BTT0	ANP32E	0	5.51	3	0	42.03	2	acidic (leucine-rich) nuclear phosphoprotein 32 family, member E	Nucleus	other

Fold Change	UniProt ID	Symbol	TB-IRIS MM			TB-IRIS MP			Entrez Gene Name	Location	Type(s)
			q-value	Barista score	# of peptides	q-value	Barista score	# of peptides			
1.281	Q9BUL8	PDCD10	0.021696	2.93	3	0.001809	10.54	2	programmed cell death 10	Cytoplasm	other
-1.423	Q9BVC6	TMEM109	0	7.01	1	0	11.78	1	transmembrane protein 109	Cytoplasm	other
-5.651	Q9H082	RAB33B	0.049129	2.37	1	0.02569	6.07	4	RAB33B, member RAS oncogene family	Cytoplasm	enzyme
1.225	Q9H2U2-2	PPA2	0	5.38	3	0	27.49	4	pyrophosphatase (inorganic) 2	Cytoplasm	enzyme
-1.568	Q9H3N1	TMX1	0	5.78	4	0	13.59	2	thioredoxin-related transmembrane protein 1	Cytoplasm	enzyme
-1.399	Q9H3U1-2	UNC45A	0.009294	3.43	3	0	14.43	5	unc-45 homolog A (C. elegans)	Plasma Membrane	other
-1.103	Q9H4B7	TUBB1	0	22.27	12	0	136.94	18	tubulin, beta 1 class VI	Cytoplasm	other
-3.319	Q9H9B4	SFXN1	0	5.36	4	0	14.63	3	sideroflexin 1	Cytoplasm	transporter
-1.487	Q9NR31	SAR1A	0	5.22	2	0	11.8	2	SAR1 homolog A (S. cerevisiae)	Cytoplasm	enzyme
-1.209	Q9NYU2-2	UGGT1	0	9.38	6	0	16.77	7	UDP-glucose glycoprotein glucosyltransferase 1	Cytoplasm	enzyme
2.213	Q9NZN3	EHD3	0	13.77	5	0	77.41	13	EH-domain containing 3	Cytoplasm	other
-1.581	Q9UBW8	COPS7A	0	9.05	2	0	18.53	1	COP9 constitutive photomorphogenic homolog subunit 7A (Arabidopsis)	Cytoplasm	other
2.284	Q9UH99	SUN2	0	7.81	4	0	47.66	8	Sad1 and UNC84 domain containing 2	Nucleus	other
1.404	Q9UJZ1	STOML2	0	6.31	2	0	26.61	3	stomatin (EPB72)-like 2	Plasma Membrane	other
4.301	Q9ULV4	CORO1C	0	4.9	2	0	56.8	6	coronin, actin binding protein, 1C	Cytoplasm	other
-1.405	Q9UM22	EPDR1	0.042544	2.47	1	0.015061	6.77	1	ependymin related protein 1 (zebrafish)	Nucleus	other
-1.498	Q9Y251	HPSE	0	32	3	0	49.71	3	heparanase	Plasma Membrane	enzyme
1.161	Q9Y277	VDAC3	0	56.45	9	0	135.22	9	voltage-dependent anion channel 3	Cytoplasm	ion channel
-1.397	Q9Y3A6	TMED5	0.002447	4.39	1	0	16.88	2	transmembrane emp24 protein transport domain containing 5	Cytoplasm	other
1.177	Q9Y3Z3	SAMHD1	0	16.44	13	0	56.44	13	SAM domain and HD domain 1	Nucleus	enzyme
1.454	Q9Y490	TLN1	0	196.63	66	0	745.47	88	talin 1	Plasma Membrane	other
4.259	Q9Y4D1-2	DAAM1	0	6.04	7	0	27.52	4	dishevelled associated activator of morphogenesis 1	Cytoplasm	other
1.930	Q9Y6C9	MTCH2	0	7.7	3	0	27.39	4	mitochondrial carrier 2	Cytoplasm	other
-2.925	Q9Y6N5	SQRDL	0	9.41	6	0	25.85	5	sulfide quinone reductase-like (yeast)	Cytoplasm	enzyme

The TBART PP/MM paired dataset (Table 5.1) was generated using proteins commonly identified in the TBART PDE PP and the TBART PDE MM datasets (Table 4.2).

Fold Change	UniProt ID	Symbol	TBART MM			TBART MP			Entrez Gene Name	Location	Type(s)
			q-value	Barista score	# of peptides	q-value	Barista score	# of peptides			
2.395	A0AVT1	UBA6	0.014640	3.29	4	0.012851	3.97	3	ubiquitin-like modifier activating enzyme 6	Cytoplasm	enzyme
-1.457	A0FGR8-2	ESYT2	0.000000	7.32	4	0.000000	9.20	4	extended synaptotagmin-like protein 2	unknown	other
1.141	A8KA46	RSU1	0.000000	9.51	6	0.009618	4.28	5	Ras suppressor protein 1	Cytoplasm	other
1.032	B0I1T2	MYO1G	0.000000	24.36	12	0.000000	19.67	15	myosin IG	Cytoplasm	other
-2.676	B7Z7R3	LIMS1	0.000000	16.06	5	0.000000	7.46	4	LIM and senescent cell antigen-like domains 1	Plasma Membrane	other
1.064	C9JCP4	RNF213	0.000000	62.86	34	0.000000	40.08	31	ring finger protein 213	Plasma Membrane	enzyme
-1.299	D6RF44	HNRNPD	0.000000	10.75	2	0.000000	12.83	4	heterogeneous nuclear ribonucleoprotein D (AU-rich element RNA binding protein 1, 37kDa)	Nucleus	transcription regulator
-2.855	E7EVX7	ANK1	0.000000	11.04	14	0.006367	4.80	9	ankyrin 1, erythrocytic	Plasma Membrane	other
-1.355	G5E977	NAPRT1	0.006650	4.85	6	0.048162	2.48	4	nicotinate phosphoribosyltransferase domain containing 1	Cytoplasm	enzyme
2.246	G5E9T1	ATL1	0.018882	3.18	3	0.000000	6.71	1	atlastin GTPase 1	Cytoplasm	enzyme
1.124	O00148	DDX39A	0.000000	16.01	5	0.000000	18.14	8	DEAD (Asp-Glu-Ala-Asp) box polypeptide 39A	Nucleus	enzyme
-1.037	O00160	MYO1F	0.000000	15.10	12	0.000000	15.16	8	myosin IF	Cytoplasm	other
1.051	O00194	RAB27B	0.000000	22.28	4	0.000000	18.16	4	RAB27B, member RAS oncogene family	Cytoplasm	enzyme
2.325	O00264	PGRMC1	0.002034	7.04	2	0.002257	6.18	1	progesterone receptor membrane component 1	Plasma Membrane	transmembrane receptor
1.046	O00299	CLIC1	0.000000	53.43	12	0.000000	36.11	10	chloride intracellular channel 1	Nucleus	ion channel
-1.797	O00303	EIF3F	0.000000	42.52	4	0.000000	35.60	1	eukaryotic translation initiation factor 3, subunit F	Cytoplasm	translation regulator
1.124	O00629	KPNA4	0.000000	9.10	1	0.000000	8.47	1	karyopherin alpha 4 (importin alpha 3)	Nucleus	transporter
1.349	O14974-2	PPP1R12A	0.006650	4.91	2	0.025928	3.14	1	protein phosphatase 1, regulatory subunit 12A	Cytoplasm	phosphatase
-1.697	O15143	ARPC1B	0.000000	23.21	3	0.000000	9.62	5	actin related protein 2/3 complex, subunit 1B, 41kDa	Cytoplasm	other
1.538	O15144	ARPC2	0.000000	19.63	9	0.000000	21.59	8	actin related protein 2/3 complex, subunit 2, 34kDa	Cytoplasm	other
1.089	O15173	PGRMC2	0.000000	19.12	4	0.000000	19.03	2	progesterone receptor membrane component 2	Nucleus	other
-1.754	O15260-2	SURF4	0.000000	11.35	1	0.000000	8.78	3	surfeit 4	Cytoplasm	other
1.038	O15533-2	TAPBP	0.002034	6.67	2	0.019350	3.65	2	TAP binding protein (tapasin)	Cytoplasm	transporter

Fold Change	UniProt ID	Symbol	TBART MM			TBART MP			Entrez Gene Name	Location	Type(s)
			q-value	Barista score	# of peptides	q-value	Barista score	# of peptides			
4.697	O43143	DHX15	0.002034	6.80	6	0.000000	10.84	7	DEAH (Asp-Glu-Ala-His) box polypeptide 15	Nucleus	enzyme
-1.717	O43169	CYB5B	0.000000	12.05	2	0.000000	9.85	1	cytochrome b5 type B (outer mitochondrial membrane)	Cytoplasm	enzyme
1.070	O43390-2	HNRNPR	0.003707	5.58	4	0.002257	6.03	4	heterogeneous nuclear ribonucleoprotein R	Nucleus	other
2.271	O43488	AKR7A2	0.005398	5.13	2	0.000000	10.70	3	aldo-keto reductase family 7, member A2 (aflatoxin aldehyde reductase)	Cytoplasm	enzyme
1.183	O43598-2	C6orf108	0.003707	6.08	1	0.011400	4.05	2	chromosome 6 open reading frame 108	Nucleus	other
1.015	O43670-2	ZNF207	0.036614	2.74	2	0.007994	4.60	1	zinc finger protein 207	Nucleus	transcription regulator
-1.056	O43707	ACTN4	0.000000	22.50	23	0.000000	15.83	17	actinin, alpha 4	Cytoplasm	other
-2.669	O43809	NUDT21	0.000000	11.83	2	0.002257	5.83	3	nudix (nucleoside diphosphate linked moiety X)-type motif 21	Nucleus	other
1.636	O60610-2	DIAPH1	0.000000	10.09	8	0.000000	13.36	8	diaphanous homolog 1 (Drosophila)	Plasma Membrane	other
1.210	O60814	HIST1H2BJ/HIST1H2BK	0.003707	5.87	5	0.016108	3.72	5	histone cluster 1, H2bk	Nucleus	other
-1.112	O75083	WDR1	0.000000	48.49	15	0.000000	32.87	15	WD repeat domain 1	Extracellular Space	other
-1.327	O75131	CPNE3	0.003707	5.20	4	0.006367	4.84	5	copine III	Cytoplasm	kinase
1.801	O75367-3	H2AFY	0.000000	11.25	5	0.000000	10.75	4	H2A histone family, member Y	Nucleus	other
1.140	O75390	CS	0.006650	4.68	4	0.007994	4.52	3	citrate synthase	Cytoplasm	enzyme
1.191	O75396	SEC22B	0.000000	12.42	2	0.000000	10.50	1	SEC22 vesicle trafficking protein homolog B (S. cerevisiae) (gene/pseudogene)	Cytoplasm	other
-1.188	O75489	NDUFS3	0.000000	31.56	8	0.000000	16.61	5	NADH dehydrogenase (ubiquinone) Fe-S protein 3, 30kDa (NADH-coenzyme Q reductase)	Cytoplasm	enzyme
1.086	O75558	STX11	0.003707	5.52	2	0.000000	6.81	2	syntaxin 11	Plasma Membrane	transporter
-1.799	O75643	SNRNP200	0.000000	18.81	14	0.000000	6.89	10	small nuclear ribonucleoprotein 200kDa (U5)	Nucleus	enzyme
-1.370	O75746	SLC25A12	0.000000	12.86	5	0.000000	11.23	3	solute carrier family 25 (aspartate/glutamate carrier), member 12	Cytoplasm	transporter
1.113	O75844	ZMPSTE24	0.000000	8.16	1	0.000000	11.12	1	zinc metallopeptidase STE24 homolog (S. cerevisiae)	Nucleus	peptidase
-1.090	O76074-2	PDE5A	0.000000	15.08	7	0.000000	10.71	6	phosphodiesterase 5A, cGMP-specific	Cytoplasm	enzyme
-1.422	O94804	STK10	0.000000	16.61	4	0.009618	4.13	4	serine/threonine kinase 10	Cytoplasm	kinase
1.000	O95674	CDS2	0.000000	12.00	3	0.000000	12.07	2	CDP-diacylglycerol synthase (phosphatidate cytidylyltransferase) 2	Cytoplasm	enzyme

Fold Change	UniProt ID	Symbol	TBART MM			TBART MP			Entrez Gene Name	Location	Type(s)
			q-value	Barista score	# of peptides	q-value	Barista score	# of peptides			
1.537	O95810	SDPR	0.000000	16.92	2	0.000000	16.79	5	serum deprivation response	Plasma Membrane	other
2.330	P00387-2	CYB5R3	0.007598	4.11	3	0.002257	5.24	4	cytochrome b5 reductase 3	Cytoplasm	enzyme
1.150	P00403	COX2	0.007598	3.64	2	0.043071	2.58	1	cytochrome c oxidase subunit II	Cytoplasm	enzyme
1.042	P00488	F13A1	0.000000	30.36	13	0.000000	22.40	7	coagulation factor XIII, A1 polypeptide	Extracellular Space	enzyme
-2.008	P00558	PGK1	0.000000	33.93	7	0.000000	21.10	5	phosphoglycerate kinase 1	Cytoplasm	kinase
3.624	P01040	CSTA	0.000000	10.85	1	0.000000	22.50	2	cystatin A (stefin A)	Cytoplasm	other
-1.791	P01137	TGFB1	0.000000	13.05	4	0.000000	10.58	4	transforming growth factor, beta 1	Extracellular Space	growth factor
1.619	P01834	IGKC	0.000000	23.61	4	0.000000	11.77	2	immunoglobulin kappa constant	Extracellular Space	other
1.065	P01857	IGHG1	0.000000	7.96	4	0.020562	3.56	1	immunoglobulin heavy constant gamma 1 (G1m marker)	Extracellular Space	other
1.109	P01911	HLA-DRB1	0.048737	2.59	3	0.023174	3.32	3	major histocompatibility complex, class II, DR beta 1	Plasma Membrane	transmembrane receptor
1.278	P02533	KRT14	0.000000	61.48	12	0.000000	58.26	16	keratin 14	Cytoplasm	other
-1.711	P02549-2	SPTA1	0.000000	9.28	16	0.032493	2.84	11	spectrin, alpha, erythrocytic 1 (elliptocytosis 2)	Cytoplasm	other
1.596	P02656	APOC3	0.000000	9.10	2	0.000000	12.20	1	apolipoprotein C-III	Extracellular Space	transporter
-1.269	P02671-2	FGA	0.000000	31.39	8	0.000000	21.29	8	fibrinogen alpha chain	Extracellular Space	other
1.381	P02675	FGB	0.000000	30.17	8	0.000000	46.83	10	fibrinogen beta chain	Extracellular Space	other
1.052	P02730	SLC4A1	0.000000	184.55	16	0.000000	142.50	13	solute carrier family 4, anion exchanger, member 1 (erythrocyte membrane protein band 3, Diego blood group)	Plasma Membrane	transporter
-2.450	P02768	ALB	0.000000	14.45	8	0.000000	15.02	8	albumin	Extracellular Space	transporter
1.183	P02775	PPBP	0.032934	2.82	2	0.027452	3.08	3	pro-platelet basic protein (chemokine (C-X-C motif) ligand 7)	Extracellular Space	cytokine

Fold Change	UniProt ID	Symbol	TBART MM			TBART MP			Entrez Gene Name	Location	Type(s)
			q-value	Barista score	# of peptides	q-value	Barista score	# of peptides			
1.540	P02788	LTF	0.000000	14.20	7	0.000000	24.31	7	lactotransferrin	Extracellular Space	peptidase
1.114	P04004	VTN	0.000000	11.52	2	0.000000	6.87	3	vitronectin	Extracellular Space	other
2.211	P04083	ANXA1	0.000000	7.79	5	0.000000	13.89	5	annexin A1	Plasma Membrane	other
7.080	P04114	APOB	0.007598	3.92	21	0.002257	5.17	21	apolipoprotein B (including Ag(x) antigen)	Extracellular Space	transporter
1.142	P04179	SOD2	0.000000	7.79	1	0.020562	3.52	2	superoxide dismutase 2, mitochondrial	Cytoplasm	enzyme
-1.254	P04264	KRT1	0.000000	223.04	25	0.000000	209.23	23	keratin 1	Cytoplasm	other
1.677	P04275	VWF	0.000000	11.32	11	0.000000	10.27	15	von Willebrand factor	Extracellular Space	other
1.000	P04406	GAPDH	0.000000	38.21	6	0.000000	25.19	6	glyceraldehyde-3-phosphate dehydrogenase	Cytoplasm	enzyme
1.112	P04632	CAPNS1	0.000000	9.37	2	0.009618	4.31	2	calpain, small subunit 1	Cytoplasm	peptidase
-1.872	P04839	CYBB	0.000000	12.33	5	0.020562	3.50	2	cytochrome b-245, beta polypeptide	Cytoplasm	enzyme
1.181	P04843	RPN1	0.000000	43.84	16	0.000000	40.60	12	ribophorin I	Cytoplasm	enzyme
1.103	P04844	RPN2	0.000000	42.01	7	0.000000	43.60	8	ribophorin II	Cytoplasm	enzyme
-1.109	P04899	GNAI2	0.000000	26.20	7	0.000000	28.44	7	guanine nucleotide binding protein (G protein), alpha inhibiting activity polypeptide 2	Plasma Membrane	enzyme
1.213	P05106	ITGB3	0.000000	46.88	13	0.000000	41.59	12	integrin, beta 3 (platelet glycoprotein IIIa, antigen CD61)	Plasma Membrane	transmembrane receptor
2.238	P05107	ITGB2	0.043655	2.62	7	0.006367	4.85	8	integrin, beta 2 (complement component 3 receptor 3 and 4 subunit)	Plasma Membrane	other
-1.839	P05109	S100A8	0.002034	6.58	1	0.002257	5.96	2	S100 calcium binding protein A8	Cytoplasm	other
-1.428	P05141	SLC25A5	0.002034	6.11	6	0.000000	17.18	10	solute carrier family 25 (mitochondrial carrier; adenine nucleotide translocator), member 5	Cytoplasm	transporter
1.274	P05164-2	MPO	0.000000	24.64	13	0.000000	18.11	9	myeloperoxidase	Cytoplasm	enzyme
1.067	P05388	RPLP0	0.003707	5.54	2	0.002257	5.50	3	ribosomal protein, large, P0	Cytoplasm	other

Fold Change	UniProt ID	Symbol	TBART MM			TBART MP			Entrez Gene Name	Location	Type(s)
			q-value	Barista score	# of peptides	q-value	Barista score	# of peptides			
1.880	P06576	ATP5B	0.000000	43.37	9	0.000000	54.60	11	ATP synthase, H+ transporting, mitochondrial F1 complex, beta polypeptide	Cytoplasm	transporter
2.720	P06733	ENO1	0.000000	7.78	7	0.000000	16.93	6	enolase 1, (alpha)	Cytoplasm	transcription regulator
1.365	P07195	LDHB	0.000000	12.40	3	0.000000	12.96	4	lactate dehydrogenase B	Cytoplasm	enzyme
-1.025	P07237	P4HB	0.000000	21.59	7	0.000000	20.60	6	prolyl 4-hydroxylase, beta polypeptide	Cytoplasm	enzyme
-1.797	P07355-2	ANXA2	0.006650	4.45	7	0.002257	6.56	7	annexin A2	Plasma Membrane	other
-1.146	P07384	CAPN1	0.000000	28.81	10	0.000000	13.44	8	calpain 1, (mu/I) large subunit	Cytoplasm	peptidase
-1.203	P07437	TUBB	0.000000	55.57	13	0.000000	59.35	13	tubulin, beta class I	Cytoplasm	other
2.258	P07737	PFN1	0.000000	9.84	3	0.000000	12.74	2	profilin 1	Cytoplasm	other
-1.206	P07900-2	HSP90AA1	0.000000	38.04	18	0.000000	29.62	20	heat shock protein 90kDa alpha (cytosolic), class A member 1	Cytoplasm	enzyme
-1.199	P07996	THBS1	0.000000	68.35	22	0.000000	55.07	23	thrombospondin 1	Extracellular Space	other
1.384	P08133	ANXA6	0.000000	13.09	12	0.000000	16.49	11	annexin A6	Plasma Membrane	other
-1.039	P08238	HSP90AB1	0.000000	66.89	20	0.000000	57.23	20	heat shock protein 90kDa alpha (cytosolic), class B member 1	Cytoplasm	enzyme
-1.722	P08567	PLEK	0.000000	30.87	6	0.000000	18.90	6	pleckstrin	Cytoplasm	other
-2.677	P08574	CYC1	0.000000	13.98	4	0.028277	3.06	1	cytochrome c-1	Cytoplasm	enzyme
1.116	P08670	VIM	0.000000	50.82	17	0.000000	47.48	18	vimentin	Cytoplasm	other
2.261	P08758	ANXA5	0.003707	5.51	1	0.002257	5.75	3	annexin A5	Plasma Membrane	other
1.391	P08779	KRT16	0.000000	15.96	13	0.000000	9.60	13	keratin 16	Cytoplasm	other
1.575	P08865	RPSA	0.000000	19.64	5	0.000000	17.03	6	ribosomal protein SA	Cytoplasm	translation regulator
-1.711	P09211	GSTP1	0.000000	9.37	3	0.014572	3.81	2	glutathione S-transferase pi 1	Cytoplasm	enzyme
1.751	P0CG47	UBB	0.002034	6.32	3	0.000000	8.81	4	ubiquitin B	Cytoplasm	enzyme
1.056	P10619	CTSA	0.000000	9.74	1	0.000000	12.77	1	cathepsin A	Cytoplasm	peptidase
1.376	P10809	HSPD1	0.000000	42.85	9	0.000000	43.50	10	heat shock 60kDa protein 1 (chaperonin)	Cytoplasm	enzyme

Fold Change	UniProt ID	Symbol	TBART MM			TBART MP			Entrez Gene Name	Location	Type(s)
			q-value	Barista score	# of peptides	q-value	Barista score	# of peptides			
1.158	P11021	HSPA5	0.000000	29.91	12	0.000000	44.04	11	heat shock 70kDa protein 5 (glucose-regulated protein, 78kDa)	Cytoplasm	enzyme
1.034	P11142	HSPA8	0.000000	51.69	13	0.000000	57.48	16	heat shock 70kDa protein 8	Cytoplasm	enzyme
1.077	P11177-2	PDHB	0.000000	12.81	3	0.000000	10.19	3	pyruvate dehydrogenase (lipoamide) beta	Cytoplasm	enzyme
1.059	P11216	PYGB	0.000000	23.95	10	0.000000	15.39	11	phosphorylase, glycogen; brain	Cytoplasm	enzyme
1.835	P11277-2	SPTB	0.000000	11.30	13	0.000000	13.06	12	spectrin, beta, erythrocytic	Plasma Membrane	other
5.270	P11310-2	ACADM	0.007598	4.23	5	0.000000	17.79	4	acyl-CoA dehydrogenase, C-4 to C-12 straight chain	Cytoplasm	enzyme
1.586	P11586	MTHFD1	0.002034	6.78	5	0.000000	9.42	4	methylenetetrahydrofolate dehydrogenase (NADP+ dependent) 1, methenyltetrahydrofolate cyclohydrolase, formyltetrahydrofolate synthetase	Cytoplasm	enzyme
1.068	P11678	EPX	0.000000	18.82	7	0.000000	14.25	6	eosinophil peroxidase	Cytoplasm	enzyme
-1.027	P12814	ACTN1	0.000000	103.97	29	0.000000	77.79	30	actinin, alpha 1	Cytoplasm	other
-1.742	P12931-2	SRC	0.000000	12.29	10	0.019350	3.64	4	v-src sarcoma (Schmidt-Ruppin A-2) viral oncogene homolog (avian)	Cytoplasm	kinase
2.167	P13489	RNH1	0.006650	4.49	3	0.006367	4.74	2	ribonuclease/angiogenin inhibitor 1	Cytoplasm	other
1.160	P13498	CYBA	0.025344	2.97	1	0.043071	2.57	1	cytochrome b-245, alpha polypeptide	Cytoplasm	enzyme
1.049	P13639	EEF2	0.000000	32.24	13	0.000000	29.87	14	eukaryotic translation elongation factor 2	Cytoplasm	translation regulator
1.000	P13645	KRT10	0.000000	213.31	21	0.000000	225.24	20	keratin 10	Cytoplasm	other
1.677	P13647	KRT5	0.000000	32.77	11	0.000000	35.48	11	keratin 5	Cytoplasm	other
-1.151	P13667	PDIA4	0.000000	15.56	5	0.007994	4.60	5	protein disulfide isomerase family A, member 4	Cytoplasm	enzyme
1.111	P13796	LCP1	0.000000	26.96	13	0.000000	26.34	13	lymphocyte cytosolic protein 1 (L-plastin)	Cytoplasm	other
-2.057	P13804	ETFA	0.000000	37.64	8	0.000000	22.09	4	electron-transfer-flavoprotein, alpha polypeptide	Cytoplasm	transporter
1.516	P14222	PRF1	0.000000	13.07	6	0.000000	17.98	6	perforin 1 (pore forming protein)	Cytoplasm	other
-1.392	P14314	PRKCSH	0.000000	23.34	3	0.000000	11.94	4	protein kinase C substrate 80K-H	Cytoplasm	enzyme
-1.457	P14618	PKM	0.000000	57.00	15	0.000000	38.90	13	pyruvate kinase, muscle	unknown	kinase
1.145	P14625	HSP90B1	0.000000	25.37	12	0.000000	17.67	14	heat shock protein 90kDa beta (Grp94), member 1	Cytoplasm	other
1.068	P14866	HNRNPL	0.000000	10.44	6	0.002257	5.57	4	heterogeneous nuclear ribonucleoprotein L	Nucleus	other
2.176	P14868	DARS	0.003707	5.65	3	0.023174	3.26	3	aspartyl-tRNA synthetase	Cytoplasm	enzyme

Fold Change	UniProt ID	Symbol	TBART MM			TBART MP			Entrez Gene Name	Location	Type(s)
			q-value	Barista score	# of peptides	q-value	Barista score	# of peptides			
2.176	P14868	DARS	0.003707	5.65	3	0.023174	3.26	3	aspartyl-tRNA synthetase	Cytoplasm	enzyme
3.319	P15153	RAC2	0.003707	5.20	3	0.000000	13.12	6	ras-related C3 botulinum toxin substrate 2 (rho family, small GTP binding protein Rac2)	Cytoplasm	enzyme
-1.430	P15311	EZR	0.000000	8.89	7	0.000000	12.68	9	ezrin	Plasma Membrane	other
1.016	P15498	VAV1	0.000000	20.07	8	0.000000	18.35	3	vav 1 guanine nucleotide exchange factor	Nucleus	transcription regulator
-1.104	P16615-2	ATP2A2	0.000000	8.08	9	0.000000	12.45	5	ATPase, Ca++ transporting, cardiac muscle, slow twitch 2	Cytoplasm	transporter
-1.824	P17655	CAPN2	0.000000	16.97	11	0.012851	3.96	5	calpain 2, (m/II) large subunit	Cytoplasm	peptidase
-2.223	P17844	DDX5	0.002034	6.23	8	0.007994	4.46	4	DEAD (Asp-Glu-Ala-Asp) box helicase 5	Nucleus	enzyme
2.242	P17987	TCP1	0.006650	4.39	7	0.002257	5.64	8	t-complex 1	Cytoplasm	other
2.171	P18054	ALOX12	0.018882	3.18	4	0.007994	4.44	6	arachidonate 12-lipoxygenase	Cytoplasm	enzyme
-1.300	P18085	ARF4	0.006650	4.61	3	0.002257	5.73	3	ADP-ribosylation factor 4	Cytoplasm	enzyme
2.351	P18124	RPL7	0.003707	5.77	2	0.000000	7.18	4	ribosomal protein L7	Nucleus	transcription regulator
1.107	P18206-2	VCL	0.000000	56.24	23	0.000000	40.69	21	vinculin	Plasma Membrane	enzyme
-1.791	P19367-2	HK1	0.000000	32.58	10	0.000000	17.06	8	hexokinase 1	Cytoplasm	kinase
1.113	P19878	NCF2	0.000000	7.68	5	0.000000	9.23	4	neutrophil cytosolic factor 2	Cytoplasm	enzyme
-1.482	P20700	LMNB1	0.000000	15.42	7	0.000000	11.86	10	lamin B1	Nucleus	other
-1.675	P21266	GSTM3	0.006650	4.82	2	0.016108	3.72	1	glutathione S-transferase mu 3 (brain)	Cytoplasm	enzyme
-1.103	P21333-2	FLNA	0.000000	312.88	82	0.000000	277.55	80	filamin A, alpha	Cytoplasm	other
1.041	P21796	VDAC1	0.000000	52.81	11	0.000000	35.04	8	voltage-dependent anion channel 1	Cytoplasm	ion channel
1.355	P22314	UBA1	0.000000	24.49	15	0.000000	25.79	14	ubiquitin-like modifier activating enzyme 1	Cytoplasm	enzyme
1.229	P22626	HNRNPA2B1	0.000000	13.81	6	0.000000	8.98	5	heterogeneous nuclear ribonucleoprotein A2/B1	Nucleus	other
-2.777	P22695	UQCRC2	0.000000	33.44	7	0.000000	20.33	4	ubiquinol-cytochrome c reductase core protein II	Cytoplasm	enzyme
1.639	P23219-2	PTGS1	0.000000	24.57	5	0.000000	22.83	4	prostaglandin-endoperoxide synthase 1 (prostaglandin G/H synthase and cyclooxygenase)	Cytoplasm	enzyme
-1.129	P23246	SFPQ	0.000000	53.64	9	0.000000	36.27	6	splicing factor proline/glutamine-rich	Nucleus	other

Fold Change	UniProt ID	Symbol	TBART MM			TBART MP			Entrez Gene Name	Location	Type(s)
			q-value	Barista score	# of peptides	q-value	Barista score	# of peptides			
-1.478	P23396	RPS3	0.000000	28.03	7	0.000000	14.42	4	ribosomal protein S3	Cytoplasm	enzyme
1.051	P23528	CFL1	0.000000	32.82	4	0.000000	40.26	5	cofilin 1 (non-muscle)	Nucleus	other
-1.908	P24539	ATP5F1	0.000000	34.88	5	0.000000	18.65	5	ATP synthase, H+ transporting, mitochondrial Fo complex, subunit B1	Cytoplasm	transporter
1.286	P25205	MCM3	0.031799	2.83	4	0.028277	2.99	6	minichromosome maintenance complex component 3	Nucleus	enzyme
1.619	P25705	ATP5A1	0.000000	65.12	12	0.000000	58.16	15	ATP synthase, H+ transporting, mitochondrial F1 complex, alpha subunit 1, cardiac muscle	Cytoplasm	transporter
-2.306	P25789	PSMA4	0.000000	8.56	4	0.020562	3.49	1	proteasome (prosome, macropain) subunit, alpha type, 4	Cytoplasm	peptidase
1.468	P26038	MSN	0.000000	27.79	12	0.000000	30.15	14	moesin	Plasma Membrane	other
-2.124	P26368-2	U2AF2	0.003707	5.94	3	0.023174	3.43	4	U2 small nuclear RNA auxiliary factor 2	Nucleus	other
-1.895	P26641	EEF1G	0.000000	10.73	4	0.041990	2.66	3	eukaryotic translation elongation factor 1 gamma	Cytoplasm	translation regulator
1.020	P27105	STOM	0.000000	42.36	9	0.000000	36.30	9	stomatin	Plasma Membrane	other
-1.134	P27338	MAOB	0.000000	19.32	6	0.000000	19.35	6	monoamine oxidase B	Cytoplasm	enzyme
-1.637	P27348	YWHAQ	0.000000	37.85	8	0.000000	33.61	6	tyrosine 3-monooxygenase/tryptophan 5-monooxygenase activation protein, theta polypeptide	Cytoplasm	other
1.014	P27797	CALR	0.020239	3.16	2	0.009618	4.30	3	calreticulin	Cytoplasm	transcription regulator
1.322	P27824	CANX	0.000000	69.33	6	0.000000	75.48	7	calnexin	Cytoplasm	other
1.117	P28331	NDUFS1	0.000000	13.76	7	0.000000	15.23	8	NADH dehydrogenase (ubiquinone) Fe-S protein 1, 75kDa (NADH-coenzyme Q reductase)	Cytoplasm	enzyme
2.158	P29350-3	PTPN6	0.000000	21.31	15	0.000000	28.84	15	protein tyrosine phosphatase, non-receptor type 6	Cytoplasm	phosphatase
-3.570	P30041	PRDX6	0.002034	6.47	2	0.002257	5.84	2	peroxiredoxin 6	Cytoplasm	enzyme
2.316	P30048	PRDX3	0.006650	4.74	3	0.014572	3.83	2	peroxiredoxin 3	Cytoplasm	enzyme
-4.664	P30084	ECHS1	0.000000	32.89	5	0.000000	10.86	4	enoyl CoA hydratase, short chain, 1, mitochondrial	Cytoplasm	enzyme
1.956	P30101	PDIA3	0.000000	14.41	8	0.000000	16.28	10	protein disulfide isomerase family A, member 3	Cytoplasm	peptidase
-1.690	P31040	SDHA	0.000000	26.26	7	0.000000	17.90	8	succinate dehydrogenase complex, subunit A, flavoprotein (Fp)	Cytoplasm	enzyme
1.243	P31146	CORO1A	0.000000	50.95	9	0.000000	33.26	7	coronin, actin binding protein, 1A	Cytoplasm	other

Fold Change	UniProt ID	Symbol	TBART MM			TBART MP			Entrez Gene Name	Location	Type(s)
			q-value	Barista score	# of peptides	q-value	Barista score	# of peptides			
-1.008	P31150	GDI1	0.038981	2.69	4	0.002257	6.57	5	GDP dissociation inhibitor 1	Cytoplasm	other
-1.748	P31930	UQCRC1	0.000000	8.53	3	0.000000	11.61	5	ubiquinol-cytochrome c reductase core protein I	Cytoplasm	enzyme
-1.250	P31942-2	HNRNPH3	0.000000	16.97	3	0.000000	6.83	3	heterogeneous nuclear ribonucleoprotein H3 (2H9)	Nucleus	other
-1.510	P31943	HNRNPH1	0.000000	32.26	6	0.000000	22.69	4	heterogeneous nuclear ribonucleoprotein H1 (H)	Nucleus	other
-3.760	P31946-2	YWHAB	0.000000	48.24	10	0.023174	3.36	6	tyrosine 3-monooxygenase/tryptophan 5-monooxygenase activation protein, beta polypeptide	Cytoplasm	transcription regulator
1.038	P31948	STIP1	0.013368	3.45	3	0.045530	2.54	5	stress-induced-phosphoprotein 1	Cytoplasm	other
2.317	P32969	RPL9	0.000000	9.31	1	0.002257	5.29	2	ribosomal protein L9	Cytoplasm	other
1.780	P35232	PHB	0.000000	22.34	4	0.000000	33.15	5	prohibitin	Nucleus	transcription regulator
-1.314	P35442	THBS2	0.003707	5.60	5	0.004406	4.94	8	thrombospondin 2	Extracellular Space	other
1.000	P35527	KRT9	0.000000	202.70	19	0.000000	201.76	19	keratin 9	Cytoplasm	other
1.013	P35579	MYH9	0.000000	174.83	56	0.000000	161.72	53	myosin, heavy chain 9, non-muscle	Cytoplasm	transporter
-1.694	P35606	COPB2	0.000000	25.20	9	0.000000	10.76	7	coatomer protein complex, subunit beta 2 (beta prime)	Cytoplasm	transporter
-1.072	P35908	KRT2	0.000000	98.30	22	0.000000	100.41	24	keratin 2	Cytoplasm	other
2.263	P36406-2	TRIM23	0.007598	3.88	2	0.012851	3.85	3	tripartite motif containing 23	Nucleus	enzyme
1.198	P36542-2	ATP5C1	0.000000	14.06	4	0.000000	20.47	6	ATP synthase, H+ transporting, mitochondrial F1 complex, gamma polypeptide 1	Cytoplasm	transporter
-1.702	P36776	LONP1	0.000000	15.89	4	0.000000	7.86	4	lon peptidase 1, mitochondrial	Cytoplasm	peptidase
2.163	P36957	DLST	0.000000	11.24	3	0.000000	9.39	4	dihydrolipoamide S-succinyltransferase (E2 component of 2-oxo-glutarate complex)	Cytoplasm	enzyme
-1.311	P37802	TAGLN2	0.000000	32.75	5	0.000000	29.67	4	transgelin 2	Cytoplasm	other
1.225	P37837	TALDO1	0.000000	10.89	4	0.000000	16.59	3	transaldolase 1	Cytoplasm	enzyme
-1.126	P38646	HSPA9	0.000000	58.48	11	0.000000	37.12	10	heat shock 70kDa protein 9 (mortalin)	Cytoplasm	other
-1.297	P39656	DDOST	0.000000	34.01	8	0.000000	42.85	6	dolichyl-diphosphooligosaccharide–protein glycosyltransferase	Cytoplasm	enzyme
-1.912	P40939	HADHA	0.000000	39.36	8	0.000000	24.43	11	hydroxyacyl-CoA dehydrogenase/3-ketoacyl-CoA thiolase/enoyl-CoA hydratase (trifunctional protein), alpha subunit	Cytoplasm	enzyme

Fold Change	UniProt ID	Symbol	TBART MM			TBART MP			Entrez Gene Name	Location	Type(s)
			q-value	Barista score	# of peptides	q-value	Barista score	# of peptides			
1.176	P42224-2	STAT1	0.000000	36.90	9	0.000000	29.13	8	signal transducer and activator of transcription 1, 91kDa	Nucleus	transcription regulator
-1.021	P42704	LRPPRC	0.000000	25.79	14	0.000000	17.71	11	leucine-rich pentatricopeptide repeat containing	Cytoplasm	other
2.191	P42765	ACAA2	0.003707	5.83	2	0.016108	3.77	3	acetyl-CoA acyltransferase 2	Cytoplasm	enzyme
1.094	P43243	MATR3	0.000000	8.45	1	0.000000	7.62	4	matrin 3	Nucleus	other
1.123	P43307-2	SSR1	0.000000	19.84	1	0.002257	6.61	1	signal sequence receptor, alpha	Cytoplasm	other
1.640	P43403	ZAP70	0.002034	6.62	6	0.000000	8.57	6	zeta-chain (TCR) associated protein kinase 70kDa	Plasma Membrane	kinase
-1.523	P45880-1	VDAC2	0.000000	31.22	7	0.000000	18.09	5	voltage-dependent anion channel 2	Cytoplasm	ion channel
-1.855	P46781	RPS9	0.000000	18.91	8	0.002257	6.15	5	ribosomal protein S9	Cytoplasm	translation regulator
1.052	P46940	IQGAP1	0.000000	61.28	25	0.000000	43.90	22	IQ motif containing GTPase activating protein 1	Cytoplasm	other
1.848	P47756-2	CAPZB	0.000000	13.34	3	0.000000	12.82	5	capping protein (actin filament) muscle Z-line, beta	Cytoplasm	other
-1.766	P48047	ATP5O	0.000000	17.84	5	0.000000	6.70	2	ATP synthase, H+ transporting, mitochondrial F1 complex, O subunit	Cytoplasm	transporter
1.175	P48147	PREP	0.007598	3.68	4	0.020562	3.60	2	prolyl endopeptidase	Cytoplasm	peptidase
-1.100	P48426	PIP4K2A	0.000000	9.37	3	0.000000	10.17	2	phosphatidylinositol-5-phosphate 4-kinase, type II, alpha	Cytoplasm	kinase
1.298	P48735	IDH2	0.000000	34.75	14	0.000000	28.18	10	isocitrate dehydrogenase 2 (NADP+), mitochondrial	Cytoplasm	enzyme
2.185	P49368-2	CCT3	0.014640	3.31	3	0.009618	4.19	4	chaperonin containing TCP1, subunit 3 (gamma)	Cytoplasm	other
-1.672	P49411	TUFM	0.000000	17.06	5	0.000000	9.21	5	Tu translation elongation factor, mitochondrial	Cytoplasm	translation regulator
1.160	P49755	TMED10	0.000000	9.49	3	0.000000	8.68	1	transmembrane emp24-like trafficking protein 10 (yeast)	Cytoplasm	transporter
1.157	P50416-2	CPT1A	0.035414	2.74	4	0.006367	4.67	4	carnitine palmitoyltransferase 1A (liver)	Cytoplasm	enzyme
1.056	P50552	VASP	0.002034	6.77	2	0.002257	5.92	3	vasodilator-stimulated phosphoprotein	Plasma Membrane	other
-3.672	P50991	CCT4	0.000000	12.70	5	0.012851	3.89	4	chaperonin containing TCP1, subunit 4 (delta)	Cytoplasm	other
1.092	P51148	RAB5C	0.000000	11.87	3	0.000000	11.84	3	RAB5C, member RAS oncogene family	Cytoplasm	enzyme
-1.120	P51149	RAB7A	0.000000	28.14	6	0.000000	16.89	6	RAB7A, member RAS oncogene family	Cytoplasm	enzyme
1.165	P51452	DUSP3	0.000000	7.64	1	0.007994	4.34	1	dual specificity phosphatase 3	Cytoplasm	phosphatase
2.869	P51571	SSR4	0.000000	20.13	3	0.000000	18.51	3	signal sequence receptor, delta	Cytoplasm	other

Fold Change	UniProt ID	Symbol	TBART MM			TBART MP			Entrez Gene Name	Location	Type(s)
			q-value	Barista score	# of peptides	q-value	Barista score	# of peptides			
-2.698	P51572	BCAP31	0.000000	15.61	2	0.007994	4.64	1	B-cell receptor-associated protein 31	Cytoplasm	transporter
1.778	P51659	HSD17B4	0.000000	26.47	11	0.000000	28.54	8	hydroxysteroid (17-beta) dehydrogenase 4	Cytoplasm	enzyme
1.150	P51991-2	HNRNPA3	0.000000	12.66	3	0.016108	3.73	2	heterogeneous nuclear ribonucleoprotein A3	Nucleus	other
-1.570	P52209	PGD	0.000000	31.73	7	0.000000	15.52	5	phosphogluconate dehydrogenase	Cytoplasm	enzyme
1.198	P52565	ARHGDIA	0.025344	2.96	1	0.002257	5.52	1	Rho GDP dissociation inhibitor (GDI) alpha	Cytoplasm	other
1.788	P52566	ARHGDIB	0.006650	4.43	2	0.002257	5.35	2	Rho GDP dissociation inhibitor (GDI) beta	Cytoplasm	other
-1.302	P52597	HNRNPF	0.000000	8.88	5	0.000000	6.81	5	heterogeneous nuclear ribonucleoprotein F	Nucleus	other
-1.226	P52907	CAPZA1	0.000000	9.80	4	0.004406	5.04	4	capping protein (actin filament) muscle Z-line, alpha 1	Cytoplasm	other
1.040	P53396	ACLY	0.003707	5.90	9	0.000000	7.93	9	ATP citrate lyase	Cytoplasm	enzyme
1.050	P53621-2	COPA	0.000000	9.63	7	0.000000	8.01	13	coatomer protein complex, subunit alpha	Cytoplasm	transporter
1.183	P54920	NAPA	0.003707	6.00	4	0.009618	4.24	3	N-ethylmaleimide-sensitive factor attachment protein, alpha	Cytoplasm	transporter
1.286	P55072	VCP	0.000000	18.56	12	0.000000	30.60	13	valosin containing protein	Cytoplasm	enzyme
1.126	P55084	HADHB	0.000000	10.07	5	0.025928	3.17	4	hydroxyacyl-CoA dehydrogenase/3-ketoacyl-CoA thiolase/enoyl-CoA hydratase (trifunctional protein), beta subunit	Cytoplasm	enzyme
-1.129	P55160	NCKAP1L	0.000000	22.81	6	0.000000	19.35	5	NCK-associated protein 1-like	Plasma Membrane	other
1.172	P55209	NAP1L1	0.003707	5.34	2	0.002257	6.09	1	nucleosome assembly protein 1-like 1	Nucleus	other
-1.429	P57737-2	CORO7/CORO7-PAM16	0.000000	16.78	8	0.000000	14.15	6	coronin 7	Cytoplasm	other
2.251	P59998	ARPC4	0.000000	15.14	4	0.000000	8.74	4	actin related protein 2/3 complex, subunit 4, 20kDa	unknown	other
-2.482	P60709	ACTB	0.000000	51.30	13	0.000000	50.34	11	actin, beta	Cytoplasm	other
1.079	P60842	EIF4A1	0.000000	20.55	7	0.000000	24.31	9	eukaryotic translation initiation factor 4A1	Cytoplasm	translation regulator
1.802	P60953	CDC42	0.000000	17.24	3	0.000000	12.61	4	cell division cycle 42 (GTP binding protein, 25kDa)	Cytoplasm	enzyme
1.179	P60981	DSTN	0.002034	7.27	2	0.006367	4.80	1	destrin (actin depolymerizing factor)	Cytoplasm	other
1.158	P61006	RAB8A	0.000000	10.93	4	0.000000	11.40	4	RAB8A, member RAS oncogene family	Plasma Membrane	other
1.062	P61009	SPCS3	0.000000	10.81	3	0.000000	17.17	4	signal peptidase complex subunit 3 homolog (S. cerevisiae)	Cytoplasm	peptidase
1.685	P61019	RAB2A	0.000000	11.93	3	0.000000	21.21	4	RAB2A, member RAS oncogene family	Cytoplasm	enzyme
2.211	P61106	RAB14	0.000000	10.86	3	0.000000	12.43	4	RAB14, member RAS oncogene family	Cytoplasm	enzyme

Fold Change	UniProt ID	Symbol	TBART MM			TBART MP			Entrez Gene Name	Location	Type(s)
			q-value	Barista score	# of peptides	q-value	Barista score	# of peptides			
-1.028	P61158	ACTR3	0.000000	32.09	9	0.000000	18.62	7	ARP3 actin-related protein 3 homolog (yeast)	Plasma Membrane	other
-1.093	P61160	ACTR2	0.000000	46.76	7	0.000000	38.88	11	ARP2 actin-related protein 2 homolog (yeast)	Plasma Membrane	other
1.162	P61204	ARF3	0.000000	19.02	6	0.000000	24.23	4	ADP-ribosylation factor 3	Cytoplasm	enzyme
1.078	P61224	RAP1B	0.000000	41.48	9	0.000000	33.42	7	RAP1B, member of RAS oncogene family	Cytoplasm	enzyme
3.258	P61225	RAP2B	0.000000	8.07	4	0.000000	8.28	4	RAP2B, member of RAS oncogene family	Plasma Membrane	enzyme
1.146	P61313	RPL15	0.002034	6.81	2	0.002257	5.55	2	ribosomal protein L15	Cytoplasm	other
-1.406	P61586	RHOA	0.000000	25.27	7	0.000000	25.13	4	ras homolog family member A	Cytoplasm	enzyme
-1.080	P61978-2	HNRNPK	0.000000	20.43	6	0.000000	14.72	7	heterogeneous nuclear ribonucleoprotein K	Nucleus	other
1.104	P61981	YWHAG	0.000000	11.47	7	0.000000	14.63	6	tyrosine 3-monooxygenase/tryptophan 5-monooxygenase activation protein, gamma polypeptide	Cytoplasm	other
-1.289	P62241	RPS8	0.000000	14.53	3	0.000000	10.63	4	ribosomal protein S8	Cytoplasm	other
-2.269	P62258	YWHAE	0.000000	24.27	7	0.002257	5.35	5	tyrosine 3-monooxygenase/tryptophan 5-monooxygenase activation protein, epsilon polypeptide	Cytoplasm	other
1.167	P62263	RPS14	0.006650	4.73	3	0.020562	3.58	2	ribosomal protein S14	Cytoplasm	translation regulator
1.695	P62330	ARF6	0.000000	8.75	4	0.006367	4.81	2	ADP-ribosylation factor 6	Plasma Membrane	transporter
1.192	P62424	RPL7A	0.002034	6.41	2	0.000000	7.25	1	ribosomal protein L7a	Cytoplasm	other
-2.600	P62491	RAB11A	0.000000	24.94	5	0.000000	11.56	6	RAB11A, member RAS oncogene family	Cytoplasm	enzyme
-1.755	P62701	RPS4X	0.000000	11.20	7	0.020562	3.61	4	ribosomal protein S4, X-linked	Cytoplasm	other
1.709	P62826	RAN	0.000000	20.01	5	0.000000	20.97	6	RAN, member RAS oncogene family	Nucleus	enzyme
1.165	P62913-2	RPL11	0.000000	9.17	1	0.000000	9.90	2	ribosomal protein L11	Cytoplasm	other
1.103	P62937	PPIA	0.013368	3.36	2	0.000000	9.15	3	peptidylprolyl isomerase A (cyclophilin A)	Cytoplasm	enzyme
-1.103	P63104	YWHAZ	0.000000	45.01	8	0.000000	42.24	9	tyrosine 3-monooxygenase/tryptophan 5-monooxygenase activation protein, zeta polypeptide	Cytoplasm	enzyme

Fold Change	UniProt ID	Symbol	TBART MM			TBART MP			Entrez Gene Name	Location	Type(s)
			q-value	Barista score	# of peptides	q-value	Barista score	# of peptides			
-1.788	P63244	GNB2L1	0.000000	9.27	4	0.023174	3.41	2	guanine nucleotide binding protein (G protein), beta polypeptide 2-like 1	Cytoplasm	enzyme
1.019	P68104	EEF1A1	0.000000	19.29	8	0.000000	19.85	9	eukaryotic translation elongation factor 1 alpha 1	Cytoplasm	translation regulator
-1.163	P68133	ACTA1	0.000000	9.42	15	0.012851	3.83	11	actin, alpha 1, skeletal muscle	Cytoplasm	other
-1.589	P68366	TUBA4A	0.000000	23.77	13	0.000000	20.85	12	tubulin, alpha 4a	Cytoplasm	other
-1.090	P68371	TUBB4B	0.000000	16.23	12	0.000000	11.87	13	tubulin, beta 4B class IVb	Cytoplasm	other
2.887	P68871	HBB	0.000000	30.67	9	0.000000	34.50	8	hemoglobin, beta	Cytoplasm	transporter
-2.601	P78371	CCT2	0.000000	14.78	5	0.000000	13.02	7	chaperonin containing TCP1, subunit 2 (beta)	Cytoplasm	kinase
1.216	P78417	GSTO1	0.000000	10.77	3	0.006367	4.79	2	glutathione S-transferase omega 1	Cytoplasm	enzyme
1.185	P84095	RHOG	0.000000	25.26	3	0.000000	22.87	4	ras homolog family member G	Cytoplasm	enzyme
1.402	Q00325-2	SLC25A3	0.000000	7.77	4	0.000000	9.20	4	solute carrier family 25 (mitochondrial carrier; phosphate carrier), member 3	Cytoplasm	transporter
-1.510	Q00610-2	CLTC	0.000000	157.42	36	0.000000	106.13	28	clathrin, heavy chain (Hc)	Plasma Membrane	other
1.135	Q00839-2	HNRNPU	0.000000	34.74	11	0.000000	30.35	9	heterogeneous nuclear ribonucleoprotein U (scaffold attachment factor A)	Nucleus	transporter
-2.011	Q01813	PFKP	0.000000	27.11	7	0.000000	14.59	7	phosphofructokinase, platelet	Cytoplasm	kinase
-3.340	Q02218	OGDH	0.000000	12.95	11	0.025928	3.20	6	oxoglutarate (alpha-ketoglutarate) dehydrogenase (lipoamide)	Cytoplasm	enzyme
1.683	Q02543	RPL18A	0.000000	12.92	3	0.000000	13.80	5	ribosomal protein L18a	Cytoplasm	other
2.311	Q02878	RPL6	0.000000	7.64	5	0.000000	8.17	5	ribosomal protein L6	Cytoplasm	other
-1.392	Q02978	SLC25A11	0.000000	31.91	6	0.000000	14.90	6	solute carrier family 25 (mitochondrial carrier; oxoglutarate carrier), member 11	Cytoplasm	transporter
1.080	Q03252	LMNB2	0.002034	7.15	4	0.006367	4.82	10	lamin B2	Nucleus	other
-1.449	Q03518	TAP1	0.000000	32.75	8	0.000000	13.68	5	transporter 1, ATP-binding cassette, sub-family B (MDR/TAP)	Cytoplasm	transporter
-1.225	Q04917	YWHAH	0.000000	22.61	7	0.000000	26.45	6	tyrosine 3-monooxygenase/tryptophan 5-monooxygenase activation protein, eta polypeptide	Cytoplasm	transcription regulator
1.191	Q05655	PRKCD	0.003707	6.07	2	0.004406	5.12	4	protein kinase C, delta	Cytoplasm	kinase
-3.619	Q06323	PSME1	0.000000	19.35	8	0.000000	6.88	5	proteasome (prosome, macropain) activator subunit 1 (PA28 alpha)	Cytoplasm	other

Fold Change	UniProt ID	Symbol	TBART MM			TBART MP			Entrez Gene Name	Location	Type(s)
			q-value	Barista score	# of peptides	q-value	Barista score	# of peptides			
-1.671	Q07021	C1QBP	0.000000	14.42	4	0.000000	10.69	2	complement component 1, q subcomponent binding protein	Cytoplasm	other
1.155	Q07812-2	BAX	0.006650	4.81	1	0.000000	9.93	1	BCL2-associated X protein	Cytoplasm	transporter
2.314	Q07955-2	SRSF1	0.007598	3.76	2	0.023174	3.37	2	serine/arginine-rich splicing factor 1	Nucleus	other
1.404	Q07960	ARHGAP1	0.000000	10.90	4	0.000000	11.72	4	Rho GTPase activating protein 1	Cytoplasm	other
1.243	Q08211	DHX9	0.000000	17.49	10	0.000000	18.72	13	DEAH (Asp-Glu-Ala-His) box polypeptide 9	Nucleus	enzyme
-1.136	Q08AF3	SLFN5	0.000000	8.53	4	0.000000	9.48	6	schlafen family member 5	Nucleus	enzyme
-1.828	Q10713	PMPCA	0.002034	6.21	4	0.002257	6.65	1	peptidase (mitochondrial processing) alpha	Cytoplasm	peptidase
-2.625	Q12769	NUP160	0.000000	14.54	7	0.000000	8.76	6	nucleoporin 160kDa	Nucleus	transporter
-2.535	Q12906-2	ILF3	0.000000	8.74	5	0.049543	2.46	4	interleukin enhancer binding factor 3, 90kDa	Nucleus	transcription regulator
1.081	Q13200	PSMD2	0.000000	16.21	7	0.000000	8.80	6	proteasome (prosome, macropain) 26S subunit, non-ATPase, 2	Cytoplasm	other
1.477	Q13201	MMRN1	0.000000	27.02	17	0.000000	26.86	13	multimerin 1	Extracellular Space	other
-1.531	Q13423	NNT	0.000000	23.25	12	0.000000	12.48	7	nicotinamide nucleotide transhydrogenase	Cytoplasm	enzyme
1.158	Q13576	IQGAP2	0.000000	46.92	25	0.000000	44.72	19	IQ motif containing GTPase activating protein 2	Cytoplasm	other
1.150	Q13951-2	CBFB	0.000000	17.12	2	0.000000	14.52	2	core-binding factor, beta subunit	Nucleus	transcription regulator
1.484	Q14204	DYNC1H1	0.000000	26.36	32	0.000000	18.18	19	dynein, cytoplasmic 1, heavy chain 1	Cytoplasm	peptidase
-1.189	Q14697-2	GANAB	0.000000	26.78	10	0.000000	10.27	5	glucosidase, alpha; neutral AB	Cytoplasm	enzyme
-1.319	Q14739	LBR	0.000000	16.14	6	0.000000	16.89	5	lamin B receptor	Nucleus	enzyme
1.352	Q14764	MVP	0.000000	9.51	4	0.000000	10.12	4	major vault protein	Nucleus	other
-1.515	Q14974	KPNB1	0.000000	23.95	6	0.000000	10.83	3	karyopherin (importin) beta 1	Nucleus	transporter
-1.842	Q15019-2	SEPT2	0.000000	9.72	4	0.000000	6.66	2	septin 2	Cytoplasm	enzyme
1.080	Q15029	EFTUD2	0.000000	12.11	6	0.000000	6.77	3	elongation factor Tu GTP binding domain containing 2	Nucleus	enzyme
1.128	Q15084-2	PDIA6	0.000000	11.26	4	0.007994	4.55	3	protein disulfide isomerase family A, member 6	Cytoplasm	enzyme
1.195	Q15149-2	PLEC	0.000000	7.83	27	0.000000	9.26	24	plectin	Cytoplasm	other
1.173	Q15185	PTGES3	0.005398	4.94	1	0.002257	5.71	1	prostaglandin E synthase 3 (cytosolic)	Cytoplasm	enzyme
1.231	Q15233	NONO	0.000000	12.50	4	0.000000	11.12	3	non-POU domain containing, octamer-binding	Nucleus	other

Fold Change	UniProt ID	Symbol	TBART MM			TBART MP			Entrez Gene Name	Location	Type(s)
			q-value	Barista score	# of peptides	q-value	Barista score	# of peptides			
-2.692	Q15365	PCBP1	0.000000	9.84	6	0.000000	6.92	7	poly(rC) binding protein 1	Nucleus	translation regulator
1.124	Q15942	ZYX	0.002034	6.82	3	0.025928	3.15	3	zyxin	Plasma Membrane	other
1.342	Q16181-2	SEPT7	0.000000	25.52	6	0.000000	16.96	5	septin 7	Cytoplasm	other
2.376	Q16666-2	IFI16	0.000000	15.46	7	0.000000	13.64	7	interferon, gamma-inducible protein 16	Nucleus	transcription regulator
-1.375	Q1KMD3	HNRNPUL2	0.000000	19.65	3	0.000000	14.44	5	heterogeneous nuclear ribonucleoprotein U-like 2	Nucleus	other
1.128	Q27J81-2	INF2	0.000000	11.64	4	0.000000	8.71	4	inverted formin, FH2 and WH2 domain containing	Cytoplasm	other
-1.210	Q562R1	ACTBL2	0.002034	6.79	6	0.004406	5.03	5	actin, beta-like 2	unknown	other
1.088	Q5BJH7-2	YIF1B	0.000000	9.44	2	0.002257	5.29	1	Yip1 interacting factor homolog B (S. cerevisiae)	unknown	other
1.080	Q6IAN0	DHRS7B	0.022772	3.11	3	0.002257	5.33	3	dehydrogenase/reductase (SDR family) member 7B	unknown	other
1.077	Q6IBS0	TWF2	0.003707	5.70	1	0.002257	5.46	1	twinfilin, actin-binding protein, homolog 2 (Drosophila)	Cytoplasm	kinase
1.043	Q6L8Q7-2	PDE12	0.007598	4.19	2	0.041990	2.68	4	phosphodiesterase 12	Cytoplasm	other
1.624	Q6P2Q9	PRPF8	0.000000	18.90	11	0.000000	8.54	11	PRP8 pre-mRNA processing factor 8 homolog (S. cerevisiae)	Nucleus	other
1.861	Q70J99-3	UNC13D	0.000000	10.18	9	0.000000	7.74	7	unc-13 homolog D (C. elegans)	Cytoplasm	other
-1.804	Q7KZF4	SND1	0.002034	7.16	7	0.002257	5.90	9	staphylococcal nuclease and tudor domain containing 1	Nucleus	enzyme
1.082	Q7Z4W1	DCXR	0.000000	16.58	2	0.000000	15.50	2	dicarbonyl/L-xylulose reductase	Cytoplasm	enzyme
2.315	Q7Z7H5-2	TMED4	0.007598	3.95	2	0.007994	4.55	2	transmembrane emp24 protein transport domain containing 4	Cytoplasm	transporter
1.067	Q86UX7-2	FERMT3	0.000000	100.29	24	0.000000	104.75	26	fermitin family member 3	Cytoplasm	enzyme
1.080	Q86WV1-2	SKAP1	0.007598	3.77	2	0.012851	3.86	2	src kinase associated phosphoprotein 1	Cytoplasm	kinase
1.142	Q8IXM6-2	NRM	0.003707	6.02	3	0.041990	2.68	1	nurim (nuclear envelope membrane protein)	Nucleus	other
3.354	Q8NBS9	TXNDC5	0.007598	3.72	3	0.020562	3.56	3	thioredoxin domain containing 5 (endoplasmic reticulum)	Cytoplasm	enzyme
1.070	Q8TC12	RDH11	0.000000	8.67	2	0.006367	4.73	3	retinol dehydrogenase 11 (all-trans/9-cis/11-cis)	Cytoplasm	enzyme
-1.131	Q8TEM1	NUP210	0.000000	23.10	16	0.000000	17.92	11	nucleoporin 210kDa	Nucleus	transporter
1.930	Q9Y6C9	MTCH2	0	7.7	3	0	27.39	4	mitochondrial carrier 2	Cytoplasm	other
1.006	Q8WUM4	PDCD6IP	0.007598	3.64	9	0.000000	8.03	7	programmed cell death 6 interacting protein	Cytoplasm	other
-1.756	Q8WY22	BRI3BP	0.000000	17.38	2	0.002257	5.32	2	BRI3 binding protein	Extracellular Space	other

Fold Change	UniProt ID	Symbol	TBART MM			TBART MP			Entrez Gene Name	Location	Type(s)
			q-value	Barista score	# of peptides	q-value	Barista score	# of peptides			
-1.254	Q92608	DOCK2	0.000000	11.21	9	0.000000	7.02	13	dedicator of cytokinesis 2	Cytoplasm	other
-1.677	Q92616	GCN1L1	0.000000	14.05	11	0.007994	4.45	8	GCN1 general control of amino-acid synthesis 1-like 1 (yeast)	Cytoplasm	translation regulator
-1.195	Q92621	NUP205	0.002034	7.00	6	0.012851	3.98	10	nucleoporin 205kDa	Nucleus	other
-3.426	Q92888-3	ARHGEF1	0.000000	12.18	4	0.028277	3.03	4	Rho guanine nucleotide exchange factor (GEF) 1	Cytoplasm	other
-1.742	Q96FW1	OTUB1	0.002034	7.24	3	0.041990	2.68	1	OTU domain, ubiquitin aldehyde binding 1	Cytoplasm	enzyme
1.021	Q96HE7	ERO1L	0.002034	6.78	3	0.000000	7.96	4	ERO1-like (S. cerevisiae)	Cytoplasm	enzyme
-1.896	Q96I99	SUCLG2	0.000000	8.30	2	0.000000	6.94	2	succinate-CoA ligase, GDP-forming, beta subunit	Cytoplasm	enzyme
1.041	Q96KP4	CNDP2	0.003707	5.71	4	0.041990	2.62	5	CNDP dipeptidase 2 (metallopeptidase M20 family)	Cytoplasm	peptidase
1.663	Q96PP8	GBP5	0.000000	8.00	3	0.000000	9.31	4	guanylate binding protein 5	Plasma Membrane	enzyme
-1.791	Q99439	CNN2	0.000000	11.01	3	0.012851	3.95	3	calponin 2	Cytoplasm	other
-1.023	Q99456	KRT12	0.007598	4.17	3	0.000000	7.67	3	keratin 12	Cytoplasm	other
-1.080	Q99623	PHB2	0.000000	38.78	9	0.000000	28.95	7	prohibitin 2	Cytoplasm	transcription regulator
1.477	Q99714-2	HSD17B10	0.000000	31.10	9	0.000000	33.07	6	hydroxysteroid (17-beta) dehydrogenase 10	Cytoplasm	enzyme
1.028	Q99798	ACO2	0.000000	40.11	10	0.000000	31.73	8	aconitase 2, mitochondrial	Cytoplasm	enzyme
1.056	Q99829	CPNE1	0.000000	11.54	3	0.002257	6.30	4	copine I	unknown	transporter
1.105	Q9BSJ8-2	ESYT1	0.000000	25.24	9	0.000000	32.08	7	extended synaptotagmin-like protein 1	unknown	other
3.326	Q9BVC6	TMEM109	0.000000	9.64	1	0.000000	7.18	1	transmembrane protein 109	Cytoplasm	other
1.226	Q9BVK6	TMED9	0.041247	2.65	1	0.019350	3.66	2	transmembrane emp24 protein transport domain containing 9	Cytoplasm	transporter
1.080	Q9BWM7	SFXN3	0.007598	3.64	1	0.032493	2.78	3	sideroflexin 3	Cytoplasm	transporter
1.079	Q9GZS3	WDR61	0.000000	14.41	1	0.000000	15.07	1	WD repeat domain 61	unknown	other
-1.248	Q9H2U2-2	PPA2	0.006650	4.63	2	0.002257	6.46	3	pyrophosphatase (inorganic) 2	Cytoplasm	enzyme
2.269	Q9H3N1	TMX1	0.000000	10.78	3	0.000000	11.14	4	thioredoxin-related transmembrane protein 1	Cytoplasm	enzyme
1.019	Q9H3U1-2	UNC45A	0.003707	5.56	5	0.019350	3.65	7	unc-45 homolog A (C. elegans)	Plasma Membrane	other
-1.138	Q9H4B7	TUBB1	0.000000	28.88	11	0.000000	13.03	11	tubulin, beta 1 class VI	Cytoplasm	other
1.116	Q9H845	ACAD9	0.022772	3.06	4	0.028277	2.97	3	acyl-CoA dehydrogenase family, member 9	Cytoplasm	enzyme

Fold Change	UniProt ID	Symbol	TBART MM			TBART MP			Entrez Gene Name	Location	Type(s)
			q-value	Barista score	# of peptides	q-value	Barista score	# of peptides			
-1.154	Q9H9B4	SFXN1	0.000000	30.86	6	0.000000	16.40	7	sideroflexin 1	Cytoplasm	transporter
-1.608	Q9HBI1-2	PARVB	0.000000	29.11	6	0.000000	27.29	4	parvin, beta	Cytoplasm	other
1.080	Q9NP72	RAB18	0.000000	23.30	3	0.000000	11.85	3	RAB18, member RAS oncogene family	Cytoplasm	enzyme
-1.334	Q9NQC3-3	RTN4	0.000000	23.30	4	0.004406	4.98	3	reticulon 4	Cytoplasm	other
-1.162	Q9NTJ5	SACM1L	0.000000	7.61	8	0.002257	5.93	5	SAC1 suppressor of actin mutations 1-like (yeast)	Cytoplasm	phosphatase
1.101	Q9NTK5-3	OLA1	0.006650	4.46	1	0.006367	4.83	2	Obg-like ATPase 1	Cytoplasm	other
1.166	Q9NVJ2	ARL8B	0.007598	3.97	2	0.012851	3.84	3	ADP-ribosylation factor-like 8B	Plasma Membrane	enzyme
-2.348	Q9NYU2-2	UGGT1	0.000000	13.03	9	0.002257	5.24	8	UDP-glucose glycoprotein glucosyltransferase 1	Cytoplasm	enzyme
-2.601	Q9NZN3	EHD3	0.000000	9.86	9	0.002257	5.84	10	EH-domain containing 3	Cytoplasm	other
1.101	Q9UBW8	COPS7A	0.016053	3.20	3	0.002257	5.26	2	COP9 constitutive photomorphogenic homolog subunit 7A (Arabidopsis)	Cytoplasm	other
1.185	Q9UFW8	CGGBP1	0.007598	3.86	1	0.025928	3.20	1	CGG triplet repeat binding protein 1	Nucleus	other
1.496	Q9UH99	SUN2	0.000000	34.81	8	0.000000	34.03	16	Sad1 and UNC84 domain containing 2	Nucleus	other
4.663	Q9UHD8-2	SEPT9	0.024046	2.99	3	0.000000	9.13	5	septin 9	Cytoplasm	enzyme
1.056	Q9UIQ6-2	LNPEP	0.000000	9.88	3	0.000000	9.43	4	leucyl/cystinyl aminopeptidase	Cytoplasm	peptidase
-1.895	Q9UJU6-2	DBNL	0.000000	10.70	4	0.002257	5.81	4	drebrin-like	Cytoplasm	other
-1.787	Q9UKM9	RALY	0.006650	4.81	3	0.000000	9.21	1	RNA binding protein, autoantigenic (hnRNP-associated with lethal yellow homolog (mouse))	Nucleus	other
-1.736	Q9UL46	PSME2	0.000000	8.28	4	0.000000	11.51	4	proteasome (prosome, macropain) activator subunit 2 (PA28 beta)	Cytoplasm	peptidase
1.744	Q9ULV4	CORO1C	0.000000	11.15	3	0.000000	15.03	5	coronin, actin binding protein, 1C	Cytoplasm	other
-1.542	Q9Y277-2	VDAC3	0.000000	35.58	7	0.000000	23.28	6	voltage-dependent anion channel 3	Cytoplasm	ion channel
1.038	Q9Y2X3	NOP58	0.003707	5.86	4	0.028277	3.03	4	NOP58 ribonucleoprotein homolog (yeast)	Nucleus	enzyme
1.040	Q9Y383-2	LUC7L2	0.000000	8.89	2	0.002257	5.58	1	LUC7-like 2 (S. cerevisiae)	unknown	other
1.032	Q9Y3Z3	SAMHD1	0.000000	50.25	18	0.000000	39.36	16	SAM domain and HD domain 1	Nucleus	enzyme
-1.126	Q9Y490	TLN1	0.000000	280.88	73	0.000000	246.99	70	talin 1	Plasma Membrane	other
1.002	Q9Y678	COPG1	0.000000	8.38	10	0.002257	5.66	4	coatomer protein complex, subunit gamma 1	Cytoplasm	transporter
1.067	Q9Y6C2	EMILIN1	0.000000	23.88	7	0.000000	27.35	7	elastin microfibril interfacer 1	Extracellular Space	other
-1.780	Q9Y6N5	SQRDL	0.000000	22.37	7	0.000000	9.71	7	sulfide quinone reductase-like (yeast)	Cytoplasm	enzyme